Interaction of mitochondrial fusion and electron transport chain function in differentiation of *Drosophila* neural stem cells

विद्या वाचस्पति की उपाधि की अपेक्षाओं की आंशिक पूर्ति में प्रस्तुत शोध प्रबंध

A thesis submitted in partial fulfilment of the requirements for the degree of

DOCTOR OF PHILOSOPHY

द्वारा / By

राहुल कुमार वर्मा / Rahul Kumar Verma

पंजीकरण सं. / Registration No.: 20203725

शोधप्रबंध पर्यवेक्षक / Thesis Supervisor: Prof. Richa Rikhy



भारतीय विज्ञान शिक्षा एवं अनुसंधान संस्थान, पुणे
INDIAN INSTITUTE OF SCIENCE EDUCATION AND RESEARCH, PUNE
2025

CERTIFICATE

This is to certify that the thesis titled **"Interaction of mitochondrial fusion and electron transport chain function in differentiation of *Drosophila* neural stem cells"**, submitted by **Mr. Rahul Kumar Verma**, is an original piece of research conducted by the candidate at IISER Pune under my guidance and supervision from January 2020 to December 2024.

I further confirm that this work, in whole or in part, has not been submitted previously for any degree or diploma at any other university or institution. To the best of my knowledge, the statements made by the candidate regarding this thesis are accurate and true.

Date:06/07/2025

Supervisor: Prof. Richa Rikhy

Declaration

I hereby declare that this written submission represents my original work, expressed in my own words. Wherever ideas or contributions from others have been included, they have been appropriately cited and referenced. I affirm that I have adhered to all academic honesty and integrity principles, ensuring that no idea, data, fact, or source has been fabricated, falsified, or misrepresented in this submission.

I fully understand that any violation of the above principles may result in disciplinary action by the Institute and potential legal consequences from improperly cited sources or those from whom permissions were required but not obtained.

The work presented in this thesis is solely my original research, carried out under the supervision of Prof. Richa Rikhy.



Date:06/07/2025 Rahul Kumar Verma

Acknowledgements

This thesis is a culmination of years of learning, growth, and support, something that would not have been possible without the many people who stood by me.
First of all, I would like to give my heartfelt thanks to my advisor, Prof. Richa Rikhy, for her unwavering guidance and trust. Working in her lab has been a transformative journey. Her scientific insights, constant encouragement, and patient mentorship made this journey very easy. I'm especially grateful for the freedom she gave me to explore ideas and the resources she made available to pursue them.
I sincerely thank my RAC members, Prof. Girish Ratnaparkhi and Prof. Nagaraj Balasubramanian, for their thoughtful feedback during reviews.

I deeply appreciate Mr Atharva Bhingare for his dedication and sharp insights during his Master's thesis in our lab. His contributions in analyzing the role of ATP synthase and cristae architecture in differentiation and mitochondrial activity in neuroblast were crucial to this project.

I'm grateful to RR lab past and present members, Ritika, Shashwat, Rajnandini, Aparna, Harsh, Debasmita, Somya, Sanjana, Anirban, Rishikesh and Shakshi for the many conversations, laughter, and support that made lab life enjoyable. I'm especially thankful to Dnyanesh Dubal and Bhavin Uttekar for their guidance early on. A special shoutout to Bhavin for teaching me a proper way of making fly combinations by using fly genetics.

Thanks to Snehal, Yashwant, and Ashwini at the IISER Fly Stock Centre for always keeping things running smoothly. I also thank Vijay and Santosh from the Microscopy Facility for their technical support and training. My appreciation goes to Piyush, Kalpesh, Mrinalini, and Mahesh from the Biology Admin team for their ever-reliable logistical help. Special thanks to BDSC and VDRC for providing fly stocks.

I would also like to thank my friends at IISER Pune, Ojal and Benjamin, for the many meaningful discussions on science, life, and career. Our conversations, tea breaks, lively debates, and shared everyday moments added joy to the research routine and made campus life truly vibrant and memorable. Their companionship greatly enriched my PhD journey, and I am sincerely grateful for it.

I would also like to thank my friends from Delhi University, Simran, Arjun, and Ishwinder, who have been a constant source of support. Their friendship provided strength during difficult phases and made the demanding moments more bearable. I am deeply grateful for their presence and support.

I am thankful to IISER Pune for providing a vibrant research environment, exceptional facilities, and financial support. I also thank Eklavya Ignite for enabling me to present my work at international conferences.

I would also like to specially acknowledge the cricket facilities at IISER Pune for providing a much-needed outlet beyond the laboratory. Playing cricket brought me immense joy and served as an important stress reliever during my PhD. I am grateful to the friends I made through the cricket community, Aman, Shivansh, Mehul, Kushankur, Soham, and Sayim, with whom I shared many enjoyable matches and moments. The time spent playing cricket with them brought balance to my life and greatly enriched my overall PhD experience.

I thank my family for everything, especially my elder brother Alesh, who was always there for me, in all the ups and downs. His love and belief in me have been my backbone always.

Table of Contents

List of figures……..……13
List of Tables……..……..20
List of Abbreviations……..…….……22
Abstract……...26
Synopsis……...27

Chapter 1: Introduction
1.1 Mitochondria……36
1.1.1 Mitochondrial structure……..37
1.1.2 Mitochondrial dynamics: fusion and fission……...38
1.1.3 Regulation of mitochondrial dynamics during cell cycle progression……41
1.1.4 Mitochondrial activity: Electron transport chain, mitochondrial membrane potential, ATP synthesis, and ROS generation……...44
1.1.5 Mitochondrial morphology and activity in stem cells and differentiated cells……47
1.1.6 Mitochondrial function in development……..…48

1.2 *Drosophila* neuroblast development
1.2.1 Formation through delamination……..49
1.2.2 Polarity formation and asymmetric cell division……51
1.2.3 Central nervous system of third instar larvae……...54
1.2.4 Neuroblast as model system to study stem cell biology……..57

1.3 Aims and objectives of the thesis……..58

Chapter 2: Materials and Methods

2.1 Materials

2.1.1 Fly stocks: Table……60

2.1.2 Antibodies: Table……67

2.1.3 Dyes and drugs: Table……..…69

2.1.4 In vitro assay kits: Table……...69

2.2 Methods

2.2.1 Fly crosses and genetics……..70

2.2.2 UAS-Gal4 binary system…….70

2.2.3 Larval brain Immunostaining……70

2.2.4 Mitochondrial membrane potential detection……71

2.2.5 Cellular ROS detection……..71

2.2.6 Cellular ATP detection……...71

2.2.7 EdU assay for cell proliferation analysis……72

2.2.8 Microscopy and image acquisition

2.2.8.1 Imaging of fixed samples……72

2.2.8.2 Live imaging of type II neuroblast in larval brain..……..…73

2.2.8.3 Transmission electron microscopy of larval neuroblasts……73

2.2.9 Quantification of neuroblast mitotic index……..74

2.2.10 Quantification of the number of mature INPs, GMCs and neurons in

type II neuroblast lineages……..……74
2.2.11 EdU incorporation analysis……74
2.2.12 Nuclear Cyclin E intensity measurement……..…75
2.2.13 Quantification of ROS intensity in type-II NBs……75
2.2.14 Mitochondrial membrane potential analysis……75
2.2.15 ATP dye fluorescence analysis……..75

Chapter 3: Neuroblast specific downregulation of electron transport chain complexes in the central nervous system of *Drosophila* larvae results in survival and behavioural defects

3.1 Introduction……..76
3.2 Materials and methods……..77
3.3 Results
3.3.1 Inhibition of electron transport chain complex I, II, III, IV, and V in *Drosophila* neuroblasts shows larval as well as adult lethality……...79

3.3.2 Knockdown of electron transport chain complex I, II, IV, and V do not change the number of neuroblasts in the third instar larval brain hemisphere……86

3.3.3 Disruption of ETC complex in neuroblasts leads to decline in neuronal population in brain lobe……..……89

3.4 Discussion……91

Chapter 4: Electron transport chain complex I and mitochondrial fusion regulate ROS for differentiation of *Drosophila* neural stem cells

4.1 Introduction……..…92
4.2 Materials and methods……..94
4.3 Results
4.3.1 ETC complex I depletion leads to a decrease in proliferation and differentiation of neuroblasts at the third instar larval stage……..…96

4.3.2 Induction of mitochondrial fusion by depletion of Drp1 in complex I deficient type II neuroblasts alleviate the proliferation and differentiation defect in the lineage…….103

4.3.3 Depletion of Drp1 suppresses the G1/S phase progression defects and cyclin E decrease in complex I downregulated type II neuroblasts…111

4.3.4 Decreased MMP, mitochondrial fragmentation, cristae and increased ROS production in complex I depleted type II neuroblasts is rescued by mitochondrial fusion……...113

4.3.5 Depletion of ROS scavenging enzymes, SOD1 and SOD2, leads to differentiation defects due to a decrease in G1-S transition……..…120

4.3.6 Overexpression of ROS scavengers, SOD2 and Catalase in complex I depleted type II neuroblast suppresses differentiation and G1/S transition defects by lowering ROS levels……125
4.4 Discussion……..134

Chapter 5: Depletion of electron transport chain complex II causes proliferation and differentiation defects in *Drosophila* neural stem cells

5.1 Introduction……137
5.2 Materials and methods……138
5.3 Results

5.3.1 ETC complex II depletion leads to an increase in proliferation of neuroblasts at the third instar larval stage……140

5.3.2 Complex II depletion in type II neuroblast leads to differentiation defects……141

5.3.3 Induction of mitochondrial fusion by depletion of Drp1 in complex II deficient type II neuroblasts do not rescue the proliferation and differentiation defects……..……144

5.3.4 Complex II downregulation in type II neuroblast increases ROS production and decreases mitochondrial membrane potential……...147

5.4 Discussion……150

Chapter 6: Perturbation of the electron transport chain complex IV results in proliferation and differentiation defects in *Drosophila* neural stem cells

6.1 Introduction……151
6.2 Materials and methods……153
6.3 Results

6.3.1 Complex IV disruption in *Drosophila* neuroblast leads to decreased proliferation at the third instar larval stage……154

6.3.2 Complex IV depletion in type II neuroblasts results in a decreased number of mature INPs, GMCs, and neurons in the lineage……156

6.3.3 Forced mitochondrial fusion by depletion of Drp1 in complex IV lacking neuroblasts rescues the proliferation defect in larval brain lobe...161

6.3.4 Induction of mitochondrial fusion by depletion of Drp1 in complex IV deficient type II neuroblasts rescues the number of mINPs, GMCs and neurons in the lineage……163

6.3.5 Complex IV downregulation in type II neuroblast increases ROS production and decreases mitochondrial membrane potential……168

6.3.6 Forced mitochondrial fusion by Drp1 depletion in complex IV perturbed neuroblast rescued MMP but not ROS generation……172

6.3.7 Mitochondrial fusion restores Cyclin E nuclear accumulation in complex IV-depleted neuroblasts……173

6.4 Discussion……..175

Chapter 7: Downregulation of electron transport chain complex V in neuroblast disrupts cristae morphology and results in proliferation and differentiation defects

7.1 Introduction……..…177
7.2 Materials and methods……178
7.3 Results
7.3.1 Disruption of complex V in *Drosophila* neuroblast leads to decreased proliferation at the third instar larval stage……..180

7.3.2 Complex V depletion in type II neuroblasts results in a decreased number of mature INPs, GMCs, and neurons in the lineage……..182

7.3.3 Mitochondrial fusion fails to rescue differentiation in complex V dimer-forming subunit (α, β, E, G) knockdowns, but rescues in B subunit depletion……..……..……185

7.3.4 Mitochondrial fusion fails to rescue differentiation in complex V dimer-forming subunit (α, β, E, G) knockdowns but rescues in B subunit depletion……..……189

7.4 Discussion……..195

8. Chapter 8: Summary of thesis…….……196

9. References……..…..200

List of Figures

Chapter 1: Introduction

Figure 1.1: A typical structure of mitochondria

Figure 1.2: Schematic representation of mitochondrial fission

Figure 1.3: Schematic representation of mitochondrial fusion.

Figure 1.4: Schematic representation of cell cycle-dependent mitochondrial dynamics.

Figure 1.5: Schematic representation of electron flow through the ETC complexes, and generation of mitochondrial membrane potential, ROS and other metabolites.

Figure 1.6: Schematic representation of *Drosophila* neuroblast specification via lateral inhibition.

Figure 1.7: Schematic representation of polarity formation and asymmetric division of *Drosophila* NBs.

Figure 1.8: Developmental timeline of *Drosophila* neurogenesis waves.

Figure 1.9: Schematic representation of the *Drosophila* 3rd instar larval nervous system and type I and type II neuroblasts development

Chapter 3: Neuroblast specific downregulation of electron transport chain complexes in the central nervous system of *Drosophila* larvae results in survival and behavioural defects

Figure 3.1: Downregulation of ETC complex I, II, III, IV, and V do not affect neuroblast number.

Figure 3.2: Downregulation of complex I (ND-51^{i}) and complex IV (Cox6C^{i}) in neuroblast using *wor*-Gal4 causes a reduction in Elav-positive neuronal population.

Chapter 4: Electron transport chain complex I and mitochondrial fusion regulate ROS for differentiation of *Drosophila* neural stem cells

Figure 4.1: Schematic showing the arrangement of *Drosophila* mitochondrial complex I subunits forming the L-shaped topology.

Figure 4.2: Deletion of complex I reduces the proliferation of neuroblasts in the third instar larval brain.

Figure 4.3: Deletion of complex I reduces division of type II neuroblasts in the third instar larval brain.

Figure 4.4: Complex I depletion in type II neuroblasts results in a decreased number of mINPs, GMCs, and neurons in the lineages.

Figure 4.5: Decrease of differentiated cells in the lineage of complex I-depleted type II neuroblast was not due to apoptosis or cell death. Differentiation abnormalities shown by the ND-51^{i} neuroblast were not caused by off-target defects.

Figure 4.6: Representative images of mitochondrial morphology in type II neuroblasts and third instar larval muscle

Figure 4.7: Forced mitochondrial fusion by Drp1^{SD} expression in complex I-depleted neuroblasts alleviates the proliferation defects.

Figure 4.8: Forced mitochondrial fusion by Drp1^{SD} overexpression in complex I-depleted neuroblasts alleviates the differentiation defects.

Figure 4.9: Forced mitochondrial fusion in complex I-depleted type II neuroblasts partially alleviates the number of neurons.

Figure 4.10: Differentiation defects rescue on Drp1^{SD} expression was not because of Gal4 dilution.

Figure 4.11: Depletion of complex I in type II neuroblasts inhibits G1-S phase progression by reducing Cyclin E levels. This cell cycle defect is rescued by promoting mitochondrial fusion.

Figure 4.12: Depletion of complex I diminishes MMP in type II neuroblast, and mitochondrial fusion alleviates it.

Figure 4.13: Disruption of complex I in neuroblast leads to mitochondrial fragmentation and decreased number of cristae per mitochondria, and Drp1 depletion rescues these defects.

Figure 4.14: Depletion of complex I in type II neuroblasts does not change the ATP levels.

Figure 4.15: Depletion of complex I increases ROS levels in type II neuroblast, and mitochondrial fusion suppresses it.

Figure 4.16: Depletion of SOD1/2 in the II neuroblast causes mitochondrial fragmentation without changing mitochondrial membrane potential.

Figure 4.17: Downregulation of SOD1 and SOD2 enzymes in type II neuroblast leads to elevated ROS levels.

Figure 4.18: Loss of SOD1 and SOD2 leads to decreased mature INPs, GMCs, and neurons in the type II neuroblast lineage.

Figure 4.19: Depletion of SOD1 and SOD2 results in G1-S phase transition defects through decreasing nuclear cyclin E in type II neuroblast.

Figure 4.20: Overexpression of SOD2 and catalase in ND-51^{i} expressing type II neuroblast decreases ROS levels compared to ND-51^{i} alone.

Figure 4.21: Overexpression of SOD2 and catalase in ND-51^{i} expressing type II neuroblast alleviates differentiation defects.

Figure 4.22: Overexpression of SOD2 and catalase independently in type II neuroblasts does not affect differentiation.

Figure 4.23: G1/S transition defect is alleviated in SOD2^{OE} in complex I depleted type II neuroblast lineages.

Figure 4.24: Overexpression of SOD2 and catalase in complex I depleted type II neuroblast did not rescue the MMP loss.

Figure 4.25: Mitochondrial fusion by Drp1 depletion rescues the differentiation defect in SOD2 depleted type II neuroblasts

Figure 4.26: A schematic diagram representing a summary of the mechanism of complex I mediated regulation of type II neuroblast differentiation.

Chapter 5: Depletion of electron transport chain complex II causes proliferation and differentiation defects in *Drosophila* neural stem cells

Figure 5.1: Schematic showing the structure of complex II (succinate dehydrogenase).

Figure 5.2: Deletion of complex II leads to increased proliferation of neuroblasts in the third instar larval brain.

Figure 5.3: Complex II depletion in type II neuroblasts results in an increased number of mature INPs and GMCs, but decreased neurons in the lineage.

Figure 5.4: Mitochondrial fusion does not alleviate the defect of high proliferation of complex II-depleted neuroblasts in the larval brain lobe.

Figure 5.5: Mitochondrial fusion by Drp1 depletion in type II neuroblasts could not rescue the differentiation defects.

Figure 5.6: Disruption of complex II in type II neuroblast leads to elevated ROS generation.

Figure 5.7: Depletion of complex II in type II neuroblast leads to decreased mitochondrial membrane potential

Chapter 6: Perturbation of the electron transport chain complex IV results in proliferation and differentiation defects in *Drosophila* neural stem cells

Figure 6.1: Schematic representation of the core subunits (I, II, and III)of complex IV (cytochrome c oxidase).

Figure 6.2: Depletion of complex IV in neuroblasts decreases their proliferation in the larval brain.

Figure 6.3: Depletion of complex IV in type II neuroblast leads to a decreased number of mature INPs and GMCs in the lineage.

Figure 6.4: Complex IV perturbation in type II neuroblast leads to decreased proliferation of mINPs.

Figure 6.5: Depletion of complex IV in type II neuroblasts leads to a decreased number of neurons in the lineage.

Figure 6.6: Induction of mitochondrial fusion in complex IV-deficient neuroblasts restores their proliferation.

Figure 6.7: Mitochondrial fusion restores the mINPs and GMCs in the lineage of complex IV-depleted type II neuroblasts.

Figure 6.8: Mitochondrial fusion restores the mINPs proliferation in the lineage of complex IV-depleted type II neuroblasts.

Figure 6.9: Mitochondrial fusion restores the neurons in the lineage of complex IV-depleted type II neuroblasts.

Figure 6.10: Disruption of complex IV in type II neuroblasts leads to loss of MMP.

Figure 6.11: Perturbation of complex IV in type II neuroblasts diminishes the ROS generation.

Figure 6.12: Mitochondrial fusion restores MMP loss in complex IV-depleted type II neuroblasts but cannot rescue ROS levels.

Figure 6.13: Mitochondrial fusion rescues nuclear cyclin E loss in complex IV-depleted neuroblasts.

Chapter 7: Downregulation of electron transport chain complex V in neuroblast disrupts cristae morphology and results in proliferation and differentiation defects

Figure 7.1: Subunit organization of mitochondrial ATP synthase (mtATPase)

Figure 7.2: Neuroblasts in the third instar larval brain proliferate less on complex V depletion.

Figure 7.3: Depletion of complex V in type II neuroblasts leads to a decreased number of mature INPs and GMCs in the lineage.

Figure 7.4: Complex V inhibition in type II neuroblasts reduces the number of neurons in the lineage.

Figure 7.5: Mitochondrial fusion does not rescue the decreased number of mature INPs and GMCs in ATP syn α, β, E, and G subunits depleted type II neuroblast lineage, but rescues in ATP syn B knockdown.

Figure 7.6: Mitochondrial fusion fails to restore the reduced numbers of neurons in the lineage of type II neuroblasts lacking ATP synthase α, β, E, and G subunits, but rescues in B subunit knockdown.

Figure 7.7: Mitochondrial fusion could not restore MMP loss in complex V-depleted type II neuroblasts.

Figure 7.8: Mitochondrial hyperfusion failed to reduce elevated ROS levels in ATP synthase α and β-depleted type II neuroblasts, but suppressed ROS generation in ATP synthase B.

Figure 7.9: Depletion of ATP syn β subunit results in fragmented mitochondrial morphology and loss of cristae, and forced mitochondrial fusion could not rescue it.

Figure 7.10: Mitochondrial hyperfusion alleviated cytoplasmic accumulation of cytochrome c in ATP synthase B-depleted type II neuroblasts but had no effect in α or β subunit knockdowns.

List of Tables

List of fly lines

List of Antibodies

List of Dyes and Drugs

List of In Vitro Assay Kits

Observation Table 1: RNAi screening of electron transport chain complexes in the *Drosophila* central nervous system

Table 2: Summary of phenotypic outcomes upon depletion of ETC complexes in the type II neuroblast

List of Abbreviations

1	aPKC	Atypical Protein Kinase C
2	Ase	Assense
3	CDK	Cyclin-Dependent kinase
4	Dpn	Deadpan
5	DRP1	Dynamin Related Protein 1
6	E(spl)	Enhancer of split
7	EdU	5-Ethynyl-2’-deoxyuridine
8	ER	Endoplasmic Reticulum
9	Espl	Enhancer of Split
10	ETC	Electron Transport Chain
11	FADH	Flavin Adenine Dinucleotide Hydrogen
12	Fis1	Fission 1
13	GMC	Ganglion Mother Cell
14	HD	Huntington's disease
15	IMM	Inner Mitochondrial Membrane
16	INP	Intermediate Neural Precursor

17	MARCM	Mosaic Analysis Repressible Cell Marker
18	Marf	Mitochondrial Assembly Related Factor
19	MB	Mushroom Body
20	MEF1	Mitochondrial Elongation Factor 1
21	MFF	Mitochondrial Fission Factor
22	MFfn	Mitofusin
23	Mira	Miranda
24	MMP	Mitochondrial Membrane Potential
25	mTOR	Mechanistic Target of Rapamycin
26	NADH	Nicotinamide Adenine Dinucleotide Hydrogen
27	NB	Neuroblast
28	NE	Neuro-Epithelium
29	NICD	Notch Intracellular Domain
30	NSCs	Neural Stem Cells
31	OL	Optic Lobe
32	OMM	Outer Mitochondrial Membrane

33	Opa1	Optic atrophy 1
34	OXPHOS	Oxidative phosphorylation
35	PAN	Posterior Asense Negative
36	PAR3	Partitioning Defective 3
37	PBS	Phosphate Buffer Saline
38	PD	Parkinson’s Disease
39	PFA	Paraformaldehyde
40	pH3	phoso-Hoston-3
41	Pnt	Pointed
42	Pros	Prospero
43	PSCs	Pluripotent Stem Cells
44	RIP	Receptor Interacting Protein
45	ROS	Reactive Oxygen Species
46	RT	Room Temperature
47	SOD	Superoxide Dismutase
48	Su(H)	Suppressor of Hairless
49	TCA	Tricarboxylic acid
50	TIC	Tumor Initiating Cells

51	UAS	Upstream Activator Sequence
52	VNC	Ventral Nerve Cord
53	Wor	Worniu
54	ZA	Zonula Adherens

Abstract

Mitochondrial fusion and fission, along with the activity of the electron transport chain in neural stem cells (NSCs), play an essential role in regulating the metabolic demands of differentiation. However, the mechanisms by which mitochondrial morphology and activity together regulate NSC differentiation are poorly understood. This study explored the interaction between mitochondrial morphology and electron transport chain complexes in *vivo* in *Drosophila* NSC (neuroblast) differentiation. We found that the inhibition of oxidative phosphorylation by depleting different subunits of complex I, II, IV and V did not affect the number of type II neuroblasts in the brain but reduced the number of intermediate precursor cells, ganglion mother cells and neurons in the type II neuroblast lineage. This differentiation defect was suppressed by forced mitochondrial fusion on additional depletion of Drp1 in complex I and IV-depleted neuroblasts but not in complex II and V-deficient neuroblasts. We further explored the mechanism by which ETC complex depletion affects differentiation and fusion rescue. We found that the depletion of complex I subunits led to a decrease in mitochondrial membrane potential, an increase in ROS, a decline in nuclear cyclin E, and a decrease in the proliferation of the neuroblasts and mature intermediate precursor cells. In addition to forced mitochondrial fusion, these defects were reversed by overexpression of ROS-scavenging enzymes such as SOD2 and catalase in the neuroblast. Together, this study reveals the role of mitochondrial morphology in regulating mitochondrial activity to control the levels of ROS for proper differentiation in the type II neuroblast lineage.

Synopsis

Title: **Interaction of Mitochondrial Fusion and Electron Transport Chain Function in Differentiation of *Drosophila* Neural Stem Cells**

Candidate: **Rahul Kumar Verma**

Registration number: **20203725**

Institute: **Indian Institute of Science Education and Research (IISER), Pune**

Supervisor: **Prof. Richa Rikhy**

---

1. Introduction

Mitochondria, known as the powerhouse of the cell, play a far more complex role than generating ATP. They regulate various cellular processes, including energy metabolism, redox signalling, calcium homeostasis, and programmed cell death (Green and Kroemer 2004; Youle and van der Bliek 2012). Mitochondria comprise the outer membrane, inner membrane, intermembrane space, and matrix. The outer membrane contains permeable porins, allowing the passage of ions and metabolites between the cytosol and the intermembrane space. In contrast, the inner membrane is highly impermeable. It forms a folded structure called cristae, which expands its surface area to house the electron transport chain (ETC) and oxidative phosphorylation (OXPHOS) machinery. These compartmentalisations are vital for efficient ATP production. The intermembrane space hosts proton gradients, metabolites and enzymes involved in oxidative phosphorylation. Meanwhile, the matrix contains mitochondrial DNA and enzymes crucial for the TCA cycle and fatty acid oxidation (Wollweber et al. 2017; Yang

et al. 2021). Mitochondrial structure and function are tightly linked; their dynamic morphology is regulated by fusion and fission events, determining their distribution, shape, and metabolic state. Mitochondrial fission is mediated by the GTPase dynamin-related protein 1 (DRP1), which is recruited to the outer mitochondrial membrane to initiate the process. This recruitment is initiated by receptor proteins such as mitochondrial fission factor (MFF) (Lee et al. 2004), mitochondrial fission protein 1 (Fis1) (Zhao et al. 2011), and mitochondrial elongation factor 1 (MEF1) (Pernas and Scorrano 2016). These proteins assemble at ER-mitochondria contact sites, forming platforms for DRP1 localization. Once bound, DRP1 oligomerizes around the mitochondria, driving membrane constriction and ultimately leading to mitochondrial fragmentation (Cipolat et al. 2004). Mitochondrial fusion starts with the outer membrane (OMM) fusion and then the inner membrane (IMM). Mfn1/2 (*Drosophila* homolog called Marf, Mitochondrial assembly regulatory factor) mediates OMM fusion followed by IMM fusion through optic atrophy 1 (Opa1) (Malka et al. 2005; Song et al. 2009).

Mitochondrial dynamics have emerged as key regulators in various physiological contexts, particularly in animal development and stem cell biology. In stem and progenitor cells, mitochondrial morphology and function shift dramatically during transitions between self-renewal and differentiation. Proliferating stem cells often exhibit a fragmented mitochondrial network with lower oxidative phosphorylation, whereas differentiated cells show fused mitochondria with higher OXPHOS activity (Chung et al. 2007; Seo et al. 2018). However, the molecular mechanisms through which mitochondrial dynamics and function influence stem cell differentiation remain incompletely understood.

Recent evidence suggests that mitochondrial morphology and ETC function regulate stem cell proliferation and differentiation. In *Drosophila* neural stem cells (NSCs), inhibiting OXPHOS by knocking down complex I or V causes mitochondrial fragmentation, reduces proliferation, and disrupts their developmental patterning. In contrast, blocking glycolysis by depleting key enzymes such as phosphofructokinase or

aldolase does not produce similar defects (van den Ameele and Brand 2019). Also, loss of Opa1 leads to fragmented mitochondria and impairs neuroblast differentiation. Interestingly, promoting fusion by knocking down Drp1 can rescue the differentiation defects caused by Opa1 depletion (Dubal et al. 2022).

In this study, we investigate the interaction between mitochondrial fusion and OXPHOS driven by complex I, II, IV, and V during the proliferation and differentiation of neuroblasts in the central brain of *Drosophila* third instar larvae. The central brain in the third instar larva contains type I and type II neuroblasts. The type I neuroblasts are approximately 90 in number, and the type II neuroblasts are 8 in number. They express transcription factors Deadpan (Dpn) and Asense (Ase). Type I neuroblasts divide to produce ganglion mother cells (GMCs). The type II neuroblast lineages contain transit-amplifying cells, similar to those in mammalian systems. Type II neuroblasts express an Ets transcription factor, *pointed P1* (*pnt*) (Zhu et al. 2011). They undergo division to produce immature intermediate neural progenitors (INPs) (Bello et al. 2008). Immature INPs undergo transcriptional changes to form mature INPs (mINPs) expressing Dpn and Ase. mINPs divide asymmetrically 5–6 times, to form GMCs. GMCs in both type I and II neuroblasts lineages express Prospero (Pros) and Ase. GMCs eventually divide symmetrically to produce neurons or glia. High nuclear Pros and Elav are expressed in neurons (Knoblich 2010; Kelsom and Lu 2012).

ETC complex I is a multi-subunit enzyme with a 1000 kDa molecular weight that catalyzes the transfer of electrons from NADH to ubiquinone. Complex I can generate ROS during electron transfer in the ETC. Electron flow starts when NADH and $FADH_2$ donate electrons to complex I and II, respectively. Electrons from these complexes are transferred to complex III via ubiquinone and then to complex IV through cytochrome c, where molecular oxygen is reduced to water. This electron flow is coupled to the pumping of protons from the mitochondrial matrix to the intermembrane space by complex I, II, and IV, establishing an electrochemical gradient across the inner

mitochondrial membrane, which manifests as the mitochondrial membrane potential (MMP)**.** Complex V (ATP Synthase) utilises the MMP to synthesise ATP from ADP.

In this study, we are trying to dissect the interplay between mitochondrial fusion and ETC function in *Drosophila*'s type II NB differentiation. By systematically perturbing complexes of the ETC and manipulating mitochondrial morphology through genetic tools, this work aims to uncover how mitochondrial structure-function relationships shape *Drosophila* neural stem cells differentiation. We have well-characterised the role of complex I in type II neuroblast proliferation and differentiation, along with some preliminary data for other ETC complexes. We found that inhibition of OXPHOS through depleting complex I, IV and V led to decreased proliferation in the central brain neuroblasts, but no change in the number of neuroblasts. There was a decrease in differentiation in the type II neuroblast lineage, characterised by reduced mINPs, GMCs, and neurons. Downregulation of complex I led to fragmented mitochondria, decreased cristae, a low MMP, and increased ROS generation. These elevated ROS levels decreased differentiation by inhibiting the G1 to S phase transition in the cell cycle. Inducing mitochondrial fusion or increasing ROS scavengers in complex I-depleted type II neuroblasts reversed the ROS levels and restored the differentiation defects. Unlike the depletion of complexes I, IV, and V, inhibition of complex II led to an increase in mature INPs and GMCs within the neuroblast lineage. However, similar to other ETC complex disruptions, the number of neurons remained low. These differentiation defects were not rescued by promoting mitochondrial fusion. Complex V is crucial in forming dimers within the IMM, which is essential for maintaining the cristae structure (Teixeira et al. 2015). Disrupting complex V in neuroblasts resulted in loss of cristae in mitochondria, likely due to impaired dimer formation. This was accompanied by reduced mitochondrial activity, marked by decreased membrane potential and elevated ROS levels. Inducing mitochondrial hyperfusion in complex V-depleted neuroblasts did not restore cristae architecture, mitochondrial function, and differentiation defects.

2. Results

2.1 ETC disruption affects proliferation and differentiation but not neuroblast numbers in the central brain of larvae

To assess the role of ETC complexes in neuroblast formation, proliferation and differentiation we depleted ETC subunits from complexes I (ND-51, ND-39, and ND-19), II (SdhD), IV (Cox5A, Cox6C, Cox7A, and Cox8), and V (ATP synthase α, β, B, E, G) using RNAi under neuroblast-specific Gal4 (pan neuronal, *worniu*-Gal4 (*wor*-Gal4) and type II pacific, *pointed P1*-Gal4 (*pnt*-Gal4)). We found that there was a significant reduction in the proportion of mitotically active NSCs within each third instar larval brain lobe. Next, to determine the effect of ETC disruption on type II neuroblast differentiation, we immunostained brains with Ase, Dpn, and Pros. Consistent with the decrease in proliferation, the number of mINPs (Dpn+), GMCs (Ase+, Dpn-), and neurons (Pros+) in the type II neuroblast were decreased. However, the number of type II NBs remained unaffected. In contrast to complexes I, IV, and V being depleted, complex II inhibition resulted in a rise in neuroblast proliferation, which resulted in an increase of mature INPs and GMCs within the neuroblast lineage. However, the number of neurons remained low, as is the case with disruption of other ETC complexes. This indicates that while ETC activity is not required for neuroblast formation, it is essential for proliferation and differentiation.

2.2 Mitochondrial hyperfusion rescues differentiation defects in specific ETC Knockdowns

Mitochondrial fusion is crucial for *Drosophila* neuroblast differentiation (Dubal et al. 2022). Depleting Opa1 in type II neuroblasts leads to mitochondrial fragmentation and differentiation defects (Dubal et al. 2022). Drp1 activity is essential for driving mitochondrial fragmentation in Opa1-depleted cells (Chowdhary et al. 2017; Trevisan et al. 2018; Deng et al. 2018). Co-depletion of Drp1 with Opa1 restores mitochondrial

fusion and alleviates the differentiation. Additionally, concurrent depletion of Drp1 with Opa1 restores mitochondrial fusion and alleviates the differentiation defects(Dubal et al. 2022). We assessed mitochondrial morphology in complex I-depleted type II neuroblasts and muscle cells by using *pnt*-Gal4 and *mhc*-Gal4, respectively. Depletion of Complex I in *Drosophila* type II neuroblasts (ND-51<*pnt*-Gal4) and larval muscle (ND-51<*mhc*-Gal4) induces mitochondrial fragmentation. Overexpression of $Drp1^{SD}$ (Drp1 dominant negative form) along with complex I downregulation results in hyperfused and clustered mitochondria. Next, we examined whether reversing mitochondrial morphology by $Drp1^{SD}$ expression in complex I-depleted neuroblasts can rescue proliferation and differentiation defects. Expression of $Drp1^{SD}$ restored neuroblast proliferation and the number of differentiated cells (mature INPs, GMCs, and neurons) in the lineages. $Drp1^{SD}$ also rescued proliferation and differentiation defects in complex IV-depleted neuroblasts. However, no rescue was observed in knockdowns of ATP synthase dimer-forming subunits (α, β, E, G). Interestingly, rescue was partial in ATP synthase B-depleted conditions, which is not involved in dimerisation. Therefore, ATP synthase dimerisation and proper cristae morphology are prerequisites for the rescue of differentiation defects by mitochondrial hyperfusion.

2.3 Mitochondrial membrane potential was reduced upon ETC complex I, II, IV and V knockdown

Disruption of the mitochondrial ETC in neuroblasts leads to mitochondrial fragmentation, decreased mitochondrial activity, and altered metabolites (Bonnay et al. 2020; Yao et al. 2019). We measured the changes in MMP in ETC-depleted type II neuroblasts by using the potentiometric dye, Tetra-methyl-rhodamine methyl ester (TMRM) in living third-instar larval brains. We found that MMP was lost on ETC complex I, II, IV and V downregulation in type II neuroblast. Mitochondrial hyperfusion by co-expression of $Drp1^{SD}$ with complex I and IV knockdown restored the MMP but had no effect in complex V-depleted type II neuroblast. Cristae exhibit ETC machinery, which generates MMP during OXPHOS. By concentrating proteins involved in oxidative phosphorylation

and lowering the mean distance between ETC complexes, cristae behave as specialised compartments that ensure favourable conditions for OXPHOS (Gilkerson et al. 2003; Vogel et al. 2006; Song et al. 2013). Therefore, cristae disruption might be the reason for reduced MMP on complex I depletion in neuroblasts. We used transmission electron microscopy to assess cristae morphology. Complex I depletion in neuroblast showed decreased and poorly organised cristae in mitochondria. $Drp1^{SD}$ expression restored the cristae number. These results suggest that rescue of MMP by mitochondrial fusion in complex I-depleted neuroblasts is due to the achievement of appropriate mitochondrial morphology and cristae architecture. But MMP was not involved in differentiation, as we did not find any change in ATP levels between the complex I downregulated and control neuroblast. In contrast to complex I, depletion of complex V in neuroblasts resulted in complete loss of cristae, and even mitochondrial hyperfusion could not restore it. Therefore, hyperfusion cannot restore cristae integrity without ATP synthase dimerisation, failing to rescue differentiation.

2.3 ETC disruption in type II neuroblast changes ROS levels

2.3.1 Complex I depletion elevates ROS generation, which results in differentiation defects through inhibiting G1/S phase progression, which is rescued by mitochondrial hyperfusion

Altering mitochondrial morphology and ETC function changes ROS levels in the mitochondria and the cytoplasm (Sharma et al. 2011; Ježek et al. 2018; Deng et al. 2018). We assessed the ROS levels in type II neuroblasts using the fluorescent dye dihydroxy ethidium (DHE). Complex I depletion resulted in elevated ROS generation, which could be rescued by mitochondrial hyperfusion. To determine if mitochondrial fusion rescued the differentiation defects (section 2.2) by lowering the ROS levels, we increased ROS generation in neuroblasts by downregulating ROS scavenging enzymes, SOD1 and SOD2. These elevated ROS levels led to a decrease in differentiation by interfering with G1/S phase transition in the cell cycle, characterised by

reduced nuclear cyclin E (regulated G1/S phase progression) accumulation in the type II neuroblast and a decreased number of EdU (S phase marker) positive cells in the lineage. Also, overexpression of ROS scavengers, SOD2 and catalase, in complex I-depleted type II neuroblasts reversed the ROS levels and restored the differentiation defects in the type II neuroblast lineage. Therefore, these data indicate that optimum levels of ROS are required for proper type II neuroblast differentiation. Elevated ROS on depletion of either complex I or SOD1/2 causes differentiation defects, and lowering ROS levels in complex I downregulated type II neuroblast by mitochondrial fusion or overexpression of ROS scavengers rescues the differentiation.

2.3.2 Complex II and V depletion increases ROS in type II neuroblasts, while complex IV depletion reduces it

Knockdown of complex IV subunits Cox5A, Cox6C, Cox7C and Cox8 in type II neuroblasts resulted in a complete loss of ROS generation, which could not be rescued by mitochondrial hyperfusion. Depleting complex II subunit, SdhD and complex V, ATP synthase subunits α, β, and B, led to an increase in ROS levels. Co-expression of $Drp1^{SD}$ reduced ROS in the ATP synthase B knockdown, and it failed to do so in α or β knockdowns. Since α and β subunits are critical for dimer formation, these findings suggest that ATP synthase dimerisation is necessary for hyperfusion-mediated rescue, and ROS regulation occurs downstream of cristae organisation and is tightly linked to type II neuroblast differentiation.

3. Discussion

Our study elucidates the interplay between mitochondrial fusion, cristae architecture, and ETC activity in regulating neural stem cell differentiation in *Drosophila*. While ETC activity is necessary for differentiation, mitochondrial hyperfusion could rescue the differentiation block in complex I and IV knockdowns, but failed in ATP synthase

dimerisation-defective conditions. Therefore, mitochondrial morphology alone is not sufficient; rather, the regulation of metabolite generation, ROS and cristae morphology is crucial. ATP synthase dimerisation, mediated by α, β, E, and G subunits, appears central to cristae formation and ROS compartmentalisation. Loss of these subunits disrupted cristae, increased ROS and prevented mitochondrial fusion from restoring redox balance or rescuing lineage progression. Conversely, ATP synthase B depletion, which does not affect dimerisation, allowed ROS reduction upon $Drp1^{SD}$ expression. Thus, this work proposes a model wherein the ETC function generates redox signals that are regulated by mitochondrial morphology. Hyperfusion buffers ROS only when cristae integrity is maintained, allowing controlled redox signalling that promotes type II neuroblast lineage differentiation.

Chapter 1

Introduction

1.1 Mitochondria

Eukaryotic cells contain numerous membrane-bound organelles, and mitochondria are one of the key organelles located in the cytoplasm. They were first identified by Altmann in 1890 (Falkenberg and Larsson 2009; O'Rourke 2010). The term "mitochondrion," derived from the Greek *mitos* (thread) and *chondros* (granule), was introduced by Karl Benda in 1898 during his study of spermatogenesis. Extensive evidence supports the idea that mitochondria originated as free-living bacteria before being integrated into eukaryotic cells through endosymbiosis (Archibald 2014). Around two billion years ago, a eukaryotic cell engulfed a free-living prokaryote, which instead of being digested, established a symbiotic relationship with the host (Lane and Martin 2010). This internalised bacterium began supplying the cell with ATP, the energy currency required for numerous cellular functions (John and Whatley 1975; Amiri et al. 2003). This event—now known as the endosymbiotic theory—is considered a landmark in the evolution of multicellular life. During the time course, the host nucleus took over the control of the production of most mitochondrial proteins (Roger et al. 2017). Today, mitochondria are indispensable organelles of eukaryotic cells, playing essential roles in executing many cellular processes.

Mitochondria are predominantly inherited maternally in sexually reproducing organisms. During fertilization, only the sperm nucleus and centriole, along with a small amount of cytoplasm, enter the egg. The midpiece of the sperm, which contains mitochondria, remains outside and is eventually lost. In *C. elegans*, although some mitochondrial components do enter the oocyte, they are rapidly degraded by the cell's autophagy machinery after fertilization (Song et al. 2014).

In the following sections, I will explore various aspects of mitochondrial architecture, dynamics, and their roles in key cellular processes.

1.1.1 Mitochondrial structure

Mitochondria are eukaryotic organelles characterised by a double-membrane structure (Figure 1.1). This architecture facilitates mitochondria to perform diverse functions like ATP synthesis through oxidative phosphorylation (OXPHOS), apoptosis, calcium

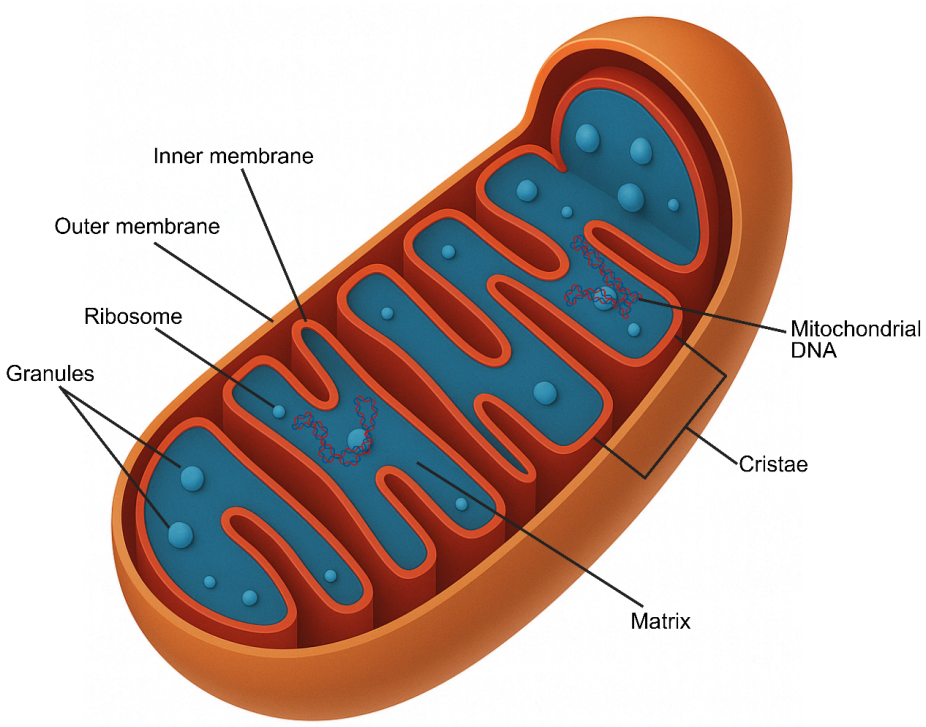


Figure 1.1: A typical structure of mitochondria. Schematic showing the architecture of mitochondria. It has the outer mitochondrial membrane (Orange), inner mitochondrial membrane (red), foldings of the inner membrane called cristae, ribosomes, DNA, and matrix. Created on BioRender.

homeostasis, ROS generation, metabolite formation, and signalling. Mitochondria consist of an outer mitochondrial membrane (OMM), an inner mitochondrial membrane

(IMM), an intermembrane space, and a matrix (Green and Kroemer 2004; Youle and van der Bliek 2012). Outer membrane possesses majorly porins, making it permeable to facilitate the exchange of various ions and metabolites between the cytoplasm and intermembrane space. The inner membrane is extensively folded into a structure known as cristae. Folding increases the surface area of the inner membrane to accommodate OXPHOS machinery (electron transport chain complexes). This compartmentalisation is essential for efficient energy production. The intermembrane space facilitates oxidative phosphorylation by harbouring, proton gradient, some metabolites and enzymes. The matrix contains the mitochondrial genome and enzymes for the TCA (Tricarboxylic acid) cycle and fatty acid oxidation, and serves as the site for crucial metabolic processes (Wollweber et al. 2017; Yang et al. 2021).

1.1.2 Mitochondrial dynamics: Fusion and fission

Mitochondria exhibit a dynamic nature, constantly oscillating between fusion and fission in response to cellular requirements. Mitochondrial fusion involves the merging of two individual mitochondria into a single, larger organelle. During mitochondrial fission, a single mitochondrion divides into two smaller mitochondria.

Mitochondrial fission is usually observed during cellular stress, including mitochondrial dysfunction or during apoptosis (Tilokani et al. 2018), during cell cycle progression, facilitating the equitable segregation of mitochondria into daughter cells during mitosis (Kashatus et al. 2011), and in response to the energy status of the cells. Fragmented mitochondria favour glycolysis and fused mitochondria facilitate OXPHOS (Mishra and Chan 2016). Mitochondrial fission also regulates the uniform distribution of mitochondria within the cytoplasm, ensuring equitable partitioning of mitochondria during cell division (Kraft and Lackner 2018) and spatial segregation of dysfunctional mitochondrial regions, which are subsequently targeted for lysosome-mediated degradation via mitophagy (Twig et al. 2008; Burman et al. 2017).

Mitochondrial fusion facilitates the exchange and distribution of mitochondrial DNA, metabolic intermediates, and electron transport chain proteins across the organelle network (Nunnari et al. 1997; Okamoto et al. 1998). This dynamic elongation of mitochondria supports cellular viability by augmenting OXPHOS efficiency (Mishra et al. 2014) and saves metabolically competent mitochondria from being targeted by autophagic pathways (Rambold et al. 2011; Gomes et al. 2011)

Mitochondrial fission is triggered at the endoplasmic reticulum (ER)-mitochondria contact site by the recruitment of fission machinery from the cytosol to the contact site. It is initiated by the recruitment of the GTPase dynamin-related protein 1 (DRP1) to the outer mitochondrial membrane (Figure 1.2). This process is facilitated by receptor proteins, including mitochondrial fission factor (MFF) (Lee et al. 2004), mitochondrial fission protein 1 (Fis1) (Zhao et al. 2011), and mitochondrial elongation factor 1 (MEF1) (Pernas and Scorrano 2016), which form complexes at ER-mitochondria contact sites. These complexes serve as platforms for DRP1 recruitment. Upon binding, DRP1 oligomerizes, constricting the mitochondria and ultimately leading to fragmentation (Cipolat et al. 2004).

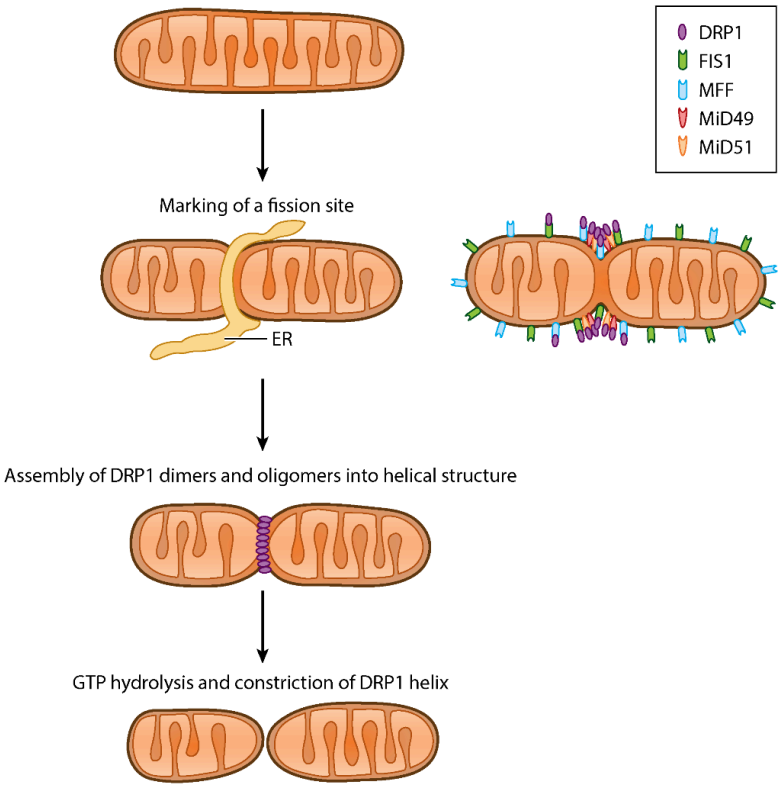


Figure 1.2: Schematic of mitochondrial fission. ER-mitochondria contact site triggers mitochondrial fission events by coordinated activities of various factors like DRP1, MFF, MEF, and Fis-1. MFF, MEF, and Fis-1 are recruited from the cytosol to the ER-mitochondria contact site, which in turn recruits DRP1 to OMM. At OMM, the multimerization of DRP1 occurs, which encircles the mitochondria that compress OMM and result in mitochondrial fragmentation.
Abbreviations: MFF, mitochondrial fission factor; MEF1, mitochondrial elongation factor 1; DRP1, dynamin-related protein 1; FIS1, fission 1; ER, endoplasmic reticulum; IMM, inner mitochondrial membrane; OMM, outer mitochondrial membrane. Figure adapted from (Pernas and Scorrano 2016).

Mitochondrial fusion is a sequential process involving fusion of OMM, followed by IMM fusion (Figure 1.3). Initially, OMM fusion is mediated by mitofusin 1 (Mfn1) and mitofusin 2 (Mfn2) isoforms; the *Drosophila* homologue of Mfn is Marf (Mitochondrial assembly regulatory factor).

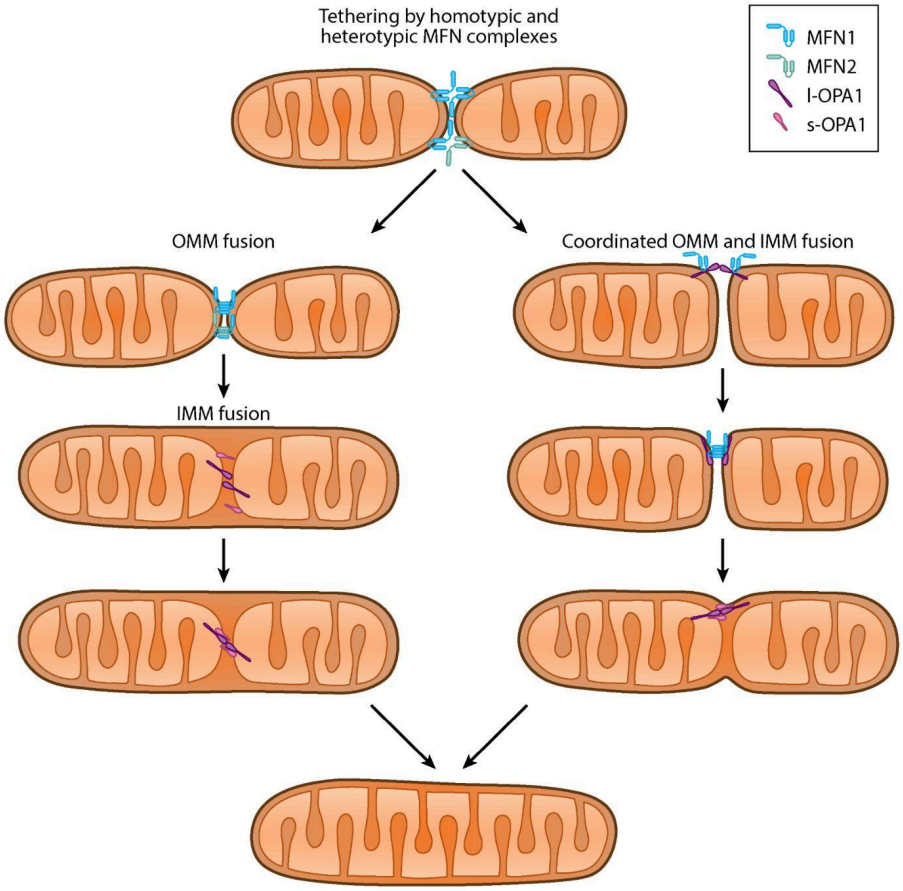


Figure 1.3: Schematic representation of the mitochondrial fusion. Fusion is executed by MFNs in OMM and OPA1 in IMM. MFN forms a heterodimer or homodimer, bringing two mitochondria together, followed by OMM fusion. Then, OPA1 leads to IMM fusion, resulting in the mixing of matrix content. Abbreviations: MFN (Mitofusin), OMM (Outer mitochondrial membrane), IMM (Inner mitochondrial membrane), Opa (Optic atrophy).
Figure adapted from (Pernas and Scorrano 2016).

The transmembrane and C-terminal domains of Mfns contain signal sequences that direct them to the OMM (Liesa et al. 2009), where they form homo- or heterodimers to initiate membrane fusion. Subsequently, optic atrophy 1 (Opa1) facilitates IMM fusion. In contrast to Mfn-mediated OMM fusion, Opa1-dependent IMM fusion requires an intact mitochondrial membrane potential. The presence of only Opa1 is sufficient to drive the fusion event (Malka et al. 2005; Song et al. 2009).

1.1.3 Regulation of mitochondrial dynamics during cell cycle progression

The precise equilibrium of mitochondrial fusion and fission events is critical for the physiological development of an organism. Mitochondrial dynamics play a crucial role during cell cycle progression (Kianian and Kianian 2014). During the G1-S phase, mitochondria typically present as an interconnected, fused network, whereas in M phase, they adopt a distinctively fragmented, punctate appearance (Figure 1.4). This cell cycle-dependent morphological shift is tightly controlled by key cell cycle regulatory proteins, cyclin-dependent kinases (CDKs) and their associated cyclins.

In the early G1 phase, mitogenic stimulation of Cyclin D–CDK4/6 complex leads to the phosphorylation, thereby inactivating the pocket proteins (pRB, p107, and p130). Consequently, this liberates E2F transcription factors, which facilitates cellular proliferation by regulating the expression of genes crucial for the synthesis of lipids, proteins, and nucleic acids (Lopez-Mejia and Fajas 2015). Before this inactivation,

non-phosphorylated pocket proteins, when bound to E2F proteins, actively repress genes vital for cellular proliferation, including Cyclin E. This suppressive effect is relieved only when the Cyclin D–CDK4/6 complex in the early G1 phase inactivates pocket proteins by phosphorylation (Lopez-Mejia and Fajas 2015).

G1-S phase transition is characterized by a state of hyperfused mitochondria, a morphology regulated by the CDK2/Cyclin E complex (Wang and Kalderon 2009; Lopez-Mejia and Fajas 2015). Intriguingly, this hyperfused mitochondria network is indispensable for the proper accumulation of Cyclin E, a critical regulator of the G1-S transition (Mitra et al. 2009). Consequently, any disruption to mitochondrial morphology, particularly through the genetic or pharmacological downregulation of fusion-promoting proteins, can precipitate a G1-S cell cycle arrest. In the S phase, CDK2 activates and forms a complex with Cyclin E. This association shifts during the G2 phase, where CDK2 instead complexes with Cyclin A. During G2-M transition, CDK1/Cyclin B1 complex activates electron transport chain complex I and phosphorylates Drp1 at serine 565, leading to its activation and the subsequent induction of mitochondrial fragmentation (Taguchi et al. 2007). The fragmentation of mitochondria during cell division ensures their equitable partitioning into daughter cells.

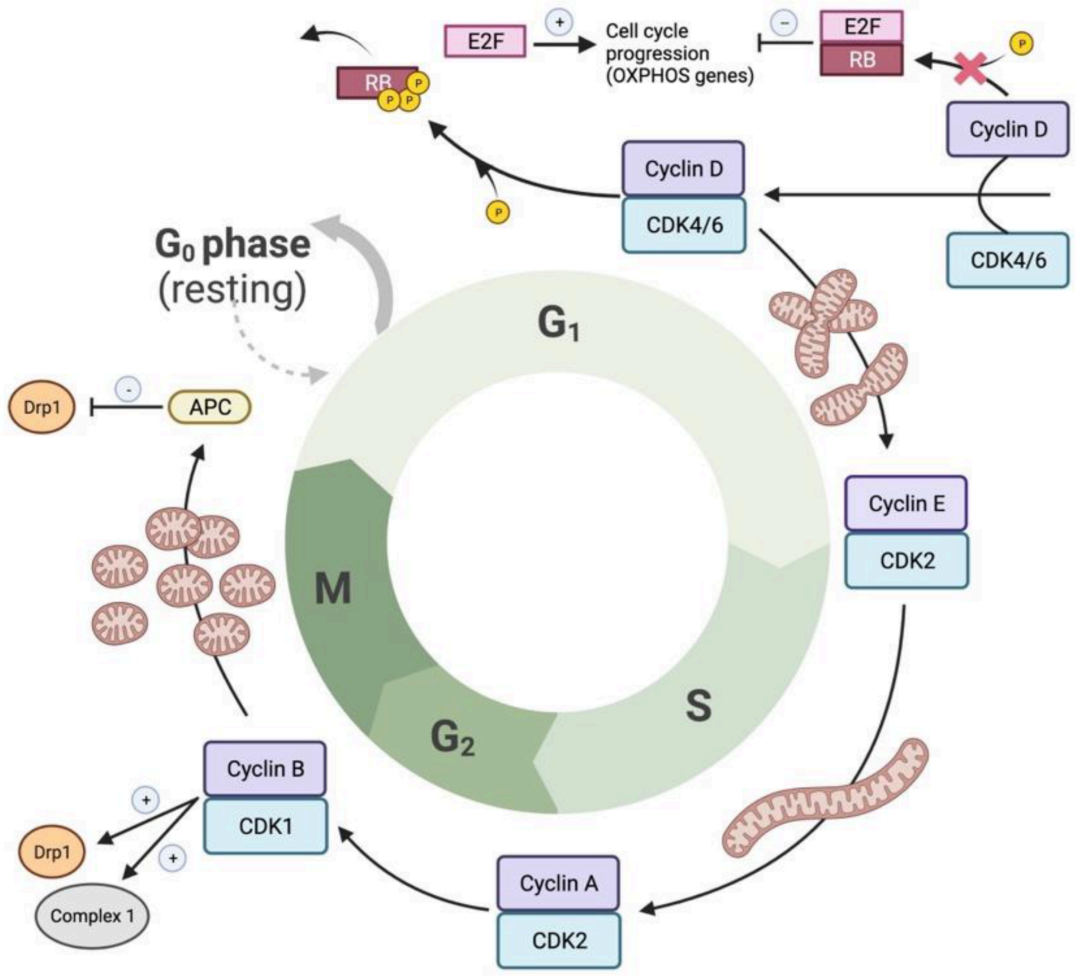


Figure 1.4: Schematic representation of cell cycle-dependent mitochondrial dynamics. This figure illustrates the dynamic changes in mitochondrial morphology throughout the cell cycle and their regulation by cyclin-dependent kinases (CDKs) and cyclins. Upon mitogenic stimulation, Cyclin D gets activated and forms a complex with CDK4/6, which leads to the retinoblastoma protein's partial phosphorylation and consequent inactivation (RB). This RB inactivation, in turn, liberates E2F transcription factors, which drive the expression of genes critical for oxidative phosphorylation (OXPHOS) and overall cell cycle progression. As cells advance from G1 into the S phase, mitochondria exhibit a characteristic hyperfused, giant morphology, a transition orchestrated by the Cyclin E/CDK2 complex. Subsequently, during the S phase itself, mitochondrial elongation is promoted through the continued activity of Cyclin

A/CDK2. Conversely, Cyclin B/CDK1 positively regulates the mitochondrial fission protein Drp1 during the M phase, inducing widespread mitochondrial fragmentation. This fragmentation, however, is transient; the Anaphase-Promoting Complex (APC) subsequently inhibits Drp1 activity during anaphase, thereby facilitating mitochondrial re-fusion as cells exit mitosis.
Furthermore, this CDK1/Cyclin B1-mediated Drp1 activation is subject to regulation by the anaphase-promoting complex (APC). APC gets activated during anaphase, leading to Cyclin B and Drp1 degradation and facilitating mitochondrial fusion and cell cycle exit. This intricate feedback loop underscores a crucial mechanism by which mitochondrial dynamics control cell cycle progression. Figure adapted from (Colpman et al. 2023).

1.1.4 Mitochondrial activity: Electron transport chain, mitochondrial membrane potential, ATP synthesis, and ROS generation

Mitochondria serve as the central regulator of cellular energy metabolism, primarily through ATP synthesis via OXPHOS (Nolfi-Donegan et al. 2020). Beyond energy production, they regulate redox homeostasis, apoptotic pathways, and intracellular signaling cascades (Shen et al. 2022). The functional efficacy of mitochondria is dependent on the coordinated activity of the electron transport chain, the establishment and maintenance of mitochondrial membrane potential (MMP), ATP synthesis, and the generation of reactive oxygen species (ROS).

The electron transport chain (ETC), localized within the inner mitochondrial membrane (Figure 1.5), is a series of protein complexes that mediate the sequential transfer of electrons derived from NADH (Nicotinamide adenine dinucleotide hydrogen) and FADH2 (Flavin adenine dinucleotide hydrogen). Electron flow terminates in the reduction of molecular oxygen to water. The ETC comprises four primary complexes (Complexes I-IV). Complex I (NADH: ubiquinone oxidoreductase) and Complex II (Succinate dehydrogenase) serve as entry points for electrons, which are subsequently transferred to ubiquinone (coenzyme Q) (Hirst 2009; Yankovskaya et al. 2003).

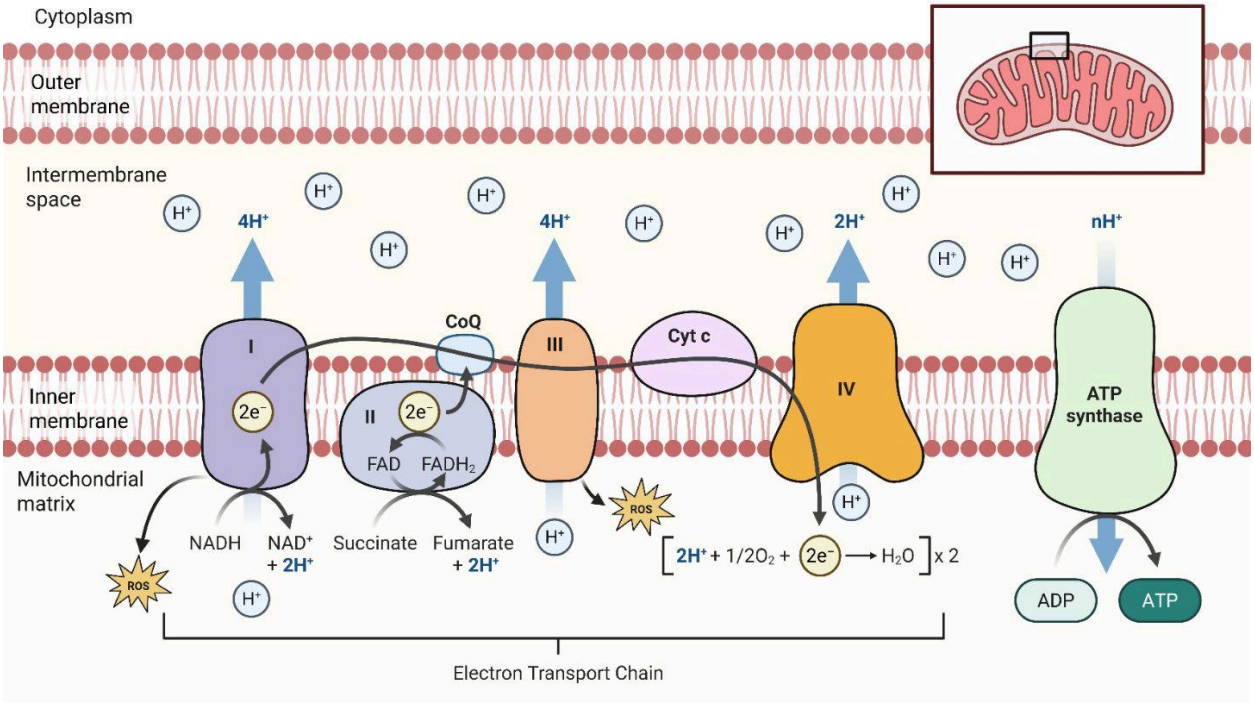


Figure 1.5: Schematic representation of electron flow through the ETC complexes, and generation of mitochondrial membrane potential, ROS and other metabolites. ETC is an assembly of protein complexes embedded in the inner mitochondrial membrane. The ETC mediates the sequential transfer of electrons from electron donors NADH and FADH2 through ETC complexes to the final electron acceptor, molecular oxygen (O_2). The chain comprises four principal complexes (Complexes I-IV). Electrons primarily enter the system via complex I (by NADH) and complex II (by FADH2), subsequently being delivered to ubiquinone (coenzyme Q). From ubiquinone, electrons are transferred to complex III, then to cytochrome c, and finally to Complex IV (cytochrome c oxidase), where molecular oxygen serves as the terminal electron acceptor and is reduced to water. The energetically favourable flow of electrons through complexes I, III, and IV are coupled to the active translocation of protons from the mitochondrial matrix into the intermembrane space. This proton pumping establishes an electrochemical gradient across the inner mitochondrial membrane, called mitochondrial membrane potential (MMP). ATP synthase (Complex V) utilises MMP to synthesise ATP. ATP synthase pumps the protons back down their concentration gradient from the intermembrane space to the matrix, and energy released by this process is utilised to convert ADP into ATP.
Image created on BioRender. (Sapkota 2024)

Electrons are then passed to Complex III (Cytochrome c reductase), followed by cytochrome c. Cytochrome c finally donates electrons one at a time to Complex IV (cytochrome c oxidase), where molecular oxygen is reduced to water (Sun et al. 2018). The energetically favourable flow of electrons through these complexes is coupled to the pumping of protons against the concentration gradient, i.e., from the mitochondrial matrix to the intermembrane space by complex I, II, and IV, establishing an electrochemical gradient across the inner mitochondrial membrane, called mitochondrial membrane potential **(MMP)** (Figure 1.5). MMP is a pivotal parameter governing mitochondrial function and bioenergetics. The impermeability of the inner mitochondrial membrane to protons maintains this gradient, which is essential for driving ATP synthesis, regulating calcium homeostasis, and facilitating the import of nuclear-encoded mitochondrial proteins. Perturbations in MMP are indicative of mitochondrial dysfunction and are implicated in the pathogenesis of diverse diseases, including neurodegenerative disorders and malignancies.

Mitochondrial ATP synthesis is mediated by ATP synthase (Complex V), a molecular rotary motor that couples the energy stored within the proton electrochemical gradient to ATP production (Figure 1.5). As protons translocate from the intermembrane space to the mitochondrial matrix through ATP synthase, conformational transitions within the enzyme catalyse the phosphorylation of ADP to ATP, called OXPHOS (Okuno et al. 2011; Junge and Nelson 2015). It constitutes the major mechanism of cellular ATP generation under aerobic conditions.

Mitochondria also represent a prominent source of **reactive oxygen species (ROS)**, which arise as byproducts of electron leakage from the electron transport chain (ETC). Complex I and III are major producers of ROS (Figure 1.5). ROS, including superoxide anions and hydrogen peroxide, exhibit a dualistic role in cellular physiology. ROS at physiological concentrations function as signaling molecules, regulating processes like

cell proliferation and differentiation. However, excessive ROS generation can induce oxidative stress, leading to damage of lipids, proteins, and DNA. To mitigate ROS-induced damage, mitochondria possess antioxidant enzymes, including superoxide dismutase 1 (SOD1), SOD2, and Catalase. SOD1 is primarily found in the cytoplasm and mitochondrial intermembrane space, but SOD2 mainly localises in the mitochondrial matrix. SOD1 and SOD2 neutralise superoxide radicals (O^{2-}) into hydrogen peroxide (H_2O_2) and oxygen. Catalase converts H_2O_2 into water and oxygen (Koju et al. 2019).

1.1.5 Mitochondrial morphology and activity in stem cells and differentiated cells

During the differentiation of stem cells, mitochondria adapt their morphology and function to meet the cell's energy needs. This dynamic mitochondrial remodelling is crucial during differentiation. As a stem cell transforms into a specialised cell type, its mitochondria undergo complex changes involving fusion, fission, and the development of cristae, all to match the cell's evolving metabolic demands.

Pluripotent stem cells (PSCs) exhibit more spherical mitochondria with less developed cristae, reflecting their primary reliance on glycolysis for their energy production. But as these cells commit to a specific fate and differentiate, their mitochondria transform. They become elongated, packed with organised and abundant cristae, allowing the mitochondria to house more components of the ETC, which are essential for efficient energy generation through OXPHOS (Chung et al. 2007; Seo et al. 2018). Inhibition of OXPHOS by knocking down complex I or complex V in *Drosophila* neural stem cells (NSCs) leads to their decreased proliferation and developmental patterning gets disrupted. Inhibition of glycolysis in NSCs by knockdown enzymes like phosphofructokinase (PFK) or aldolase typically doesn't have the same detrimental effects (van den Ameele and Brand 2019). Differentiated cells have other mitochondrial characteristics like an increased number of mitochondrial DNA (mtDNA) copies, a

denser internal matrix, a more spread-out distribution within the cell, and overall more complex and intricate mitochondrial structures (Facucho-Oliveira et al. 2007; Jasra et al. 2023). Parallel to these morphological changes, mitochondria also undergo functional shifts during PSCs differentiation like, increase in their overall function and mass. Enzymes involved in the TCA cycle and components of the ETC become more abundant. There's also a rise in ROS levels and oxygen consumption, due to a metabolic shift towards oxidative phosphorylation. The cell relies less on glycolysis by decreasing the expression of glycolytic enzymes (Chung et al. 2007).

1.1.6 Mitochondrial function in development

The core theme of developmental biology is how a single totipotent cell gives rise to many specialised cell types that develop into an organism. A specialised mitochondrial morphology—fission, fusion, and mitophagy—plays a key role in this transformation. During mouse embryonic development, cells comprising the inner cell mass exhibit fragmented and with less OXPHOS capacity. But as they commit to differentiation, their mitochondria transform into an elongated state, which is more metabolically active and supports high OXPHOS (Acton et al. 2004; Chung et al. 2007). Depletion of mitochondrial fusion proteins such as Opa1 and Mfn1/2 in embryonic stem cells halts their differentiation into cardiomyocytes, which results in defective heart development and causes developmental lethality, highlighting the necessity of mitochondrial architecture in organogenesis (Kasahara et al. 2013). During *Drosophila* central nervous system development, mitochondrial fusion promotes neural stem cell differentiation, and mitochondrial fusion facilitates the transition from a glycolytic to an oxidative metabolic state, essential for proper lineage specification. Disruption of fusion proteins such as Opa1 or Marf in *Drosophila* neuroblasts leads to differentiation defects and developmental arrest (Homem et al. 2014; Dubal et al. 2022; van den Ameele and Brand 2019; Bonnay et al. 2020).

During mouse embryogenesis, mitophagy, the selective removal of damaged mitochondria, is essential for maintaining mitochondrial quality during development. Mitophagy is upregulated in differentiating neurons to ensure that only healthy mitochondria are preserved during axonal outgrowth (Ashrafi et al. 2014).

1.2 *Drosophila* neuroblast development

1.2.1 Formation through delamination

In *Drosophila* embryogenesis, neural precursor cells or neuroblasts delaminate from the ventral neuroepithelial layer. The precise allocation and specification of these neuroblasts are governed by lateral inhibition, a cell-cell communication mechanism in which the Notch-Delta signalling pathway plays a vital role (Figure 1.6). This mechanism initiates within a proneural cluster, a group of cells characterised by the expression of proneural genes, including *achaete-scute* (Cabrera 1990).

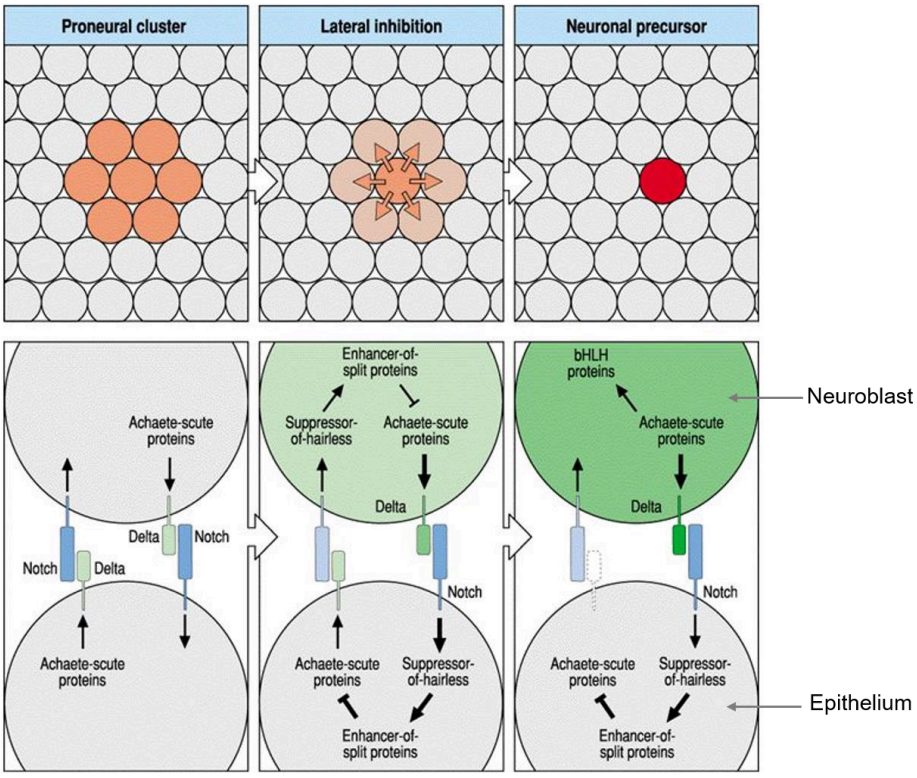


Figure 1.6: Schematic representation of *Drosophila* neuroblast specification via lateral inhibition. *Drosophila* neuroblasts are specified from the neuroepithelium layer during embryonic development. Initially, cells within a proneural cluster (depicted in orange) express proneural transcription factors, such as Achaete-scute proteins. Proneural factors are expressed by the orange cells in the proneural cluster. Delta, a ligand for Notch receptors, is activated by achaete-scute proteins. High Delta expression in the centre cell of the proneural cluster triggers Notch signalling in neighbouring cells. Enhancer of Split (Espl) is expressed in surrounding cells when Notch is activated via Suppressor of Hairless (SuH). Delta downregulation and neural fate suppression occur in surrounding cells when Espl inhibits the production of Achaete scute proteins. Achaete scute activates bHLH proteins in the central cell, triggering the gene expression pathway necessary for neural fate. Image adapted from Chapter 11: Development of Nervous System, Principles of Developmental Biology, Lewis Wolpert.

During lateral inhibition, the neuroblast within a proneural cluster upregulates its expression of the transmembrane ligand Delta. This Delta ligand interacts with the Notch receptor on adjacent cells. Serrate, another transmembrane protein, also functions as a ligand for Notch. Interaction of Notch by either Delta or Serrate induces conformational alterations in the receptor, leading to its subsequent processing via regulated intramembrane proteolysis (RIP). RIP proceeds through a two-step proteolytic cascade: an initial ectodomain cleavage followed by an intramembranous cleavage. This event releases the Notch Intracellular Domain (NICD). Following translocation to the nucleus, it forms a complex with the transcription factor Suppressor of Hairless [Su(H)]. This NICD-Su(H) complex drives the transcriptional activation of the Enhancer of split (E(spl)) genes. The resulting E(spl) gene products function as transcriptional repressors, effectively downregulating proneural gene expression in Notch-activated cells, which leads to delta downregulation in these cells and inhibition of neural fate. In the central cell, Achaete scute switches on bHLH (basic Helix-Loop-Helix) transcription factor, activating the genes necessary for the cell to acquire neuronal fate. Consequently, this inhibitory feedback ensures that the central cell adopts the neural

precursor fate, while its surrounding cells maintain their epithelial identity (Cabrera 1990).

Following their specification, neuroblasts delaminate from the neuroepithelium (Yu et al. 2006). Ventral neuroepithelial cells are typically interconnected through zonula adherens (ZA) junctions, circumferential adhesive complexes positioned at the apico-lateral aspect of each cell. These junctions are predominantly composed of DE-cadherin and catenin proteins. The integrity of these adherens junctions typically constrains the inherent capacity of neuroepithelial cells to undergo asymmetric cell division (Lu et al. 2001).

During the epithelial-to-neuroblast transition, ZA junctions are actively disassembled, enabling the cells to adopt a rounded morphology and subsequently ingress from the epithelial layer. The dissolution of these intercellular adhesions and the acquisition of a spherical cellular shape represent a hallmark of the delamination process. This morphological shift from a columnar to a spherical shape is considered a pivotal event in neuroblast formation. These newly delaminated, spherical neuroblasts possess apicobasal polarity (Lu et al. 2001).

1.2.2 Polarity formation and asymmetric division

Investigation on *Drosophila* neuroblasts has advanced our understanding of how distinct protein complexes localize and influence cell fate determination. Neuroblast polarity is established independently of the polarity mechanisms governing the surrounding neuroepithelium. Proteins like Stardust (Std) and Crumbs (Crb) are indispensable for neuroblast polarity but are required for neuroepithelial polarity (A. Wodarz & Huttner, 2003). Crb is a transmembrane protein crucial for establishing epithelial cell polarity, and Sdt is a cytoplasmic scaffold that interacts with Crumbs (Hong et al. 2001). This intrinsic cellular polarity is crucial for accurate spindle orientation during proper asymmetric division (Wodarz and Huttner 2003).

The precise localization of specific protein complexes characterizes the apical domain of the neuroblast (Figure 1.7). One such key entity is the *Drosophila* atypical protein kinase C (DaPKC)/PAR6 complex (Wodarz and Huttner 2003). This complex itself comprises various PAR family members, including PDZ domain-containing protein Bazooka (Baz) (vertebrate PAR3 homolog), PAR6 , and aPKC (Doerflinger et al. 2010). Disruptions of components of this aPKC/PAR6 complex lead to the aberrant localization of Miranda (Mira). Mira, an adaptor protein (Atwood and Prehoda 2009; Hannaford et al. 2018), exhibits a membrane-binding domain and distinct docking sites for segregating determinants such as Staufen (Stau), Prospero (Pros), a vertebrate ortholog of Prox1, and brain tumor (Brat), a mammalian ortholog of Trim2, Trim3, Trim32 (Shen et al., 1998).

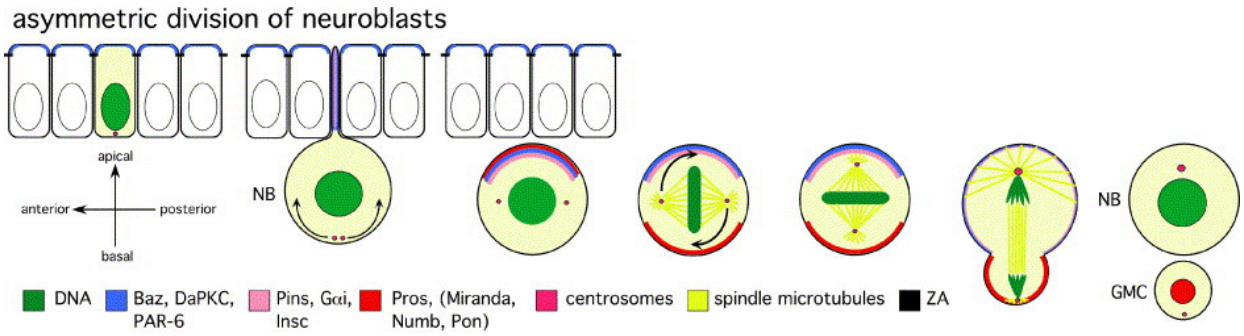


Figure 1.7: Schematic representation of polarity formation and asymmetric division of *Drosophila* NBs. After neuroblast delamination from neuroepithelia recruits an apical complex, including the Baz-DaPKC-PAR6(blue) and centrioles at the base move to the AP pole. With the aid of the Insc-Pins complex (pink), spindle fibres originating from these centrioles rotate the division plane by 90^{c} angle. The apically situated Pros-Mira-Numb-Pon (red) complex moves to the basal pole during spindle rotation, giving the neuroblast apicobasal polarity. The neuroblast then divides asymmetrically, forming one distinct GMC while maintaining its identity by self-renewal. Pros (red) are released into the nucleus when the basal complex enters the newly formed GMC, and Miranda is destroyed. In GMC, pros turn on the differentiated program, which

leads to the development of two differentiated neurons or glia. Image adapted from (Wodarz and Huttner 2003).

Another critical apical complex is Inscuteable (Insc), which consists of Insc itself, Partner of Insc (Pins, the mammalian orthologs of Ags3 and Lgn), and the G protein family member Gαi (Wodarz and Huttner 2003). The Insc complex physically associates with Baz via the Insc protein, thereby securing its apical confinement.
Research reveals a remarkable conservation of apicobasal polarity mechanisms across evolution. Proteins found at the apical region of *Drosophila* neuroblasts exhibit homologous localization in the neural progenitors of vertebrates. The observation further highlights this functional conservation that genetic impairment of these conserved proteins often manifests in analogous developmental phenotypes in both flies and vertebrates.

Drosophila neuroblasts divide asymmetrically for their own self-renewal and the precise segregation of fate determinants. In early anaphase, the cleavage plane migrates toward the basal cortex, from which a smaller basal cell, ganglion mother cell (GMC), eventually buds off. The mitotic spindle exhibits an asymmetric arrangement during anaphase, resulting in apical and basal poles of unequal dimensions; the apical pole consistently remains larger than the basal pole (Wodarz and Huttner 2003). Upon completion of telophase, a single neuroblast yields two morphologically distinct daughter cells: a larger neuroblast, which represents the self-renewed lineage, and a smaller GMC, committed to differentiation. Basally localized protein complexes are partitioned throughout this division into the nascent GMC. Within the GMC, Miranda undergoes degradation (Doerflinger et al. 2010), consequently liberating Prospero to translocate into the nucleus. Nuclear Prospero then activates a transcriptional program essential for differentiation. Subsequently, the GMC undergoes a terminal division to generate neurons or glial cells (Urbach et al. 2003).

1.2.3 Central nervous system of third instar larvae

The *Drosophila* nervous system development initiates from the embryonic stage, which undergoes two distinct phases of neurogenesis. The initial wave arises during embryonic stages 8 to 11. As previously discussed, embryonic neuroblasts are specified within the ventral neuroepithelium via lateral inhibition. Following stage 11, most of these NBs undergo apoptosis, while a subset enters a quiescent G_0 phase, halting their cell cycle (Homem and Knoblich 2012).

Larval neurogenesis and neuroblast types

Upon larval hatching and initiation of feeding on a nutrient-rich medium, the fat body, a key nutrient-sensing organ, detects amino acid signals. This triggers the activation of the mTOR pathway, which subsequently relays signals to the glial cells surrounding the brain. In response, these glial cells stimulate the quiescent neuroblasts to re-enter the cell cycle and divide extensively, generating a vast array of new neurons and glia. This second wave of neurogenesis is remarkably productive, yielding approximately 90% of the entire *Drosophila* nervous system's neuronal population (Homem and Knoblich 2012). The bilobed *Drosophila* larval brain, connected to a single ventral nerve cord (VNC), hosts four primary categories of neuroblasts.

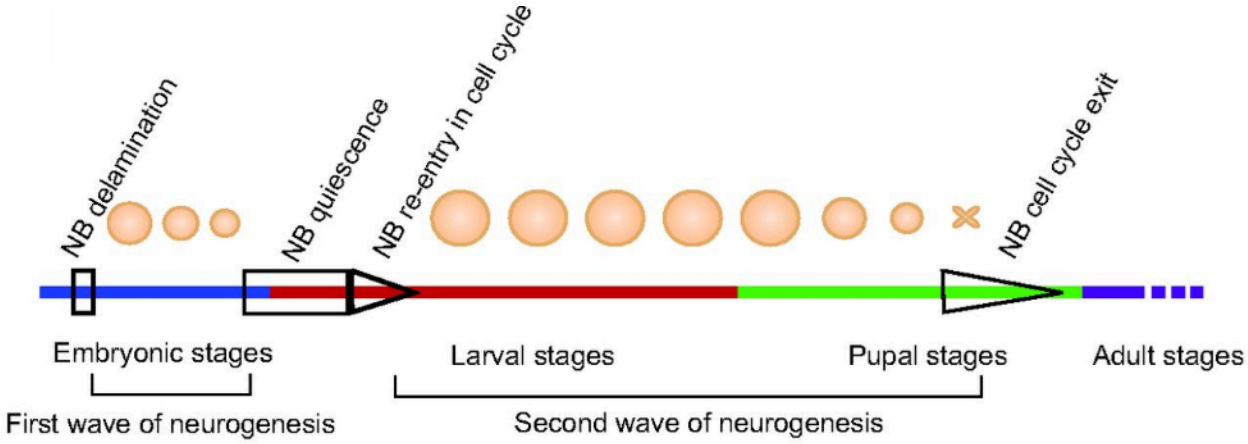


Figure 1.8: Developmental timeline of *Drosophila* neurogenesis waves. The two waves of neurogenesis throughout *Drosophila* development are shown chronologically. Embryonic

neuroblasts (beige) enter a quiescent G_0 state during late embryogenesis. However, larval neuroblasts reenter the cell cycle to initiate a second wave of neurogenesis. They undergo substantial growth after each cell division, enabling them to execute more proliferative cycles. The second wave of neurogenesis terminates when neuroblasts vanish during the pupal stages. Different neuroblasts exit the cell cycle at different time points, but the cartoon illustrates the cell-cycle exit mechanism for thoracic neuroblasts, which shrink in size until they divide and differentiate in a size-wise symmetric manner, followed by terminal differentiation. Image adapted from (Homem and Knoblich 2012).

Central Brain (CB) neuroblasts originate from embryonic lineages and are situated in the central brain region. This group encompasses both type I and type II neuroblasts. Each lobe of the *Drosophila* larval brain typically contains around 90 type I and 8 type II neuroblasts (Bayraktar et al. 2010) (Figure 1.9).

Type I neuroblasts are found in both anterior and posterior sides of the brain and constitute the majority of NBs in the central brain region. They express transcription factors Asense and Deadpan. They undergo an asymmetric division to self-renew and generate a GMC (ganglion mother cell) that further divides symmetrically to form two neurons or glial cells (Buescher et al. 1998). **Type II neuroblasts** present at posterior side of brain and are distinguished by their absence of a transcription factor, Asense, hence they are called Posterior Asense Negative (PAN) neuroblasts. They express a key transcription factors, Deadpan (Dpn) and asymmetrically localized cell fate determinant proteins Brat, and Numb. Notably, the differentiation factor Pros, which acts as a tumour suppressor, is absent in these cells, rendering these lineages more susceptible to tumour formation.

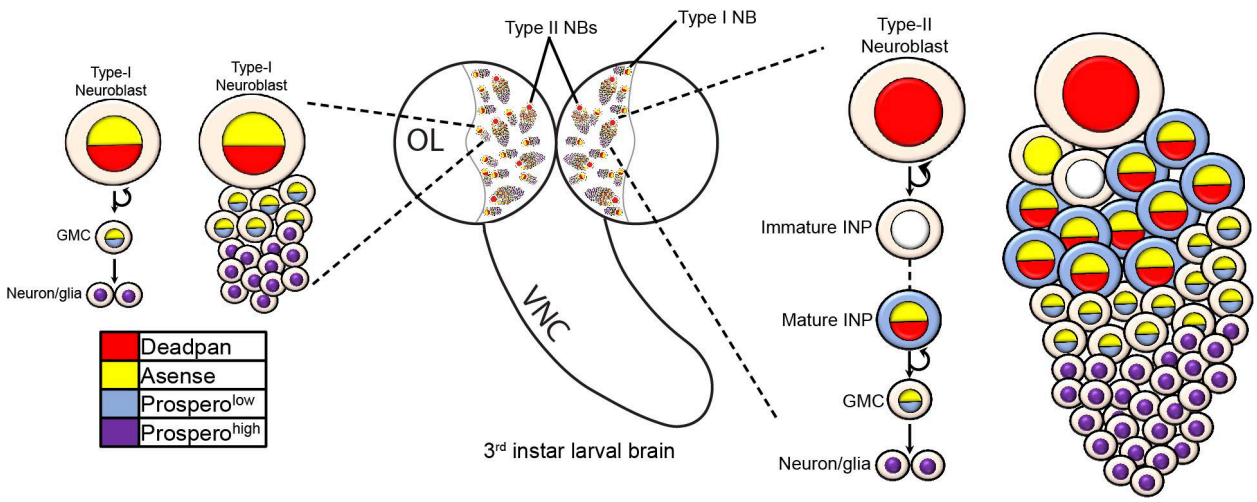


Figure 1.9. Schematic representation of the *Drosophila* 3rd instar larval nervous system and type I and type II neuroblasts development. The *Drosophila* third instar larval central nervous system consists of two distinct cerebral lobes and a single ventral nerve cord (VNC). Each cerebral lobe is further delineated into an optic lobe and a central brain (CB) region. The CB specifically harbours two neuroblasts, type I neuroblasts (have Asense/yellow, Deadpan/red) and type II neuroblasts (have Deadpan/red), both of which undergo asymmetric cell divisions. type I neuroblasts divide asymmetrically to self-renew and generate a single ganglion mother cell (GMC). This GMC then undergoes one terminal symmetric division, giving rise to two differentiated neurons or glial cells. In contrast, type II neuroblasts employ a more complex lineage strategy. They self-renew while producing an immature intermediate neural precursor (INP). Following a maturation phase, these INPs function as transit-amplifying cells, undergoing 4-5 rounds of asymmetric division. Each INP division yields a self-renewed INP and a GMC. These GMCs subsequently divide symmetrically to generate differentiated neurons or glial cells. Each specific progenitor population within these neuroblast lineages is characterised by distinct cellular markers: Deadpan (red), Asense (yellow), low cytoplasmic Prospero (blue), and high nuclear Prospero (purple). Image created on PowerPoint.

Type II neuroblast division applies to the production of intermediate neural progenitor cells (INPs) (Bello et al. 2008). These INPs serve as transit-amplifying cells, undergoing 4-5 rounds of division to expand the pool of differentiated neurons. INP-mediated

amplification allows a single type II neuroblast lineage to produce a considerably larger number of differentiated neurons than a type I neuroblast lineage (Boone and Doe 2008; Bayraktar et al. 2010). Instead of division, newly generated, immature INPs undergo a maturation phase lasting approximately 5-6 hours. This maturation is marked by a sequential expression of transcription factors, beginning with Ase, followed by Dpn and Pros. Once mature, INPs resemble type I neuroblasts in their behaviour: they divide asymmetrically to generate GMCs, which then give rise to a pool of differentiated neurons or glia (Boone and Doe 2008). type II neuroblasts collectively contribute roughly 5000 neurons, which are instrumental in forming the adult brain's central complex (Bayraktar et al. 2010). This central complex is vital for various adult fly behaviours, including orientation, navigation, and courtship, and also plays a significant role in forming and recalling short- and long-term memories.

Other neuroblast population

Beyond the Central Brain neuroblasts, other distinct populations include VNC neuroblasts, Mushroom Body (MB) neuroblasts, and Optic Lobe (OL) neuroblasts. VNC neuroblasts, encompassing both abdominal and thoracic subtypes, also derive from embryonic neuroblast lineages. MB neuroblasts, numbering four per brain lobe, are responsible for forming the brain's olfactory learning and memory centres (Lee et al. 1999; Kunz et al. 2012). In contrast to other neuroblast types, OL neuroblasts uniquely emerge solely during larval growth, originating from the optic lobe neuroepithelium (Apitz and Salecker 2016; Egger et al. 2008).

1.2.4 Neuroblast as a model system to study stem cell biology

Drosophila neuroblasts represent an excellent model for investigating fundamental principles of stem cell biology, including lineage formation and differentiation. These neural stem cells recapitulate key stem cell properties, such as asymmetric cell division, the uneven distribution of polarity markers, self-renewal, and the capacity for differentiation (Homem and Knoblich 2012).

Neuroblasts have been instrumental in elucidating various molecular signalling pathways, including Notch, JNK, ROS, EGFR, and Fat-Hippo. The developmental patterns and neuronal progeny of specific neuroblast lineages are also thoroughly documented in the literature (Egger et al. 2008; Isshiki et al. 2001; Spana et al. 1995; Lai et al. 2008; Kunz et al. 2012).

Furthermore, *Drosophila* neuroblasts are highly amenable to genetic manipulation. The availability of powerful tools like the Gal4-UAS binary system, Mosaic Analysis with a Repressible Cell Marker (MARCM), and advanced gene editing techniques such as CRISPR-Cas facilitates detailed functional analyses. The existence of lineage-specific Gal4 drivers, such as *pointed (Pnt)-Gal4,* which targets type II neuroblast lineages, enables precise, lineage-restricted investigations into protein function. Due to the presence of various differentiation markers at different stages of type II neuroblast development (Figure 1.9), we can track differentiation. Also, they are not required for the survival of animals, making it a sound model system for the study of stem cell biology. Recent advancements also permit the *in vitro* culture of neuroblasts without compromising their stemness, opening avenues for high-throughput analyses such as RNA sequencing and metabolic assays.

1.3 Aims and objectives of the thesis

As previously elaborated, the significance of mitochondrial dynamics and metabolism in stem cell proliferation and differentiation is well-established. However, a gap persists in our understanding of the mechanism by which mitochondrial morphology and activity together regulate the process of stem cell differentiation.

Drosophila neuroblasts offer an experimental system to address these lacunae systematically. This model allows for investigations such as: How do mitochondrial morphology and functional states regulate neural stem cell proliferation and differentiation? Furthermore, what are the quantitative and lineage-specific

consequences of perturbing mitochondrial dynamics, metabolism, or both on neuroblast populations? A pivotal question also concerns how neuroblasts respond and adapt to shifts in their cellular metabolic environment in response to their development.

Collectively, these unresolved questions underpin the central hypothesis of this thesis: that mitochondrial morphology and metabolic state are fundamentally crucial for the proper formation and subsequent differentiation of *Drosophila* neural stem cells.

To investigate this hypothesis, I have designed the following objectives:

1. *Analysing the effect of downregulating electron transport chain components on animal survival, mitochondrial morphology and differentiation of type II neuroblasts.*

2. *To examine the rescue of differentiation defects caused by disrupting electron transport chain components by mitochondrial hyperfusion on additional depletion of mitochondrial fission protein, Drp1.*

3. *Analysis of mitochondrial activity, ROS generation and mitochondrial membrane potential in electron transport chain-depleted type II neuroblast.*

4. *To analyse the mechanism of mitochondrial fusion-mediated regulation of type II neuroblast differentiation.*

Chapter 2

Materials and Methods

2.1 Materials

2.1.1 Fly stocks

Gal4 Lines			
S.No.	**Flies**	**Target**	**Fly line information**
1	*pnt*-Gal4,UAS-mCD8-GFP	Expressed only in type II neuroblasts in the central brain region from embryonic stages	Gift from Juergen Knoblich, Vienna, Austria
2	*wor*-Gal4,UAS-mCD8-GFP	Expressed in all types of NBs in the whole larval brain from embryonic stages	Gift from Juergen Knoblich, Vienna, Austria
3	*mhc*-Gal4	Expressed in all muscle types	-
RNAi lines			
4	$Drp1^{SD}$ ($Drp1^{S193D}$)	Downregulate expression of Dynamin-related protein (Drp1)	Generated by Darshika Tomer in

			the Richa Rikhy lab
5	mCherry^{i} (Control)	Expresses dsRNA for RNAi of mCherry	Bloomington number, BL35785
6	ND-PDSW RNAi (^{i})	Downregulate expression of NADH dehydrogenase (ubiquinone) PDSW subunit, complex I	BL 29592 (Perkins et al. 2015)
7	ND-39^{i}	Downregulate expression of NADH dehydrogenase (ubiquinone) 39 kDa subunit, complex I	BL 52922 (Perkins et al. 2015)
8	ND-19^{i}	Downregulate expression of NADH dehydrogenase (ubiquinone) 19 kDa subunit, complex I	BL 50577 (Perkins et al. 2015)
9	ND-49^{i}	Downregulate expression of NADH dehydrogenase (ubiquinone) 49 kDa subunit, complex I	BL 57499 (Perkins et al. 2015)
10	ND-42^{i}	Downregulate expression of NADH dehydrogenase (ubiquinone) 42 kDa subunit, complex I	BL 34526 (Perkins et al. 2015)

11	ND-51^{i}	Downregulate expression of NADH dehydrogenase (ubiquinone) 51 kDa subunit, complex I	BL 36701 (Perkins et al. 2015)
12	ND-51^{i}	Downregulate expression of NADH dehydrogenase (ubiquinone) 51 kDa subunit, complex I	BL 29534 (Perkins et al. 2015)
13	SdhC^{i}	Downregulate expression of Succinate dehydrogenase, subunit C, complex II	BL 53281 (Perkins et al. 2015)
14	SdhD^{i}	Downregulate expression of Succinate dehydrogenase, subunit D, complex II	BL 65040 (Perkins et al. 2015)
15	SdhBL^{i}	Downregulate expression of Succinate dehydrogenase, subunit B, complex II	BL 58100 (Perkins et al. 2015)
16	UQCR 11^{i}	Downregulate expression of Ubiquinol-cytochrome c reductase 11 kDa subunit, complex III	BL 64896 (Perkins et al. 2015)

17	cyt-c1L^{i}	Downregulate expression of Cytochrome c1-like, complex III	BL 34916 (Perkins et al. 2015)
18	Cox6C^{i}	Downregulate expression of Cytochrome c oxidase subunit 6C, complex IV	BL 33878 (Perkins et al. 2015)
19	Cox5A^{i}	Downregulate expression of Cytochrome c oxidase subunit 5A, complex IV	BL 27548 (Perkins et al. 2015)
20	Cox8^{i}	Downregulate expression of Cytochrome c oxidase subunit 8, complex IV	BL65223 (Perkins et al. 2015)
21	Cox 7C^{i}	Downregulate expression of Cytochrome c oxidase subunit 7C, complex IV	BL62877 (Perkins et al. 2015)
22	ATP Syn E^{i}	Downregulate expression of ATP Synthase, subunit E, complex V	BL67826 (Perkins et al. 2015)
23	ATP Syn G^{i}	Downregulate expression of ATP Synthase, subunit G, complex V	BL67347

			(Perkins et al. 2015)
24	ATP Syn D^i	Downregulate expression of ATP Synthase, subunit D, complex V	BL 33740 (Perkins et al. 2015)
25	ATP Syn B^i	Downregulate expression of ATP Synthase, subunit B, complex V	BL28062 (Perkins et al. 2015)
26	ATP Syn O^i	Downregulate expression of ATP Synthase, subunit O, complex V	BL65180 (Perkins et al. 2015)
27	ATP Syn C^i	Downregulate expression of ATP Synthase, subunit C, complex V	BL35464 (Perkins et al. 2015)
28	ATP Syn α^i	Downregulate expression of ATP Synthase, subunit α, complex V	BL28059 (Perkins et al. 2015)
29	ATP Syn β^i	Downregulate expression of ATP Synthase, subunit β , complex V	BL 27712 (Perkins et al. 2015)

30	ATP Syn γ^{i}	Downregulate expression of ATP Synthase, subunit γ , complex V	BL28723 (Perkins et al. 2015)
31	ATP Syn γ^{i}	Downregulate expression of ATP Synthase, subunit γ , complex V	BL15641 (Perkins et al. 2015)
32	SOD1^{i}	Downregulate expression of SOD1	BL34616 (Perkins et al. 2015)
33	SOD2^{i}	Downregulate expression of SOD2	BL25969 (Perkins et al. 2015)
34	hSOD1A4V, dominant negative mutant of hSOD1	Downregulate expression of SOD1	(Chowdhary et al. 2020)
35	Catalase^{i}	Downregulate expression of Catalase	BL34020 (Perkins et al. 2015)
36	Sod1^{OE} (Overexpression)	Overexpress SOD1	BL24750 (Shaka et al. 2022)

37	Sod2^{OE}	Overexpress SOD2	BL24494 (Sorianello et al. 2025)
38	Catalase^{OE}	Overexpress Catalase	-
39	Drp1^{SD};*pnt*-Gal4, UAS-CD8-GFP	*pnt*-Gal4 overexpression of Drp1^{SD}	Generated by genetic crosses
40	Drp1^{SD};mCherry^{i}	Downregulate expression of Drp1 and expresses dsRNA for RNAi of mCherry	Generated by genetic crosses
41	Drp1^{SD} ;ND-51^{i}	Downregulate expression of ND-51 and Drp1	Generated by genetic crosses
42	Drp1^{SD} ;ND-19^{i}	Downregulate expression of ND-19 and Drp1	Generated by genetic crosses
43	Drp1^{SD} ;Cox 6C^{i}	Downregulate expression of Drp1 and Cox6C	Generated by genetic crosses
44	Drp1^{SD};ATP syn E^{i}	Downregulate expression of Drp1 and ATP syn E	Generated by genetic crosses
45	Drp1^{SD};ATP syn G^{i}	Downregulate expression of Drp1 and ATP syn G	Generated by genetic crosses
46	Drp1^{SD};ATP syn B^{i}	Downregulate expression of Drp1 and ATP syn B	Generated by genetic crosses

47	Drp1^{SD};ATP syn α^{i}	Downregulate expression of Drp1 and ATP syn α	Generated by genetic crosses
48	Drp1^{SD};ATP syn β^{i}	Downregulate expression of Drp1 and ATP syn β	Generated by genetic crosses
49	SOD2^{OE};ND-51^{i}	Overexpress Sod2 and downregulate expression of ND-51	Generated by genetic crosses
50	Catalase^{OE};ND-51^{i}	Overexpress Catalase and downregulate expression of ND-51	Generated by genetic crosses
51	mitoGFP;*pnt*-Gal4	Express mitochondrial localised GFP driven by *pnt*-Gal4	Generated by genetic crosses
52	mitoGFP;ND-51^{i}	Express mitochondrial localised GFP and downregulate expression of ND-51	Generated by genetic crosses

2.1.2 Antibodies

Type	Name	Dilution used	Source
Primary Antibodies	Chicken anti-GFP	1:1000	Invitrogen, A10262
	Rat anti-Deadpan	1:130	Abcam, ab195173

	Rabbit anti-Deadpan	1:500	Yuh-Nung Jan, UCSF, USA
	Rabbit anti-Asense	1:10,000	Yuh-Nung Jan, UCSF, USA
	Mouse anti-Prospero	1:20	DSHB, MR1A
	Rabbit anti-Cytochrome c	1:200	Cell Signaling, 4272S
	Rabbit anti-phospho-Histone 3	1:500	Invitrogen, PA5-17869
	Rat anti-Elav	1:200	9F8A9
	Rab anti-Cyclin E	1:200	Santacruz, sc-33748
	Mouse anti-ATP B	1:200	Abcam, ab14730
	Rabbit-anti-phosphoAMPK	1:200	Cell Signaling, 2535L
	Rat-anti-Miranda	1:600	Abcam, 197788
	Rabbit-anti-cleaved Caspase 3	1:100	Cell Signaling, D175
Secondary Antibodies	Anti-Chicken Alexa Fluor 488	1:1,000	Molecular probes
	Anti-Mouse Alexa Fluor 488, 568, 647	1:1,000	Molecular probes

	Anti-Rat Alexa Fluor 488, 568, 647	1:1,000	Molecular probes
	Anti-Rabbit Alexa Fluor 488, 568, 647	1:1,000	Molecular probes

2.1.3 Dyes and drugs

Type	Name	Dilution used	Source
Dyes and drugs	Hoechst (label DNA)	1:1,000	Molecular Probes
	TMRE (mitochondrial membrane potential indicator) (100μM)	1:1,000	Thermo Fisher Scientific, T668
	DHE (detect ROS) (30mM)	1:1,000	Invitrogen, D1168
	ATP-Red (detect ATP) (30μM)	1:1,000	Merck Millipore, SCT045
	SlowFade Gold (Anti-fading agent)	-	Invitrogen, S36937

2.1.4 In vitro assay kits

Kit name	Used for	Source
Click-iT EdU Assay Kit	Mark cells in S-phase	Invitrogen C10340

2.2 Methods

2.2.1 Fly crosses and genetics

Fly crosses were conducted as follows: 10 female flies were placed along with 5-6 male flies in polystyrene vials containing cornmeal agar media at 29°C. After 48 hours, the flies were transferred to fresh vials. 5-6 days after, third instar larvae emerged, and subsequent analysis was performed.

2.2.2 UAS-Gal4 binary system

For tissue-specific perturbation of target genes in neuroblasts, we used the yeast-derived UAS-Gal4 binary expression system. Gal4 is a yeast transcription factor that binds to the upstream activator sequence (UAS) (Duffy, 2002). In this system, flies expressing Gal4 under tissue-specific promoters are crossed with flies carrying UAS-driven RNAi or overexpression constructs. When Gal4 binds to the UAS, it activates transcription of the downstream gene or RNAi. In our experiments, we used Gal4 lines driven by neuroblast-specific promoters such as *worniu* and *pointed*, and *inscuteable*, in combination with UAS-linked target genes.

2.2.3 Larval brain Immunostaining

After 5-6 days of cross, wandering third instar larvae were collected and dissected in Schneider's media, followed by 4% paraformaldehyde (PFA) fixation for 25 minutes. The brains were then washed in 0.1% PBST (1X PBS, O.1% Triton X-100) for 30 minutes at room temperature (RT) and blocked with 1% BSA in 0.1% PBST for 1 hour at RT. Following this, the brains were incubated with the required primary antibodies (diluted in 1% BSA) overnight (~14 hours) at 4℃ on a shaker. The next day, brains were washed thrice (20min, 10min, 10min) with 0.1% PBST. Subsequently, the brains were incubated with secondary antibodies (diluted in 0.1% PBST) for 1 hour at RT, followed by 20 minutes of washing with 0.1% PBST. The brains were stained with DNA dye

Hoechst for 10 minutes, washed for 10 minutes with 0.1% PBST, and finally mounted in Slow-Fade Gold (Molecular Probes).

2.2.4 Mitochondrial membrane potential detection

Larval brains were dissected out in Schneider's media and treated with 1:150 D(+) Limonene (Lobachemie) (diluted in Schneider's media) for 4 minutes. Subsequently, brains were immersed in 100 nM Tetramethylrhodamine, methyl ester (TMRM) for 30 minutes. Afterwards, the brains were washed with Schneider's media for 5 minutes and mounted in a poly-L-lysine-coated LabTEK chamber, immersed in Schneider's media. Imaging was done immediately using the Zeiss LSM 710 confocal system with 63X/1.4 NA Oil objective using 561 nm laser. We have used the routine confocal mode in the Zeiss LSM 710 microscope throughout all our experiments. We quantified the relative TMRM intensity of type II neuroblasts to the surrounding type I neuroblasts.

2.2.5 Cellular ROS detection

Third instar larval brains were dissected in Schneider's media and each of the brain lobes was delicately cut at the outer margin of the optic lobe to facilitate the penetration of DHE into brain tissue. Subsequently, the brains were incubated in 30 μM Dihydroethidium (DHE) for 15 minutes at RT. Following this, the brains were washed with Schneider's media for 10 minutes before being mounted in a poly-L-lysine-coated LabTEK chamber, immersed in Schneider's media. The coverslip was placed over the brains very gently to avoid tissue damage. Imaging was done immediately using the Zeiss LSM 710 confocal system with 63X/1.4 NA Oil objective using 561 nm laser. We quantified the relative DHE intensity of type II neuroblasts to surrounding type I neuroblasts.

2.2.6 Cellular ATP detection

Third instar larval brains were dissected out in Schneider's media and treated with 1:150 D(+) Limonene (Lobachemie) (diluted in Schneider's media) for 4 minutes. Subsequently, brains were immersed in 30μM ATP-red dye for 30 minutes. Afterwards,

the brains were washed with Schneider's media for 5 minutes and mounted in a poly-L-lysine-coated LabTEK chamber, immersed in Schneider's media. Imaging was done immediately using the Zeiss LSM710 confocal inverted system with 63X/1.4 NA Oil objective using 561 nm laser. We quantified the relative ATP-red dye intensity of type II neuroblasts to surrounding type I neuroblasts.

2.2.7 EdU assay for cell proliferation analysis

EdU assay was performed by using a Click-iTTM EdU Alexa FluorTM 647 imaging kit (C10340). Third instar larvae were dissected in Schneider's medium and immediately treated with 10μM EdU (5-ethynyl-2'-deoxyuridine) for 15 minutes at RT. EdU incorporation reaction in DNA was stopped by fixing the brains in 4% PFA for 25 minutes. The brains were washed in 0.1% PBST for 30 minutes at room temperature (RT) and blocked with 1% BSA in 0.1% PBST for 1 hour at RT. Following this, the brains were incubated with the required primary antibodies overnight (~14 hours) at 4℃ on a shaker. The next day, brains were washed for 20 minutes with 0.1% PBST. Subsequently, the brains were incubated with secondary antibodies against primary antibodies for 1 hour at RT, followed by 20 minutes of washing with 0.1% PBST. Subsequently, the brains were washed for 20 minutes with 0.1% PBST. A Click-iT reaction cocktail was prepared according to the manufacturer's instructions. Along with other reagents, it contains Alexa Fluor 647, which binds to EdU in the DNA of cells. The brains were incubated in it for 30 minutes at RT, followed by 10 minutes of washing with 0.1%PBST. For DNA staining, the brains were treated with Hoechst (1:1000) in 0.1%PBST for 10 minutes and then washed for 10 minutes with 0.1% PBST before being mounted in Slow-Fade Gold. Subsequent imaging was performed using a Zeiss LSM710 with a 40x/1.4NA oil objective.

2.2.8 Microscopy and image acquisition

2.2.8.1 Imaging of fixed samples

Fixed samples were imaged at room temperature using a Zeiss LSM710 or LSM780 inverted confocal microscope at the IISER Pune microscopy facility. A Plan-Apochromat 40x (1.4 NA) or 63x (1.4 NA) oil objective was used for image acquisition. Images were captured at 1024x1024 pixels with an averaging of 2 and an acquisition speed of 8 using Zen2010 software. Fluorescence intensity was maintained within the 8-bit scale (0-255). During confocal microscopy, Hoechst, a DNA dye, was excited using a Diode laser. Argon laser (488 nm) was employed for Alexa Fluor 488, while a DPSS laser was used to image Alexa Fluor 568. Finally, Alexa Fluor 647 signals were acquired using a 633 nm HeNe laser.

Representative images in figures depict type II lineage, chosen to display the maximum number of cells within that lineage.

2.2.8.2 Live imaging of type II neuroblast in larval brain

For live imaging of type II neuroblasts, third instar larval brains were dissected at room temperature in Schneider's *Drosophila* media. An inverted ZMP LSM710 confocal microscope was used to scan the brains on a 35 mm dish in Schneider's media supplemented with 10% FBS and 10 mM insulin (I0516, Sigma) at 3-minute intervals for three hours at 25°C.

2.2.8.3 Transmission electron microscopy of larval neuroblasts

Third instar larval brains were dissected in Schneider's *Drosophila* media at room temperature. Brains were immediately fixed in 3% glutaraldehyde for 2hr at 4°C. Washed twice with 0.1 M Sodium cacodylate buffer, pH 7.4, for 10 min each. Then, tissues were further fixed in 1 % Osmium tetroxide (OsO_4) for 1 hr at 4^{o}C. Brains were en-block stained with 2% uranyl acetate and dehydrated for ten minutes each in an increasing alcohol series. Araldite resins A and B were used to infiltrate the tissues, and Araldite resin B was used to embed the tissues and polymerize them for 48 hours at 60^{o}C. Using an ultra-microtome (LeicaUC7), ultrathin brain slices of 70 nm were cut and collected on copper slot grids. Lead citrate was used to contrast the sections. The

transmission electron microscope, JEM 1400 Plus, JEOL (Japan), at 120 kV, was used to take the images.

2.2.9 Quantification of neuroblast mitotic index

Neuroblasts in the central brain hemisphere were quantified using Miranda as a cortical marker in conjunction with mCD8-GFP<*worniu*-Gal4 across various genotypes. The percentage of pH3-positive neuroblasts was then determined and plotted to assess NB proliferation. Type II NB mitotic index was calculated by counting pH3-positive mCD8-GFP<*pnt*-Gal4 cells within each brain lobe. Statistical significance was assessed using a non-parametric Mann-Whitney t-test.

2.2.10 Quantification of the number of mature INPs, GMCs and neurons in type II neuroblast lineages.

Dpn-positive cells were classified as mature INPs. Ase marked mature INPs and GMCs. Dpn-negative, Ase-positive cells were counted as GMCs within each type II neuroblast lineage. Young neurons, characterized by high nuclear Pros expression at the lineage base (Bayraktar et al. 2010; Samuels et al. 2020), were quantified from all Z-sections of the type II neuroblast lineage. The lineage boundary was delineated by anti-GFP staining to enhance the mCD8-GFP signal. ImageJ's brightness and contrast tools further ensured that only cells belonging to the same lineage were counted. Cell counts were plotted using GraphPad Prism, and statistical analysis was performed with a non-parametric Mann-Whitney t-test.

2.2.11 EdU incorporation analysis

We quantified EdU-positive cells across different planes within single type II lineages for various genotypes using the ImageJ cell counter. Proliferating mature INPs were specifically identified by co-localization of Dpn and EdU. Cell counts were then plotted using GraphPad Prism software, and a non-parametric Mann-Whitney t-test was applied for statistical analysis.

2.2.12 Nuclear Cyclin E intensity measurement

We quantified nuclear Cyclin E intensity in GFP-positive type II neuroblasts. Using ImageJ's freehand tool, we delineated the nuclear region of interest for each neuroblast. The ratio of nuclear to cytoplasmic Cyclin E fluorescence intensity was then calculated for all genotypes. These ratios were plotted using GraphPad Prism software, and a non-parametric Mann-Whitney t-test was applied for statistical analysis.

2.2.13 Quantification of ROS intensity in type-II NBs

We measured ROS by quantifying DHE uptake intensity in type II neuroblasts (mCD8-GFP positive) across different genotypes. For comparison, we also analysed neighbouring wild-type, type I NBs (mCD8-GFP negative) within the same samples. Using ImageJ's freehand tool, we defined a region of interest (cytoplasmic area) for each neuroblast. The ratio of DHE fluorescence intensity of the GFP-positive neuroblast to a neighbouring GFP-negative neuroblast (in the same optical plane) was calculated for all genotypes. These ratios were then plotted using GraphPad Prism software, and a non-parametric Mann-Whitney t-test was performed for statistical analysis.

2.2.14 Mitochondrial Membrane Potential Analysis

Mitochondrial membrane potential in GFP-positive type II neuroblasts was quantified by measuring TMRM dye intensity. The methodology for both quantification and data plotting was identical to that employed for the DHE analysis.

2.2.15 ATP dye fluorescence analysis

ATP in GFP-positive type II neuroblasts was quantified by measuring ATP-red dye intensity. The methodology for both quantification and data plotting was identical to DHE analysis.

Chapter 3

Neuroblast specific downregulation of electron transport chain complexes in the central nervous system of *Drosophila* larvae results in survival and behavioural defects

---

3.1 Introduction

Studies on the dynamics and function of mitochondria have highlighted the importance of mitochondria for both cellular survival and the organism's overall health. One of the primary functions of mitochondria is OXPHOS through electron transport chain activity, which constitutes the primary mechanism for ATP generation in aerobic eukaryotes, providing the vast majority of cellular energy required to sustain life. Beyond its quintessential role in bioenergetics, OXPHOS is now recognized as a pivotal regulator of animal survival, overall health and pathogenesis of numerous diseases (Nicholls 2002). In *Drosophila*, brain cancer formation and subsequent organismal lethality, driven by neural stem cell-derived tumor initiating cells (TICs), rely on OXPHOS to sustain their uncontrolled proliferation. Inhibiting OXPHOS, through the depletion of Complex V, effectively abrogates the tumor-forming capacity of these TICs (Bonnay et al. 2020). Also, dysfunctional OXPHOS contributes to energy deficiency and increased oxidative stress, which are hallmarks of Alzheimer's disease (AD), Parkinson's disease (PD), and Huntington's disease (HD).

In Alzheimer's Disease (AD), the accumulation of amyloid-beta (Aβ) protein, a process initiated by ROS, directly instigates lysosomal membrane degradation and leads to neuronal death (Zhang et al. 2009). The most prevalent flaw in the ETC in AD is a cytochrome c oxidase (Complex IV) deficiency, which causes an increase in ROS production, a decrease in energy storage, and a disturbance in energy metabolism (Rak

et al. 2016). Similarly, in PD and HD, Oxphos dysfunction due to ETC complex perturbation causes high ROS, which promotes oxidative stress and neuronal death (Shoffner et al. 1991; Tassone et al. 2023).

Drosophila melanogaster offers a versatile and robust model for investigating the developmental repercussions of mitochondrial genetic alterations. Its utility is further highlighted by the high degree of evolutionary conservation, with approximately 60% of human genes associated with cancer and other genetic diseases possessing orthologs within the *Drosophila* genome (Mirzoyan et al. 2019). The rapid life cycle, spanning approximately 10 days at ambient temperature, accelerates the analysis of multiple generations. The high fecundity of a single female, capable of laying between 800 and 1500 eggs, facilitates the screening of large progenies within individual experimental designs.

The *Drosophila* development starts with an egg that hatches into a larva and progresses through three distinct instar stages. This larval phase is followed by pupation, during which the organism undergoes complete metamorphosis—an intricate process involving the development of adult functional organs from specialized imaginal discs. Adult flies eclose from the pupal case, typically within 8 days post-larval hatching (Fernández-Moreno et al. 2007). This well-defined progression through distinct developmental stages enables precise, stage-specific analysis of genetic manipulations. In the present chapter, we harnessed this model to analyse the effects of perturbing ETC complexes on animal survival and differentiation of neuroblasts. We downregulated target proteins utilising various RNA interference (RNAi) lines with neuroblasts specific Gal4 drivers.

3.2 Materials and methods

3.2.1 Fly stocks

3.2.1.1 Gal4 flies: *pnt*-Gal4,UAS-mCD8-GFP and *wor*-Gal4,UAS-mCD8-GFP

3.2.1.2 RNAi flies: ND-PDSW^{i} (BL29592), ND-39^{i} (BL52922), ND-19^{i} (BL50577), ND-49^{i} (BL57499), ND-42^{i} (BL34526), and ND-51^{i} (BL36701), SdhC^{i} (BL53281), SdhD^{i} (BL65040), SdhBL^{i} (BL58100), UQCR11^{i} (BL64896), Cyt-c1L^{i} (BL34916), Cox6C^{i} (BL33878), Cox5A^{i} (BL27548), Cox8^{i} (BL65223), Cox7C^{i} (BL62877), ATP Syn G^{i} (BL67347), ATP Syn B^{i} (BL28062), ATP Syn D^{i} (BL33740), ATP Syn O^{i} (BL65180), ATP Syn α^{i} (28059), ATP Syn β^{i} (BL27712), ATP Syn β^{i} (BL28056), ATP Syn E^{i} (BL67826), ATP Syn C^{i} (BL35464), ATP Syn γ^{i} (BL28723), ATP Syn γ^{i} (BL15641).

3.2.2 Antibodies

Primary antibodies: Chicken anti-GFP (1:1000, Invitrogen, A10262), rabbit anti-Ase (1:10000, Yuh-Nung Jan, UCSF, USA), rat-anti-Deadpan (1:150, Abcam, ab195173), rabbit anti-Deadpan (1:800, Yuh-Nung Jan, UCSF, USA), mouse-anti-Prospero (1:20, DSHB, MR1A), rabbit anti-phosphohistone 3 (1:500, Invitrogen, PA5-17869), mouse-anti- ATPβ (1:200, Abcam, ab14730), rabbit-anti-cleaved Caspase 3 (1:100, Cell Signaling, D175).

Secondary antibodies: Alexa fluor coupled secondary antibodies (Invitrogen) were used in 1:1000 dilution: anti-chicken 488, anti-mouse 568/647, anti-rabbit 488/568/647, anti-rat 488/568/647.

3.2.3 Immunostaining

Third instar larval brains of ETC RNAi and control were dissected and processed for immunostaining following the protocol mentioned in section 2.2.3

3.2.4 Image acquisition and analysis

Fixed samples were processed for Confocal microscopy done at room temperature using LSM710 or LSM780 inverted microscope with a Plan apochromat 40x 1.4NA and 63x 1.4NA oil objective. Refer to sections 2.2.8,2.2.9, and 2.2.10 for detailed information about image acquisition and analysis.

3.3 Results

3.3.1 Inhibition of electron transport chain complex I, II, III, IV, and V in *Drosophila* neuroblasts shows larval as well as adult lethality

Mitochondrial activity and morphology are critical regulators of mammalian stem cell proliferation and differentiation, notably influencing these processes through the modulation of cyclin levels (Parker et al. 2015; Chen and Chan 2017). Perturbations in mitochondrial function, such as inhibiting the ETC, have been shown to disrupt mitochondrial morphology and concurrently impair stem cell proliferation (van den Ameele and Brand 2019; Teixeira et al. 2015).

To study the role of various ETC components on the neural stem cell differentiation and its impact on *Drosophila* development, we carried out an in vivo RNA interference (RNAi) screening in *Drosophila* brain by using *worniu*-Gal4 (Table 1). *Worniu*-Gal4 expresses in all neuroblasts of the brain from embryonic stages onwards. Table 1 shows that, inhibition of ETC complexes by down-regulating various nuclear encoded subunits causes developmental defects of three types,, **i) Pupae lethal**, third instar larvae were developed into pupae but failed to develop into flies, **ii) Adult lethal**, adult flies eclose out of the pupae but die immediately **iii) Partially lethal**, few escaper flies eclosed out of pupae but they were sluggish. We crossed Gal4 virgin females in duplicates to ETC RNAi expressing males on standard cornmeal agar media and incubated them at 29^{o}C and then we observed the F1 progeny development of RNAi and control flies. We depleted ETC complex I by expressing RNAi lines against its multiple subunits (ND-PDSW, ND-39, ND-19, ND-49, ND-42, and ND-51) by using *wor*-Gal4 and *pnt*-Gal4 to determine their role in animal survival and behaviour (Observation table 1). With *wor*-Gal4, knockdown of each subunit resulted in developmental defects. We observed two kinds of defects: pupae lethal and partially lethal. Downregulation of ND-PDSW, ND-49, and ND-42 in NSCs showed partial lethality; most of the pupae failed to eclose, but a few flies emerged from pupae exhibiting sluggishness. Depletion of ND-51,

ND-39, and ND-19 showed a more severe phenotype; all the F1 larvae proceeded to pupation but could not develop into flies.

Observation table 1: RNAi screening of electron transport chain complexes in *Drosophila* central nervous system

ETC	Gal4	RNAi	Source	Embryo	Larvae	Pupae	Adults
Complex I	*wor*	ND-PDSW	BL29592	+	+	+	Died immediately after eclosion
		ND-39	BL52922	+	+	+	Not emerged from pupae
		ND-19	BL50577	+	+	+	Not emerged from pupae
		ND-49	BL57499	+	+	+	Died immediately after eclosion
		ND-42	BL34526	+	+	+	Died immediately after eclosion
		ND-51	BL36701	+	+	+	Not emerged from pupae
	pnt	ND-PDSW	BL29592	+	+	+	Sluggish

		ND-39	BL52922	+	+	+	Sluggish
		ND-19	BL50577	+	+	+	Sluggish
		ND-49	BL57499	+	+	+	Sluggish
		ND-42	BL34526	+	+	+	Sluggish
		ND-51	BL36701	+	+	+	Sluggish
Complex II	*wor*	SdhC	BL53281	+	+	+	Nonlethal
		SdhBL	BL58100	+	+	+	Nonlethal
		SdhD	BL 65040	+	+	+	Not emerged from pupae
	pnt	SdhC	BL53281	+	+	+	Normal
		SdhBL	BL58100	+	+	+	Normal
		SdhD	BL 65040	+	+	+	Sluggish

Complex III	*wor*	UQCR 11	BL64896	+	+	+	Nonlethal
		Cyt-c1L	BL34916	+	+	+	Nonlethal
		Cyt-c1	BL34583	+	+	+	Died immediately after eclosion
	pnt	UQCR 11	BL64896	+	+	+	Normal
		cyt-c1L	BL34916	+	+	+	Normal
		Cyt-c1	BL34583	+	+	+	Sluggish
Complex IV	*wor*	Cox5A	BL27548	+	+	+	Died immediately after eclosion
		Cox6C	BL33878	+	+	+	Not emerged from pupae
		Cox 7C	BL62877	+	+	+	Died immediately after eclosion
		Cox8	BL65223	+	+	+	Not emerged from pupae

	pnt	Cox5A	BL27548	+	+	+	Sluggish
		Cox6C	BL33878	+	+	+	Sluggish
		Cox8	BL65223	+	+	+	Sluggish
		Cox 7C	BL62877	+	+	+	Sluggish
Complex V	*wor*	ATP Syn E	BL67826	+	+	+	Not emerged from pupae
		ATP Syn G	BL67347	+	+	+	Not emerged from pupae
		ATP Syn D	BL33740	+	+	+	Died immediately after eclosion
		ATP Syn β	BL27712	+	+	+	Died immediately after eclosion
		ATP Syn α	BL28059	+	+	+	Not emerged from pupae
		ATP Syn B	BL28062	+	+	+	Died immediately after eclosion

		ATP Syn β	BL28056	+	+	+	Not emerged from pupae
		ATP Syn γ	BL28723	+	+	+	Not emerged from pupae
		ATP Syn O	BL65180	+	+	+	Nonlethal
		ATP Syn C	BL35464	+	+	+	Nonlethal
	pnt	ATP Syn E	BL67826	+	+	+	Sluggish
		ATP Syn G	BL67347	+	+	+	Sluggish
		ATP Syn D	BL33740	+	+	+	Sluggish
		ATP Syn β	BL27712	+	+	+	Sluggish
		ATP Syn α	BL28059	+	+	+	Sluggish
		ATP Syn B	BL28062	+	+	+	Sluggish
		ATP Syn β	BL28056	+	+	+	Sluggish

		ATP Syn γ	BL28723	+	+	+	Sluggish
		ATP Syn O	BL65180	+	+	+	Normal
		ATP Syn C	BL35464	+	+	+	Normal

Observation table 1. *wor*-Gal4 and *pnt*-Gal4 drivers were crossed with RNAi lines against subunits of ETC complexes at 29ºC and lethality or behavioural phenotype was recorded in the F1 adults. *wor*-Gal4 expresses in all neuroblasts but *pnt*-Gal4 expresses in only type II neuroblasts. *wor*-Gal4-mediated depletion of ETC complex I, II, III, IV, and V showed lethality of animals at different stages of development. But *pnt*-Gal4 driven downregulation of ETC complexes showed a less severe phenotype; animals emerged from pupae, but they were sluggish. They died within 10-15 days after eclosion.

Depletion of ND-PDSW, ND-39, ND-19, ND-49, ND-42, and ND-51 subunits specifically in type II neuroblasts using *pnt*-Gal4 did not affect the development of F1 flies. Flies emerged normally out of pupae but were less active and sluggish. They died within 10-15 days after eclosion.

We depleted Complex II by downregulating its subunits, SdhD, SdhBL, and SdhC (Observation Table 1). $SdhD^{i}$ showed pupae lethality with *wor*-Gal4, but flies were sluggish with *pnt*-Gal4. $SdhBL^{i}$ and SdhCi were found to be non-lethal, and flies were normal with both *wor*-Gal4 and *pnt*-Gal4.

We impaired the complex III by knocking down its subunits, UQCR11, Cyt-c1L, and Cyt-c1 (Observation table 1). We found that *wor*-Gal4 driven expression of $Cyt\text{-}c1^{i}$ in neuroblasts leads to lethality of F1 flies just after their eclosion from pupae. *pnt*-Gal4 mediated expression of $Cyt\text{-}c1^{i}$ in type II neuroblasts made F1 flies sluggish, and they

died within 10-15 days after eclosion. But UQCR11^{i} and Cyt-c1L^{i} were non-lethal and showed no sign of sluggishness with both *worniu*-Gal4 and *pnt*-Gal4.

We disrupted complex IV by inhibiting subunits, Cox6C, Cox5A, Cox8, and Cox7C (Observation table 1). *wor*-Gal4>Cox6C^{i} F1 showed pupae lethality, development arrested at the pupal stage. Cox5A^{i} and Cox7C^{i} F1 developed till the adult stage. They were quite sluggish as they emerged from pupae and died immediately after eclosion. Cox8^{i} F1 progenies showed pupal lethality; pupae could not develop into flies. F1 flies generated by utilizing *pnt*-gal4 to downregulate the Cox6C, Cox5A, Cox8, and Cox7C subunits in type II neuroblasts were sluggish and perished 10–15 days after eclosion.

We depleted complex V downregulating its subunits, ATP syn G, ATP syn B, ATP syn D^{i}, ATP syn O, ATP syn α, ATP syn β, ATP syn E, ATP syn C, ATP syn γ (Observation table 1). *worniu*-Gal4 driven ATP syn G^{i}, ATP syn E^{i}, ATP syn α^{i}, ATP syn β^{i} (BL28056), ATP syn γ^{i}, produced F1 flies which developed till pupae stage but failed to develop into flies. But ATP syn B^{i}, ATP syn β^{i} (BL27712), ATP syn D^{i}, F1 flies emerged from pupae and died immediately. ATP syn O^{i} and ATP syn C^{i} F1 flies were non-lethal. When the ATP syn G^{i}, ATP syn E^{i}, ATP syn α^{i}, ATP syn β^{i} (BL28056), ATP syn γ^{i}, ATP syn B^{i}, ATP syn β^{i} (BL27712), ATP syn D^{i}, were expressed in type II neuroblasts using *pnt*-gal4, the resulting F1 flies were sluggish and died 10–15 days after eclosion. But ATP syn O^{i} and ATP Syn C^{i} expression F1 flies were normal.

3.3.2 Knockdown of electron transport chain complex I, II, IV, and V do not change the number of neuroblasts in third instar larval brain hemisphere

Within each lobe of the *Drosophila* larval central nervous system, the total neuroblast population ranges from 90 to 100. This population predominantly comprises type I neuroblasts, approximately 85-90 per lobe, whereas type II neuroblasts are only 8 in number (Homem and Knoblich 2012). To analyse the effect of ETC perturbation on

neuroblast number, we expressed RNAi against various subunits of ETC complexes using *wor*-Gal4,UAS-mCD8-GFP and *pnt*-Gal4,UAS-mCD8-GFP. All experimental crosses were maintained at 29°C to maximize the downregulation of target mitochondrial proteins. For subsequent analysis, brains were dissected from third-instar wandering larvae of each genotype and processed for immunofluorescent staining, utilizing Miranda as a neuroblast marker. The total number of neuroblasts within the central brain was then quantified based on Miranda and mCD8-GFP immunolabeling. A minimum of 5 brains were analyzed per genotype, and the resulting data were subjected to statistical analysis via Mann-Whitney t-test, with comparisons made against mCherry^{i} control. The number of neuroblasts were unchanged on knockdown of ETC complexes. There were approximately 100 NBs on knockdown of Complex I (ND-51^{i}, ND-39^{i}, and ND-19^{i}), complex II (SdhD^{i}), complex IV (Cox6C^{i}), and complex V (ATP synE^{i}, ATP synG^{i}, and ATP synβ^{i}) using *wor*-Gal4 (Figure 3.1 A and B). Similarly, knockdown of ETC complexes by using type II neuroblasts specific *pnt*-Gal4 did not change the number of neuroblasts, and they remained 8 (Figure 3.1 C and D). Therefore, the downregulation of ETC complexes in the *Drosophila* central nervous system does affect neuroblast formation.

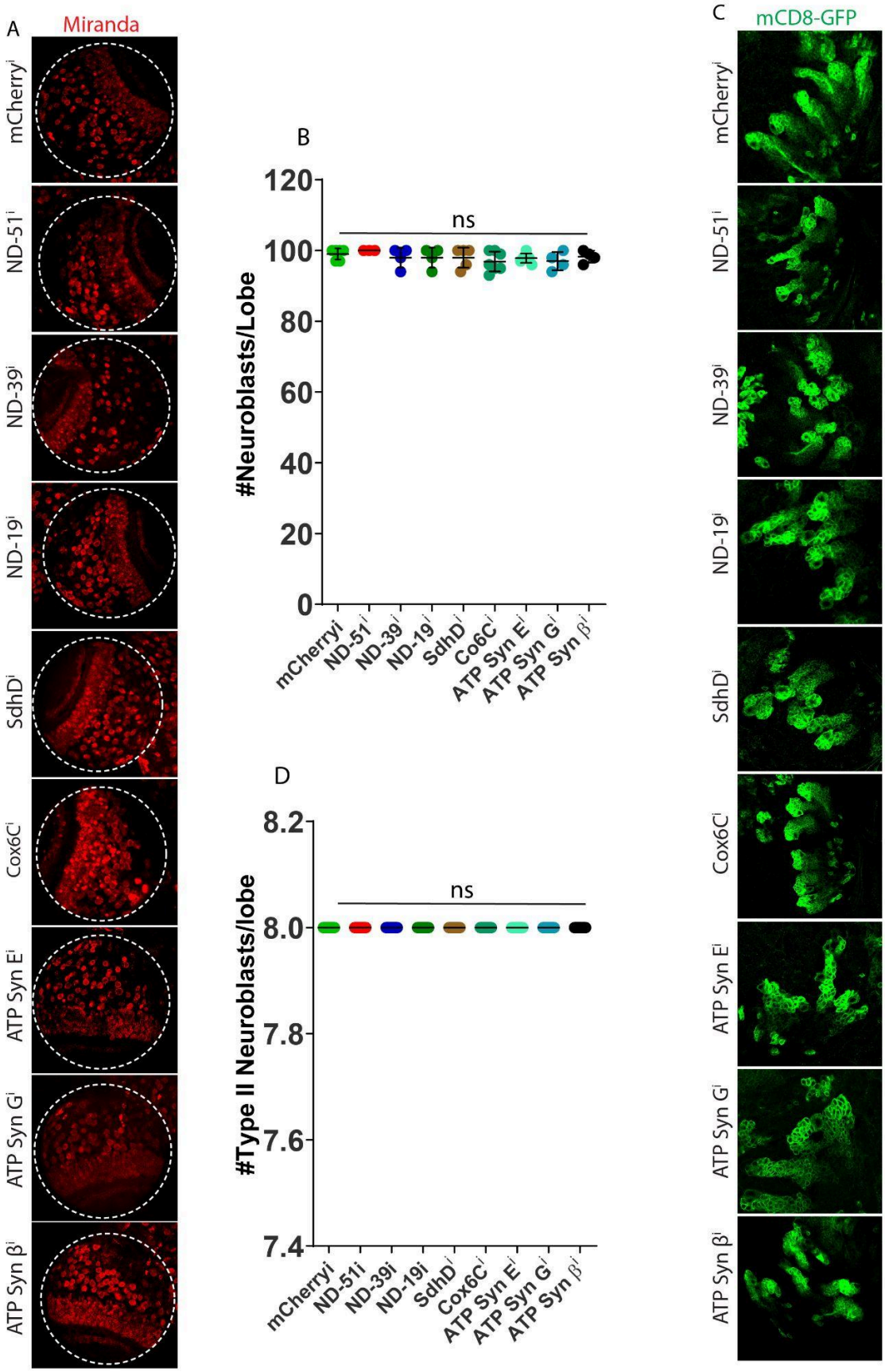

A
Miranda
mCherryi
ND-51i
ND-39i
ND-19i
SdhDi
Cox6Ci
ATP Syn Ei
ATP Syn Gi
ATP Syn βi
B
#Neuroblasts/Lobe
120
100
80
60
40
20
0
ns
mCherryi
ND-51i
ND-39i
ND-19i
SdhDi
Co6Ci
ATP Syn Ei
ATP Syn Gi
ATP Syn βi
C
mCD8-GFP
mCherryi
ND-51i
ND-39i
ND-19i
SdhDi
Cox6Ci
ATP Syn Ei
ATP Syn Gi
ATP Syn βi
D
#Type II Neuroblasts/lobe
8.2
8.0
7.8
7.6
7.4
ns
mCherryi
ND-51i
ND-39i
ND-19i
SdhDi
Cox6Ci
ATP Syn Ei
ATP Syn Gi
ATP Syn βi

Figure 3.1: Downregulation of ETC complex I, II, III, IV, and V do not affect neuroblast number. (A) Representative confocal images of larval brain lobes stained for Miranda (red) show no change in neuroblast number. The expression of all the indicated RNAi was done using *wor*-Gal4. **(B)** Quantification of neuroblast number in larval brain lobes mCherryi (6 lobes,15 brains), ND-51^{i} (3,3), ND-39^{i} (4,4), ND-19^{i} (4,4), SdhD^{i} (5,5), Cox6C^{i} (6,5), ATP synE^{i} (4,4), ATP synG^{i} (4,4), and ATP synβ^{i} (4,4). Scale bar- 10μm. **(C)** Representative confocal images of the brain lobe showing type II neuroblasts lineages (green). **(D)** Quantification of the number of type II neuroblasts per lobe in mCherryi (10 lobes, 5 brains), ND-51^{i} (10,5), ND-39^{i} (10,5), ND-19^{i} (10,5), SdhD^{i} (10,5), Cox6C^{i} (10,5), ATP synE^{i} (10,5), ATP synG^{i} (10,5), and ATP synβ^{i} (10,5). Mann-Whitney's t-test was performed for statistical analysis. ns=non-significant

3.3.3 Disruption of the ETC complex in neuroblasts leads to a decline in the neuronal population in brain lobe

We observed previously that disrupting the ETC complexes in the central nervous system impacted the overall development of the animals but didn't alter the number of neuroblasts. Type I neuroblasts undergo asymmetrical division, producing one neuroblast and one differentiated GMC. These GMCs then divide further to generate a pair of neurons or glial cells. To assess if ETC depletion in neuroblasts affects neuron generation in the larval brain, we probed neuronal populations by immunostaining against Elav. Elav is a *Drosophila* neuron-specific RNA-binding protein found in the nucleus. We examined immunofluore scence images from both control and RNAi brains. We found that depletion of complex I (ND-51^{i}) and complex IV (Cox6C^{i}) by using *worniu*-Gal4 resulted in a decrease of neuronal population in each brain lobe (Figure 3.2). Representative images of control and ETC-depleted brain belong to the same plane. Therefore, this loss of neurons might be the cause of developmental defects or sluggishness in animals.

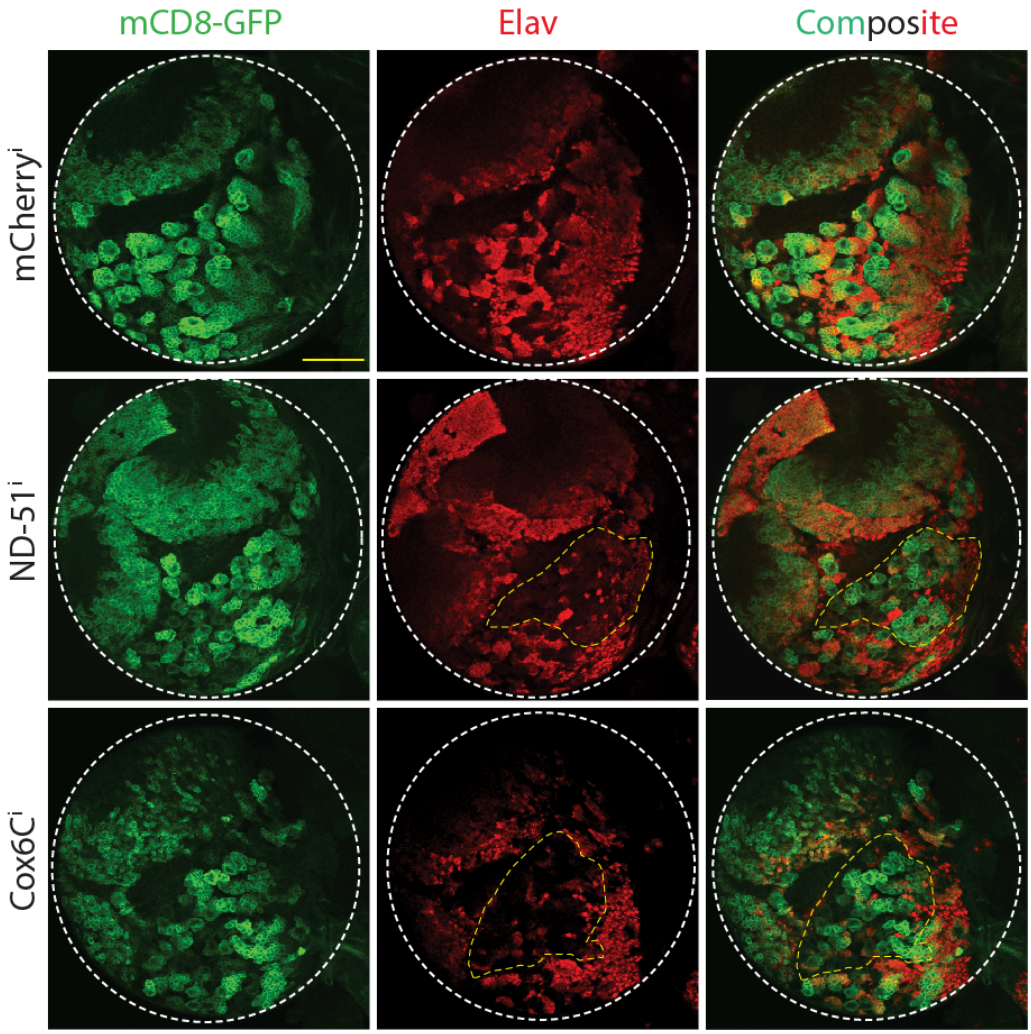


Figure 3.2: Downregulation of complex I (ND-51^{i}) and complex IV (Cox6C^{i}) in neuroblast using *wor*-Gal4 causes a reduction in Elav-positive neuronal population. Representative images of brain lobes showing reduced Elav positive neuronal population (enclosed by yellow dased lines) in third instar larval brain of genotypes: mCherry^{i} control (5 lobes,5 brains), ND-51^{i} (5,5), Cox6C^{i} (5,5). Scale bar- 50µm.

3.4 Discussion

The above results highlight the importance of ETC complexes in *Drosophila* neuroblasts for proper animal development. ETC complexes in neuroblasts are not required for their formation but are essential for their differentiation into neurons. The decreased neuronal population on ETC depletion might be responsible for the observed developmental defects. Some of the subunits of complex II (SdhB and SdhBL), complex III (UQCR11 and Cyt-c1L), and complex V (ATP Syn Oi and ATP Syn Ci) did not show a phenotype after depletion in neuroblasts. It suggests that these subunits are not essential for survival or that the RNAi lines are not working. We can check it by depleting them using a ubiquitous Gal4, Tubulin Gal-4. We found that distinct RNAi that target the same protein exhibit diverse phenotypes. Several plausible explanations account for this observed variability. Inherent knockdown efficiency of the RNAi lines might be the reason that dictates the extent of target protein depletion.

Furthermore, the targeted proteins' variable half-life within the cell can significantly influence the resulting phenotype. The kind of vector utilized to deliver this RNAi also affects its efficiency. These factors allow us to obtain phenotypic variance even when we use numerous RNA interferences to target the same protein. For further experiments, we chose RNAi lines showing survivability defects in *wor-Gal4-driven* ETC knockdown and used them to investigate their role in the differentiation and proliferation of neuroblasts.

Chapter 4

Electron transport chain complex I and mitochondrial fusion regulate ROS for differentiation of *Drosophila* neural stem cells

---

4.1 Introduction

Mitochondrial dynamics and activity regulate stem cell differentiation. In mammals, pluripotent stem cells predominantly rely on glycolysis for energy production. They contain fragmented or globular mitochondria, with poorly organised cristae and perinuclear localisation. These fragmented mitochondria have low electron transport chain activity, decreased mitochondrial membrane potential and ATP generation ability. During differentiation, mitochondria transition to OXPHOS, facilitated by fused or tubular mitochondrial architecture with well-developed cristae. Fused mitochondrial morphology has high OXPHOS, MMP, and ATP generation ability (Son et al. 2013; Liu et al. 2013; Schieke et al. 2008; Varum et al. 2009). An equilibrium between the fusion and fission events determines the mitochondrial architecture. Mitochondrial dynamics and activity regulate proliferation and differentiation in *Drosophila* neural stem cells or neuroblasts. In larval stages, proliferating neuroblasts rely on glycolysis, but during the larval to pupal transition, they undergo cell cycle exit and terminal differentiation (Homem et al. 2015). Mitochondrial fusion driven by Opa1 is essential for differentiation in the central brain neuroblasts (Dubal et al. 2022). Increase in Notch signaling gives rise to excessive proliferation of neuroblasts, which also requires mitochondrial activity and fusion (van den Ameele and Brand 2019; Bonnay et al. 2020). Even though mitochondrial dynamics and activity are important for neuroblast proliferation and differentiation, the mechanisms by which they interact to produce differentiation outcomes remains largely unexplored.

In this chapter, we investigate the interaction between mitochondrial fusion and electron transport chain complex I in the proliferation and differentiation of neuroblasts in the central brain in *Drosophila*. ETC activity is important for neuroblast proliferation and differentiation in *Drosophila*. Reduction of ETC activity leads to mitochondrial fragmentation. We study the interaction of the activity of complex I and mitochondrial fusion in the proliferation and differentiation of type II neuroblasts. ETC complex I, known as NADH dehydrogenase or NADH:ubiquinone oxidoreductase, is a multi-subunit enzyme with a 1000kDa molecular weight that catalyzes the transfer of electrons from NADH to ubiquinone. Complex I can generate ROS under conditions of forward and reverse electron transfer in the ETC. It is an L-shape in structure, consisting of one hydrophobic arm, embedded in the inner mitochondrial membrane and one hydrophilic arm, present at the periphery toward matrix (Garcia et al. 2017; Agip et al. 2023; Guarani et al. 2014) (Figure 4.1).

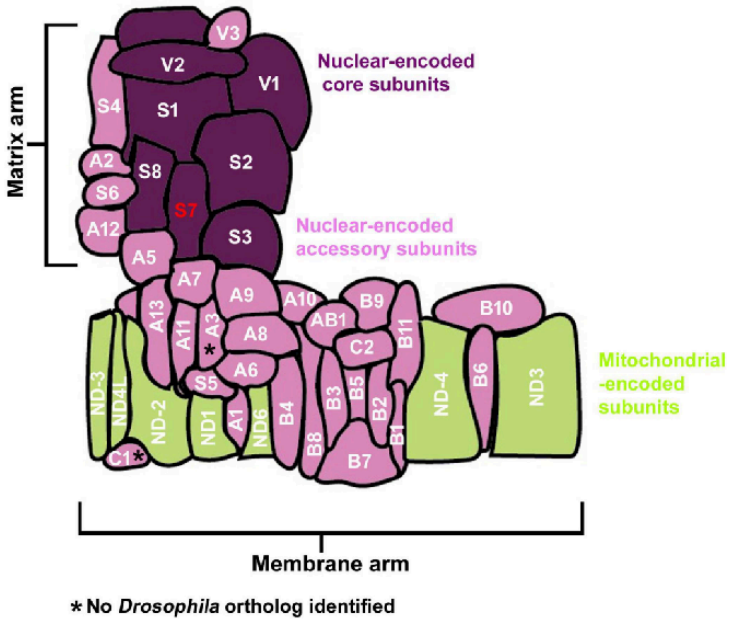


Figure 4.1. Schematic showing the arrangement of Drosophila mitochondrial complex I subunits forming the L-shaped topology. Asterisks indicate subunits with no identified Drosophila orthologs according to DIOPT. Figure adapted from (Mallik and Frank 2022).

The *Drosophila* mitochondrial complex I is composed of 43 subunits, a catalytic core of 14 evolutionarily conserved subunits alongside 29 accessory subunits (Garcia et al. 2017; Agip et al. 2023). Although these accessory subunits are not directly involved in the catalytic process, their perturbation can disrupt the assembly of the entire complex, leading to elevated ROS generation (Berger et al. 2008; Stroud et al. 2016).In this chapter, it was analysed that depletion of complex I subunits led to decreased proliferation in the central brain neuroblasts. There was a decrease in differentiation in the type II neuroblast lineage, characterized by reduced mINPs, GMCs, and neurons. Notably, complex I downregulation led to fragmented mitochondria, low MMP and increased ROS generation. These elevated ROS levels were identified as the cause of differentiation impairment by disrupting G1-S phase transition. Inducing mitochondrial fusion or increasing ROS scavengers in complex I-depleted type II neuroblasts reversed the ROS levels and restored the differentiation defects in the type II neuroblast lineage.

4.2 Materials and methods

4.2.1 Fly stocks

4.2.1.1 Gal4 flies: *pnt*-Gal4,UAS-mCD8-GFP; *wor*-Gal4,UAS-mCD8-GFP; and *mhc*-Gal4

4.2.1.2 RNAi flies: ND-51^{i} (Bloomington stock, BL36701, BL29534), ND-39^{i} (BL 52922), ND-19^{i} (BL50577), Drp1^{S193D} (Drp1^{SD}) (Chowdhary et al. 2020; Dubal et al. 2022), UAS-hSOD1A4V (BL33607), mCherry^{i} (BL35785), mito-GFP (BL8442), SOD1^{i} (BL34616), SOD2^{i}(BL25969), Catalase^{i} (BL34020), SOD1^{OE} (BL24750), SOD2^{OE} (BL24494), Catalase^{OE}. The following combinations of transgenes were made by using standard fly genetics and appropriate balancers to bring the lines together:

Drp1^{SD}/CyOGFP;mCherry^{i}/TM6B, Drp1^{SD}/CyOGFP;ND-51^{i} (36701)/TM6B, Drp1^{SD}/CyOGFP;ND-19^{i} (50577)/TM6B, Drp1^{SD}/CyOGFP;*pnt*-Gal4,CD8-GFP/TM6B, mitoGFP^{OE}/CyOGFP;*pnt*-Gal4/TM6B, SOD2^{OE}/CyOGFP;ND-51^{i}(BL36701)/TM6B, Catalase^{OE}/CyOGFP;ND-51^{i}(BL36701)/TM6B.

The *worniu*-Gal4,UAS-mCD8-GFP was used to express transgenes in all third-instar larval neuroblasts and *pnt*-Gal4, UAS-mCD8-GFP was utilised specifically for type II neuroblasts.

4.2.2 Antibodies

Primary antibodies: chicken anti-GFP (1:1000, Invitrogen, A10262), rabbit anti-Ase (1:10000, Yuh-Nung Jan, UCSF, USA), rat-anti-Deadpan (1:150, Abcam, ab195173), rabbit anti-Deadpan (1:800, Yuh-Nung Jan, UCSF, USA), mouse-anti-Prospero (1:20, DSHB, MR1A), rabbit anti-phosphohistone 3 (1:500, Invitrogen, PA5-17869), mouse-anti- ATPβ (1:200, Abcam, ab14730), rabbit anti-cyclin E (1:200, Santacruz, sc-33748), rabbit-anti-phosphoAMPK (1:200, Cell Signaling, 2535L), rat-anti-Miranda (1:600, Abcam, 197788), rabbit-anti-cleaved Caspase 3 (1:100, Cell Signaling, D175), rabbit-anti-Cytochrome C (1:200, Cell Signaling, 4272S).

Secondary antibodies: Alexa fluor coupled secondary antibodies (Invitrogen) were used in 1:1000 dilution: anti-chicken 488, anti-mouse 568/647, anti-rabbit 488/568/647, anti-rat 488/568/647.

4.2.3 Immunostaining

Third instar larval brain of ETC RNAi and control were dissected and proceeded for immunostaining following the protocol mentioned in section, 2.2.3

4.2.4 Image acquisition and analysis

Fixed samples were processed for Confocal microscopy done at room temperature using LSM710 or LSM780 inverted microscope with a Plan apochromat 40x 1.4NA and 63x 1.4NA oil objective. Refer to sections 2.2.8,2.2.9, and 2.2.10 for detailed information about image acquisition and analysis.

4.3 Results

4.3.1 ETC complex I depletion leads to a decrease in proliferation and differentiation of neuroblasts at the third instar larval stage

To evaluate the function of ETC complex I in the proliferation of neuroblasts, we depleted individual subunits in type I and II neuroblasts by combining *wor*-Gal4,mCD8-GFP and *pnt*-Gal4,mCD8-GFP with shRNA lines against them. mCD8-GFP marked the plasma membrane in the cells expressing the Gal4 and the shRNA. RNAi depletion was carried out against the complex I subunits, ND-51/dNDUFV1 belonging to the core hydrophilic matrix arm, ND-39/dNDUFSA9, and ND-19/dNDUFA8 subunits belonging to the accessory hydrophobic membrane arm by crossing the corresponding shRNA lines with *wor*-Gal4 and staining for neuroblasts with Miranda and phospho-Histone 3 (pH3) which marks dividing cells. There was a significant reduction in the proportion of mitotically active neuroblasts within each brain lobe of ND-51^{i}, ND-39^{i} and ND-19^{i} expressing genotypes than mCherry^{i} control (Figure 4.2 A and B).

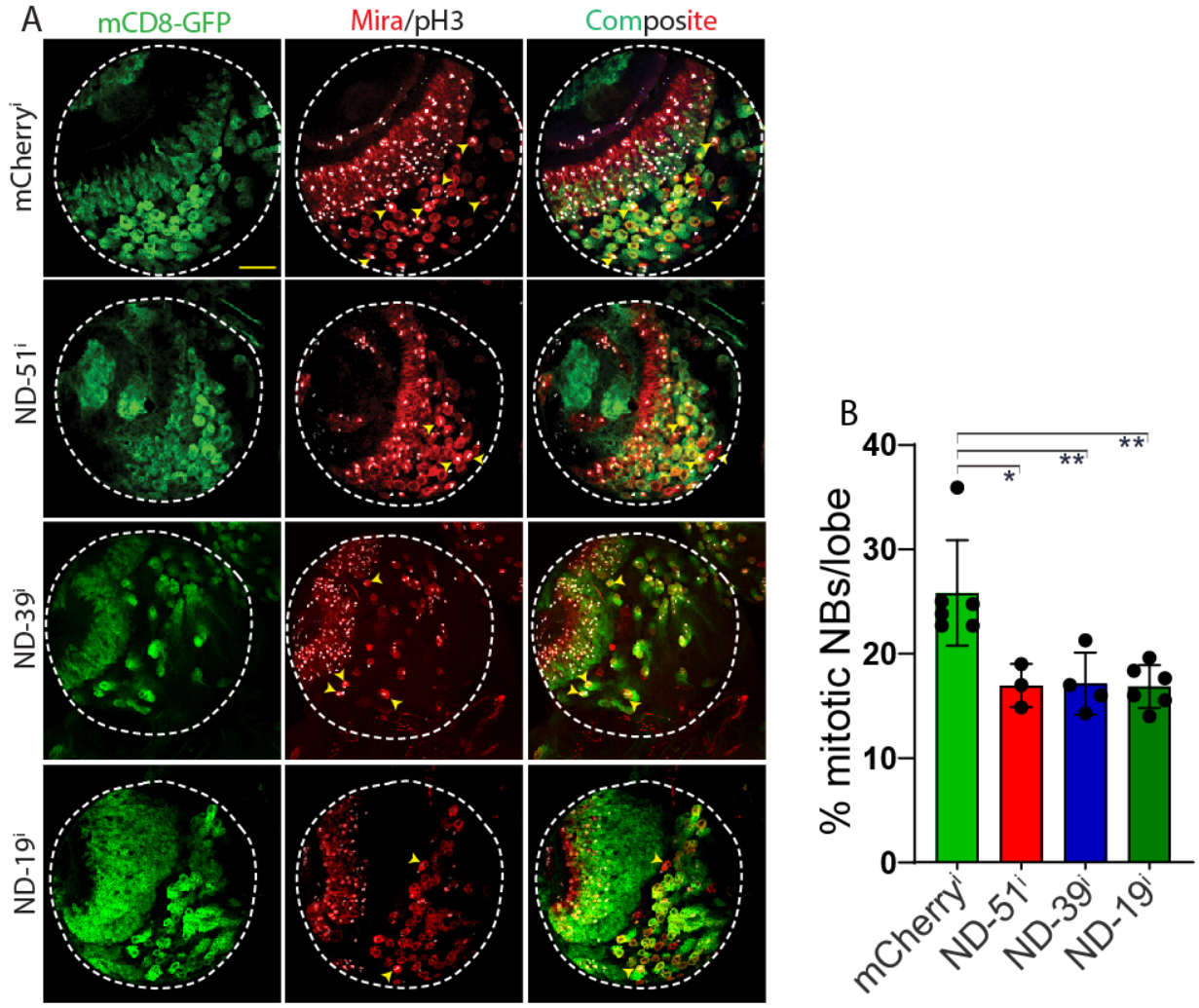


Figure 4.2: Depletion of complex I reduces the proliferation of neuroblasts in the third instar larval brain. (A) Representative images of mitotically dividing neural stem cells (NSCs) (Yellow arrowheads) in the *Drosophila* third instar larval brain lobe (white dashed outline) of indicative genotypes. *wor*-Gal4 driven UAS-mCD8-GFP marks the boundary of stem cells and its lineage (green). Miranda label stem cell cortex (red) and mitotically dividing cells are labelled by phospho-Histone H3 (pH3) (grey). Scale bar-50µm. **(B)** Graph showing the quantification of percent mitotically dividing NSCs present in each brain lobe of third instar larvae, expressing *worniu*-Gal4 driven mCherry^{i} (n=607 NSCs, 6 brains), ND-51^{i} (301, 3), ND-391^{i} (473, 5), and ND-19^{i} (605, 6). Mann-Whitney's t-test was performed for statistical analysis. *- $p<0.05$, **- $p<0.01$.

Furthermore, knockdown of ND-51, ND-39, and ND-19 in type II neuroblasts using the *pnt*-Gal4 driver also yielded a decreased number of mitotically dividing neuroblasts as compared to control (Figure 4.3 A and B). Live imaging of third instar larval brains expressing ND-51^{i} in type II neuroblasts also showed decreased division. Control neuroblasts divided at least once during live imaging in 40 mins but ND-51 depleted neuroblasts did not show a division (Figure 4.3 C). Collectively, these observations show that complex I is a crucial regulator of neuroblast proliferation.

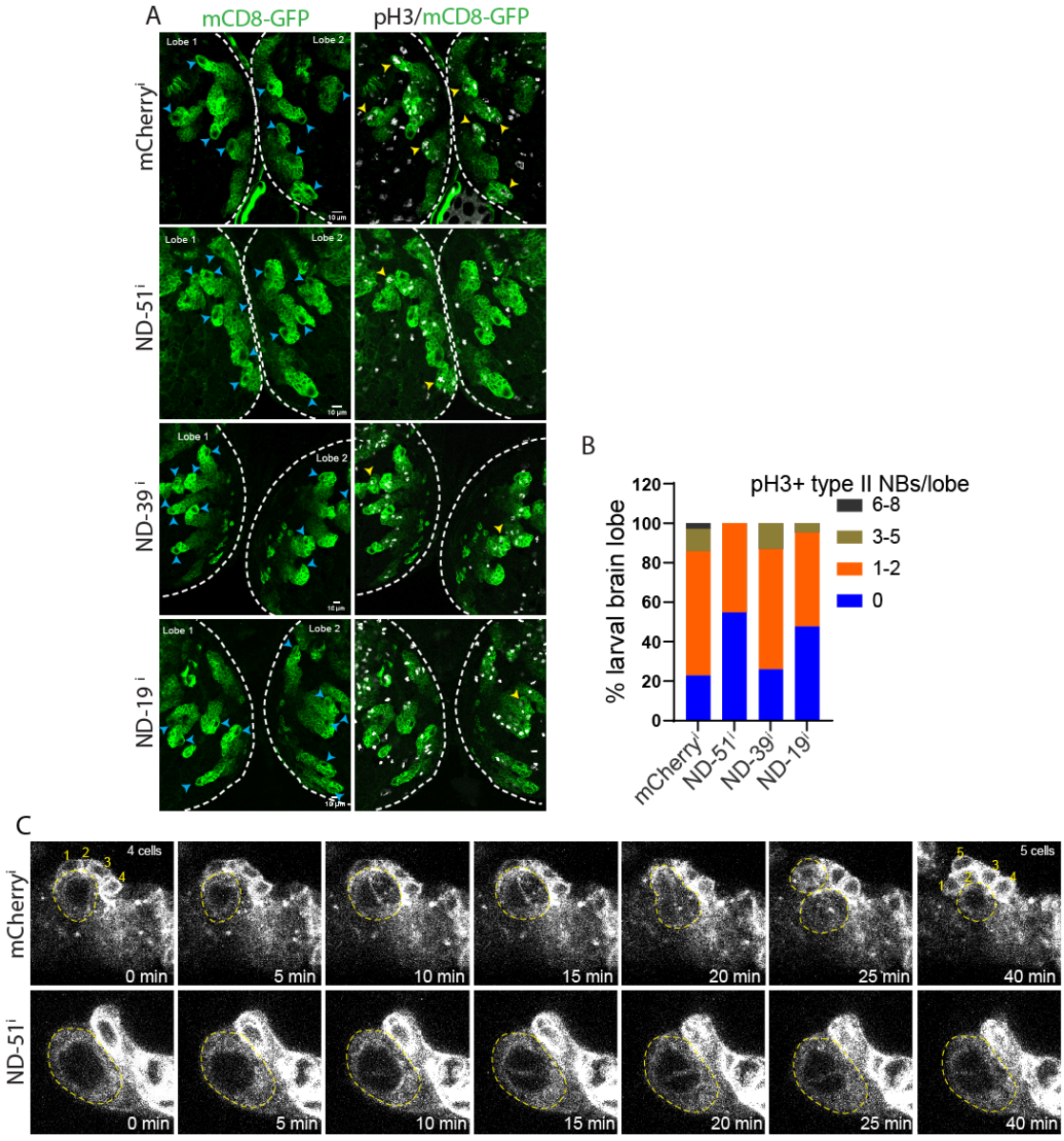


Figure 4.3: Deletion of complex I reduces division of type II neuroblasts in the third instar larval brain. (A) Representative images of mitotically dividing type II neuroblasts (Yellow arrowheads) in the *Drosophila* third instar larval brain of indicative genotypes. *pnt*-Gal4 driven mCD8-GFP marks the boundary of neuroblast (Blue arrowheads) and its lineage (green), and mitotically dividing cells are labelled by pH3 (grey). Scale bar- 10µm. **(B)** Quantification of mitotically dividing type II neuroblasts expressing *pnt*-Gal4 driven mCherry^{i} (n=144 NSCs, 9 brains), ND-51^{i} (176, 11), ND-39^{i} (192, 12), and ND-19^{i} (176, 11). **(C)** Representative images of snapshots during live imaging of type II neuroblasts of indicative genotypes. mCherry^{i} (n=15 neuroblast, 3 brains) and ND-51^{i} (25,5). Control, mCherry^{i} type II neuroblasts divided at least once during a live imaging period of 40 minutes, but ND-51^{i} neuroblasts failed to do so. Yellow dashed circle marks type II neuroblast. Before starting of division, four cells of lineage labelled as 1,2,3 and 4. After the completion of one division, a newly generated cell labelled as 5.

We further evaluated the impact of complex I depletion on differentiation in the type II neuroblast lineage. We quantified the number of distinct progenitor cells, mINPs, GMCs and neurons within the type II neuroblast lineage by immunostaining for specific markers. We found that the numbers of mINPs (Ase+, Dpn+) were decreased in ND-51^{i}, ND-39^{i} and ND-19^{i} expressing lineages as compared to mCherry^{i} expressing controls (Figure 4.4 A-C). mINPs undergo asymmetric division to produce GMCs (Ase+, Dpn-), which further symmetrically divide to form a pair of neurons or glia. Neurons show Prospero in the nucleus and are present at the base of the lineage (Bello et al. 2008; Walsh and Doe 2017). We assessed the proliferation of mINPs by co-staining with Dpn and pH3. Depletion of ND-51, ND-39, and ND-19 resulted in a decreased number of pH3-labelled mINPs within the lineage compared to controls (Figure 4.4 D and E). This reduction in mINP proliferation corresponded with a decrease in the population of GMCs (Ase+ Dpn-) (Figure 4.4 A and C), subsequently leading to a diminished production of neurons (high nuclear Prospero) (Figure 4.4 F and G).

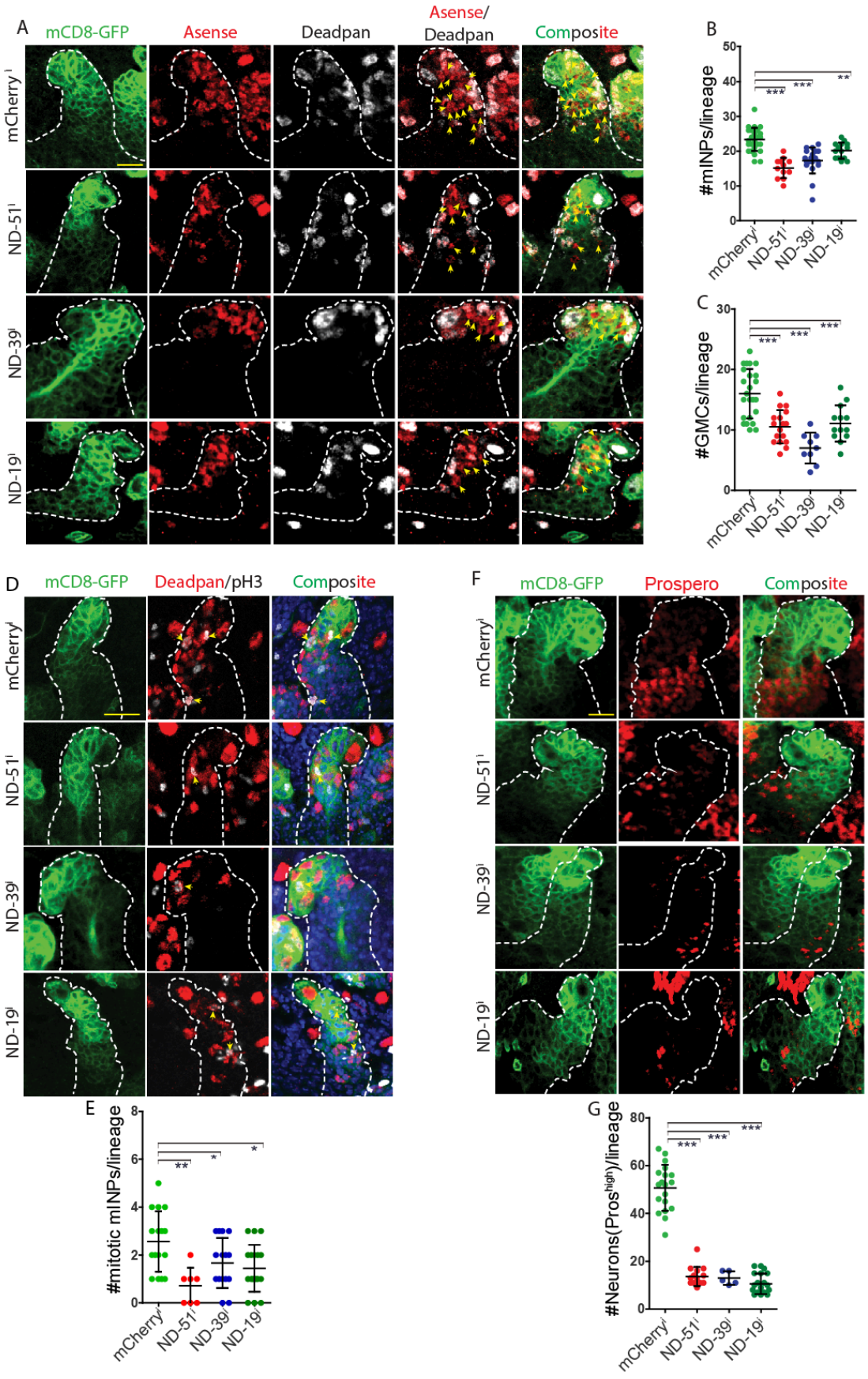

A
mCD8-GFP
Asense
Deadpan
Asense/
Deadpan
Composite
mCherry^i
ND-51^i
ND-39^i
ND-19^i
B
#mINPs/lineage
C
#GMCs/lineage
D
mCD8-GFP
Deadpan/pH3
Composite
E
#mitotic mINPs/lineage
F
mCD8-GFP
Prospero
Composite
G
#Neurons(Pros^{high})/lineage

Figure 4.4: Complex I depletion in type II neuroblasts results in decreased number of mINPs, GMCs, and neurons in the lineages. (A) Representative images of differentiated progenies in the type II neuroblast lineage of the mentioned genotypes. Deadpan positive cells are mature INPs (gray). Deadpan negative/Asense (red) positive cells are GMCs (yellow arrowheads). Scale bar- 10μm. **(B)** Quantification of mature INPs in type II neuroblast lineages of genotypes, mCherry^{i} (n=28 type II neuroblast lineages, 8 brains), ND-51^{i} (12, 6), ND-391^{i} (20, 11), and ND-19^{i} (14, 9). **(C)** Quantification of GMCs in type II neuroblast lineages of genotypes, mCherry^{i} (n=24 type II neuroblast lineages, 11 brains), ND-51^{i} (17, 9), ND-391^{i} (9, 5), and ND-19^{i} (13, 9). **(D)** Representative images showing detection of proliferating mature INP present in type II neuroblast lineage of the mentioned genotypes. Deadpan positive cells in the lineage mark mature INPs (red). pH3-labelled cells mark mitotically dividing cells (gray). We analysed mitotically dividing mature INPs by counting cells labelled for both pH3 and Deadpan. **(E)** Quantification of mitotically dividing mature INPs in type II neuroblast lineages of genotypes, mCherry^{i} (n=16 type II neuroblast lineages, 5 brains), ND-51^{i} (7, 5), ND-391^{i} (15, 5), and ND-19^{i} (18, 5). **(F)** Representative images of neurons staining in type II neuroblast lineages of indicative genotypes. High nuclear Prospero-positive cells are neurons (red). Scale bar- 10μm. **(G)** Neurons quantification in type II neuroblast lineages of genotypes, mCherry^{i} (n=19 type II neuroblast lineages, 5 brains), ND-51^{i} (15, 3), ND-39^{i} (5, 2), and ND-19^{i} (20, 4). Mann-Whitney's t-test was performed for statistical analysis. *- $p<0.05$, **- $p<0.01$, ***- $p<0.001$.

We ascertained that cell death was not a cause for depletion of cells in the type II neuroblast lineage by immunostaining the brains with an apoptosis marker, cleaved Caspase 3. We did not find any discernible difference between control and complex I depleted neuroblast lineages, showing that cell death was not a cause of the decrease in numbers of cells in each type II neuroblast lineage (Figure 4.5 A). To confirm the specificity of RNAi-mediated complex I depletion, we utilized an independent RNAi line targeting ND-51^{i} (BL29534). Expressing this line in type II neuroblasts with *pnt*-Gal4 recapitulated the differentiation defects, including a significant decrease in mature INPs, GMCs, and neurons within the lineage (Figure 4.5 B-F).

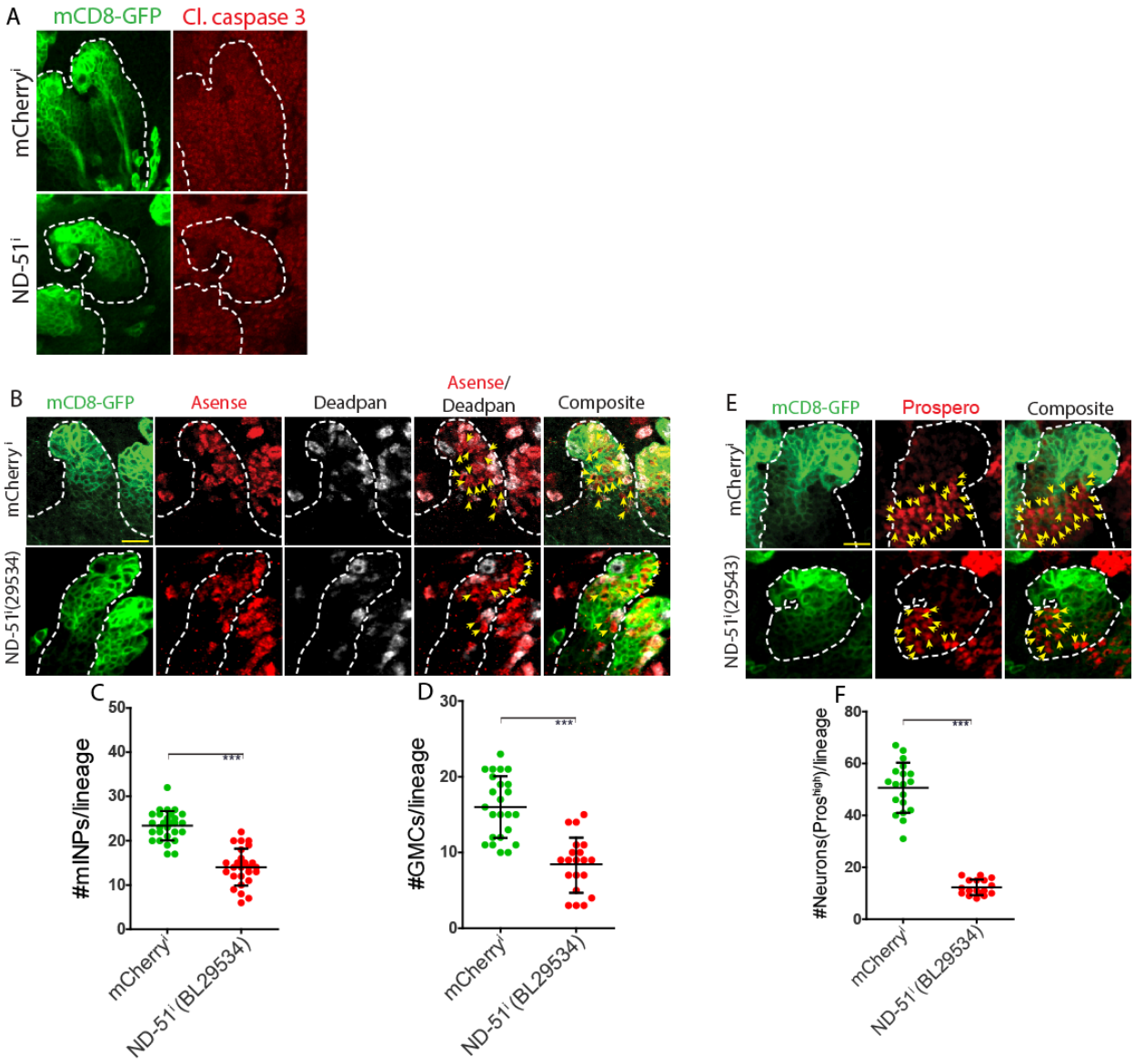


Figure 4.5: Decrease of differentiated cells in the lineage of complex I-depleted type II neuroblast was not due to apoptosis or cell death. Differentiation abnormalities shown by ND-51^i neuroblast were not because of off-target defects. (A) Representative images of cleaved caspase 3 immunostaining (red) in type II neuroblast lineage of the indicated genotype. There was no difference observed in caspase 3 expression between ND-51^i and mCherry^i control. **(B)** Representative images of differentiated progenies in the type II neuroblast lineage of the mentioned genotypes. Deadpan positive cells are mature INPs (gray). Deadpan

negative/Asense (red) positive cells are GMCs (Yellow arrowheads). Scale bar- 10µm **(C)** Quantification of mature INPs in type II neuroblast lineages of genotypes, mCherry^{i} (n=28 type II neuroblast lineages, 8 brains), ND-51^{i} BL 29534 (26, 6). **(D)** Quantification of GMCs in type II neuroblast lineages of genotypes, mCherry^{i} (n=24 type II neuroblast lineages, 8 brains), ND-51^{i} BL 29534 (20, 6). **(E)** Representative images of neurons staining in type II neuroblast lineages of indicative genotypes. High nuclear Prospero positive cells are neurons (red). Scale bar- 10µm. **(F)** Neurons quantification in type II neuroblast lineages of genotypes, mCherry^{i} (n=19 type II neuroblast lineages, 5 brains), ND-51^{i} BL 29534 (17, 6). Mann-Whitney's t-test was performed for statistical analysis.***- $p<0.001$.

In summary, the reduction in neuroblast and mINP proliferation resulting from complex I depletion in type II neuroblasts led to a decreased proliferation of transit amplifying cells and differentiated cells within the type II neuroblast lineages.

4.3.2 Induction of mitochondrial fusion by depletion of Drp1 in complex I deficient type II neuroblasts alleviates the proliferation and differentiation defect in the lineage

Complex I disruption causes mitochondrial fragmentation and co-depletion of Drp1 in the background restored the fused state

Our prior analysis demonstrated that depleting Opa1 in type II neuroblasts leads to mitochondrial fragmentation and differentiation defects (Dubal et al. 2022). Similar observations of mitochondrial fragmentation and impairment of differentiation have been reported in *Drosophila* intestinal stem cells upon Opa1 depletion (Deng et al. 2018). Drp1 activity is essential for driving mitochondrial fragmentation in Opa1-depleted cells (Chowdhary et al. 2017; Trevisan et al. 2018; Deng et al. 2018). Additionally, concurrent depletion of Drp1 with Opa1 restores mitochondrial fusion and alleviates the differentiation defects, underscoring the necessity of a fused mitochondrial morphology for proper stem cell differentiation (Dubal et al. 2022; Deng et al. 2018). Depletion of

ETC complex I and complex V in type I neuroblasts causes mitochondrial fragmentation (van den Ameele and Brand 2019). We assessed mitochondrial morphology in ND-51-depleted type II neuroblasts and muscle cells by using *pnt*-Gal4 and *mhc*-Gal4, respectively (Figure 4.6).

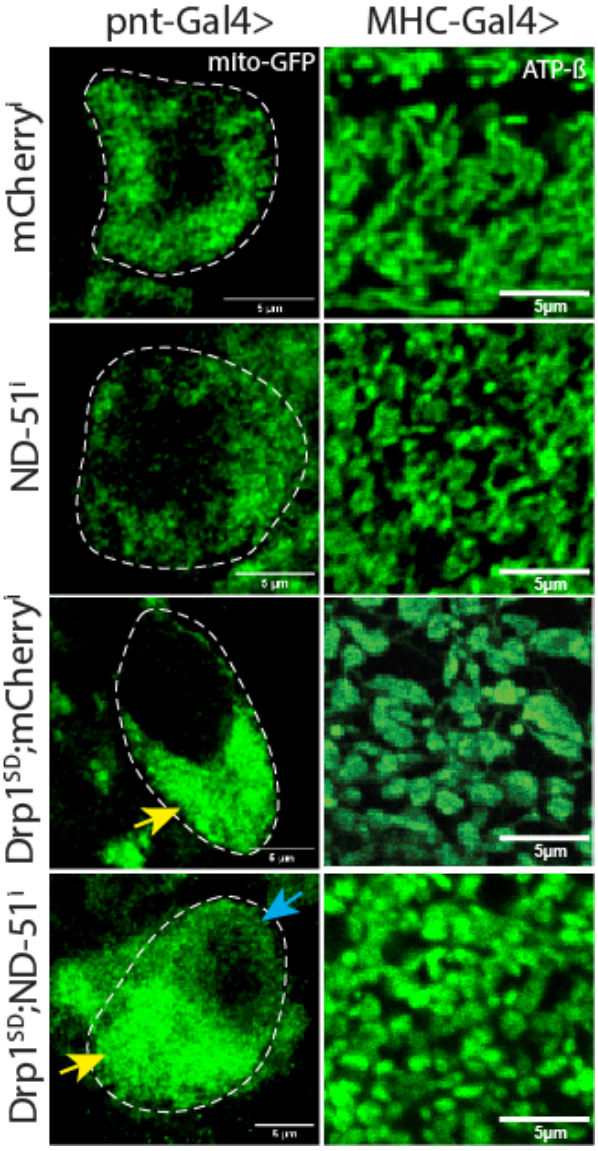


Figure 4.6: Representative images of mitochondrial morphology in type II neuroblasts and third instar larval muscle. In neuroblast, mitochondria are stained by using anti-GFP antibody against the mitochondrial tag, mito-GFP. In muscle, mitochondria were stained using

anti-ATP Syn β antibody. Depletion of Complex I in *Drosophila* type II neuroblasts (ND-51<*pnt*-Gal4) and larval muscle (ND-51<*mhc*-Gal4) induces mitochondrial fragmentation. Overexpression of $Drp1^{SD}$ in $ND\text{-}51^{i}$ neuroblasts results in clustered mitochondria (yellow arrowhead). In contrast to $Drp1^{SD}$;$mCherry^{i}$ neuroblasts, which show highly clustered mitochondria localized predominantly to one side (yellow arrowhead), $Drp1^{SD}$;$ND\text{-}51^{i}$ neuroblasts exhibit clustered and fewer punctuated mitochondrial populations (blue arrowhead).

As expected, ND-51 depleted type II neuroblasts showed fragmented mitochondria surrounding the nucleus and relatively smaller mitochondria in muscle cells. We investigated whether Drp1 depletion by co-expression of the dominant negative form of Drp1 ($Drp1^{SD}$) alongside complex I depletion could reverse the mitochondrial morphology. For this, we generated the combinations, $Drp1^{SD}$;$ND\text{-}51^{i}$ and $Drp1^{SD}$;$mCherry^{i}$ as a control and crossed them to *pnt*-Gal4 and MHC-Gal4 to assess mitochondrial morphology. Mitochondria in $Drp1^{SD}$;$mCherry^{i}$ neuroblasts were clustered and localised predominantly to one side of the neuroblasts as compared to $mCherry^{i}$ alone. $Drp1^{SD}$;$mCherry^{i}$ expression in muscle cells leads to bigger and interconnected mitochondria than $mCheery^{i}$. $Drp1^{SD}$;$ND\text{-}51^{i}$ neuroblasts exhibit a mixed population of clustered mitochondria localised to one side of the neuroblast and fragmented mitochondria. Muscle cells expressing $Drp1^{SD}$;$ND\text{-}51^{i}$ showed more fused mitochondria than $ND\text{-}51^{i}$ alone.

Mitochondrial fusion by Drp1 depletion in $ND\text{-}51^{i}$ neuroblast restores the decreased proliferation index of type I and type II neuroblasts

We further assessed the proliferation of $Drp1^{SD}$;$ND\text{-}51^{i}$ neuroblasts by crossing this with *wor*-gal4. In each brain lobe, the proportion of mitotically dividing neuroblasts was found to be increased significantly in $Drp1^{SD}$;$ND\text{-}51^{i}$ as compared to $ND\text{-}51^{i}$ alone (Figure 4.7 A and B). *pnt*-Gal4 mediated expression of $Drp1^{SD}$;$ND\text{-}51^{i}$ specifically in type II neuroblast also restored their proliferation as compared to $ND\text{-}51^{i}$ alone (Figure 4.7 C

and D). Next, we analysed the consequence of Drp1 depletion on the differentiation of ND-51^{i} type II neuroblast lineage.

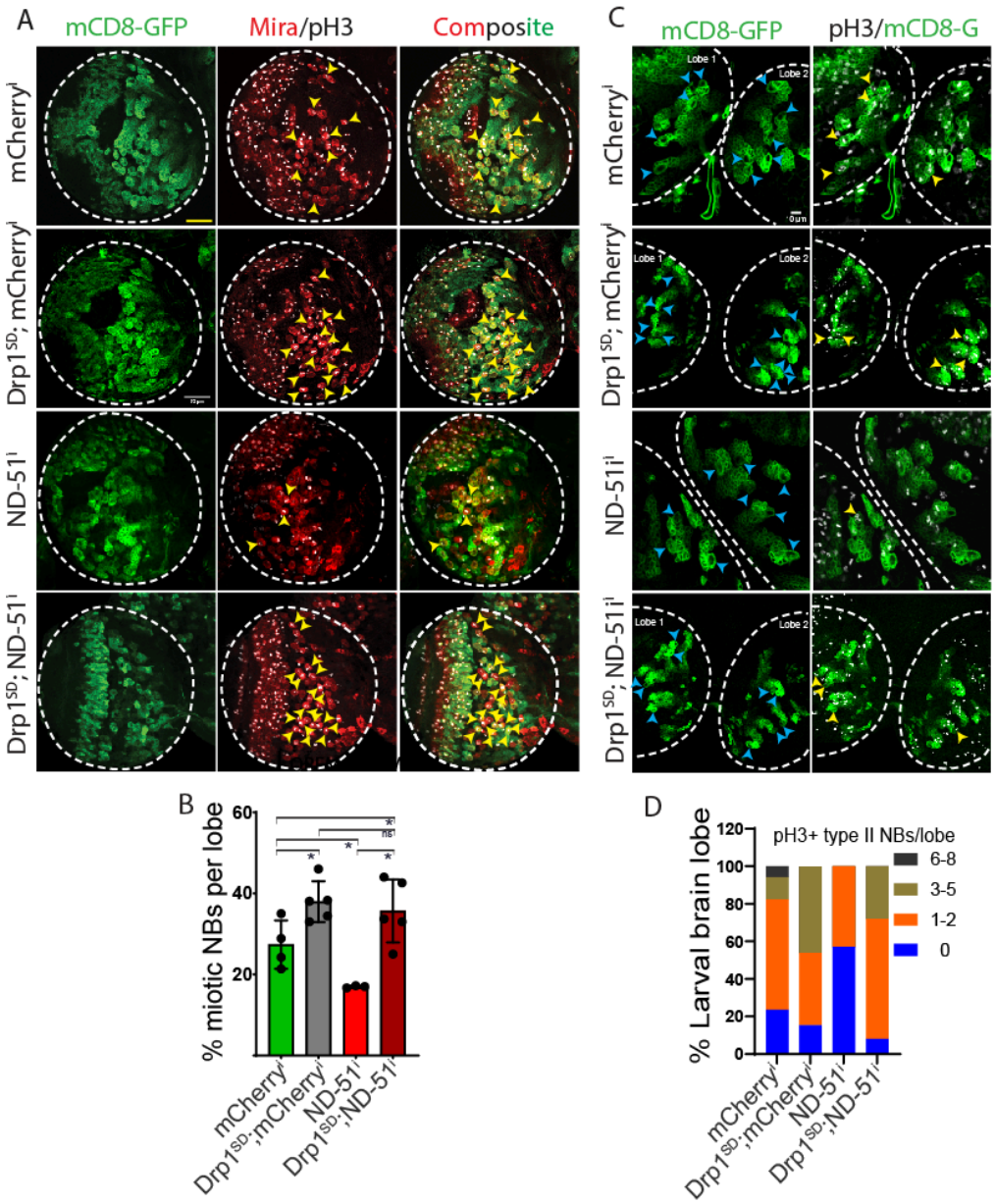


Figure 4.7: Forced mitochondrial fusion by Drp1^{SD} expression in complex I-depleted neuroblasts alleviates the proliferation defects. (A) Representative images of mitotically

dividing neuroblasts (yellow arrowheads) in the *Drosophila* third instar larval brain lobe of indicative genotypes. *wor*-Gal4 driven UAS-mCD8-GFP marks the boundary of stem cells and its lineage (green). Miranda label stem cell cortex (red) and mitotically dividing cells are labelled by phospho-Histone H3 (pH3) (grey). Scale bar- 50µm. **(B)** Graph showing the quantification of percent mitotically dividing NSCs present in each brain lobe of third instar larvae, expressing *worniu*-Gal4 driven mCherry^{i} (n=295 NSCs, 3 brains), Drp1^{SD}; mCherry^{i} (476, 5), ND-51^{i} (267, 3), Drp1^{SD}; ND-51^{i} (488, 5). **(C)** Representative figures of mitotically dividing type II neuroblasts (Yellow arrowheads) in the *Drosophila* third instar larval brain of indicative genotypes. pnt-Gal4 driven mCD8-GFP marks the boundary of stem cells (Blue arrowheads) and its lineage (green), and mitotically dividing cells are labelled by pH3 (grey). Scale bar- 10µm. **(D)** Quantification of the number of proliferating and non-proliferating type II neuroblasts in each brain lobe of the larval brain of genotype, mCherry^{i} (n=144 NSCs, 9 brains), Drp1^{SD}; mCherry^{i} (112, 7), ND-51^{i} (160, 10), Drp1^{SD}; ND-51^{i} (200,13). Mann-Whitney's t-test was performed for statistical analysis. ns=non-significant, *- $p<0.05$.

Mitochondrial fusion alleviates the type II neuroblast differentiation defects caused by depletion of complex I

Consistent with the rescue of proliferating neuroblasts (Figure 4.7), the number of mINPs increased in Drp1^{SD};ND-51^{i} compared to ND-51^{i} (Figure 4.8 A and B). Furthermore, we observed an increase in mitotically dividing mature INPs within the lineage of Drp1^{SD};ND-51^{i} neuroblast compared to ND-51^{i} (Figure 4.8 D and E). This increased division of mature INPs in Drp1^{SD};ND-51^{i} type II neuroblast lineage resulted in the rescue of the number of GMCs (Figure 4.8 A and C). However, the neurons were only partially rescued (Figure 4.9 A and B).

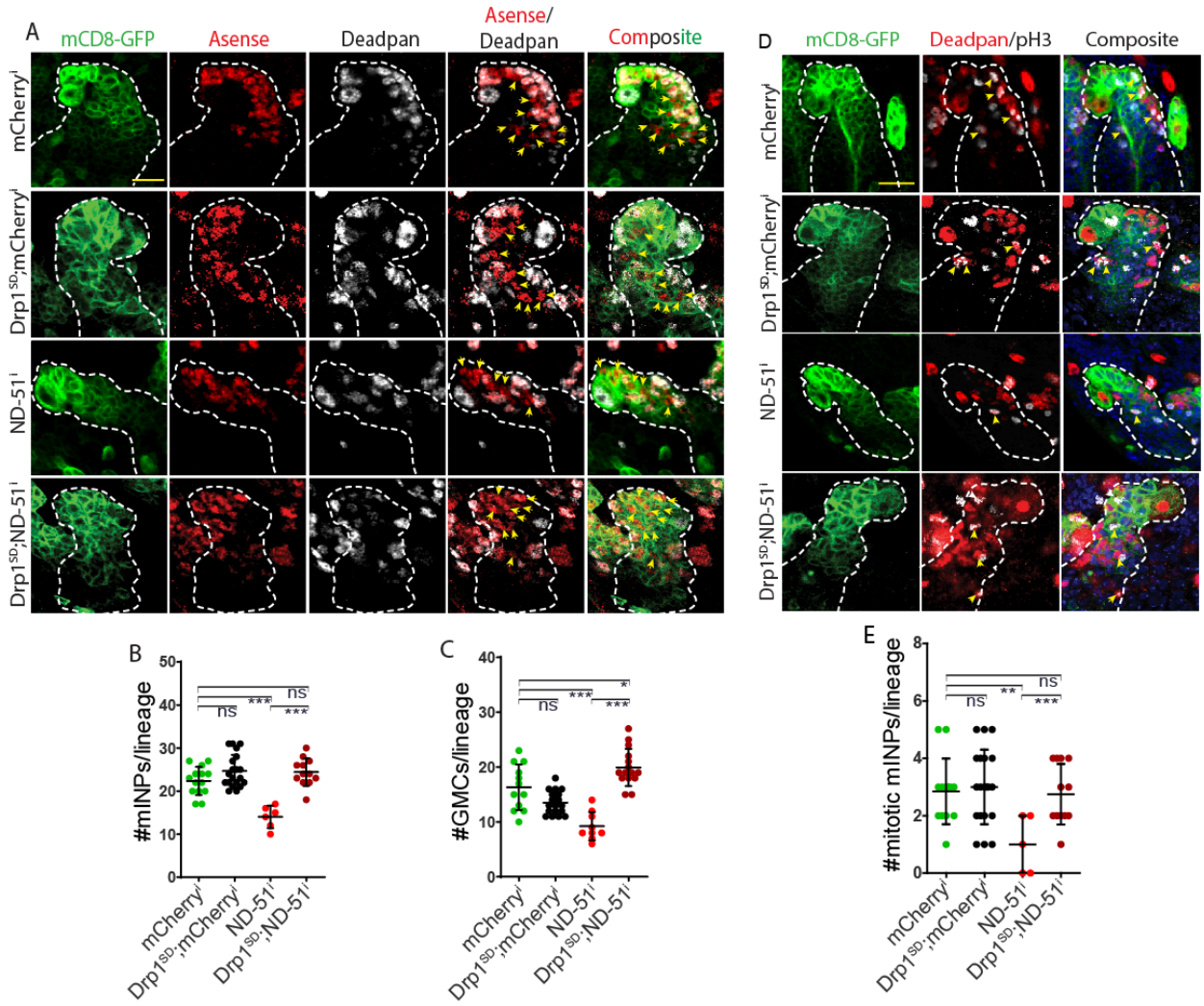


Figure 4.8: Forced mitochondrial fusion by Drp1^{SD} overexpression in complex I-depleted neuroblasts alleviates the differentiation defects. (A) Representative images of staining of mINPs and GMCs in type II neuroblast lineage of indicative genotypes. Deadpan positive cells are mature INPs (gray). Asense positive (red)/Deadpan negative cells are GMCs (Yellow arrowheads). Scale bar- 10µm. **(B)** Quantification of mature INPs in type II neuroblast lineages of genotypes, mCherry^{i} (n=28 type II neuroblast lineages, 11 brains), Drp1^{SD}; mCherry^{i} (20, 7), ND-51^{i} (12, 9), Drp1^{SD}; ND-51^{i} (12, 6). **(C)** Quantification of GMCs in type II neuroblast lineages of genotypes, mCherry^{i} (n=12 type II neuroblast lineages, 3 brains), Drp1^{SD};mCherry^{i} (18, 5), ND-51^{i} (14, 3), Drp1^{SD};ND-51^{i} (15, 5). **(D)** Representative images for mitotically dividing mature

INPs in type II neuroblast lineage of the mentioned genotypes. Deadpan positive cells in the lineage mark mature INPs (red). pH3-labelled cells mark mitotically dividing cells (gray). We analysed mitotically dividing mature INPs by counting cells labelled for both pH3 and Deadpan. **(E)** Quantification of mitotically dividing mature INPs in type II neuroblast lineages of genotypes, mCherry^{i} (n=13 type II neuroblast lineages, 5 brains), Drp1^{SD};mCherry^{i} (20, 5), ND-51^{i} (5, 4), Drp1^{SD};ND-51^{i} (12, 3). Mann-Whitney's t-test was performed for statistical analysis. ns=non-significant, *- p<0.05, **- p<0.01, ***- p<0.001.

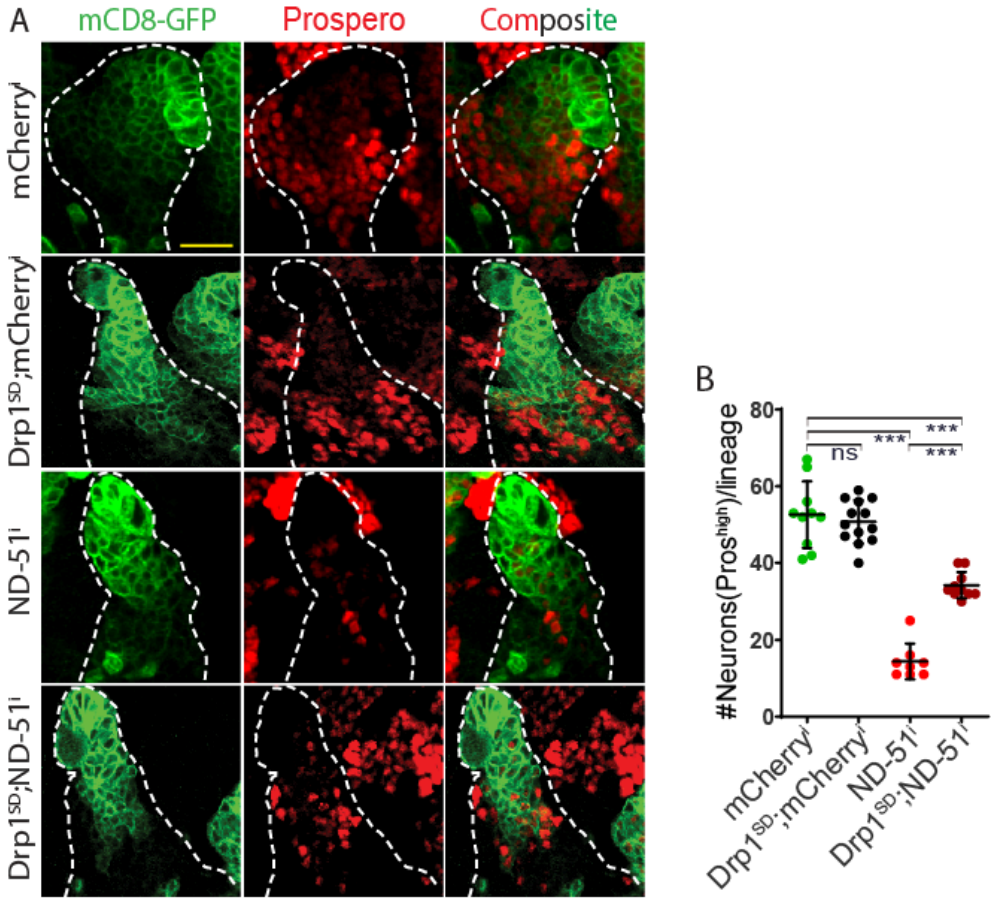


Figure 4.9: Forced mitochondrial fusion in complex I-depleted type II neuroblasts partially alleviates the number of neurons. (A) Representative images of neurons staining in type II neuroblast lineages of indicative genotypes. High nuclear Prospero-positive cells are neurons (red). Scale bar- 10µm. **(B)** Neurons quantification in type II neuroblast lineages of

genotypes,mCherry^{i} (n=10 type II neuroblast lineages, 5 brains), Drp1^{SD};mCherry^{i} (13, 5), ND-51^{i} (8, 5), Drp1^{SD};ND-51^{i} (10, 3). Mann-Whitney's t-test was performed for statistical analysis. ns=non-significant, ***- p<0.001.

To confirm that the rescue of differentiation defects upon Drp1^{SD} expression was not a consequence of Gal4 dilution, we expressed UAS-mito-GFP with ND-51^{i} and found that the numbers of mature INPs, GMCs, and neurons were similar to ND-51^{i} alone. (Figure 4.9 A-E). In summary, mitochondrial fusion could rescue the differentiation defects mediated by complex I depletion in type II neuroblasts.

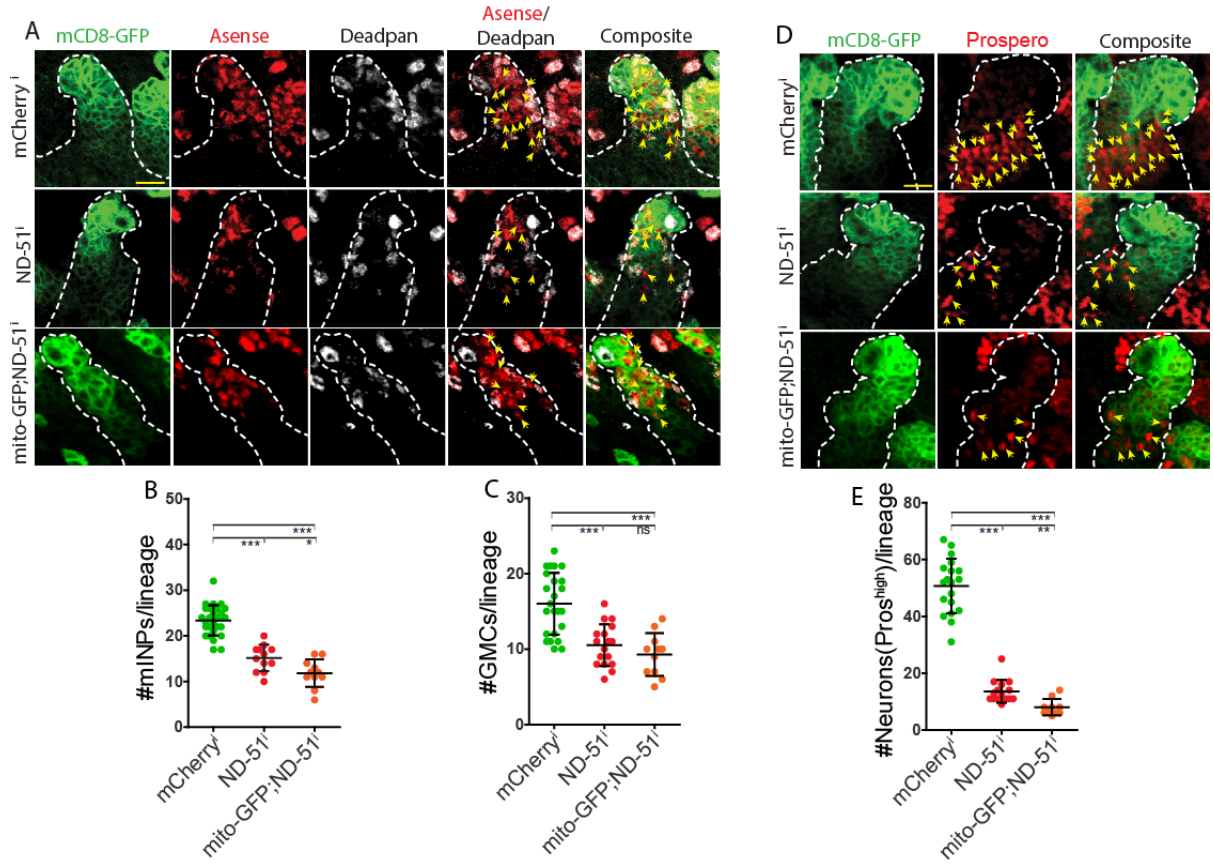


Figure 4.10: Differentiation defects rescue on Drp1^{SD} expression was not because of Gal4 dilution. (A) Representative images of mature INPs and GMCs staining in the type II neuroblast lineage of the mentioned genotypes. Deadpan positive cells are mature INPs (gray). Deadpan

negative/Asense (red) positive cells are GMCs (Yellow arrowheads). Scale bar- 10μm. **(B)** Quantification of mature INPs in type II neuroblast lineages of genotypes, mCherry^{i} (n=28 type II neuroblast lineages, 8 brains), ND-51^{i} (12,3), and mito-GFP;ND-51^{i} (11, 3). **(C)** Quantification of GMCs in type II neuroblast lineages of genotypes, mCherry^{i} (n=24 type II neuroblast lineages, 8 brains), ND-51^{i} (17,6), and mito-GFP;ND-51^{i} (11, 3). **(D)** Representative images of neurons staining in type II neuroblast lineages of indicative genotypes. High nuclear Prospero-positive cells are neurons (red). Scale bar- 10μm. **(E)** Neurons quantification in type II neuroblast lineages of genotypes, mCherry^{i} (n=19 type II neuroblast lineages, 5 brains), ND-51^{i} (15,5), and mito-GFP;ND-51^{i} (10, 3). Mann-Whitney's t-test was performed for statistical analysis. ns=non-significant, *- p<0.05, **- p<0.01, ***- p<0.001.

4.3.3 Depletion of Drp1 suppresses the G1/S phase progression defects and cyclin E decrease in complex I downregulated type II neuroblasts

Mitochondrial activity regulates cell cycle progression through the G1/S phase. Depletion of complex I in *Drosophila* eye discs causes a delay in the G1/S transition, mediated by high ROS levels and JNK-pathway activity (Mandal et al. 2010; Owusu-Ansah et al. 2008). We assessed the impact of complex I depletion on cell cycle progression in type II neuroblasts and mature INPs by incubating live brains with EdU (5-ethynyl-2'-deoxyuridine). EdU is a thymidine nucleoside analogue that is taken up by cells and incorporates into newly synthesised DNA during the S-phase of cell cycle. ND-51^{i} type II neuroblasts lineage showed a decreased number of EdU-positive cells compared to mCherry^{i} control (Figure 4.11 A and B). Also, the percentage of EdU-positive mature INPs was found to be decreased on ND-51 depletion (Figure 4.11 A and C). These S-phase defects were restored in Drp1^{SD};ND-51^{i} expressing type II neuroblast lineage (Figure 4.11 A-C). ETC dysfunction and mitochondrial fragmentation decrease cellular cyclin E levels (Mandal et al. 2005; Mitra et al. 2012). Because complex I perturbation leads to a decline of S-phase cells in lineage and cyclin E mediates G1 to S-phase transition (Mazumder et al. 2004), we used immunostaining to

quantify cyclin E levels in complex I RNAi and control type II neuroblasts. There was a decrease in the nuclear accumulation of cyclin E in ND-51^{i} neuroblast compared to the controls (Figure 4.11 *D* and *E*). Further cyclin E levels in Drp1^{SD};ND-51^{i} neuroblasts were comparable to control and greater than ND-51^{i} alone (Figure 4.11 *D* and *E*). Therefore, complex I disruption perturbs type II neuroblast differentiation by inducing G1/S phase transition defects through decreasing cyclin E.

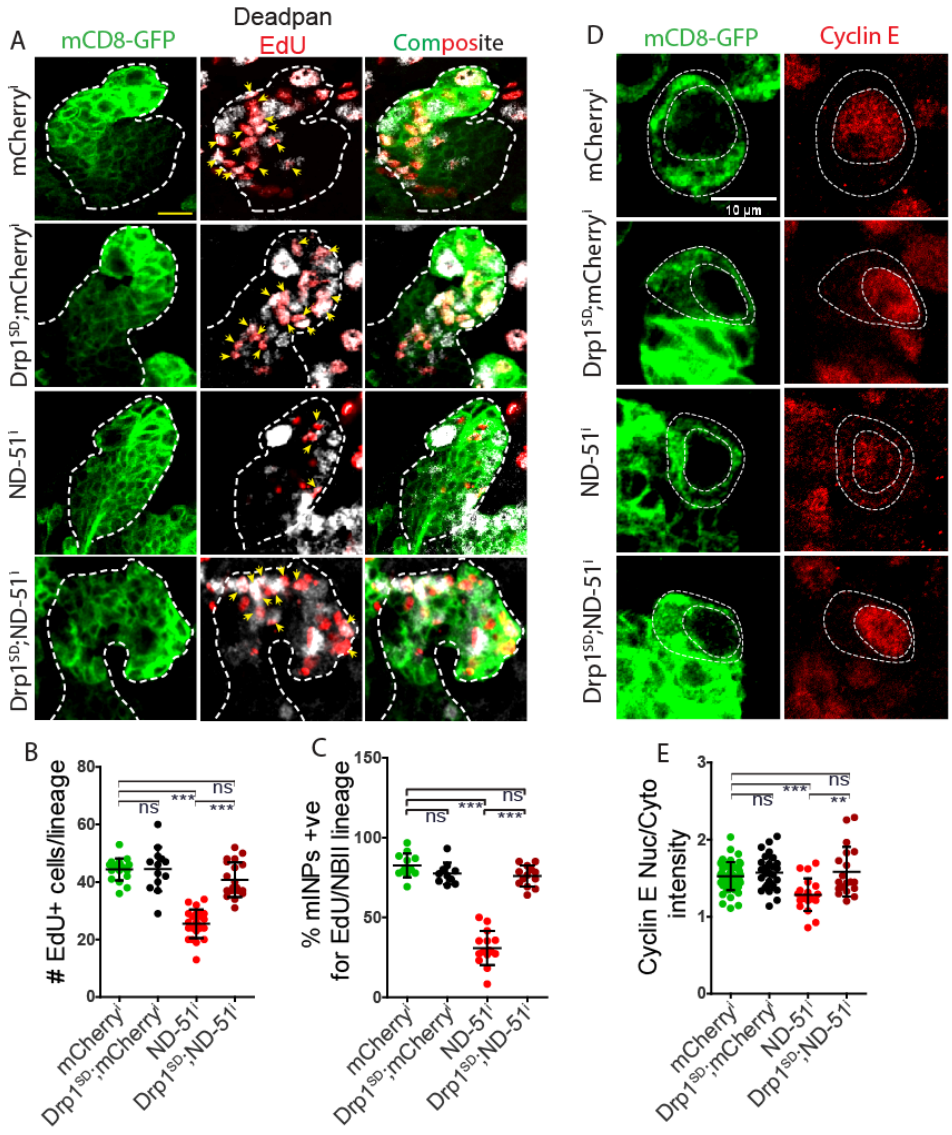


Figure 4.11: Depletion of complex I in type II neuroblasts inhibits G1-S phase progression by reducing Cyclin E levels. This cell cycle defect is rescued by promoting mitochondrial

fusion. (A) Representative images showing the labelling of mature INPs (gray) and EdU positive cells (red) in the lineages of type II neuroblasts of the mentioned genotypes. We analysed mature INPs present in S-phase by counting cells labelled for both Deadpan and EdU. Scale bar- 10µm. **(B)** Quantification of total EdU positive cells in the lineages of type II neuroblasts of genotypes:mCherry^{i} (n=19 type II neuroblasts lineages, 6 brains), Drp1^{SD};mCherry^{i} (13, 5), ND-51^{i} (23, 6), Drp1^{SD};ND-51^{i} (20, 4). **(C)** Quantification of % EdU positive mINPs (Yellow arrowheads) in the lineages of type II neuroblasts of genotypes:mCherry^{i} (n=12 type II neuroblasts lineages, 6 brains), Drp1^{SD};mCherry^{i} (11, 5), ND-51^{i} (15, 6), Drp1^{SD};ND-51^{i} (13, 4). **(D)** Representative images of cyclin E immunostaining (red) in type II neuroblasts of indicative genotypes. Type II neuroblasts are shown as encircled by white dashed line. Scale bar- 10µm. **(E)** Quantification of cyclin E intensity in the nucleus with respect to the cytoplasm of type II neuroblasts of the following genotypes: mCherry^{i} (n=62 type II neuroblasts, 9 brains), Drp1^{SD};mCherry^{i} (28, 3), ND-51^{i} (20, 3), Drp1^{SD};ND-51^{i} (19, 3). Mann-Whitney's t-test was performed for statistical analysis. ns=non-significant, **- $p<0.01$, ***- $p<0.001$.

4.3.4 Decreased MMP, mitochondrial fragmentation, cristae and increased ROS production in complex I depleted type II neuroblasts is rescued by mitochondrial fusion

Disruption of the ETC in neuroblasts leads to mitochondrial fragmentation, decreased mitochondrial activity, and altered metabolites (Bonnay et al. 2020; Yao et al. 2019). We measured the changes in MMP, cristae organization, and ROS generation to assess mitochondrial functionality in complex I-depleted type II neuroblasts. We used the potentiometric dye, Tetra-methyl-rhodamine methyl ester (TMRM), to assess MMP in living third instar larval brains. TMRM fluorescence was measured in type II neuroblasts and expressed as a ratio to neighbouring control type I neuroblasts. We observed a significant reduction in MMP in ND-51 and ND-19 depleted type II neuroblasts (Figure 4.12 A and B). Mitochondrial fusion by Drp1 depletion did not alter the MMP, and

co-expression of Drp1^{SD} with ND-51^{i} and ND-19^{i} in type II neuroblasts restored the MMP.

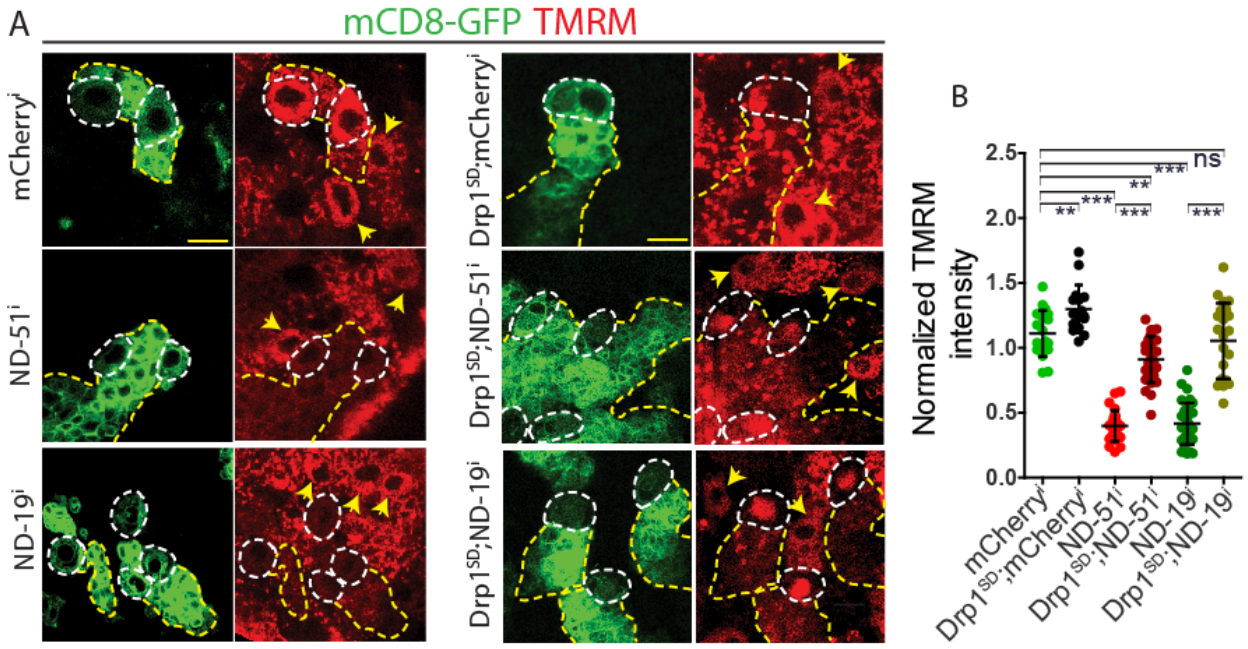


Figure 4.12: Depletion of complex I diminishes MMP in type II neuroblast and mitochondrial fusion alleviates it. (A) Representative images depicting MMP detection in type II neuroblasts of indicative genotypes using TMRM dye (red, circled by white dashed line). Surrounding control type I neuroblasts are shown by yellow arrowheads. Scale bar-10µm. **(B)** Quantification of TMRM intensity in type II neuroblast, normalized to the intensity of neighbouring type I neuroblast. The following genotypes were assessed: mCherry^{i} (n=19 type II neuroblasts, 5 brains), Drp1^{SD};mCherry^{i} (16, 5), ND-51^{i} (17, 9), Drp1^{SD};ND-51^{i} (28, 5), ND-19^{i} (34, 6), Drp1^{SD};ND-19^{i} (22, 4). Mann-Whitney's t-test was performed for statistical analysis. ns=non-significant, **- p<0.01, ***- p<0.001.

The inner mitochondrial membrane exists in a folded structure, forming a sack-like structure called cristae. Fused mitochondria can accommodate well-organised lamellar cristae, whereas fragmented mitochondria exhibit poor cristae morphology. From a

functional perspective, cristae expand the surface area of the inner mitochondrial membrane, thereby increasing ETC components, for increasing OXPHOS and higher MMP (Ikon and Ryan 2017). By concentrating ETC complexes and lowering the mean distance between them, cristae behave as a specialised compartment that ensures proper conditions for ATP synthesis (Gilkerson et al. 2003; Vogel et al. 2006; Song et al. 2013). Thus, in cristae, a local MMP is established more favourably than outside (Song et al. 2013). Therefore, cristae disruption might be the reason for reduced MMP on complex I depletion in neuroblasts. To study cristae organization, we used transmission electron microscopy in brains expressing ND-51^{i} and mCherry^{i} with *wor*-Gal4 (Figure 4.13 A-C). Control neuroblasts have elongated mitochondria that exhibit cristae-rich morphology. ND-51^{i} neuroblasts possess fragmented mitochondria and have less area than control (Figure 4.13 A and B). Also, they have fewer numbers and poorly organised cristae than mCherry^{i} control (Figure 4.13 A and C).

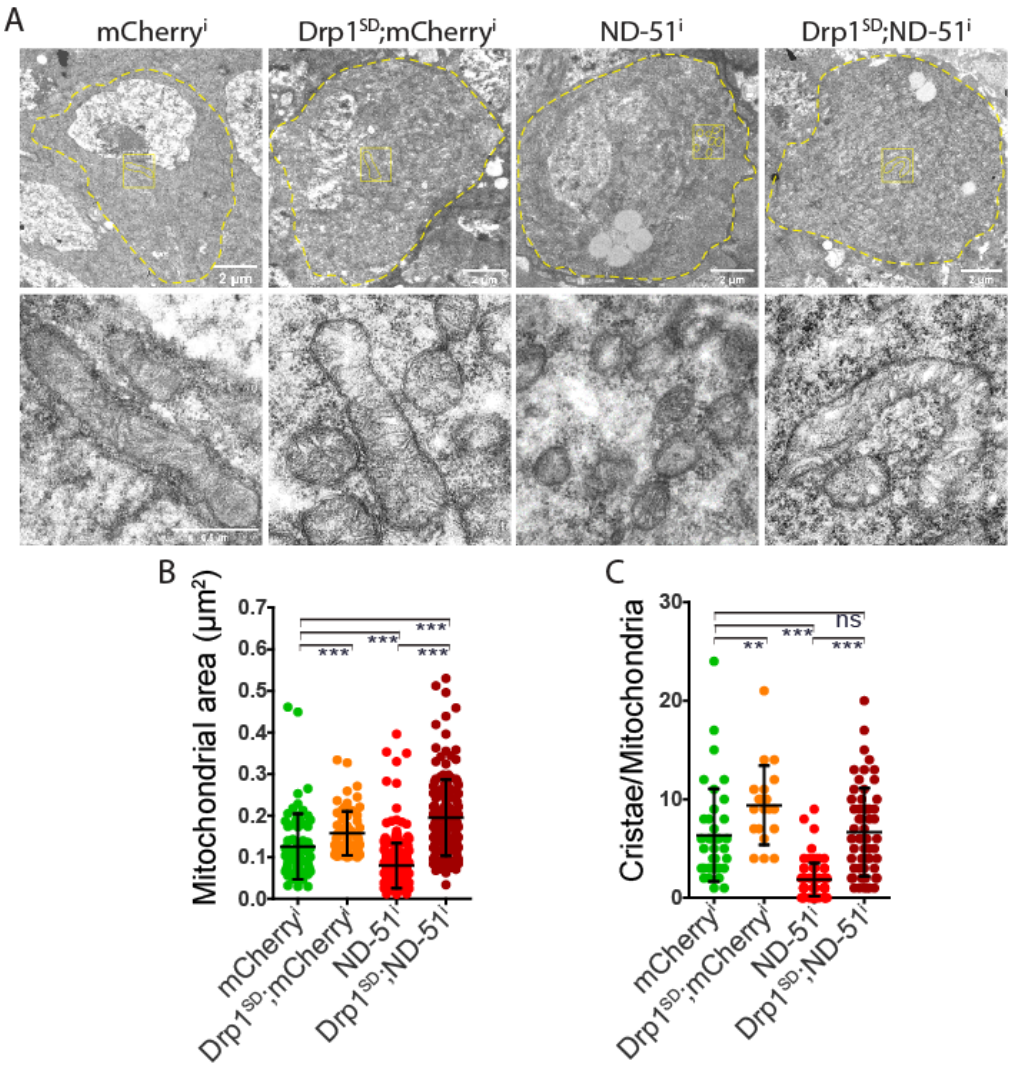


Figure 4.13: Disruption of complex I in neuroblast leads to mitochondrial fragmentation and decreased number of cristae per mitochondria, and Drp1 depletion rescues these defects. (A) Representative electron micrographs show distinct mitochondrial morphology across different genotypes. Control mCherry^{i} neuroblasts exhibit elongated mitochondria with well-developed cristae. Overexpression of Drp1^{SD} (Drp1^{SD};mCherry^{i}) results in more fused, cristae-rich mitochondria clustered on one side of the neuroblasts. Complex I depletion (*wor*-Gal4>ND-51i) leads to fragmented/circular mitochondria with less surface area than control mitochondria. In Drp1^{SD};ND-51^{i} neuroblasts, mitochondria display a mixed morphology of

fragmented and fused forms, predominantly clustered on one side with a greater number of cristae than ND-51^{i} alone. **(B)** Quantification of mitochondrial area of the following genotypes: mCherry^{i} (n=76 mitochondria, 10 neuroblasts, 3 brains), Drp1^{SD};mCherry^{i} (66, 8, 3), ND-51^{i} (247, 12, 3), Drp1^{SD};ND-51^{i} (138, 16, 3). **(C)** Quantification of cristae number in the following genotypes: mCherry^{i} (n=39 mitochondria, 10 neuroblasts, 3 brains), Drp1^{SD};mCherry^{i} (20, 8, 3), ND-51^{i} (85 mitochondria, 12, 3), Drp1^{SD};ND-51^{i} (60, 16, 3). Mann-Whitney's t-test was performed for statistical analysis. ns=non-significant, **- p<0.01, ***- p<0.001.

In Drp1^{SD};ND-51^{i} neuroblasts mitochondrial morphology and cristae number were rescued and were similar to Drp1^{SD};mCherry^{i} control (Figure 4.13 A-C). These results suggest that rescue of MMP by fusion in complex I-depleted neuroblasts is possibly through rescue of mitochondrial morphology and cristae architecture.

In *Drosophila* embryos, inhibiting ETC activity induces cellular ATP stress (Chowdhary et al. 2017). To investigate if complex I depletion induced ATP stress in type II neuroblasts, we assessed ATP levels in ND-51-depleted type II neuroblasts using the BioTracker ATP-Red Live Cell Dye. The fluorescence of the ATP-Red dye was found to be similar in complex I-depleted and control type II neuroblasts (Figure 4.14 A and B). Additionally, we examined phosphorylated AMP-activated protein kinase (p-AMPK) levels in ND-51-depleted type II neuroblasts using immunostaining. Low ATP levels elevate AMP, leading to increased p-AMPK (Willows et al. 2017). p-AMPK fluorescence was found to be similar to controls in ND-51^{i} expressing type II neuroblasts (S5 *C* and *D*). Thus, despite complex I depletion inhibiting OXPHOS, type II neuroblasts were able to sustain normal ATP levels, most likely via the glycolytic route. Literatures indicates that many stem cells rely on glycolysis for ATP generation, compared to differentiated cells, to support cellular growth and division (Ning et al. 2022; Gu et al. 2016; Liu and Chen 2021).

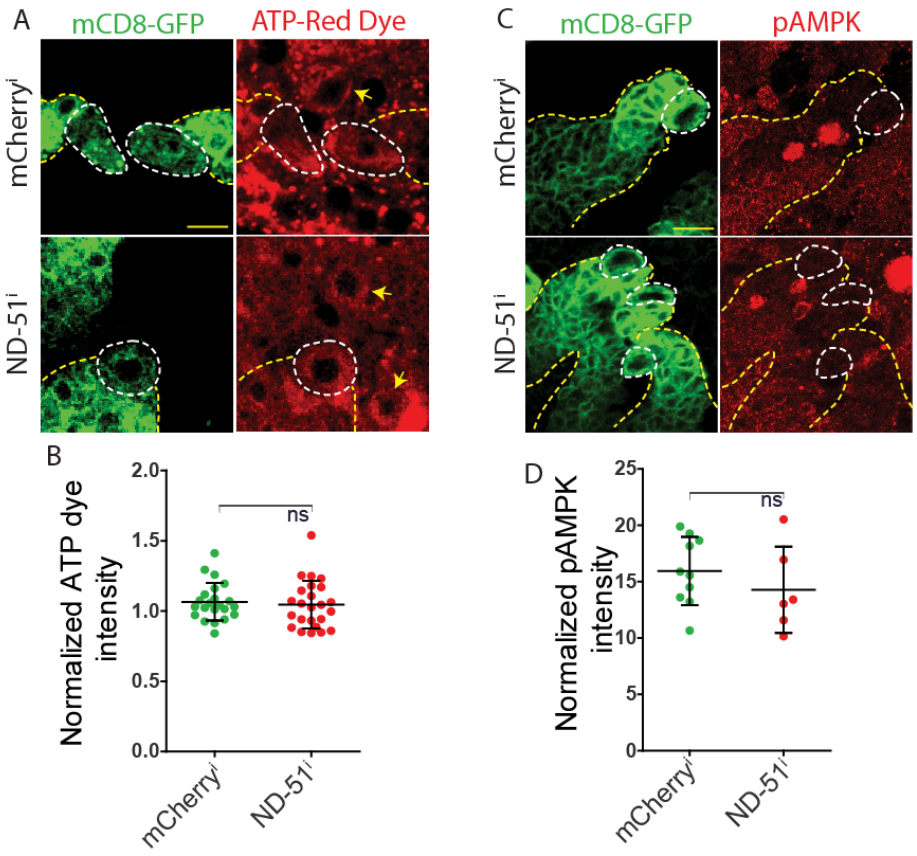


Figure 4.14: Depletion of complex I in type II neuroblast does not change the ATP levels. **(A)** Representative images of ATP detection in type II neuroblast using ATP-Red dye (red). mCD8-GFP marks the boundary of neuroblasts and lineage cells (green). White dashed circle label type II neuroblast and surrounding wild type, type I neuroblast shown by yellow arrowheads. Scale bar-10μm. **(B)** Quantification of ATP-red dye intensity normalised to surrounding type I neuroblast in genotypes, mCherry^{i} (22 neuroblast, 3 brain) and ND-51^{i} (24,3). **(C)** Representative figure of phospho-AMPK immunostaining (red) for ATP detection in type II neuroblast. There was no difference of p-AMPK in between control and complex I-depleted neuroblast. mCD8-GFP marks the boundary of neuroblasts and lineage cells (green). White dashed circle label type II neuroblast. Scale bar-10μm. **(D)** Quantification of phospho-AMPK intensity in type II neuroblast of genotypes, mCherry^{i} (10 neuroblast, 3 brain) and ND-51^{i} (6,3). Mann-Whitney's t-test was performed for statistical analysis. ns=non-significant.

Alterations in mitochondrial morphology and ETC change ROS levels in the mitochondria and the cytoplasm (Sharma et al. 2011; Ježek et al. 2018; Deng et al. 2018). The mitochondrial ETC generates ROS (Muller 2000). ROS are recognised as crucial signalling molecules in cellular processes, including stem cell maintenance and differentiation (Khacho et al. 2016; Deng et al. 2018; Owusu-Ansah and Banerjee 2009). We assessed the ROS levels in type II neuroblasts using dihydroxy ethidium (DHE) dye. DHE fluorescence in type II neuroblasts is represented as a ratio to neighbouring control type I neuroblasts. Knockdown of complex I subunits ND-51 and ND-19 in type II neuroblasts resulted in a significant elevation in ROS levels (Figure 4.15 A and B).

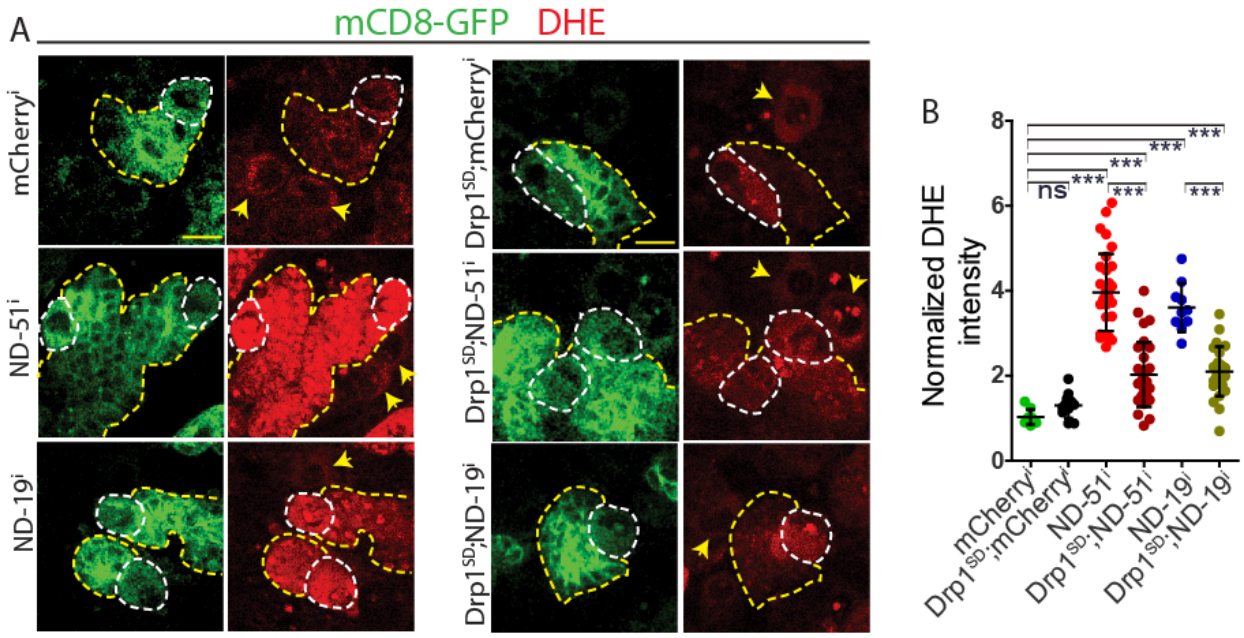


Figure 4.15: Depletion of complex I increases ROS levels in type II neuroblast, and mitochondrial fusion suppresses it. (A) Representative images showing ROS detection in type II neuroblasts ofthe mentioned genotypes using DHE dye (red, encircled by white dashed line). Control type I neuroblasts are marked by yellow arrowheads. Scale bar- 10µm. **(B)** Quantification of DHE intensity in type II neuroblast normalized to surrounding type I neuroblast of following genotypes: mCherry^{i} (n=9 type II neuroblasts, 5 brains), Drp1^{SD};mCherry^{i} (11, 5),

ND-51^{i} (32, 7), Drp1^{SD};ND-51^{i} (30, 5), ND-19^{i} (10, 3), Drp1^{SD};ND-19^{i} (26, 5). Mann-Whitney's t-test was performed for statistical analysis. ns=non-significant, ***- p<0.001.

These high ROS levels were restored in Drp1^{SD};ND-51^{i} and Drp1^{SD};ND-19^{i} neuroblasts (Figure 4.15 A and B). Existing literature suggests that, in complex I-deficient neuroblasts, mitochondrial fusion might reduce ROS generation through ETC supercomplex formation. Mitochondrial fusion facilitates supercomplex formation in the cristae. These supercomplexes make electron transport more efficient between ETC complexes by minimising the distance between them. Consequently, it reduces electron leakage and ROS production (Kohler et al. 2023; Berndtsson et al. 2020).

4.3.5 Depletion of ROS scavenging enzymes, SOD1 and SOD2 leads to differentiation defects due to a decrease in G1-S transition

To verify whether ROS indeed regulates type II neuroblast differentiation, we manipulated ROS levels in type II neuroblasts by knocking down the ROS scavenger enzymes SOD1 and SOD2. SOD2 is present in the mitochondrial matrix. However, SOD1 is mostly found in the cytosol, albeit some also localise in the intermembrane space (Koju et al. 2019). We downregulated SOD2 using RNAi (SOD2^{i}). SOD1 knockdown was done by expressing RNAi (SOD1^{i}) and expressing a dominant negative form (hSOD1). Depleting SOD enzymes in type II neuroblasts and larval muscle showed mitochondrial fragmentation (Figure 4.16A), but interestingly, MMP was not altered in SOD1^{i} type II neuroblasts but decreased slightly in SOD2^{i} (Figures 4.16B and 4.16C).

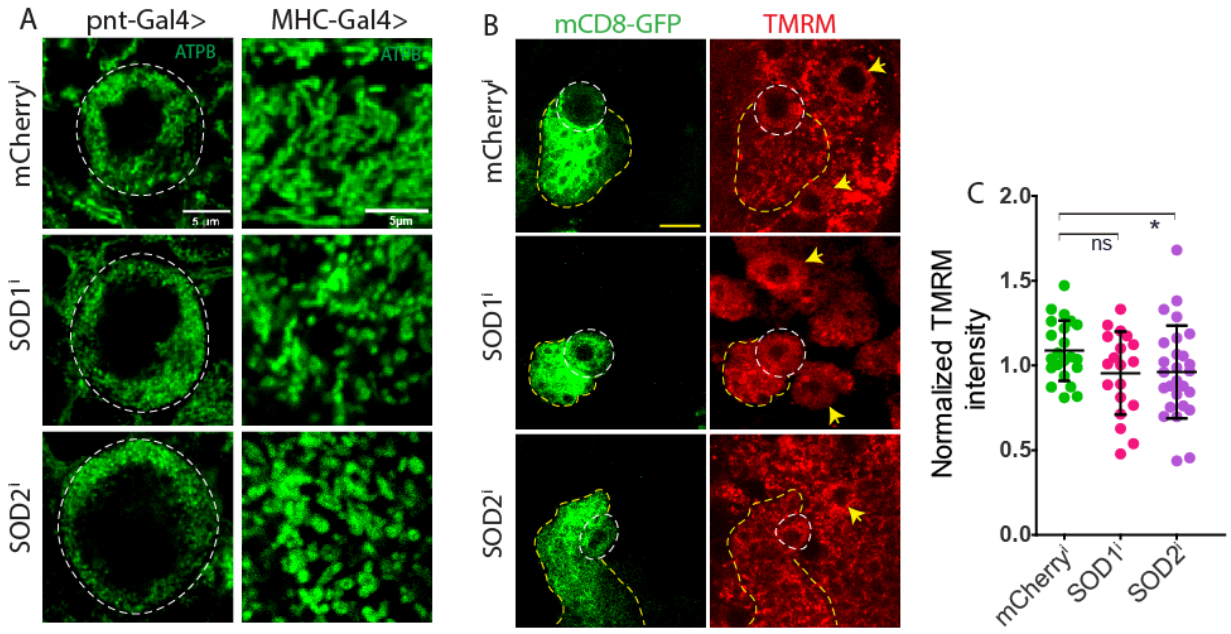


Figure 4.16: Depletion of SOD1/2 in the II neuroblast causes mitochondrial fragmentation without changing mitochondrial membrane potential. (A) Representative images of type II neuroblasts (white dashed outline) and muscle mitochondria stained by using anti-ATPB antibody (green). Knockdown of SOD1 and SOD2 in *Drosophila* type II neuroblasts and larval muscle was done using *pnt*-Gal4 and *mhc*-Gal4 respectively, induces mitochondrial fragmentation. **(B)** Representative images depicting TMRM fluorescence (red, circled by white dashed line) in type II neuroblasts. Surrounding control type I neuroblasts are shown by yellow arrowheads. Scale bar-10µm. **(C)** Quantification of TMRM fluorescence intensity in type II neuroblast, as compared to the intensity of neighbouring type I neuroblast. The following genotypes were assessed: mCherry^i (n=18 type II neuroblasts, 5 brains), SOD1^i (19,5), and SOD2^i (27,7).

Depleting SOD enzymes in type II neuroblasts using *pnt*-Gal4 resulted in elevated ROS levels (Figure 4.17 A and B).

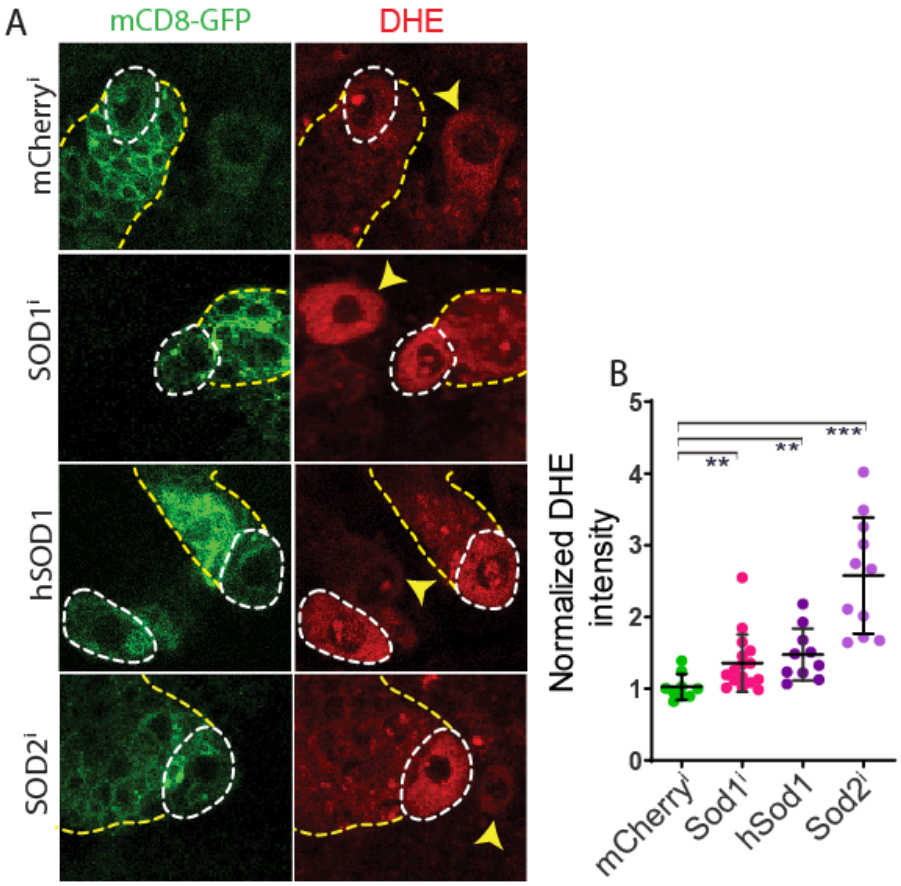


Figure 4.17: Downregulation of SOD1 and SOD2 enzymes in type II neuroblast leads to elevated ROS levels. (A) Representative images of DHE-mediated ROS detection in type II neuroblasts of the mentioned genotype. White dashed circle denotes type II neuroblast. mCD8-GFP marks the lineage cell (green). Surrounding type I neuroblast are shown by yellow arrowheads. **(B)** Quantification of DHE intensity in type II neuroblast normalized to surrounding type I neuroblasts of the following genotypes: mCherry^{i} (9 type II neuroblasts, 3 brains), SOD1^{i} (16, 3), hSOD1^{OE} (11, 3), SOD2^{i} (11, 3). Mann-Whitney's t-test was performed for statistical analysis. **- $p<0.01$, ***- $p<0.001$.

If ROS itself regulates differentiation of type II neuroblast, we expected a perturbation in its differentiation on SOD depletion. As expected, SOD1 and SOD2 downregulation in

type II neuroblasts resulted in decreased numbers of mature INPs, GMCs, and neurons in the lineages as compared to control (Figure 4.18 A-E).

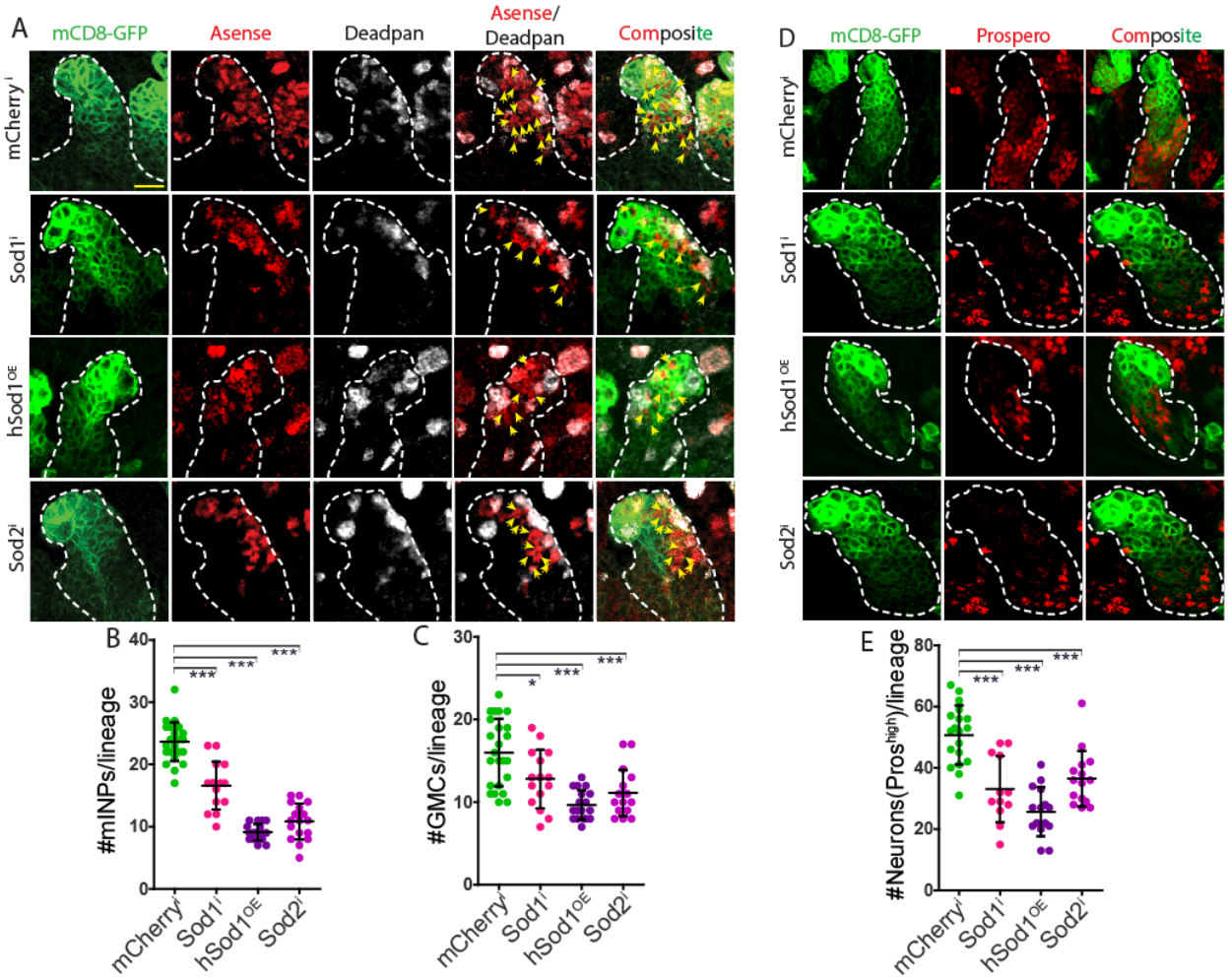


Figure 4.18. Loss of SOD1 and SOD2 leads to decreased mature INPs, GMCs, and neurons in type II neuroblasts. (A) Representative image showing staining of mINPS and GMCs of the mentioned genotypes. Deadpan positive cells are mature INPs (gray). Asense positive (red)-Deadpan negative cells are GMCs (Yellow arrowheads). **(B)** Quantification of mature INPs in type II neuroblast lineages of genotype: mCherry^{i} (n=25 type II neuroblast lineages, 5 brains), Sod1^{i} (15, 4), hSod1^{OE} (18, 4), and Sod2^{i} (17, 4). **(C)** Quantification of GMCs in type II neuroblast lineages of genotypes: mCherry^{i} (n=24 type II neuroblast lineages, 5 brains), Sod1^{i} (15, 4), hSod1^{OE} (18, 4), and Sod2^{i} (17, 4). **(D)** Representative images of neurons staining in type II neuroblast lineages of indicative genotypes. High nuclear Prospero positive

cells are neurons (red). Scale bar- 10µm. **(E)** Neurons quantification in type II neuroblast lineages of genotypes: mCherry^{i} (n=19 type II neuroblast lineages, 5 brains), Sod1^{i} (12, 3), hSod1^{OE} (15, 4), and Sod2^{i} (15, 4). Mann-Whitney's t-test was performed for statistical analysis. *- p<0.05, ***- p<0.001.

Next, we want to determine if the lower number of differentiated cells in the type II neuroblast lineage is due to cell cycle abnormalities. Therefore, we did the cell proliferation assay in SOD1 and SOD2-depleted type II neuroblasts using EdU. Downregulation of SOD1 and SOD2 leads to a decreased number of total EdU-positive cells in the lineage, and the proportion of mature INPs positive for EdU also declines (Figure 4.19 A-C). This decreased proliferation of cells in type II neuroblast lineage was

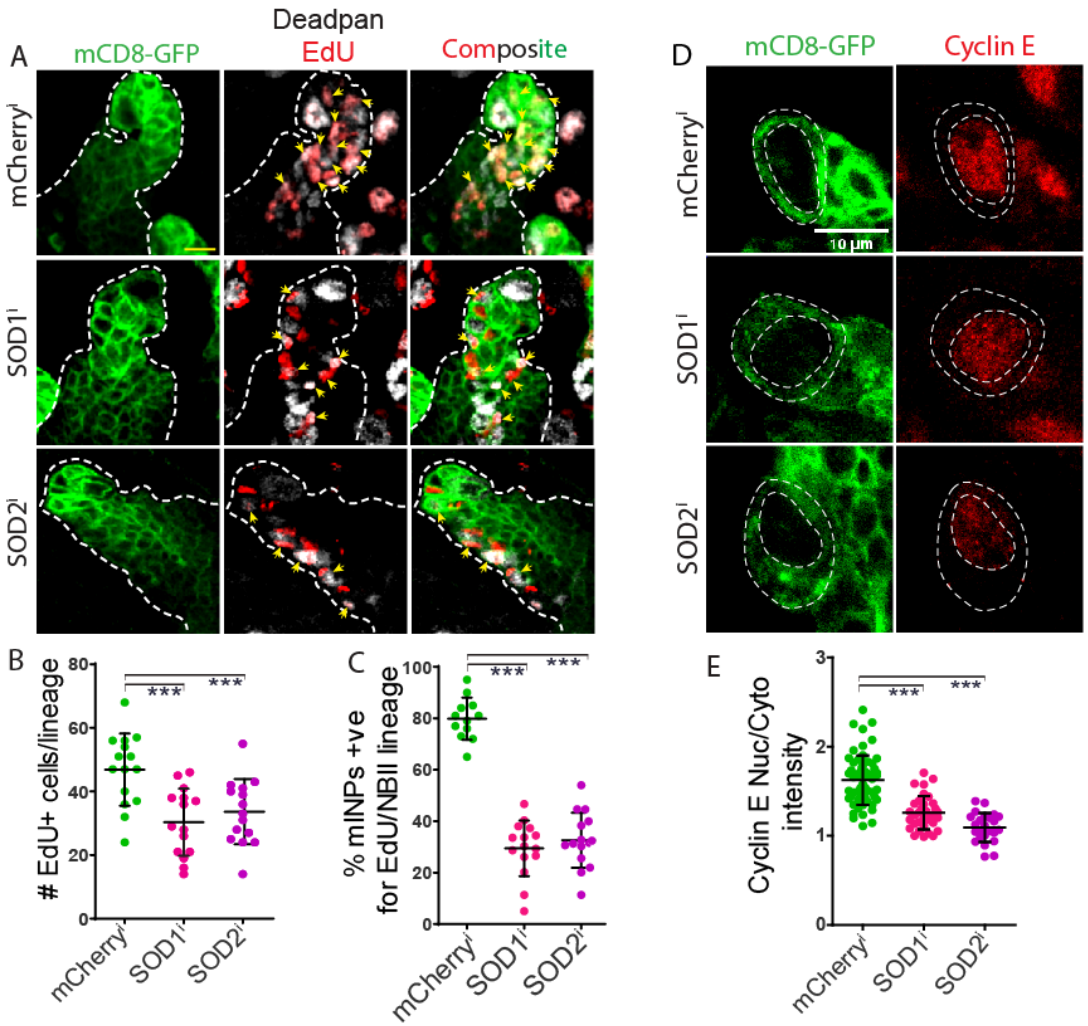


Figure 4.19: Depletion of SOD1 and SOD2 results in G1-S phase transition defects through decreasing nuclear cyclin E in type II neuroblast. (A) Representative images showing staining of mINPs and EdU-positive cells (red) in the lineages of type II neuroblasts of the mentioned genotypes. Scale bar- 10µm. **(B)** Quantification of total EdU-positive cells (red) in the lineages of type II neuroblasts of genotypes:mCherry^{i} (n=15 type II neuroblast lineages, 5 brains), Sod1^{i} (15, 5), and Sod2^{i} (15, 3). **(C)** Quantification of % EdU positive mINPs (Yellow arrowheads) in the lineages of type II neuroblasts of genotypes: mCherry^{i} (n=12 type II neuroblast lineages, 5 brains), Sod1^{i} (15, 5), and Sod2^{i} (15, 3). **(D)** Representative figures showing cyclin E immunostaining (red) in type II neuroblasts of indicative genotypes. Type II neuroblasts are shown as encircled by white dashed line. Scale bar- 10µm. **(E)** Quantification of cyclin E intensity in nucleus with respect to cytoplasm of type II neuroblast of following genotypes: mCherry^{i} (n=64 type II neuroblast lineages, 9 brains), Sod1^{i} (12, 34), and Sod2^{i} (24, 4).Mann-Whitney's t-test was performed for statistical analysis. ns=non-significant, **- $p<0.01$, ***- $p<0.001$.

consistent with the decrease of nuclear cyclin E localisation on SOD1 and SOD2 depletion (Figure 4.19 D and E).

These results imply that enhanced ROS generation in type II neuroblasts impedes nuclear cyclin E localisation, leading to proliferation defects and ultimately resulting in a decreased number of differentiated cells in the lineage.

4.3.6 Overexpression of ROS scavengers, SOD2 and Catalase in complex I depleted type II neuroblast suppresses differentiation and G1/S transition defects by lowering ROS levels

Our results show that, elevated ROS via complex I depletion or depletion of superoxide scavenging enzymes led to loss of differentiation in the type II neuroblasts, we assessed if decreasing the ROS levels in ND-51^{i} by overexpression of SOD2 and catalase would alleviate the differentiation defect in ND-51^{i}. Therefore, we generated

flies expressing SOD2^{OE};ND-51^{i} and Cat^{OE};ND-51^{i} . Overexpression of SOD2 and catalase in ND-51 depleted type II neuroblasts decreased ROS levels compared to ND-51^{i} alone (Figure 4.20 A and B).

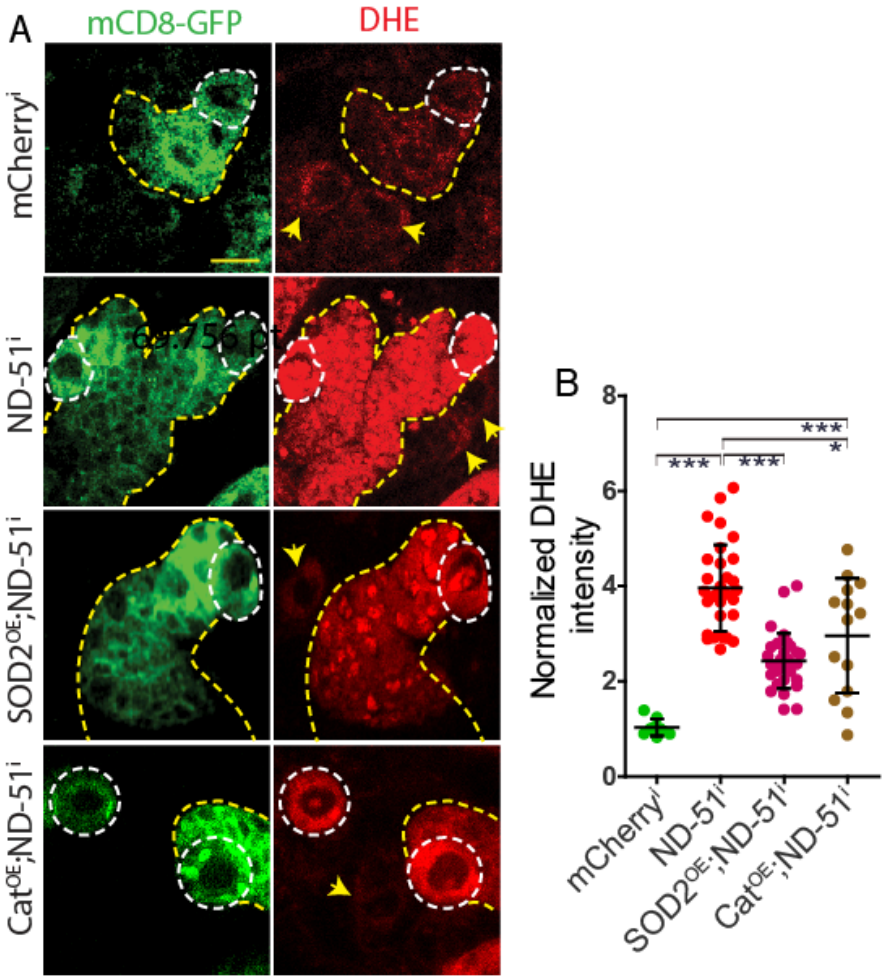


Figure 4.20: Overexpression of SOD2 and catalase in ND-51^{i} expressing type II neuroblast decreases ROS levels than ND-51^{i} alone. (A) Representative images showing ROS detection using DHE in type II neuroblast of the mentioned genotype. White dashed circle outline demarcates type II neuroblast. mCD8-GFP marks the lineage cell (green). Surrounding type I neuroblasts shown by yellow arrowheads. **(B)** Quantification of DHE intensity in type II neuroblast normalized to surrounding type I neuroblast of the following genotypes: mCherry^{i} (9 type II neuroblasts, 3 brains), ND-51^{i} (30, 5), and SOD2^{OE};ND-51^{i} (31,4) and Cat^{OE};ND-51^{i} (14,3). Mann-Whitney's t-test was performed for statistical analysis. *- p<0.05, ***- p<0.001.

Decrease of ROS levels in SOD2^{OE};ND-51^{i} and Cat^{OE};ND-51^{i} type II neuroblasts results in restoration of ND-51^{i}-mediated differentiation defects (Figure 4.21 A-E). The number of mature INPs, GMCs and neurons were higher in SOD2^{OE};ND-51^{i} and Cat^{OE}ND-51^{i} type II neuroblast lineage than ND-51^{i} alone.

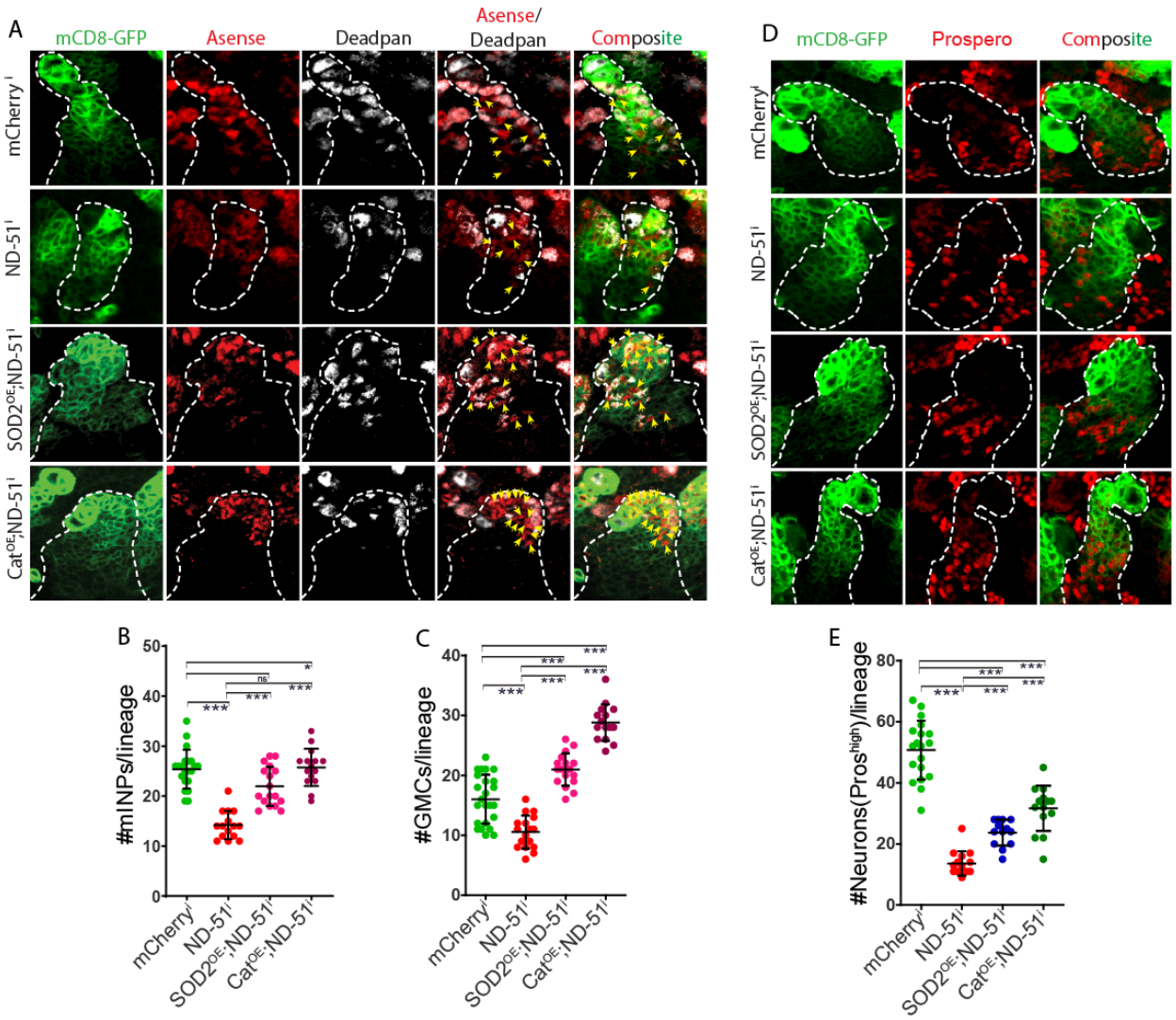


Figure 4.21: Overexpression of SOD2 and catalase in ND-51^{i} expressing type II neuroblast alleviates differentiation defects. (A) Representative image showing staining of mINPS and GMCs if type II neuroblast lineage of the mentioned genotypes. Deadpan positive cells are mature INPs (Gray). Asense positive (red)/Deadpan negative cells are GMCs (Yellow arrowheads). **(B)** Quantification of mature INPs in type II neuroblast lineages of genotype:

mCherry^{i} (n=21 type II neuroblast lineages, 6 brains), ND-51^{i} (15, 3), Sod2^{OE};ND-51^{i} (17, 5), and Catalase(Cat)^{OE} (15,5). **(C)** Quantification of GMCs in type II neuroblast lineages of genotypes: mCherry^{i} (n=24 type II neuroblast lineages, 6 brains), ND-51^{i} (17, 3), Sod2^{OE};ND-51^{i} (18, 5), and Cat^{OE} (15, 5). **(D)** Representative images of neurons staining in type II neuroblast lineages of indicative genotypes. Scale bar- 10µm. **(E)** Neurons quantification in type II neuroblast lineages of genotypes: mCherry^{i} (n=19 type II neuroblast lineages, 5 brains), ND-51^{i} (15, 3), Sod2^{OE};ND-51^{i} (13, 4), and Cat^{OE} (15, 5). Mann-Whitney's t-test was performed for statistical analysis. ns=non-significant, *- p<0.05, **- p<0.01, ***- p<0.001.

Overexpression of independent SOD2 and catalase in type II neuroblasts did not affect differentiation; the number of mature INPs, GMCs and neurons were similar to control (Figure 4.22 A-E).

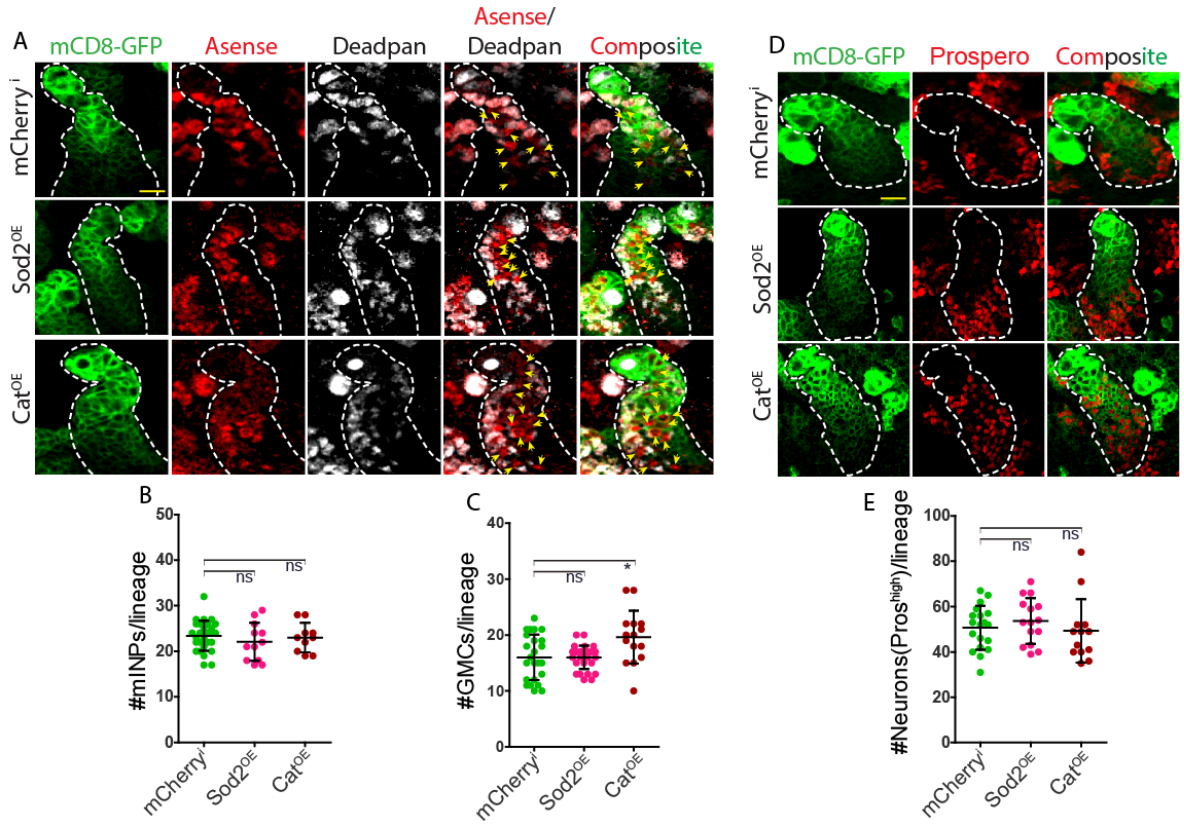


Figure 4.22: Overexpression of SOD2 and catalase independently in type II neuroblasts does not affect differentiation. (A) Representative images showing detection of mINPS and GMCs in type II neuroblast lineage of the mentioned genotypes. Deadpan positive cells are mature INPs (gray). Asense positive (red)/Deadpan negative cells are GMCs (Yellow arrowheads). **(B)** Quantification of mature INPs in type II neuroblast lineages of genotype: $mCherry^{i}$ (n=21 type II neuroblast lineages, 6 brains), $Sod2^{OE}$ (12, 3), and $Catalase(Cat)^{OE}$ (10, 5). **(C)** Quantification of GMCs in type II neuroblast lineages of genotypes: $mCherry^{i}$ (n=24 type II neuroblast lineages, 6 brains), $Sod2^{OE}$ (18, 3), and Cat^{OE} (15, 5). **(D)** Representative images of neurons staining in type II neuroblast lineages of indicative genotypes. Scale bar- 10μm. **(E)** Neurons quantification in type II neuroblast lineages of genotypes: $mCherry^{i}$ (n=19 type II neuroblast lineages, 5 brains), $Sod2^{OE}$ (15, 5), and Cat^{OE} (13, 5). Mann-Whitney's t-test was performed for statistical analysis. ns=non-significant, *- $p<0.05$.

Rescue of differentiation defects in $SOD2^{OE}$;$ND\text{-}51^{i}$ type II neuroblasts was consistent with the rescue of S-phase proliferation defects in the lineage, the number of EdU positive cells and proportion of EdU positive mINPs were higher than the $ND\text{-}51^{i}$ alone (Figure 4.23 A-C). Also, nuclear cyclin E levels in $SOD2^{OE}$;$ND\text{-}51^{i}$ type II neuroblasts were similar to those observed in controls (Figure 4.23 D and E).

$SOD2^{OE}$;$ND\text{-}51^{i}$ and expressing type II showed a loss of MMP as compared to controls and this was similar to $ND51^{i}$ (Figure 4.24 A and B), suggesting that proliferation and differentiation defects on complex I depletion are because of high ROS but not MMP loss. Since mitochondrial fusion by Drp1 depletion in complex I downregulated type II neuroblast rescued differentiation defects (Figure 4.8 and 4.9) by lowering ROS levels (Figure 4.15), we expressed $Drp1^{SG}$ (dominant negative form of Drp1) in $SOD2^{i}$ type II neuroblast. We observed that $SOD2^{i}$ mediated differentiation defects were rescued; the number of mINPs, GMCs and neurons were increased compared to $SOD2^{i}$ alone and were non-significantly different from control (Figure 4.24 A-E). These findings show a crucial role for maintenance of appropriate ROS levels by mitochondrial fusion and complex I activity in regulating differentiation in the type II neuroblast lineage.

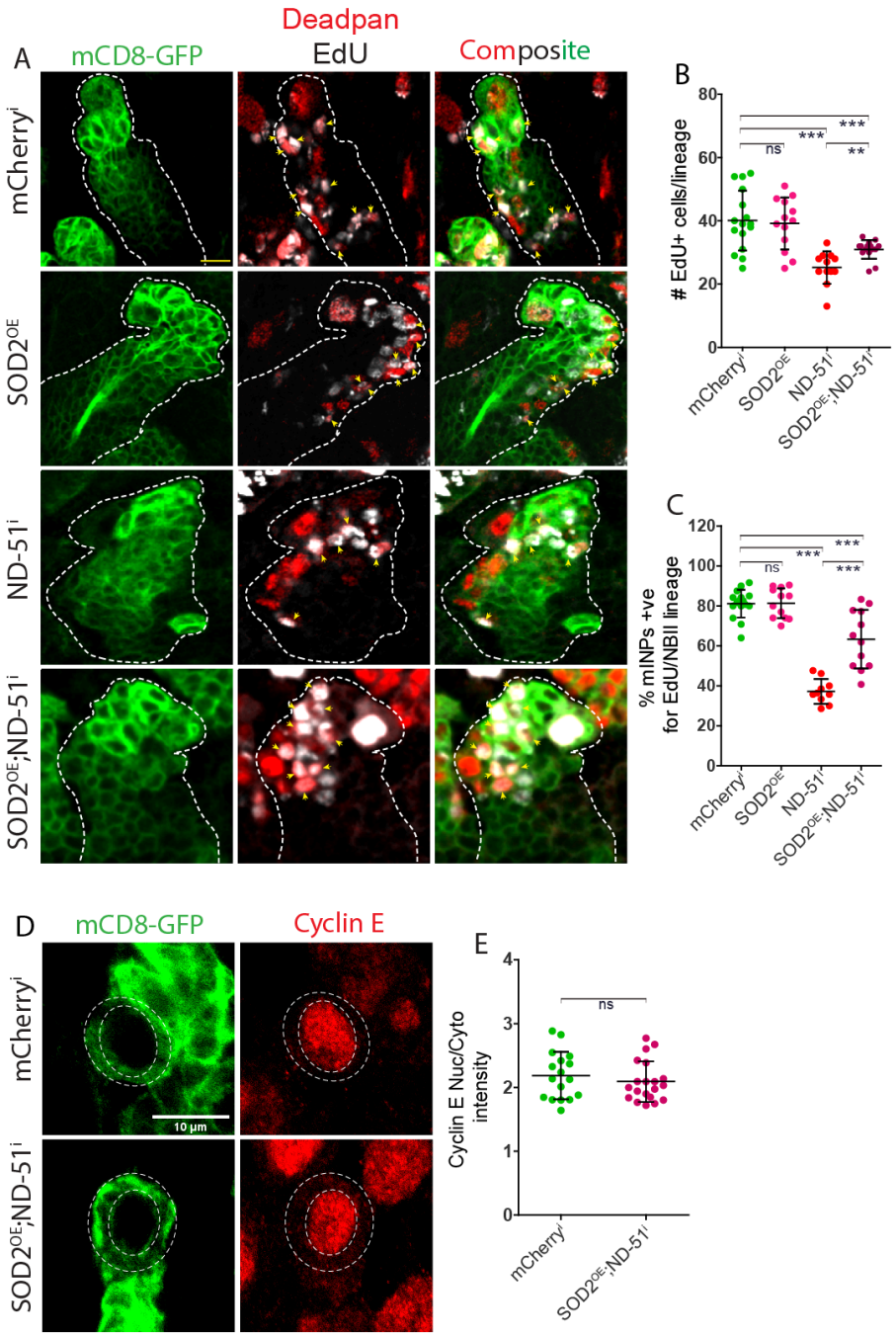


Figure 4.23: G1/S transition defect is alleviated in SOD2^{OE} in complex I depleted type II neuroblast lineages. (A) Representative images showing immunostaining of mINPs (Dpn, red) and EdU-positive cells (grey) in the lineages of type II neuroblasts of the mentioned genotypes. mINPs present in S-phase are labelled for both Dpn and EdU. Scale bar- 10µm. **(B)**

Quantification of total EdU-positive cells (grey) in the lineages of type II neuroblasts of genotypes:mCherry^{i} (n=16 type II neuroblast lineages, 3 brains), SOD2^{OE} (12,4), ND-51^{i} (15, 5), and SOD2^{OE};ND-51^{i} (12,5). **(C)** Quantification of percent EdU positive mINPs (yellow arrowheads) in the lineages of type II neuroblasts of genotypes: mCherry^{i} (n=16 type II neuroblast lineages, 3 brains), SOD2^{OE} (13,4), ND-51^{i} (10, 3), and SOD2^{OE};ND-51^{i} (15,5). **(D)** Representative images of cyclin E immunostaining (red) in type II neuroblasts (encircled by a dashed line) of indicated genotypes. Scale bar- 10µm. **(E)** Quantification of cyclin E intensity in nucleus with respect to cytoplasm of type II neuroblasts of following genotypes: :mCherry^{i} (n=17 type II neuroblasts, 3 brains) and SOD2^{OE};ND-51^{i} (20,4). Graphs show mean ± sd. Statistical analysis is done using Mann Whitney test. ns= not significant, ***- p<0.001.

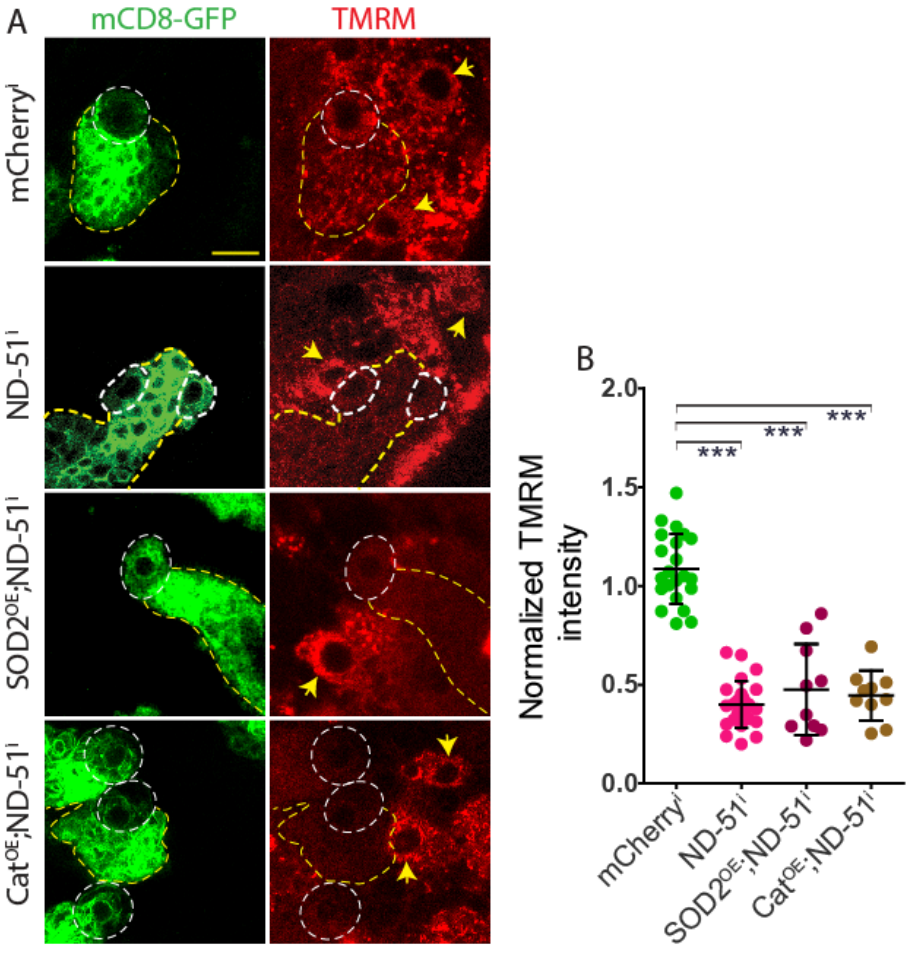


Figure 4.24: Overexpression of SOD2 and catalase in complex I depleted type II neuroblast did not rescue the MMP loss. (A) Representative images depicting TMRM

fluorescence (red, circled by white dashed line) in type II neuroblasts. Surrounding control type I neuroblasts are shown by yellow arrowheads. Scale bar-10µm. **(B)** Quantification of TMRM fluorescence intensity in type II neuroblast, as compared to the intensity of neighbouring type I neuroblast. The following genotypes were assessed: mCherry^{i} (n=18 type II neuroblasts, 5 brains), ND-51^{i} (17, 9), SOD2^{OE};ND-51^{i} (10, 4), and Cat^{OE};ND-51^{i} (10, 3).

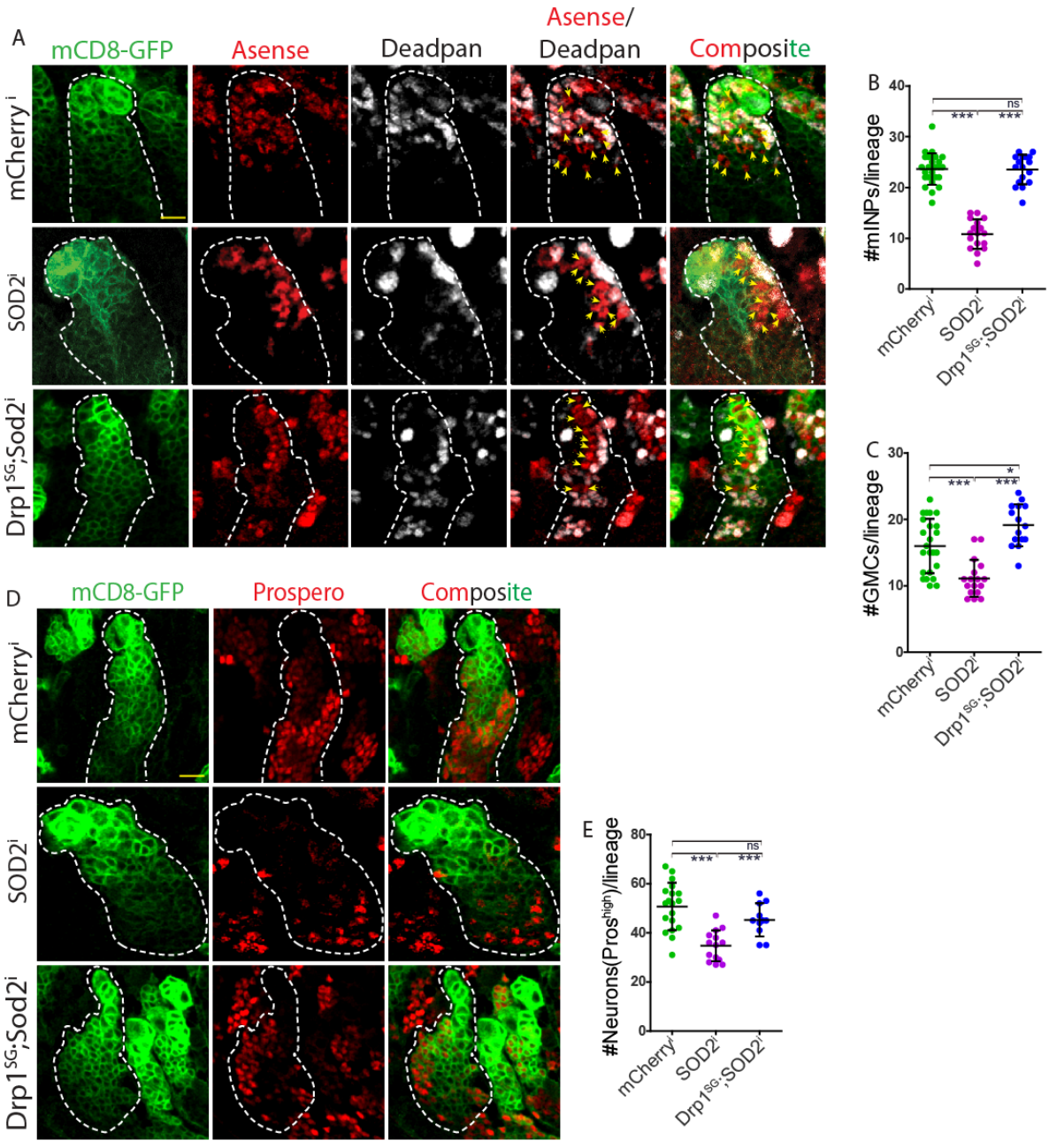


Figure 4.25: Mitochondrial fusion by Drp1 depletion rescues the differentiation defect in SOD2 depleted type II neuroblasts. (A) Representative images showing immunostaining for mINPs and GMCs of the mentioned genotypes. Dpn positive mINPs (grey). Ase positive (red)/Dpn negative cells GMCs (yellow arrowheads). **(B)** Quantification of mINPs in type II neuroblast lineages of genotype: $mCherry^{i}$ (n=25 type II neuroblast lineages, 5 brains), and $SOD2^{i}$ (17, 4), and $Drp1^{SG}$;$SOD2^{i}$ (17,4). **(C)** Quantification of GMCs in type II neuroblast lineages of genotypes: $mCherry^{i}$ (n=24 type II neuroblast lineages, 5 brains), $SOD2^{i}$ (17, 4), and $Drp1^{SG}$;$SOD2^{i}$ (15,4). **(D)** Representative images of immunostaining of neurons with high nuclear Pros (red) in type II neuroblast lineages of indicated genotypes. Scale bar- 10μm. **(E)** Quantification of neurons in type II neuroblast lineages of genotypes: $mCherry^{i}$ (n=19 type II neuroblast lineages, 5 brains), $SOD2^{i}$ (14, 4), and $Drp1^{SG}$;$SOD2^{i}$ (11,3). Data for $mCherry^{i}$ and $SOD2^{i}$ are repeated from Figure 6. Graphs show mean ± sd. Statistical analysis is done using Mann Whitney test. ns= not significant, *- $p<0.05$, **- $p<0.001$, ***- $p<0.001$.

In summary, the elevation of ROS levels in type II neuroblasts, induced by either complex I or SOD depletion, leads to mitochondrial fragmentation and differentiation defects by abrogating the G1/S phase transition. However, restoring ROS levels by overexpressing scavenging enzymes or fusing mitochondria by depleting Drp1 in these neuroblasts rescues the differentiation defects (Figure 4.26). Our studies demonstrate that relatively fused mitochondrial morphology plays a crucial role as an essential regulator of ETC activity and ROS, facilitating progression through the cell cycle for differentiation in neuroblasts of *Drosophila*.

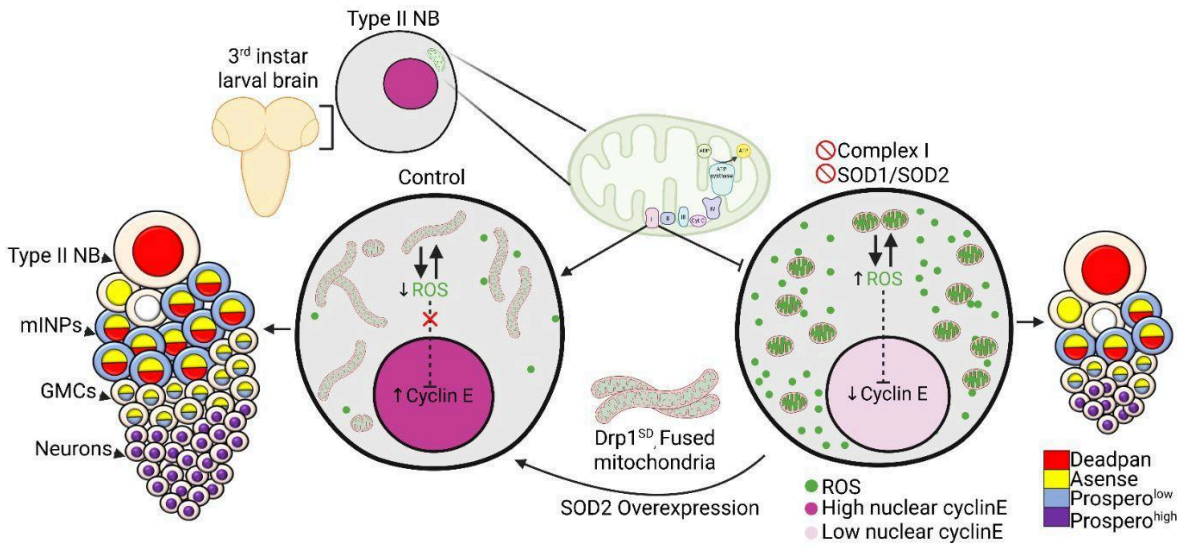


Figure 4.26: A schematic diagram representing a summary of the mechanism of complex I mediated regulation of type II neuroblast differentiation. Complex I depletion impairs neuroblast proliferation and differentiation through mitochondrial dysfunction and ROS-mediated cell cycle defects. Depletion of complex I (ND-51^{i}) in type I and type II neuroblasts results in a reduced mitotic index and a significant decrease in the number of differentiated progeny in type II neuroblast lineages. Complex I depletion increases ROS production and reduces Cyclin E levels, which is rescued by promoting mitochondrial fusion by reducing ROS levels.

4.4 Discussion

In this study, we show that complex I activity is essential for regulating proliferation and differentiation of the *Drosophila* type II neuroblast. ROS is maintained at an optimal level by mitochondrial fusion and complex I activity. This study elucidates the role of ROS and cell cycle progression as a mechanism by which complex I activity and mitochondrial dynamics control differentiation in the type II neuroblast lineage. We discuss our results in the context of the following: 1] the mechanism by which there is a change in ROS by complex I depletion and how mitochondrial fusion impacts this

change and 2] the mechanism of control of mitochondrial activity and morphology in *vivo* in stem cell differentiation.

During electron transport through ETC complexes, 0.2-2% of electrons escape ETC and interact with oxygen to form hydrogen peroxide or superoxide. (Cadenas and Davies 2000). Complex I and complex III, are the main sites of ROS production in mitochondria (Brand 2010). Dysfunctionality of complex I or its inhibition by rotenone leads to inefficient transfer of electrons, leading to their build up and increase in ROS by reaction with oxygen in the mitochondria (Sharma et al. 2009). We observed an increase of ROS on complex I depletion by depleting its subunits ND-51 or mammalian NDUFV1 and ND-19 or mammalian NDUFA8. ND-51 belongs to the core hydrophilic matrix and catalyses the oxidation of NADH to NAD+ and is part of ~815kDa complex I assembly intermediate. Downregulation of ND-51 and ND-19 in *Drosophila* muscle decreases complex I assembly (Garcia et al. 2017). Thus, disruption of complex I formation in type II neuroblasts on ND-51 and ND-19 knockdown may cause complex I to lose electrons and produce ROS.

Reverse electron transfer (RET) may be another possibility. RET catalyses the reduction of matrix NAD+ with electrons provided by $CoQH_2$. The electrons from complex I and II are transferred to $CoQH_2$, some of which are further moved to complex III (FET, forward electron transfer), and others flow back to complex I (RET). Excessive ROS is generated during RET compared to FET, presumably due to the dissociation of $FMNH_2$ from complex I and the reaction with matrix O_2 (Ten and Galkin 2019). FMN and the CoQ reduction sites of complex I are centres for ROS production during RET (Lambert and Brand 2004; Murphy 2016). In complex I deficient neuroblasts, mitochondrial fusion might reduce ROS generation via facilitating ETC supercomplex formation in the cristae. These supercomplexes make electron transport more efficient between ETC complexes by minimising the distance between them (Kohler et al. 2023; Berndtsson et al. 2020).

Decrease in complex I subunits leads to mitochondrial fragmentation. This is likely to occur due to alteration of mitochondrial fusion and fission proteins or impact of ROS on

mitochondrial fusion and fission proteins. Complex I inhibition by rotenone induces mitochondrial fission in a Drp1 dependent manner in neurons in the Parkinson's disease model (Barsoum et al. 2006). Decreasing mitochondrial fission by expressing a dominant-negative Drp1 or overexpressing Mfn led to the inhibition of apoptosis of these neurons. Increase in ROS has also been shown to increase expression of Drp1 and activate Drp1 fission by increasing phosphorylation at the 616 residue in mouse hippocampal neurons (Chang et al. 2023; Ježek et al. 2018). ROS can also lead to mitochondrial fission by reducing fusion proteins by leading to their damage due to oxidation.

Chapter 5

Depletion of electron transport chain complex II causes proliferation and differentiation defects in *Drosophila* neural stem cells

---

5.1 Introduction

Complex II, also called succinate dehydrogenase. It takes electrons from succinate, an intermediate metabolite in the TCA cycle. It's the only ETC complex that shares an intermediate with the TCA cycle. FAD in complex II accepts two electrons when succinate oxidizes to fumarate and transforms into $FADH_2$. Like complex I, $FADH_2$ transfers 2 electrons to Fe-S clusters before passing them on to coenzyme Q (Ubiquinone). However, complex II does not translocate any protons across the membrane; therefore, this pathway produces less ATP (Yankovskaya et al. 2003; Horsefield et al. 2004). Mammalian and many bacterial complex II exhibit two hydrophobic subunits anchored into the inner membrane, SdhD and SdhC, their interface have one heme b, which forms the binding site for ubiquinone (Figure 5.1). Complex II have two hydrophilic subunits located to the matrix side of the inner mitochondrial membrane, a FAD binding (SdhA) subunit, catalyze succinate to fumarate conversion and iron-sulfur (FeS) cluster binding subunit, SdhB. Disruption of complex II has been shown to perturb cellular energy homeostasis. Many cancers and individuals with mitochondrial respiratory insufficiency have been shown to contain mutations in Complex II subunits (Astuti et al. 2001; Niemann and Müller 2000; Baysal et al. 2000; Bourgeron et al. 1995). In our study of RNAi screening in *Drosophila* neuroblast, we

found complex II subunit SdhD lethal; therefore, we further used this line to study its role in neuroblast proliferation and differentiation.

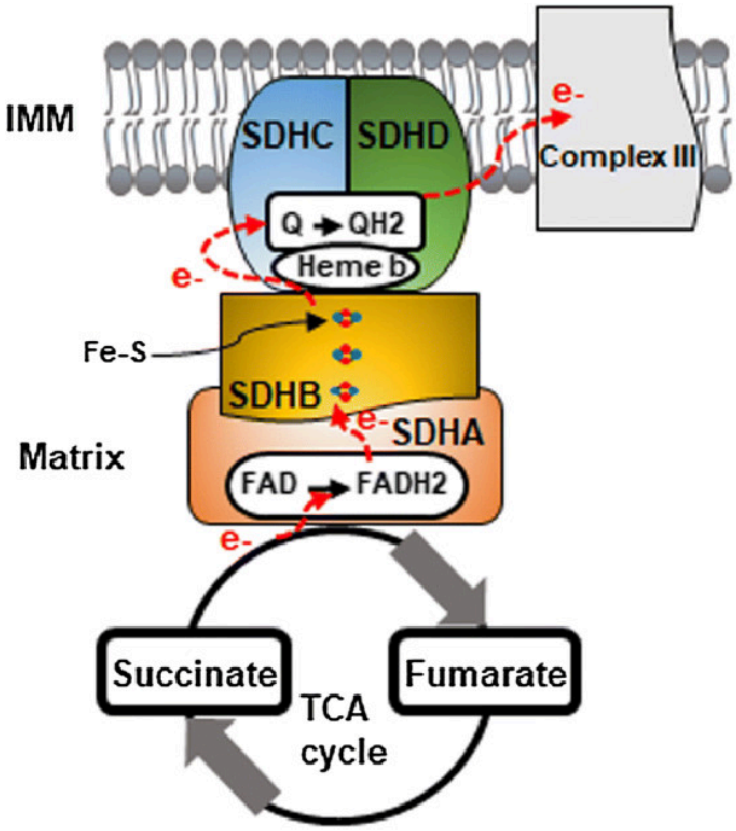


Figure 5.1: Schematic showing the structure of complex II (succinate dehydrogenase), which links the TCA cycle to OXPHOS. SDHA and SDHB oxidize succinate to fumarate. Electrons derived from this process reduce FAD into FADH2 catalysed by SDHA. FADH2 then donates electrons to Fe–S clusters in SDHB, and ultimately reduces ubiquinone before transfer to complex III. Figure adapted from (Moosavi et al. 2019).

5.2 Materials and methods

5.2.1 Fly stocks

5.2.1.1 Gal4 flies: *pnt*-Gal4,UAS-mCD8-GFP and *wor*-Gal4,UAS-mCD8-GFP

5.2.1.2 RNAi flies: mCherry^{i} (BL35785) and SdhD^{i} (BL65040)

The following combinations of transgenes were made by using standard fly genetics and appropriate balancers to bring the lines together: Drp1^{SD}/CyOGFP;mCherry^{i}/TM6B and Drp1^{SD}/CyOGFP;*pnt*-Gal4,UAS-mCD8-GFP/TM6B.

The *wor*-Gal4,UAS-mCD8-GFP was employed to express transgenes in all third-instar larval neuroblasts and *pnt*-Gal4,UAS-mCD8-GFP was utilised specifically for type II neuroblasts.

5.2.2 Antibodies

Primary antibodies: chicken anti-GFP (1:1000, Invitrogen, A10262), rabbit anti-Ase (1:10000, Yuh-Nung Jan, UCSF, USA), rat-anti-Deadpan (1:150, Abcam, ab195173), rabbit anti-Deadpan (1:800, Yuh-Nung Jan, UCSF, USA), mouse-anti-Prospero (1:20, DSHB, MR1A), rabbit anti-phosphohistone 3 (1:500, Invitrogen, PA5-17869), rat-anti-Miranda (1:600, Abcam, 197788).

Secondary antibodies: Alexa fluor coupled secondary antibodies (Invitrogen) were used in 1:1000 dilution: anti-chicken 488, anti-mouse 568/647, anti-rabbit 488/568/647, anti-rat 488/568/647.

5.2.3 Immunostaining

Third instar larval brains of ETC RNAi and control were dissected and processed for immunostaining following the protocol mentioned in section 2.2.3

5.2.4 Image acquisition and analysis

Fixed samples were processed for Confocal microscopy done at room temperature using LSM710 or LSM780 inverted microscope with a Plan apochromat 40x 1.4NA and

63x 1.4NA oil objective. Refer to sections 2.2.8, 2.2.9, and 2.2.10 for detailed information about image acquisition and analysis.

5.3 Results

5.3.1 ETC complex II depletion leads to an increase in the proliferation of neuroblasts at the third instar larval stage

Mitochondrial activity is a crucial regulator of mammalian stem cell proliferation and differentiation (Parker et al. 2015; Chen and Chan 2017). Blocking mitochondrial function by disrupting the electron transport chain has been shown to impair stem cell proliferation (van den Ameele and Brand 2019; Teixeira et al. 2015). Depletion of SdhD subunit of complex II perturbs cellular growth and metabolism (Bandara et al. 2021). To investigate the role of ETC **complex II** in *Drosophila* neuroblast proliferation, we assessed their mitotic index in the central nervous system of third instar larvae. Larval brains were dissected out and mitotically dividing neuroblasts were identified by co-staining them with Miranda (a neuroblast marker) and phospho-Histone 3 (pH3) ,which marks mitotic cells. We utilised the *worn*-Gal4 to express RNAi lines targeting Complex II subunit, SdhD. mCD8-GFP marked the plasma membrane in cells expressing Gal4 and RNA^{i}. Unlike complex I depletion, we observed a significant increase in the proportion of mitotically active neuroblasts within each brain lobe (Figure 5.2 A and B).

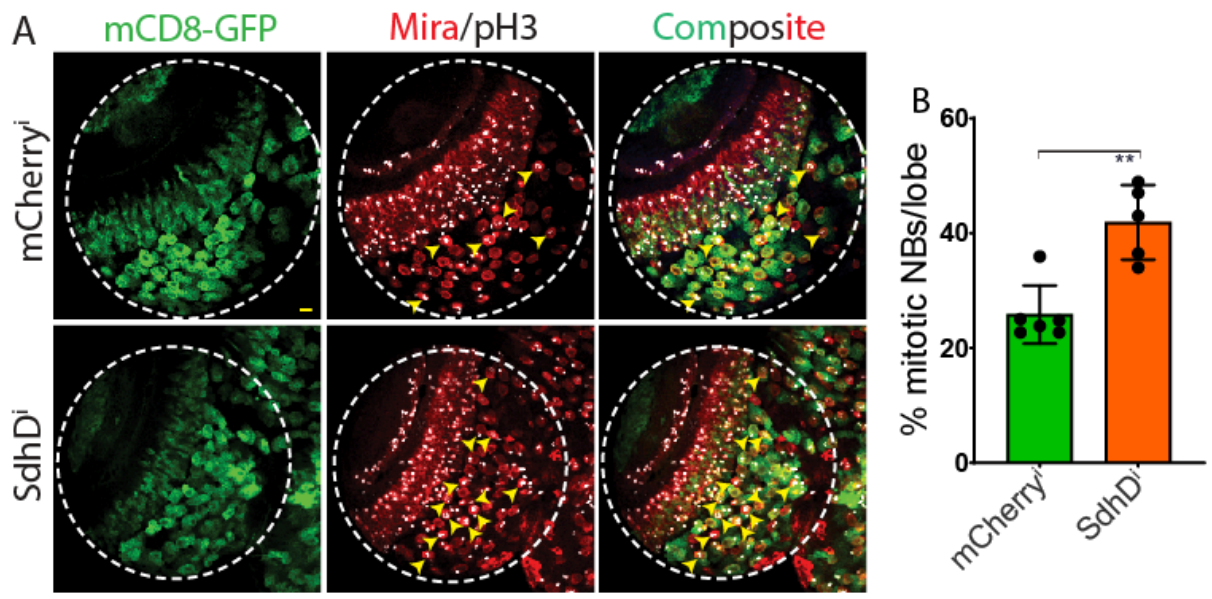


Figure 5.2: Deletion of complex II leads to increased proliferation of neuroblasts in the third instar larval brain. (A) Representative images of mitotically dividing neuroblasts (Yellow arrowheads) in the *Drosophila* third instar larval brain lobe (white dashed outline) of indicative genotypes. *wor*-Gal4 driven UAS-mCD8-GFP marks the boundary of stem cells and its lineage (green). Miranda label neuroblast cortex (red) and mitotically dividing cells are labelled by phospho-Histone H3 (pH3) (grey). Scale bar- 10µm. **(B)** Graph showing the quantification of percent mitotically dividing neuroblasts present in each brain lobe of third instar larvae, expressing *wor*-Gal4 driven mCherry^{i} (607 NSCs, 6 brains) and SdhD^{i} (490, 4).Mann-Whitney's t-test was performed for statistical analysis. **- $p<0.01$.

5.3.2 Complex II depletion in type II neuroblasts leads to differentiation defects

We further evaluated the consequence of complex II depletion (SdhD^{i}) on the differentiation of type II neuroblasts. We quantified the number of distinct progenitor cells, mINPs, GMCs and neurons within the type II neuroblast lineage by immunostaining of RNAi and control third instar larval brain for specific markers. Consistent with the increased proliferation of neuroblasts on SdhD depletion (Figure

5.2), we found that the numbers of mINPs (Ase+, Dpn+) were increased in SdhD^{i} expressing type II neuroblast lineages as compared to mCherry^{i} expressing controls (Figure 5.3 A and B). mINPs undergo asymmetric division to produce GMCs (Ase+, Dpn-), which further symmetrically divide to form a pair of neurons or glia. Neurons show Prospero in the nucleus and are present at the base of the lineage (Bello et al. 2008; Walsh and Doe 2017). We assessed the proliferation of mINPs by co-staining with Dpn and pH3. Depletion of SdhD in type II neuroblasts resulted in an increased number of pH3-labelled mINPs within the lineage compared to control (Figure 5.3 D and E). This increased proliferation corresponded with a rise in the population of GMCs (Ase+ Dpn-) (Figure 5.3 A and C). In Spite of a larger number of GMCs in the lineage we observed that the number of neurons (high nuclear Prospero) were less as compared to control (Figure 5.3 F and G).

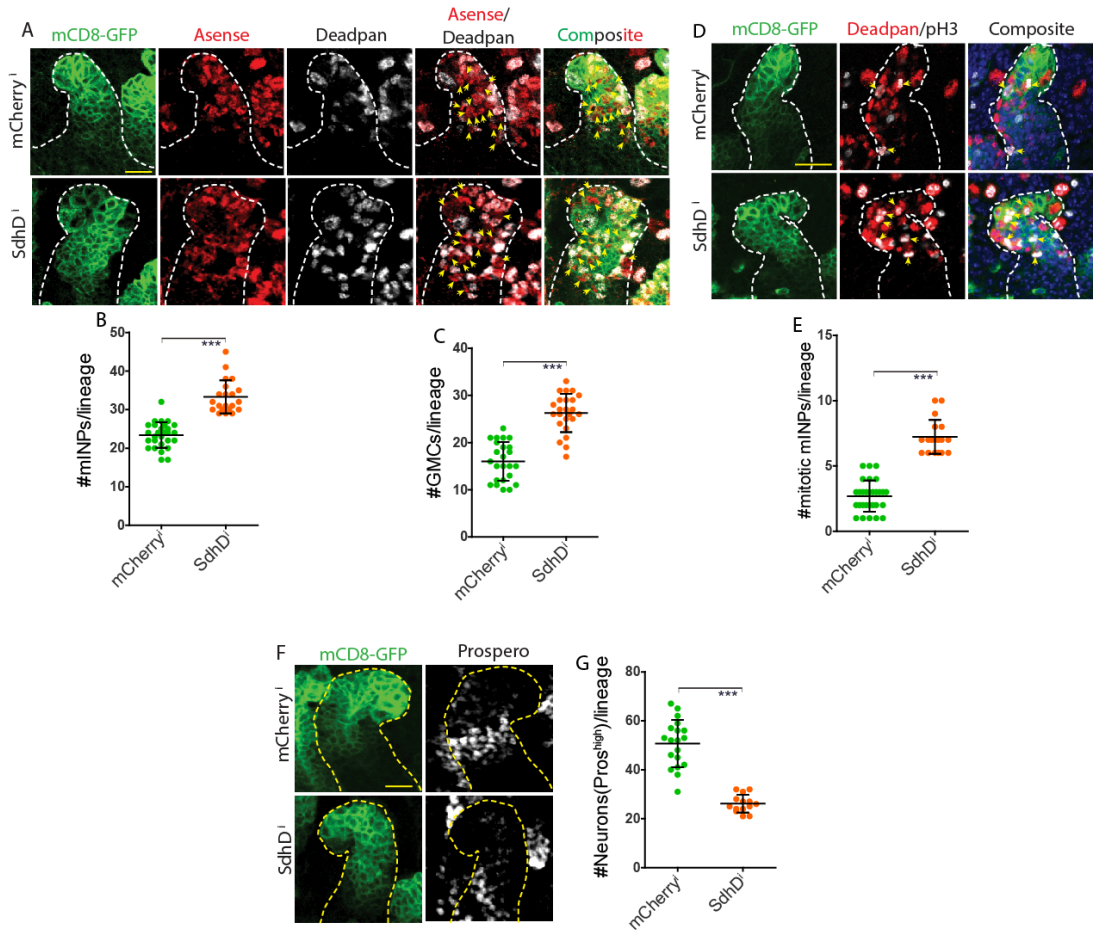


Figure 5.3: Complex II depletion in type II neuroblasts results in an increased number of mature INPs and GMCs, but decreased neurons in the lineage. (A) Representative images showing staining of mINPs and GMCs in type II neuroblast lineage of indicative genotypes. Deadpan positive cells are mature INPs (gray). Asense positive (red)-Deadpan negative cells are GMCs (yellow arrowheads). Scale bar- 10µm. **(B)** Quantification of mature INPs in type II neuroblast lineages of genotypes, mCherry^{i} (n=28 type II neuroblast lineages, 11 brains), and SdhD^{i} (21, 7). **(C)** Quantification of GMCs in type II neuroblast lineages of genotypes, mCherry^{i} (n=12 type II neuroblast lineages, 3 brains), and SdhD^{i} (24, 5). **(D)** Representative images for mitotically dividing mature INPs in the type II neuroblast lineage of the mentioned genotypes. Deadpan positive cells in the lineage mark mature INPs (red). pH3-labelled cells mark mitotically dividing cells (gray). We analysed mitotically dividing mature INPs by counting cells labelled for

both pH3 and Deadpan. **(E)** Quantification of mitotically dividing mature INPs in type II neuroblast lineages of genotypes, mCherry^{i} (n=13 type II neuroblast lineages, 5 brains), and SdhD^{i} (18, 5). **(F)** Representative images showing staining of neurons in type II neuroblast lineages of indicative genotypes. High nuclear Prospero positive cells are neurons (gray). Scale bar- 10µm. **(G)** Neurons quantification in type II neuroblast lineages of genotypes, mCherry^{i} (n=19 type II neuroblast lineages, 5 brains), and SdhD^{i} (14, 5). Mann-Whitney's t-test was performed for statistical analysis. ***- p<0.001.

5.3.3 Induction of mitochondrial fusion by depletion of Drp1 in complex II deficient type II neuroblasts does not rescue the proliferation and differentiation defects

Mitochondrial fusion is important for *Drosophila* neuroblast proliferation and differentiation (Chapter 4). Although we have not checked the mitochondrial morphology in complex II-depleted neuroblast but existing literatures show that perturbation of complex II results in mitochondrial fragmentation, decreased membrane potential, less ATP production and high ROS generation (Liot et al. 2009; Senoo-Matsuda et al. 2003). Therefore, to check if inducing mitochondrial fusion by depletion of Drp1 in complex II lacking neuroblasts could rescue the proliferation defects or not, we expressed Drp1^{SD}/SdhD^{i} in neuroblasts by crossing this with *wor*-gal4 and dissected F1 third instar larval brain. Then we stained these brains with Miranda (neuroblast marker) and pH3 (mitosis marker). In each brain lobe, the proportion of mitotically dividing neuroblasts was still similar to the SdhD^{i} alone, which was higher than the control (Figure 5.4 A and B).

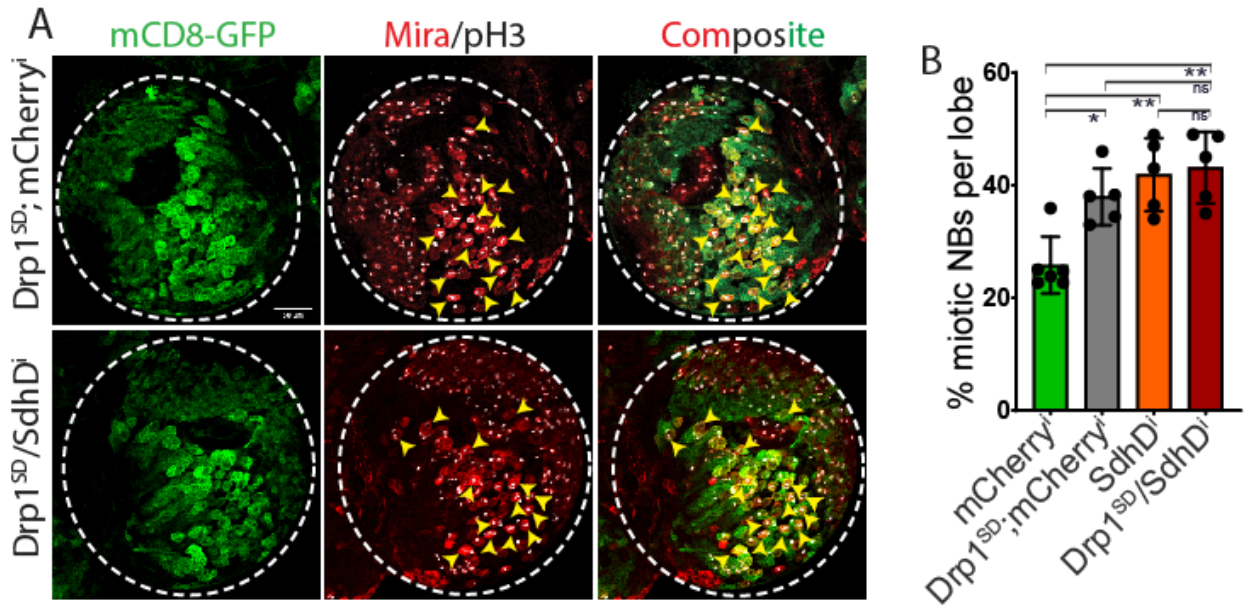


Figure 5.4: Mitochondrial fusion does not alleviate the defect of high proliferation of complex II-depleted neuroblasts in the larval brain lobe. (A) Representative images of mitotically dividing neuroblasts (yellow arrowheads) in the *Drosophila* third instar larval brain lobe (white dashed outline) of indicative genotypes. *wor*-Gal4 driven UAS-mCD8-GFP marks the boundary of stem cells and its lineage (green). Miranda label stem cell cortex (red) and mitotically dividing cells are labelled by phospho-Histone H3 (pH3) (grey). Scale bar- 50µm. **(B)** Graph showing the quantification of percent mitotically dividing neuroblast present in each brain lobe of third instar larvae, expressing *worniu*-Gal4 driven mCherry^{i} (607 NSCs, 6 brains), Drp1^{SD}; mCherry^{i} (476, 5), SdhD^{i} (490, 4), Drp1^{SD}/SdhD^{i} (488, 5). Data for all the single RNAi is repeated from section 5.3.1 for comparison. Mann-Whitney's t-test was performed for statistical analysis. ns=non-significant, *- $p<0.05$, **- $p<0.01$.

Next, we analysed the consequence of Drp1 depletion on the differentiation of SdhD^{i} type II neuroblasts. We determined the number of mINPs and GMCs in the lineages of Drp1^{SD}/SdhD^{i} expressing type II neuroblasts. The number of mature INPs and GMCs in Drp1^{SD}/SdhD^{i} was similar to SdhD^{i}, which is significantly higher than the control (Figure 5.5 A-C). Investigating the proliferation of mature INPs by co-staining with Dpn and pH3

revealed that they were dividing more, which was non-significantly different from SdhD^{i} alone Figure 5.5 D and E).

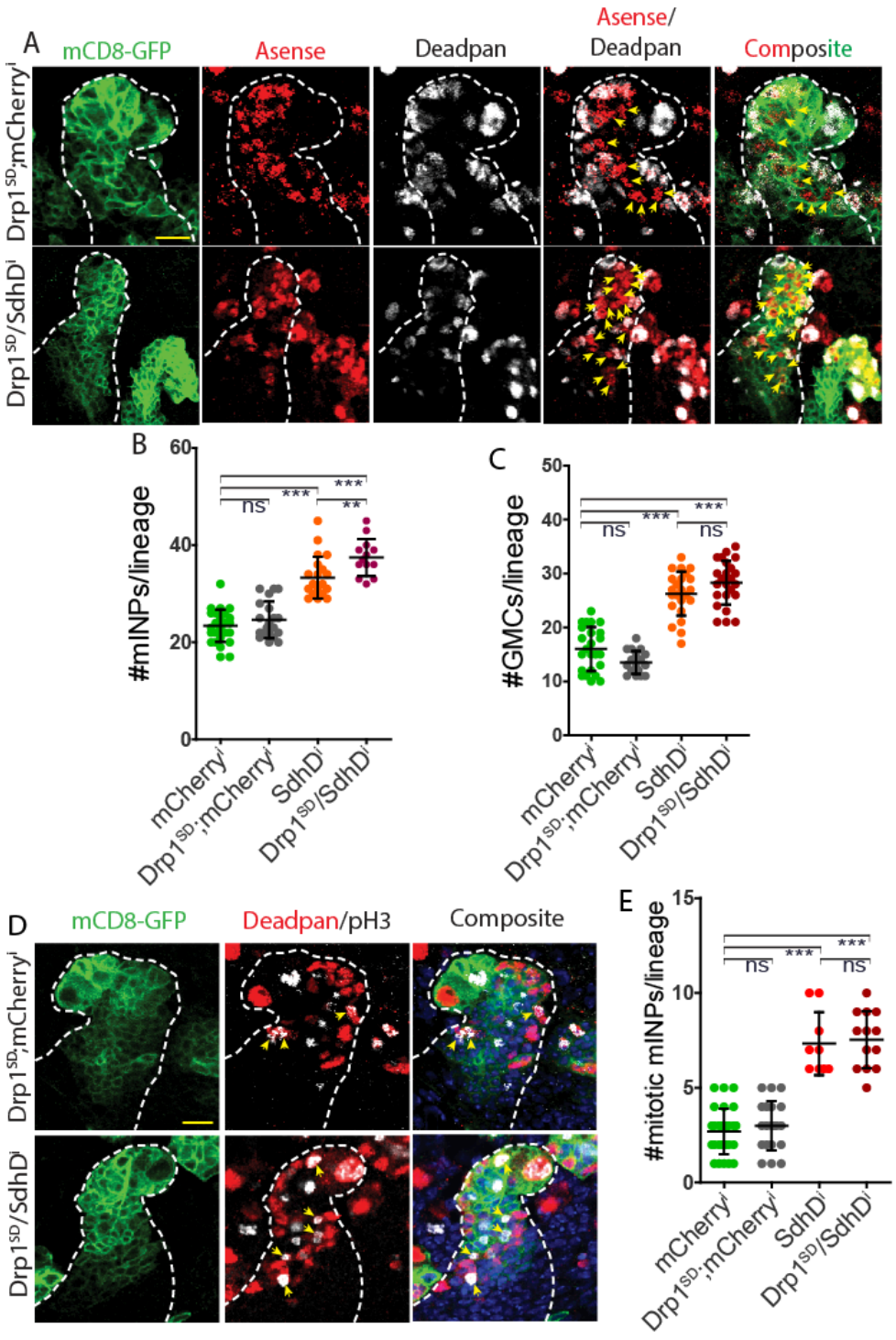


Figure 5.5: Mitochondrial fusion by Drp1 depletion in type II neuroblasts could not rescue the differentiation defects. (A) Representative images of staining of mINPs and GMCs cells in type II neuroblast lineage of indicative genotypes. Deadpan positive cells are mature INPs (gray). Asense positive (red)-Deadpan negative cells are GMCs (yellow arrowheads). Scale bar-10µm. **(B)** Quantification of mature INPs in type II neuroblast lineages of genotypes, mCherry^{i} (n=28 type II neuroblast lineages, 11 brains), Drp1^{SD}; mCherry^{i} (20, 5), SdhD^{i} (21,7), Drp1^{SD}/SdhD^{i} (21, 5). Data for all the single RNAi is taken from section 5.3.2.**(C)** Quantification of GMCs in type II neuroblast lineages of genotypes, mCherry^{i} (n=12 type II neuroblast lineages, 3 brains), Drp1^{SD};mCherry^{i} (20, 5), and SdhD$^{i\ i}$ (24, 5), Drp1^{SD}/SdhD^{i} (25, 5). Data for all the single RNAi is taken from section 6.3.2. **(D)** Representative images for mitotically dividing mature INPs in type II neuroblast lineage of the mentioned genotypes. Deadpan positive cells in the lineage marks mature INPs (red). pH3 labelled cells mark mitotically dividing cells (grey). We analyzed mitotically dividing mature INPs by counting cells labelled for both pH3 and Deadpan. **(E)** Quantification of mitotically dividing mature INPs in type II neuroblast lineages of genotypes, mCherry^{i} (n=13 type II neuroblast lineages, 5 brains), Drp1^{SD};mCherry^{i} (20, 5), SdhD^{i} (18, 5), and Drp1^{SD}/SdhD^{i} (13,5). Data for all the single RNAi is taken from section 6.3.1. Mann-Whitney's t-test was performed for statistical analysis. ns=non-significant,**-$p<0.01$, ***-$p<0.001$.

5.3.4 Complex II downregulation in type II neuroblast increases ROS production and decreases mitochondrial membrane potential

Alterations in mitochondrial ETC function change MMP and ROS levels in the mitochondria (Sharma et al. 2011; Ježek et al. 2018; Deng et al. 2018). We assessed mitochondrial activity in complex II-depleted type II neuroblasts by measuring MMP and ROS generation. Recent studies show that ROS is a crucial signalling molecule that regulates stem cell maintenance and differentiation (Khacho et al. 2016; Deng et al. 2018; Owusu-Ansah and Banerjee 2009). We assessed the ROS levels in type II neuroblasts using DHE dye. DHE fluorescence in control and RNAi type II neuroblasts was measured by quantifying its intensity using the Image J tool. We observed that

Knockdown of complex II subunit SdhD in type II neuroblasts by using *pnt*-Gal4 resulted in a significant elevation of ROS levels (Figure 5.6 A and B). Increased ROS levels suggest that depletion of SdhD subunit destabilizes the complex II assembly and resulting in leakage of electrons and combining with molecular oxygen and forming ROS.

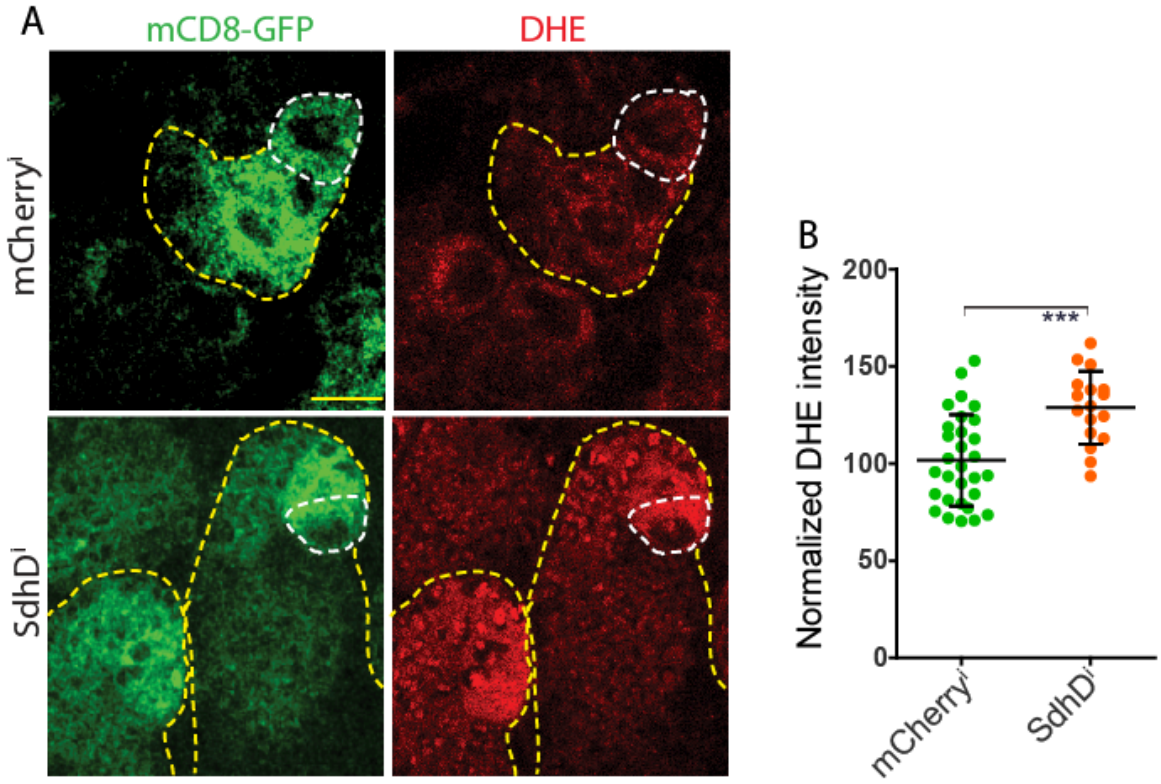


Figure 5.6. Disruption of complex II in type II neuroblast leads to elevated ROS generation. (A) Representative images showing ROS in type II neuroblasts of the mentioned genotypes using DHE dye (red, encircled by white dashed outline). Scale bar- 10µm. **(B)** Quantification of DHE intensity in type II neuroblasts normalised to background following genotypes: mCherry^i (n=30 type II neuroblasts, 5 brains), SdhD^i (17,5). Mann-Whitney's t-test was performed for statistical analysis. ***- p<0.001.

Next, we used the potentiometric dye, TMRM, to measure MMP in third-instar larval brains. TMRM fluorescence was measured in type II neuroblasts and expressed as a ratio to neighbouring control type I neuroblasts. We observed a significant reduction in MMP in SdhD-depleted type II neuroblasts (Figure 5.7 A and B).

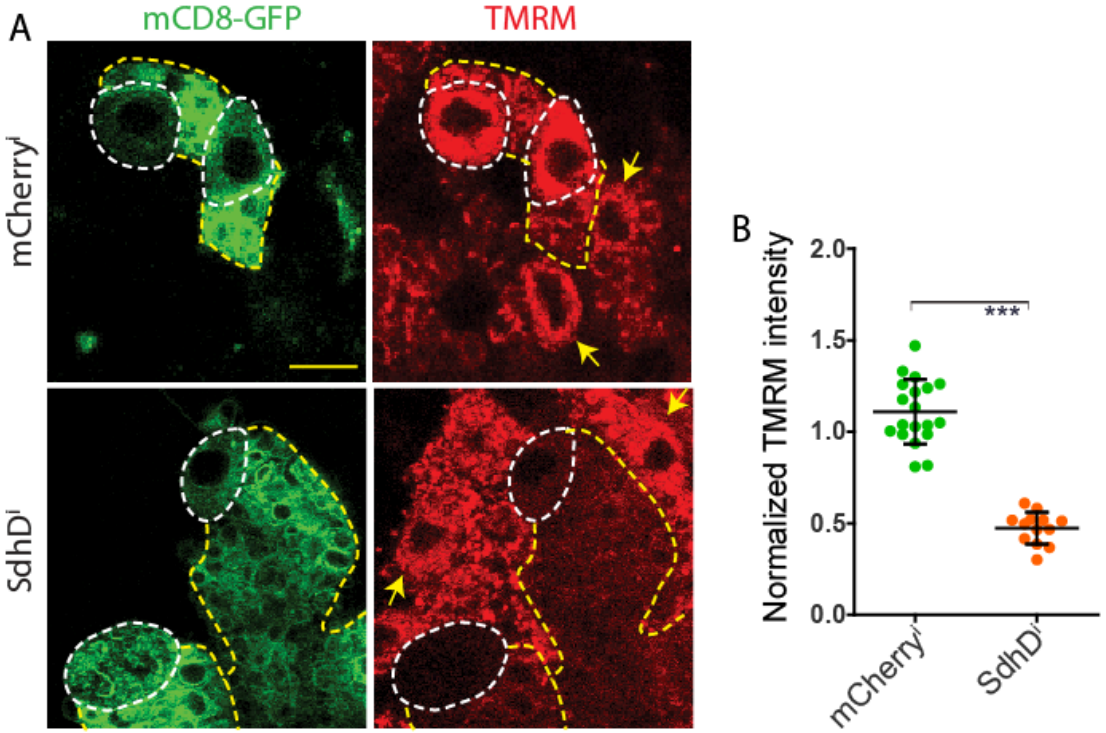


Figure 5.7: Depletion of complex II in type II neuroblasts leads to decreased mitochondrial membrane potential. (A) Representative images depicting mitochondrial membrane potential detection in type II neuroblasts of indicative genotypes using TMRM dye (red, circled by white dashed outline). Surrounding control type I neuroblasts are shown by yellow arrowheads. Scale bar- 10µm. **(B)** Quantification of TMRM intensity in type II neuroblast, normalised to the intensity of neighbouring type I neuroblast. The following genotypes were assessed: mCherry^i (n=19 type II neuroblasts, 5 brains), and SdhD^i (13,5). Mann-Whitney's t-test was performed for statistical analysis. ***- p<0.001.

5.4 Discussion

We observed that depletion of complex II subunit SdhD in type II neuroblasts increases the number of mature INPs and GMCs in the lineage, but in spite of the increased number of GMCs, neurons were fewer than control lineages. It may be because of either the decreased proliferation of GMCs or their failure to differentiate into neurons. To dissect the proliferation defect of GMCs, we can do co-staining of a GMC marker and phospho-Histone3 (mitosis marker) or EdU. We can check the GMCs differentiation into neurons by knocking down SdhD specifically in GMCs and analysing the number of neurons produced by them. We found that complex II depletion in type II neuroblasts resulted in decreased mitochondrial membrane potential and elevation of ROS generation. Knockdown of the SdhD subunit likely destabilised the entire complex, causing electron leakage and subsequent ROS accumulation. Complex II catalyses the oxidation of succinate to fumarate, and the two electrons released by this process are taken up by FAD to form $FADH_2$. $FADH_2$ then donates these electrons to ubiquinone at the site of the SdhD-SdhC interface, contributing to electron transport and membrane potential generation. Loss of SdhD may impair electron transfer to ubiquinone, thereby reducing membrane potential and increasing oxidative stress. Complex II disruption in type II neuroblasts leads to increased proliferation of neuroblasts and mature INPs, resulting in more mature INPs and GMCs in the lineage. However, complex I depletion shows decreased proliferation and fewer differentiated cells in the lineage. Although both complex I and II depletion cause similar mitochondrial activity defects (high ROS and MMP loss), they produce opposite proliferation and differentiation defects, suggesting that complex II might regulate this process by another mechanism, which is downstream of ROS. Complex II is involved in the TCA cycle and regulates FAD/$FADH_2$ levels; these metabolic functions may impact proliferation and differentiation. In future, we can check the TCA cycle intermediates and FAD/FADH2 levels in control versus complex II-depleted neuroblasts to dissect the role of complex II in regulating lineage progression.

Chapter 6

Perturbation of the electron transport chain complex IV results in proliferation and differentiation defects in *Drosophila* neural stem cells

---

6.1 Introduction

Complex IV, also known as cytochrome c oxidase (COX), is the final electron acceptor in the electron transport chain. It takes up electrons from cytochrome c to reduce molecular oxygen into water, meanwhile pumping protons from the matrix to the intermembrane space and generating membrane potential. Eukaryotic complex IV is composed of 13 subunits. The eukaryotic mitochondrial genome encodes complex IV subunits I, II, and III, which are conserved from bacteria to humans. These three subunits are present in the catalytic core of complex IV (Figure 6.1) (Tomizaki et al. 1999; Iwata 1998; Svensson-Ek et al. 2002).

Subunit I exhibit Heme a_3, a copper atom (Cu_B), and a tyrosyl group. Subunit I permits the simultaneous transfer of four electrons to O_2, inhibiting the production of intermediate ROS. Cytochrome c electrons are transmitted to heme in subunit I, then to the oxygen binding site heme a_3/Cu_B in subunit I (Ludwig et al. 2001), and lastly to the Cu_A site in subunit II, which is made up of two copper atoms (Bombelka et al. 1986). Subunit III is necessary for effective proton pumping and stabilises the core subunits (Svensson-Ek et al. 2002). Other than the mitochondrial DNA-encoded catalytic subunits I-III, the nuclear genome encodes other supernumerary subunits. Supernumerary subunits provide structural stability to the whole complex IV but are also involved in catalytic activity. Complex IV undergoes "allosteric ATP-inhibition" when bound ADP is exchanged for ATP at the matrix domain of subunit IV (Arnold and

Kadenbach 1997), and its affinity for cytochrome c is reduced when bound ADP is exchanged for ATP at the cytosolic domain of subunit IV (Napiwotzki and Kadenbach 1998).

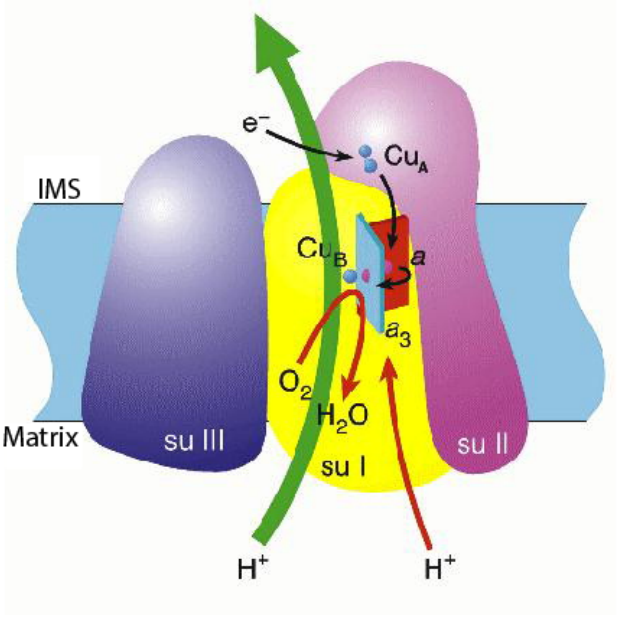


Figure 6.1: Schematic representation of the core subunits (I, II, and III)of complex IV (cytochrome c oxidase). Figure showing the spatial arrangement of the subunits within the membrane (cyan) and the orientation of metal centers (Cu_A, Cu_B, and hemes a and a3). IMS denotes interemembarne space. The diagram highlights the electron-transfer pathway (black arrow), proton uptake from matrix during oxygen reduction (red arrow), and the proton pumping activity from matrix to IMS (green arrow). Cooper atoms are shown as blue spheres, and iron atoms as magenta spheres. Figure adopted from (Scott 1995).

Binding of 3,5-diiodothyronine to Cox5A subunit eliminated "allosteric ATP-inhibition" (Arnold et al. 1998), and in complex IV from the bovine heart, an antibody to subunit Cox5A-H prevented a decrease in H^+/e^- stoichiometry from 1 to 0.5 at high ATP/ADP-ratios (Frank and Kadenbach, 1996). Furthermore, Cox4 subunit is necessary for the holoenzyme assembly (Li et al. 2006). In this chapter, we have examined the impact of nuclear-encoded supernumerary subunits of complex IV, Cox5A, Cox6C,

Cox7C, and Cox8 depletion on the proliferation and differentiation of *Drosophila* neuroblasts.

6.2 Materials and methods

6.2.1 Fly stocks

6.2.1.1 Gal4 flies: *pnt*-Gal4,UAS-mCD8-GFP, and *wor*-Gal4,UAS-mCD8-GFP

6.2.1.2 RNAi flies: mCherry^{i} (Bloomington stock, BL35785), Drp1^{S193D} (Drp1^{SD}) (Chowdhary et al. 2020; Dubal et al. 2022), Cox6C^{i} (BL33878), Cox5A^{i} (BL27548), Cox8^{i} (BL65223), Cox7C^{i} (BL62877). The following combinations of transgenes were made by using standard fly genetics and appropriate balancers to bring the lines together: Drp1^{SD}/CyOGFP;mCherry^{i}/TM6B, Drp1^{SD}/CyOGFP;Cox6C^{i} (BL33878)/TM6B, Drp1^{SD}/CyOGFP;Cox5A^{i} (BL27548)/TM6B, Drp1^{SD}/CyOGFP;*pnt*-Gal4,CD8-GFP/TM6B. The *wor*-Gal4,UAS-mCD8-GFP was employed to express transgenes in all third-instar larval neuroblasts and *pnt*-Gal4,UAS-mCD8-GFP was used specifically for type II neuroblasts.

6.2.2 Antibodies

Primary antibodies: chicken anti-GFP (1:1000, Invitrogen, A10262), rabbit anti-Ase (1:10000, Yuh-Nung Jan, UCSF, USA), rat-anti-Deadpan (1:150, Abcam, ab195173), rabbit anti-Deadpan (1:800, Yuh-Nung Jan, UCSF, USA), mouse-anti-Prospero (1:20, DSHB, MR1A), rabbit anti-phosphohistone 3 (1:500, Invitrogen, PA5-17869), mouse-anti- ATPβ (1:200, Abcam, ab14730), rabbit-anti-Cytochrome C (1:200, Cell Signaling, 4272S).

Secondary antibodies: Alexa fluor coupled secondary antibodies (Invitrogen) were used in 1:1000 dilution: anti-chicken 488, anti-mouse 568/647, anti-rabbit 488/568/647, anti-rat 488/568/647.

6.2.3 Immunostaining

Third instar larval brains of ETC RNAi and control were dissected and processed for immunostaining following the protocol mentioned in section 2.2.3

6.2.4 Image acquisition and analysis

Fixed samples were processed for Confocal microscopy done at room temperature using LSM710 or LSM780 inverted microscope with a Plan apochromat 40x 1.4NA and 63x 1.4NA oil objective. Refer to sections 2.2.8, 2.2.9, and 2.2.10 for detailed information about image acquisition and analysis.

6.3 Results

6.3.1 Complex IV disruption in *Drosophila* neuroblast leads to decreased proliferation at the third instar larval stage

Complex IV plays a significant role in regulating stem cells' proliferation, maintenance and differentiation by regulating cellular metabolism and signaling pathways. Complex IV depletion in *Drosophila* intestinal stem cells decreases their proliferation and hampers the differentiation into enteroblasts and enterocytes by overactivating FOXO signaling (Zhang et al. 2020). Deficiency of copper in Dermal papilla cells of Rex rabbit (present at the base of hair follicles) disrupts the complex IV and reduces cellular ATP production and leads to reduced proliferation (Li et al. 2022).

To assess the role of electron transport chain Complex IV in *Drosophila* neuroblast proliferation, we measured the mitotically dividing neuroblast in the brain lobe. Mitotically dividing neuroblasts were identified by co-staining with Miranda (a neuroblast marker) and pH3 (marks mitotic cells). We used *wor*-Gal4 to express RNAi lines targeting Complex IV subunits, Cox6C and Cox7C. We observed a significant reduction in the proportion of mitotically dividing neuroblasts within each brain lobe compared to

the mCherry^{i} control (Figure 6.2 A and B). In the control larval brain lobe, 25-35% of total neuroblasts (~100 neuroblasts) are present in the mitotic stage but in Cox6C and COX7C RNAi brains possess only 7-15 % dividing neuroblasts. Then, we measured the impact of complex IV depletion specifically on type II neuroblast proliferation. We depleted complex IV by downregulating its subunits, Cox5A, Cox6C, and Cox8 in type II neuroblast using *pnt*-Gal4,mCD8-GFP and immunostained the brains with anti–pH3 and anti-GFP antibody. We identified the type II neuroblast by the mCD8-GFP signal driven by *pnt*-Gal4. We observed that downregulation of each subunit of complex IV resulted in the generation of fewer dividing neuroblasts in each brain lobe (Figure 6.2 C and D).

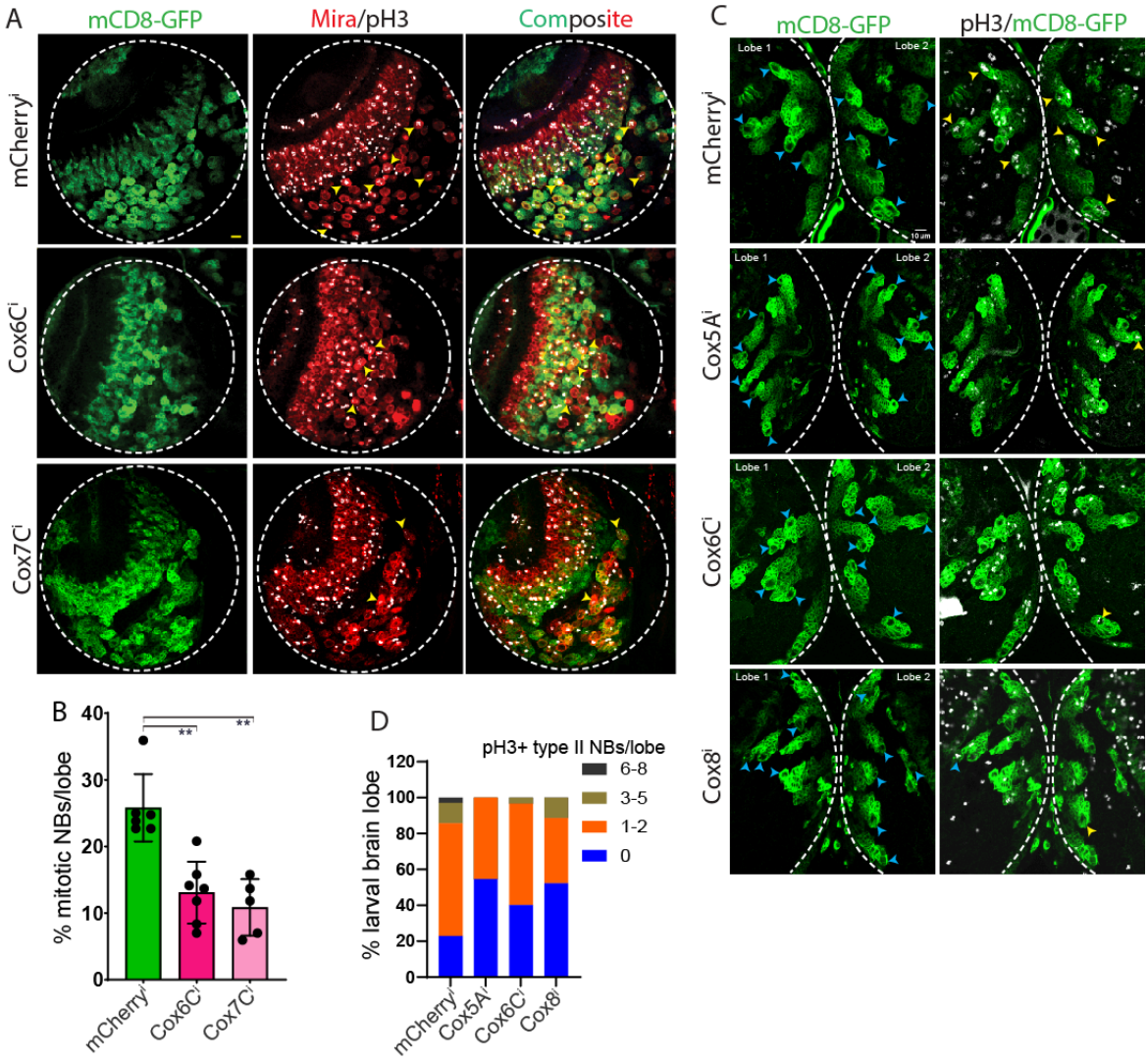


Figure 6.2: Depletion of complex IV in neuroblasts decreases their proliferation in the larval brain. (A) Representative images showing detection of mitotically dividing neuroblasts (type I and type II neuroblasts) (yellow arrowheads) inthe *Drosophila* third instar larval brain lobe (white dashed circle outline) of indicative genotypes. *wor*-Gal4 driven UAS-mCD8-GFP marks the boundary of stem cells and its lineage (green). Miranda label stem cell cortex (red) and mitotically dividing cells are labelled by phospho-Histone H3 (pH3) (grey). Scale bar- 10µm. **(B)** Graph showing the quantification of percent mitotically dividing neuroblasts present in each brain lobe of third instar larvae, expressing *wor*-Gal4 driven mCherry^{i} (n=607 NSCs, 6 brains), Cox6C^{i} (679, 6) and Cox7C (467,5). **(C)** Representative images of mitotically dividing type II neuroblasts (yellow arrowheads) in the *Drosophila* third instar larval brain of indicative genotypes. *pnt*-Gal4 driven mCD8-GFP marks the boundary of the neuroblast (blue arrowheads) and its lineage (green) and mitotically dividing cells are labelled by pH3 (grey). Scale bar- 10µm. **(D)** Quantification of mitotically dividing type II neuroblasts expressing *pnt*-Gal4 driven mCherry^{i} (n=144 NSCs, 9 brains), Cox5A^{i} (88,6), Cox6C^{i} (304,19), and Cox8^{i} (352,22). Mann-Whitney's t-test was performed for statistical analysis. ns=non-significant, *- p<0.05, **- p<0.01, ***- p<0.001.

6.3.2 Complex IV depletion in type II neuroblasts results in a decreased number of mature INPs, GMCs, and neurons in the lineage

As discussed in the previous section, the inhibition of complex IV perturbs stem cell differentiation. We assessed the role of complex IV in *Drosophila* type II neuroblast differentiation. We analysed the number of distinct progenitor cells, mINPs, GMCs and neurons within the type II neuroblast lineage by immunostaining of complex IV RNAi and control third instar larval brain for specific markers. We depleted complex IV in type II neuroblast by downregulating its subunits, Cox5A, Cox6C, Cox7C and Cox8 using *pnt*-Gal4. Consistent with the decreased proliferation of neuroblast on complex IV depletion (Figure 6.2), we found that the numbers of mature INPs (Ase+, Dpn+) were decreased in Cox5A^{i}, Cox6C^{i}, Cox7C^{i} and Cox8^{i} expressing type II neuroblast lineages as compared to mCherry^{i} expressing control (Figure 6.3 A and B). mINPs undergo asymmetric division to produce GMCs (Ase+, Dpn-).

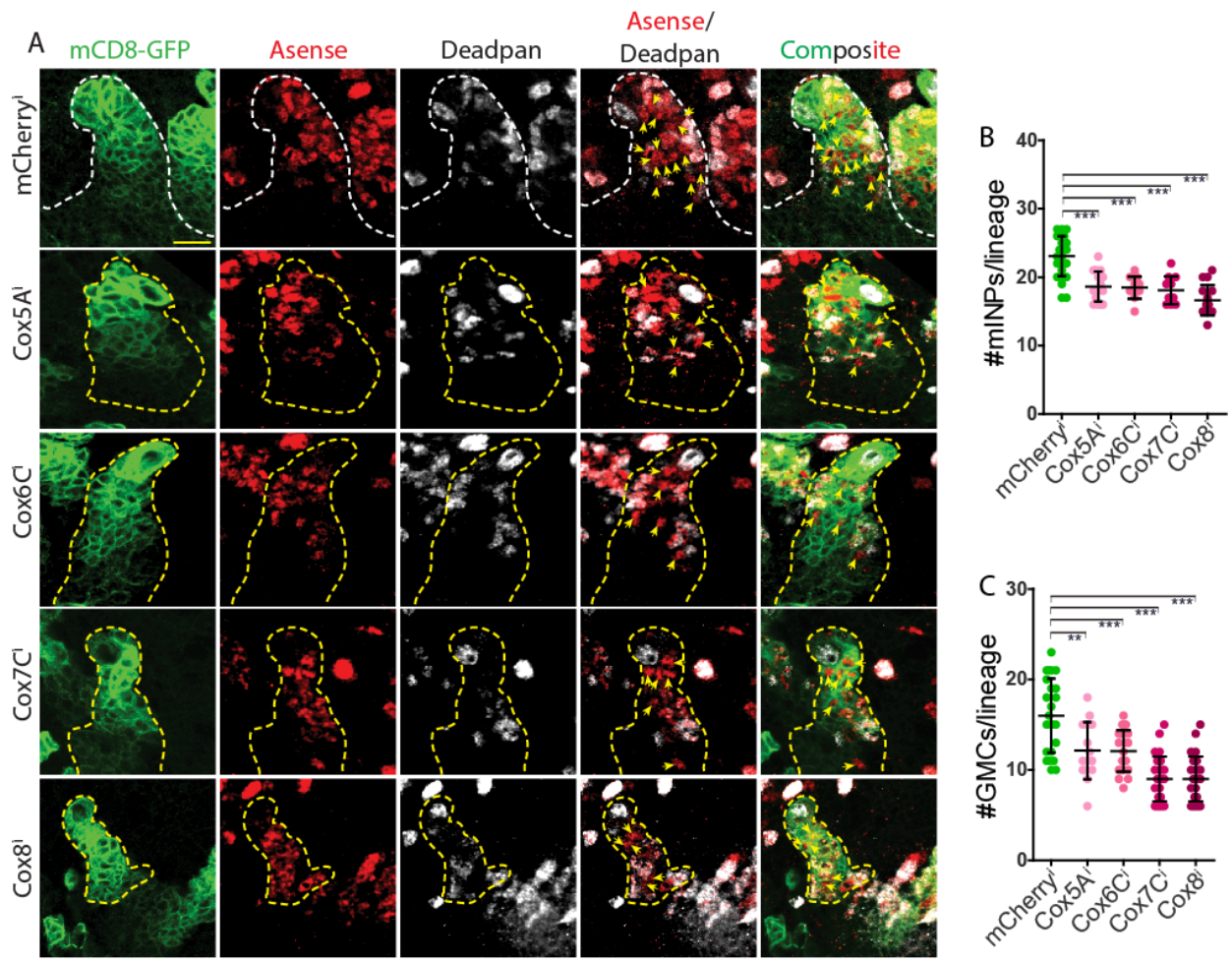


Figure 6.3: Depletion of complex IV in type II neuroblast leads to decreased number of mature INPs and GMCs in the lineage. (A) Representative figures of mINPs and GMCs detection by immunostaining in type II neuroblast lineage of indicative genotypes. Deadpan positive cells are mature INPs (gray). Asense positive (red)-Deadpan negative cells are GMCs (yellow arrowheads). Scale bar- 10µm. **(B)** Quantification of mature INPs in type II neuroblast lineages of genotypes, mCherry^i (n=28 type II neuroblast lineages, 11 brains), Cox5A^i (16,6), Cox6C^i (11,5), Cox7C^i (11,4), and Cox8^i (16,5). **(C)** Quantification of GMCs in type II neuroblast lineages of genotypes, mCherry^i (n=12 type II neuroblast lineages, 3 brains), Cox5A^i (15,6), Cox6C^i (23,5), Cox7C^i (26,4), and Cox8^i (26,5).Mann-Whitney's t-test was performed for statistical analysis. **- p<0.01, ***- p<0.001.

We further assessed the proliferation of mINPs in the lineages of Cox5A^{i}, Cox6C^{i}, Cox7C^{i} and Cox8^{i} expressing type II neuroblast by co-staining with Dpn and pH3. Knockdown of each of these subunits resulted in a decreased number of pH3-labelled mature INPs within the lineage compared to controls (Figure 6.4 A and B). This reduction in mINP proliferation resulted in producing fewer GMCs (Ase+ Dpn-) population in the lineages (Figure 6.4 A and C).

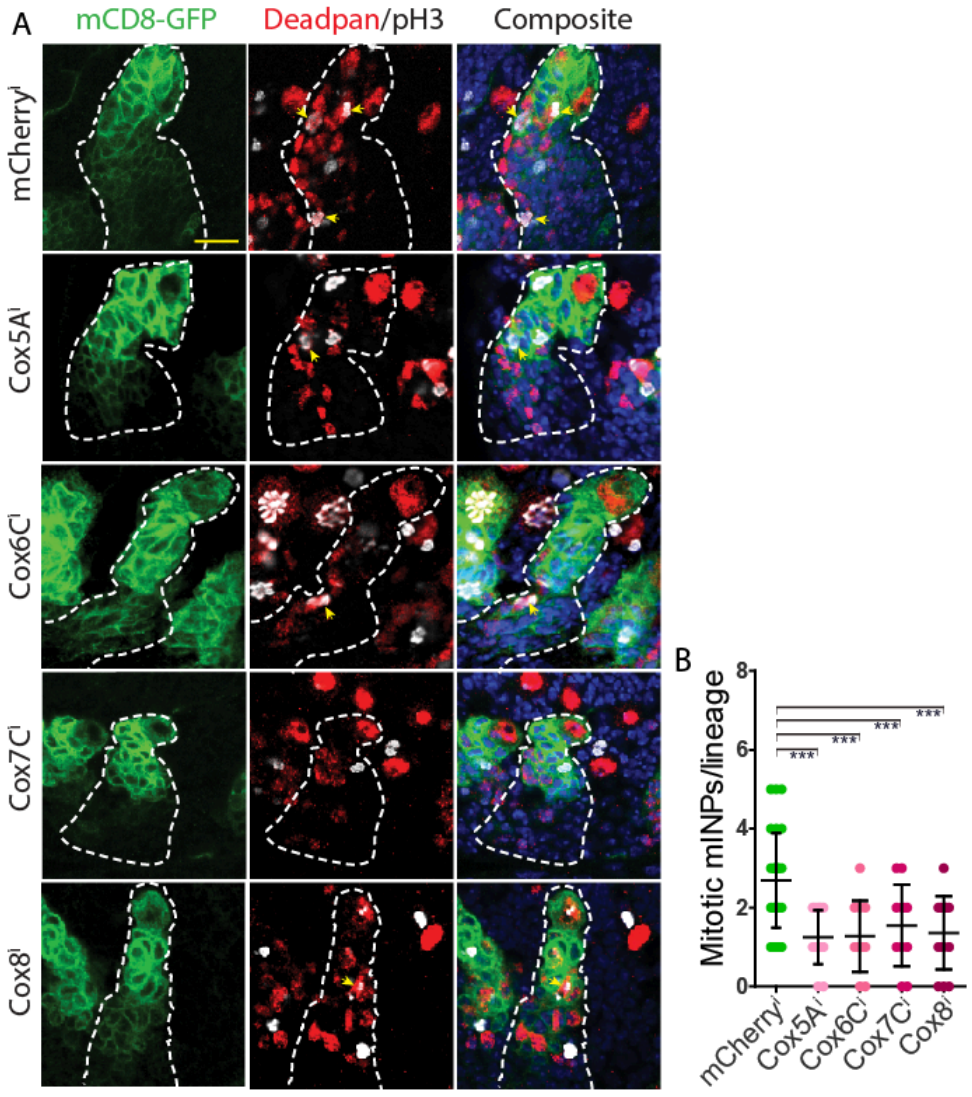


Figure 6.4: Complex IV perturbation in type II neuroblast leads to decreased proliferation of mINPs. (A) Representative images showing mitotically dividing mature INPs in the type II

neuroblast lineage of the mentioned genotypes. Deadpan positive cells in the lineage mark mature INPs (red). pH3-labelled cells mark mitotically dividing cells (gray). We analysed mitotically dividing mature INPs by counting cells labelled for both pH3 and Deadpan. **(B)** Quantification of mitotically dividing mature INPs in type II neuroblast lineages of genotypes, mCherry^{i} (n=13 type II neuroblast lineages, 5 brains), Cox5A^{i} (16,5), Cox6C^{i} (11,6), Cox7C^{i} (11,8), and Cox8^{i} (14,6).Mann-Whitney's t-test was performed for statistical analysis.***-$p<0.001$.

GMCs divide symmetrically to form a pair of neurons or glia. Neurons show Prospero in the nucleus and are present at the base of the lineage (Bello et al. 2008; Walsh and Doe 2017). For the detection of neurons in the type II neuroblast lineages, we immunostained the brains with anti-Prospero antibodies. As expected, fewer GMCs generated fewer neurons in the complex IV depleted lineage than control (Figure 6.5 A and B).

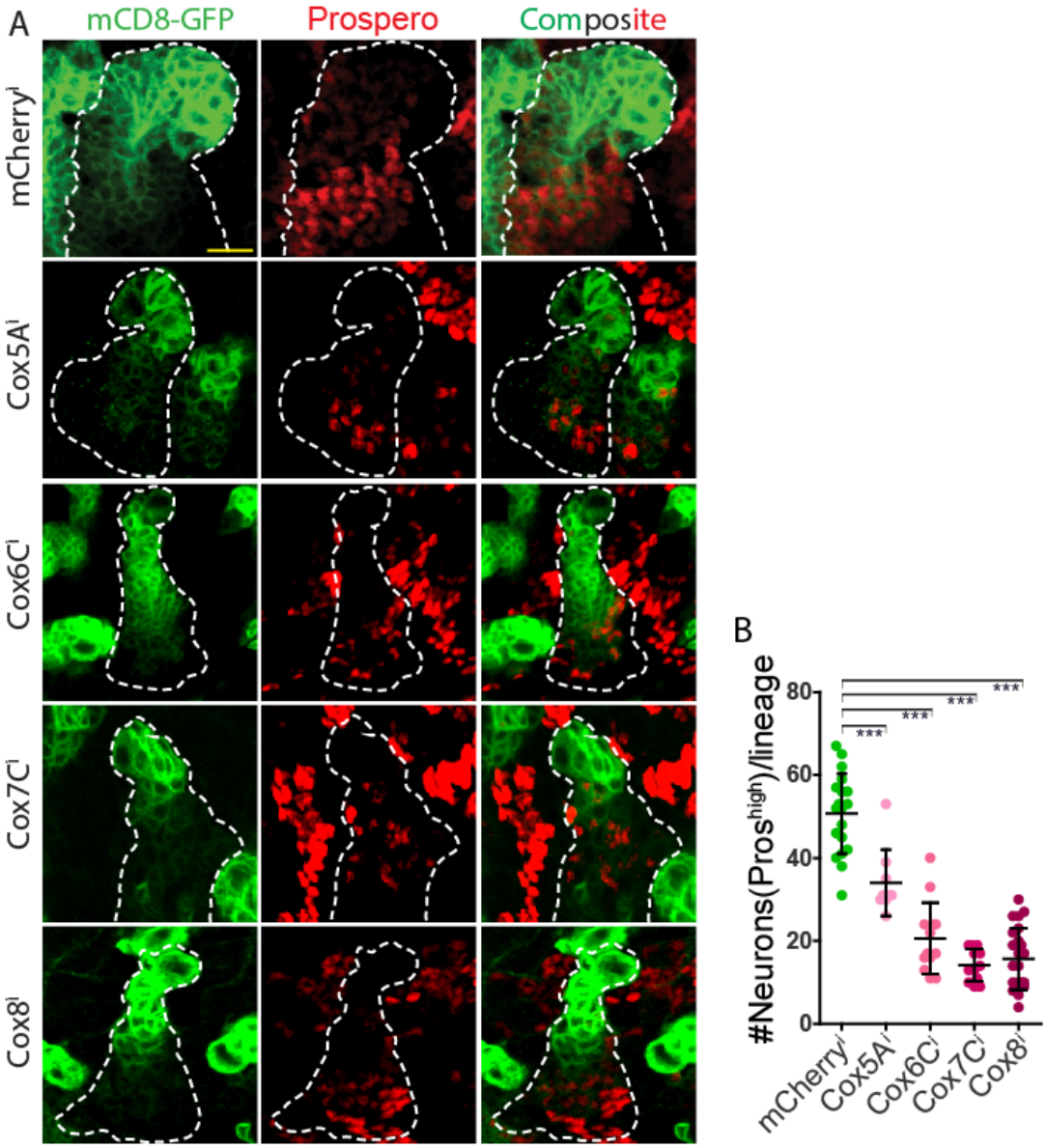


Figure 6.5: Depletion of complex IV in type II neuroblast leads to a decreased number of neurons in the lineage. **(A)** Representative images showing Prospero staining for detection of neurons in type II neuroblast lineages of indicative genotypes. High nuclear Prospero positive cells are neurons (red). Scale bar- 10µm. **(B)** Neurons quantification in type II neuroblast lineages of genotypes, mCherry^i (n=19 type II neuroblast lineages, 5 brains), Cox5A^i (9,4), Cox6C^i (13,5), Cox7C^i (12,4), and Cox8^i (23,4).Mann-Whitney's t-test was performed for statistical analysis. ***- p<0.001.

6.3.3 Forced mitochondrial fusion by depletion of Drp1 in complex IV lacking neuroblasts rescues the proliferation defect in larval brain lobe

Mitochondrial fused morphology is crucial for *Drosophila* neuroblast proliferation and differentiation (Chapter 4) (Dubal et al. 2022). Although we have not checked the mitochondrial morphology in complex IV-depleted neuroblast, literature shows that disruption of complex IV results in mitochondrial fragmentation (Rolland et al. 2013). Therefore, to assess whether inducing mitochondrial fusion by depletion of Drp1 in complex IV-deficient neuroblasts could rescue the proliferation defects or not, we generated $Drp1^{SD}$;$Cox6^{i}$ fly line. We crossed this line with *wor*-gal4 virgins and dissected F1 third instar larval brain. Then we stained these brains with Miranda (neuroblast marker) and pH3 (mitosis marker). We found that in the brain lobe, the proportion of mitotically dividing neuroblasts was found to be increased significantly in $Drp1^{SD}$;$Cox6C^{i}$ as compared to $Cox6C^{i}$ alone (Figure 6.6 A and B). $Drp1^{SD}$;$Cox6C^{i}$ neuroblasts mitotic index was similar to the mitochondrial fusion control, $Drp1^{SD}$;$mCherry^{i}$. Type II neuroblast specific expression of $Drp1^{SD}$;$Cox6C^{i}$ by using *pnt*-Gal4 restored their proliferation as compared to $Cox6C^{i}$ alone (Figure 6.6 C and D).

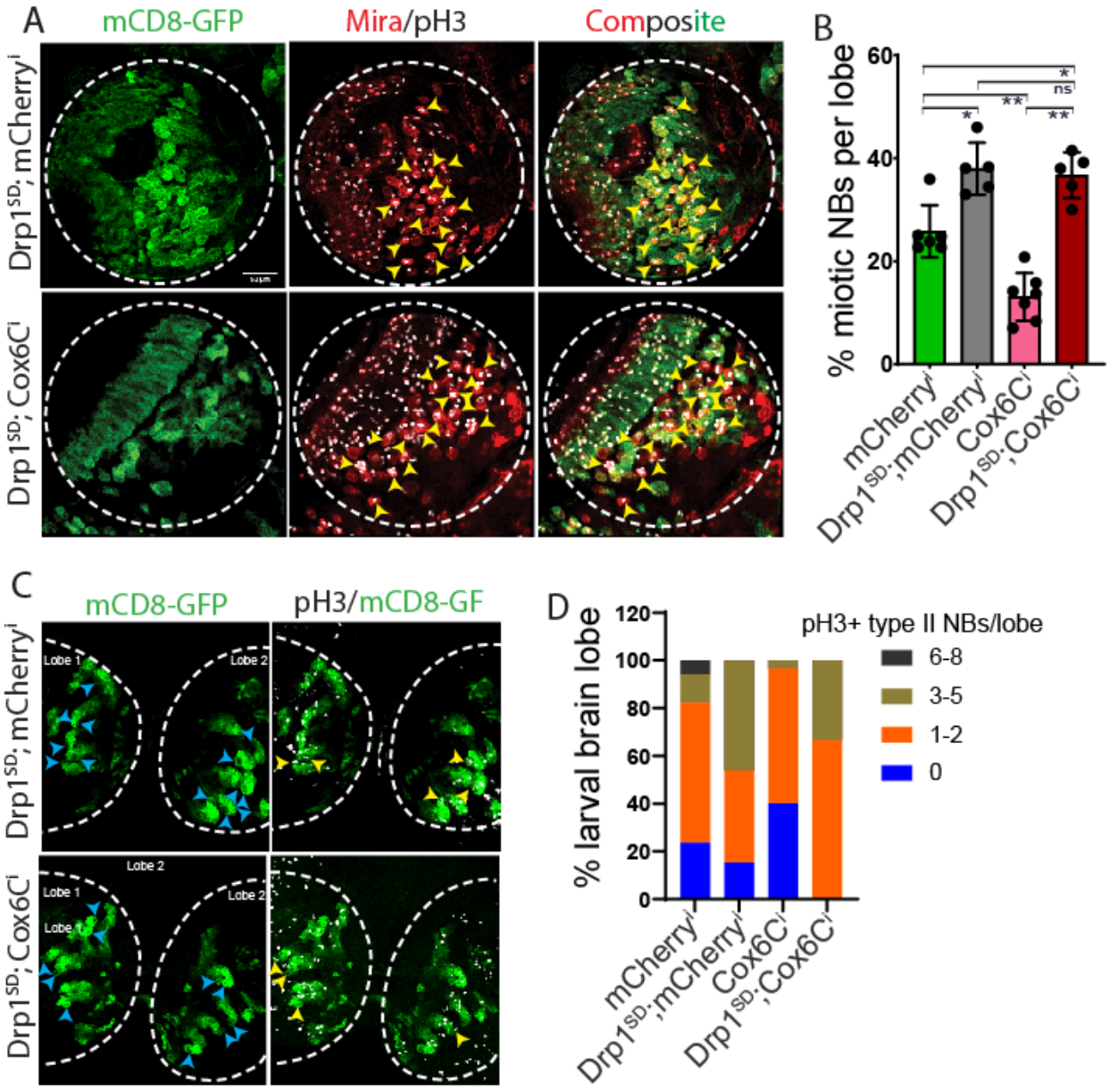


Figure 6.6: Induction of mitochondrial fusion in complex IV-deficient neuroblasts restores their proliferation. (A) Representative figures showing staining of third instar larval brain lobe for detecting mitotically dividing neuroblasts (type I/type II neuroblasts, yellow arrowheads) of indicative genotypes. *wor*-Gal4 driven UAS-mCD8-GFP marks the boundary of stem cells and its lineage (green). The white dashed circle outline marks the brain lobe. Miranda label stem cell cortex (red) and mitotically dividing cells are labelled by phospho-Histone H3 (pH3) (grey). Scale bar- 10µm. **(B)** Graph showing the quantification of percent mitotically dividing

neuroblasts present in each brain lobe of third instar larvae expressing *wor*-Gal4 driven mCherry^{i} (n=607 NSCs, 6 brains), Drp1^{SD};mCherry^{i} (476, 5), Cox6C^{i} (679, 6), and Drp1^{SD};Cox6C^{i} (489, 5). Data for all the single RNAi is taken from section 6.3.1. **(C)** Representative images of mitotically dividing type II neuroblasts (yellow arrowheads) in the *Drosophila* third instar larval brain of indicative genotypes. *pnt*-Gal4 driven mCD8-GFP marks the boundary of the neuroblast (blue arrowheads) and its lineage (green), and mitotically dividing cells are labelled by pH3 (grey). **(D)** Quantification of mitotically dividing type II neuroblasts expressing *pnt*-Gal4 driven mCherry^{i} (n=144 NSCs, 9 brains), Drp1^{SD};mCherry^{i} (112, 7), Cox6C^{i} (304,19), and Drp1^{SD};Cox6C^{i} (72, 5). Data for all the single RNAi is taken from section 6.3.1. Mann-Whitney's t-test was performed for statistical analysis. ns=non-significant, *- p<0.05, **- p<0.01.

Next, we analysed the consequence of Drp1 depletion on the differentiation of complex IV-depleted type II neuroblast.

6.3.4 Induction of mitochondrial fusion by depletion of Drp1 in complex IV deficient type II neuroblasts rescues the number of mINPs, GMCs and neurons in the lineage

We observed that mitochondrial fusion in complex IV-depleted neuroblasts rescues the proliferation defects (Figure 6.6). Next, we analysed the effect of inducing mitochondrial fusion on differentiation of complex IV deficient type II neuroblast (Cox6C^{i}, Cox7C^{i}, Cox8^{i}). To address this, we generated flies that express Drp1^{SD};Cox6C^{i}, Drp1^{SD}/Cox7C^{i}, and Drp1SD/Cox8^{i} in type II neuroblasts by crossing them with *pnt*-Gal4 and stained the F1 third instar larval brain with Asense and Deadpan together for marking mINPs and GMCs. We found that the number of mINPs in the lineages of Drp1^{SD};Cox6C^{i}, Drp1^{SD}/Cox7C^{i}, and Drp1SD/Cox8^{i} genotypes was increased compared to Cox5A^{i}, Cox6C^{i}, Cox7C^{i}, and, Cox8^{i} expressing neuroblasts respectively (Figure 6.7 A and B). Mature INPs divide to generate GMCs.

Then we analysed the proliferation of mINPs in control and complex IV RNAi lineage by immunostaining with Deadpan and pH3. We observed that the proliferation of mature INPs was restored in $Drp1^{SD}$;$Cox6C^{i}$, $Drp1^{SD}$/$Cox7C^{i}$, and Drp1SD/$Cox8^{i}$ type II neuroblast lineages than RNAi alone (Figure 6.8 A and B). Consistent with the rescue of mINPs mitotic index the number of GMCs were rescued (Figure 6.7 A and C). Fusion-mediated rescue of GMCs also restored the number of neurons in the lineages (Figure 6.9 A and B). Although the number of rescued GMCs was comparable to the control, but number of neurons were only partially rescued by mitochondrial fusion (Figure 6.9 A and B). Thus, type II NBs differentiation defects caused by complex IV perturbation can be rescued by mitochondrial fusion.

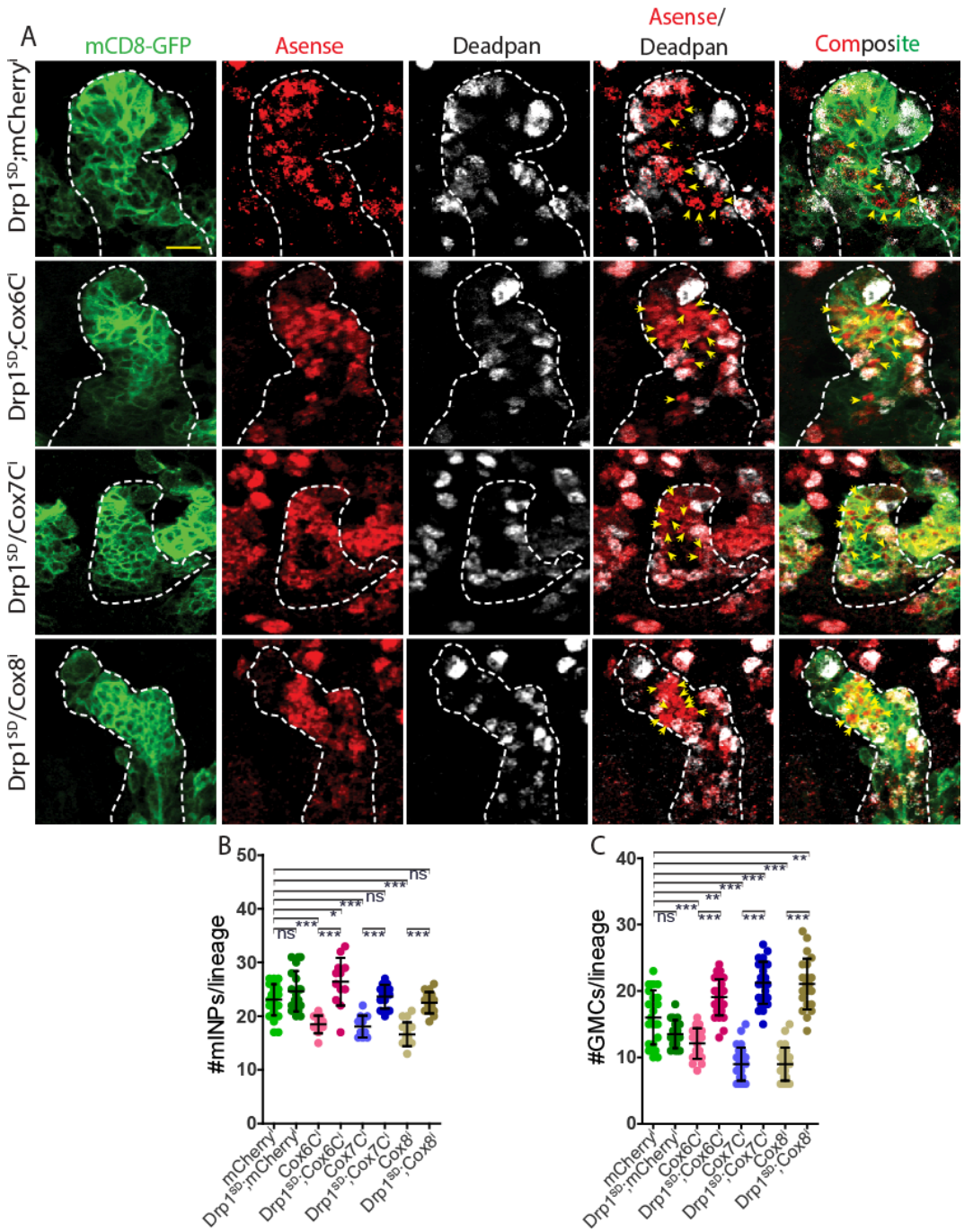


Figure 6.7: Mitochondrial fusion restores the mINPs and GMCs in the lineage of complex IV-depleted type II neuroblasts. (A) Representative figures showing detection of mINPs and

GMCs by immunostaining in type II neuroblast lineage of indicative genotypes. Deadpan positive cells are mature INPs (gray). Asense positive (red)-Deadpan negative cells are GMCs (yellow arrowheads). Scale bar- 10µm. **(B)** Quantification of mature INPs in type II neuroblast lineages of genotypes, mCherry^{i} (n=28 type II neuroblast lineages, 11 brains), Drp1^{SD}; mCherry^{i} (20, 5), Cox6C^{i} (11,5), Drp1^{SD};Cox6C^{i} (13,4), Cox7C^{i} (11,4), Drp1^{SD}/Cox7C^{i} (14,5), Cox8^{i} (16,5), and Drp1^{SD}/Cox8^{i} (16,5). Data for all the single RNAi is taken from section 6.3.2. **(C)** Quantification of GMCs in type II neuroblast lineages of genotypes, mCherry^{i} (n=12 type II neuroblast lineages, 3 brains), Drp1^{SD}; mCherry^{i} (20, 5), Cox6C^{i} (23,5), Drp1^{SD};Cox6C^{i} (29,4), Cox7C^{i} (26,4), Drp1^{SD}/Cox7C^{i} (25,5), Cox8^{i} (26,5), and Drp1^{SD}/Cox8^{i} (22,5). Data for all the single RNAi is taken from section 6.3.2.Mann-Whitney's t-test was performed for statistical analysis. ns=non-significant, *- p<0.05, **- p<0.01, ***- p<0.001.

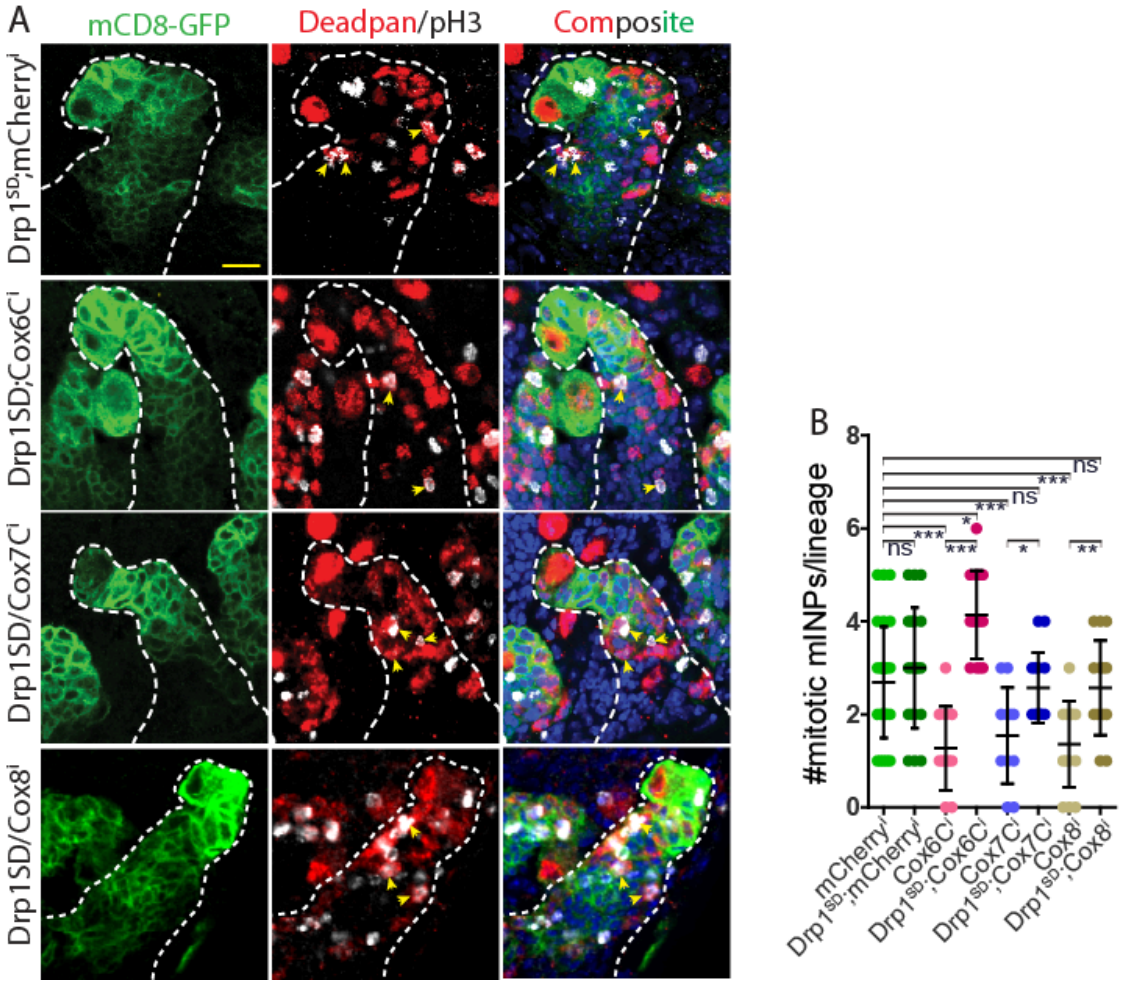


Figure 6.8: Mitochondrial fusion restores the mINPs proliferation in the lineage of complex IV-depleted type II neuroblasts. (A) Representative images showing mitotically dividing mature INPs in the type II neuroblast lineage of the mentioned genotypes. Deadpan positive cells in the lineage mark mature INPs (red). pH3 labelled cells mark mitotically dividing cells (gray). We analysed mitotically dividing mature INPs by counting cells labelled for both pH3 and Deadpan. **(B)** Quantification of mitotically dividing mature INPs in type II neuroblast lineages of genotypes, mCherry^{i} (n=13 type II neuroblast lineages, 5 brains), Drp1^{SD};mCherry^{i} (20, 5), Cox6C^{i} (11,6), Drp1^{SD};Cox6C^{i} (14,4), Cox7C^{i} (11,8), Drp1^{SD}/Cox7C^{i} (14,4), Cox8^{i} (14,6), and Drp1^{SD}/Cox8^{i} (14,4). Data for all the single RNAi is taken from section 6.3.2. Mann-Whitney's t-test was performed for statistical analysis. ns=non-significant, *- p<0.05, **- p<0.01, ***- p<0.001.

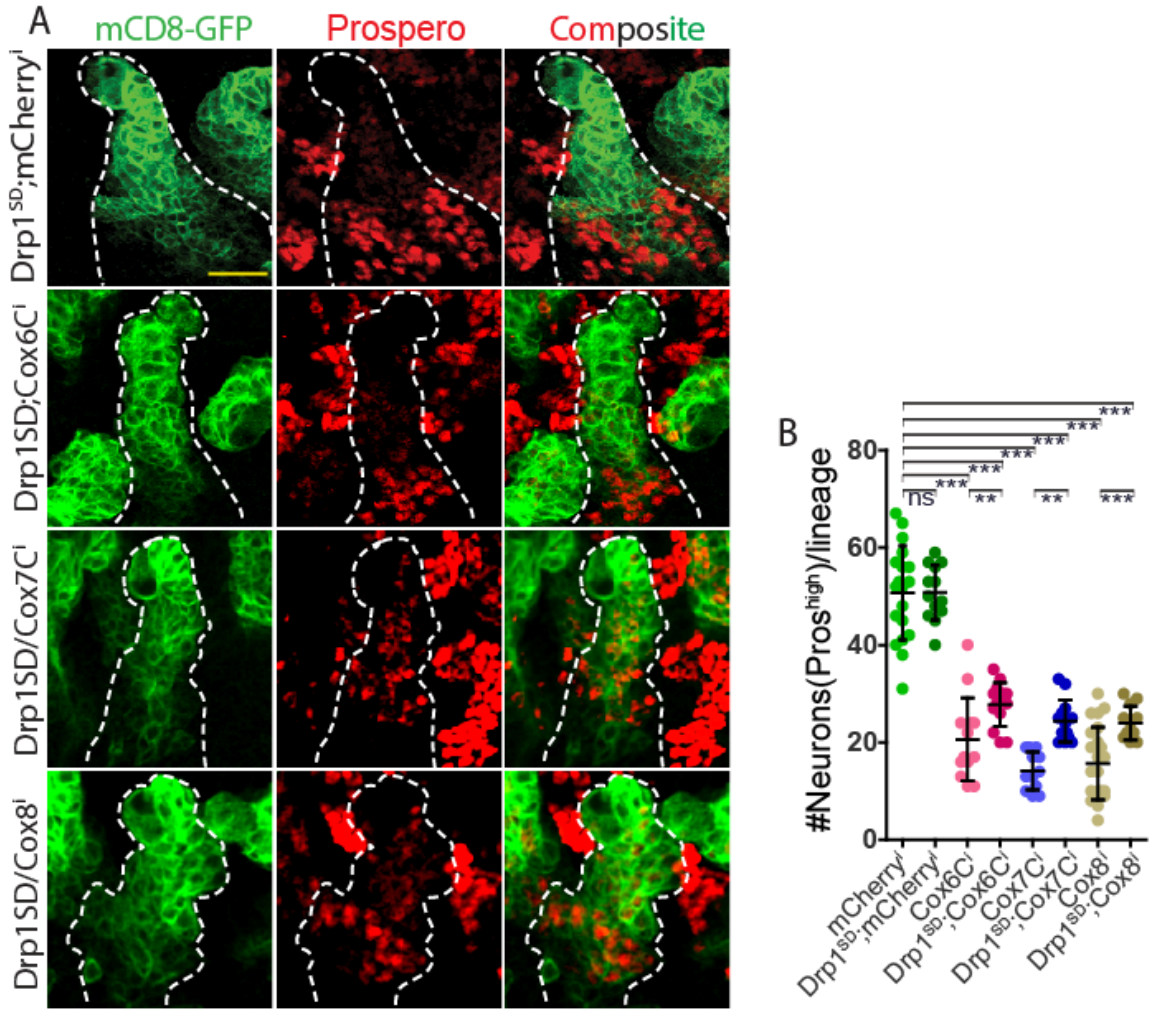


Figure 6.9: Mitochondrial fusion restores the neurons in the lineage of complex IV depleted type II neuroblasts. (A) Representative images of neurons staining in type II neuroblast lineages of indicative genotypes. High nuclear Prospero positive cells are neurons (red). Scale bar-10μm. **(B)** Neurons quantification in type II neuroblast lineages of genotypes, $mCherry^{i}$ (n=19 type II neuroblast lineages, 5 brains), $Drp1^{SD}$;$mCherry^{i}$ (13, 5), $Cox6C^{i}$ (13,5), $Drp1^{SD}$;$Cox6C^{i}$ (12,5), $Cox7C^{i}$ (12,4), $Drp1^{SD}$/$Cox7C^{i}$ (13,5), $Cox8^{i}$ (23,4), and $Drp1^{SD}$/$Cox8^{i}$ (14,5). Mann-Whitney's t-test was performed for statistical analysis. ns=non-significant, **- $p<0.01$, ***- $p<0.001$.

6.3.5 Complex IV downregulation in type II neuroblast deccreases ROS production and mitochondrial membrane potential

As we discussed in section 6.1, the electron transport chain complex IV is crucial for maintaining mitochondrial activity through OXPHOS. During electron transport, it pumps out protons from the matrix to the intermembrane space and generates mitochondrial membrane potential (MMP), which is utilised by ATP synthase to generate ATP. Therefore, to assess the role of complex IV in maintaining mitochondrial activity in type II neuroblasts, we measured MMP and ROS levels in complex IVRNAi and control neuroblasts. TMRM dye was employed to measure MMP in live third-instar larval brains. Immediately after dissecting control and complex IV RNAi third instar larval brains, they were treated with TMRM dye, followed by imaging. Type II neuroblasts' TMRM fluorescence was quantified and represented as a ratio to nearby control type I neuroblasts. We depleted complex IV in type II neuroblast by downregulating its subunits, Cox6C and Cox8 using *pnt*-Gal4,UAS-mCD8-GFP. A loss of MMP was observed in Cox6C and Cox8 downregulated type II neuroblasts (Figure 6.10 A and B).

ROS levels in the cytoplasm and mitochondria are altered by changes in mitochondrial shape and ETC activity (Sharma et al. 2011; Ježek et al. 2018; Deng et al. 2018). Oxidative phosphorylation generates ROS as a byproduct, and they have recently been recognised as crucial signalling molecules in cellular processes, including stem cell

maintenance and differentiation (Khacho et al. 2016; Deng et al. 2018; Muller 2000). Therefore, to check the role of complex IV in regulating ROS generation in type II neuroblasts, we assessed the ROS levels in type II neuroblasts using DHE dye.

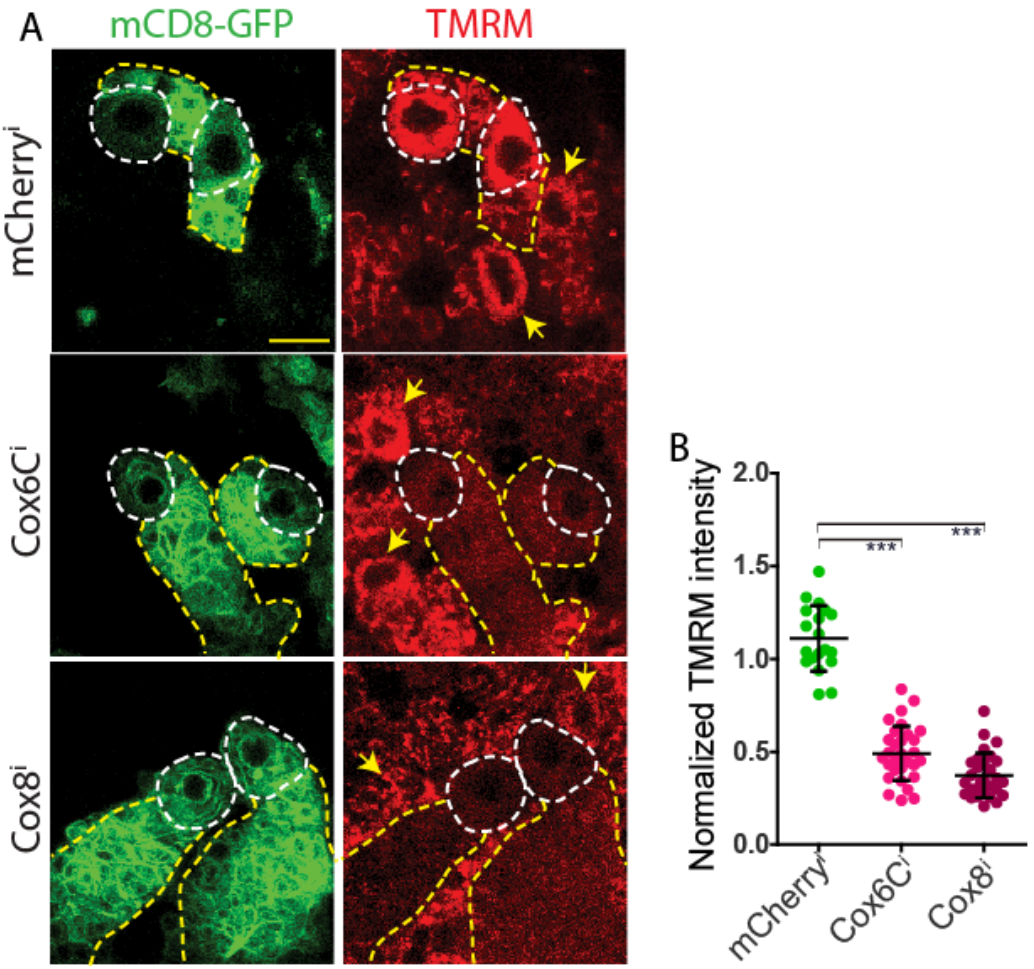


Figure 6.10: Disruption of complex IV in type II neuroblasts leads to loss of MMP. (A) Representative images depicting MMP detection in type II neuroblasts of indicative genotypes using TMRM dye (red). *pnt*-Gal4 mediated expression of mCD8-GFP marks the boundary of neuroblasts and lineage cells. The white dashed outline denotes type II neuroblast. Surrounding control type I neuroblasts are shown by yellow arrowheads. Scale bar- 10µm. **(B)** Quantification of TMRM intensity in type II neuroblast, normalised to the intensity of neighbouring type I neuroblast. The following genotypes were assessed: mCherry^{i} (n=19 type II neuroblasts, 5

brains), Cox6C^{i} (32,3) and Cox8^{i} (29,6). . Mann-Whitney's t-test was performed for statistical analysis. ***- $p<0.001$.

Following dissection, DHE dye treatment and imaging were performed on the third-instar larval brains of the control and complex IV RNAi. DHE fluorescence in type II neuroblasts was normalised to the background. Knockdown of complex IV subunits Cox5A,Cox6C, Cox7C and Cox8 in type II neuroblasts resulted in a complete loss of ROS generation (Figure 6.11 A and B).

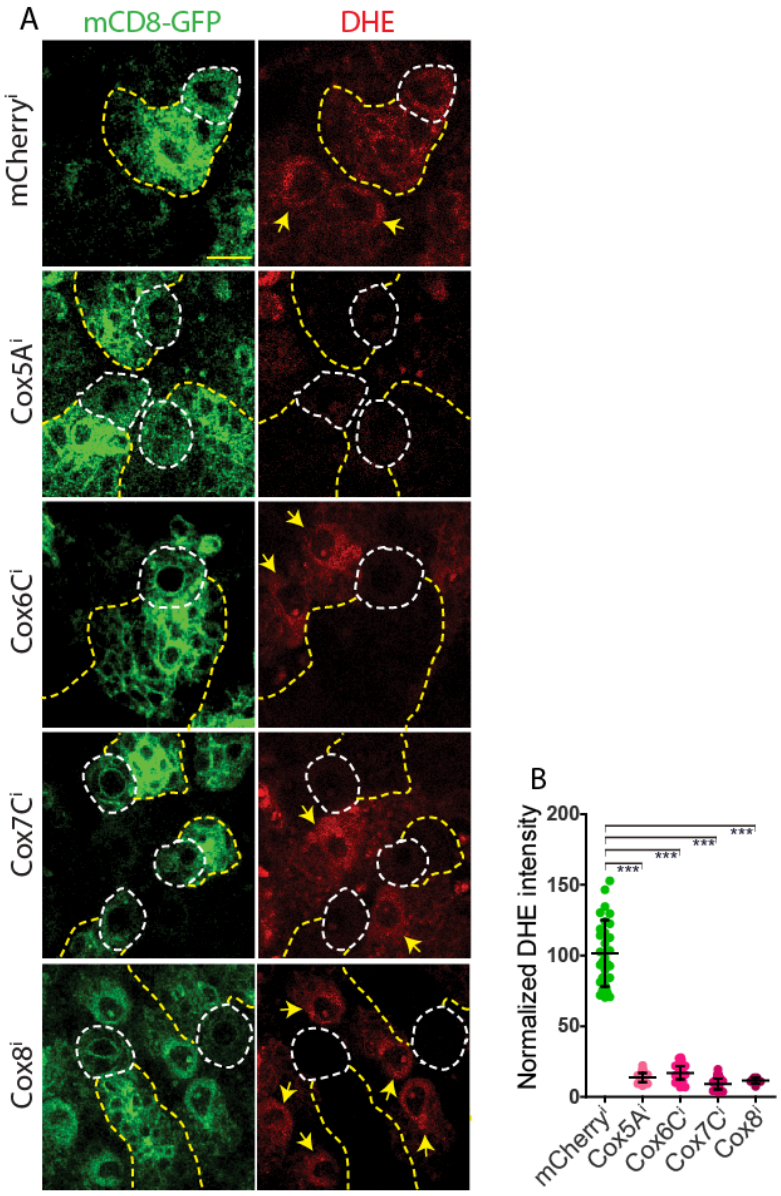


Figure 6.11: Perturbation of complex IV in type II neuroblasts diminishes the ROS generation. (A) Representative images of ROS detection in type II neuroblasts of the mentioned genotypes using DHE dye. The white dashed outline denotes type II neuroblast. Yellow arrowheads mark the surrounding type I neuroblast. Scale bar-10µm. **(B)** Quantification of DHE intensity normalised to background in type II neuroblasts of genotypes: mCherry^{i} (n=37 type II neuroblasts, 4 brains), Cox5A^{i} (37,4), Cox6C^{i} (42,5), Cox7C (42,5), and Cox8^{i} (7,3). . Mann-Whitney's t-test was performed for statistical analysis. ***- p<0.001.

6.3.6 Forced mitochondrial fusion by Drp1 depletion in complex IV perturbed neuroblast rescued MMP but not ROS generation

In complex IV-depleted neuroblasts, mitochondrial fusion corrects the differentiation abnormalities (Section 6.3.4). Our objective was to determine which mitochondrial activity parameter may be retained by fusion and rectify the abnormalities in differentiation. Therefore, we measured the MMP and ROS levels in $Drp1^{SD}$;$Cox6C^{i}$ and $Drp1^{SD}$;$mCherry^{i}$ (fusion control) expressing type II neuroblasts. We measured MMP using TMRM dye. MMP was significantly restored in $Drp1^{SD}$;$Cox6C^{i}$ type II neuroblast, than $Cox6C^{i}$ alone (Figure 6.12 A and B). Then we detected the ROS levels in complex IV-depleted type II neuroblast in a fused mitochondria background ($Drp1^{SD}$;$Cox6C^{i}$) by using DHE dye. We found that ROS levels in $Drp1^{SD}$;$Cox6C^{i}$ type II neuroblast remain low as $Cox6C^{i}$ alone (Figure 6.12 C and D).

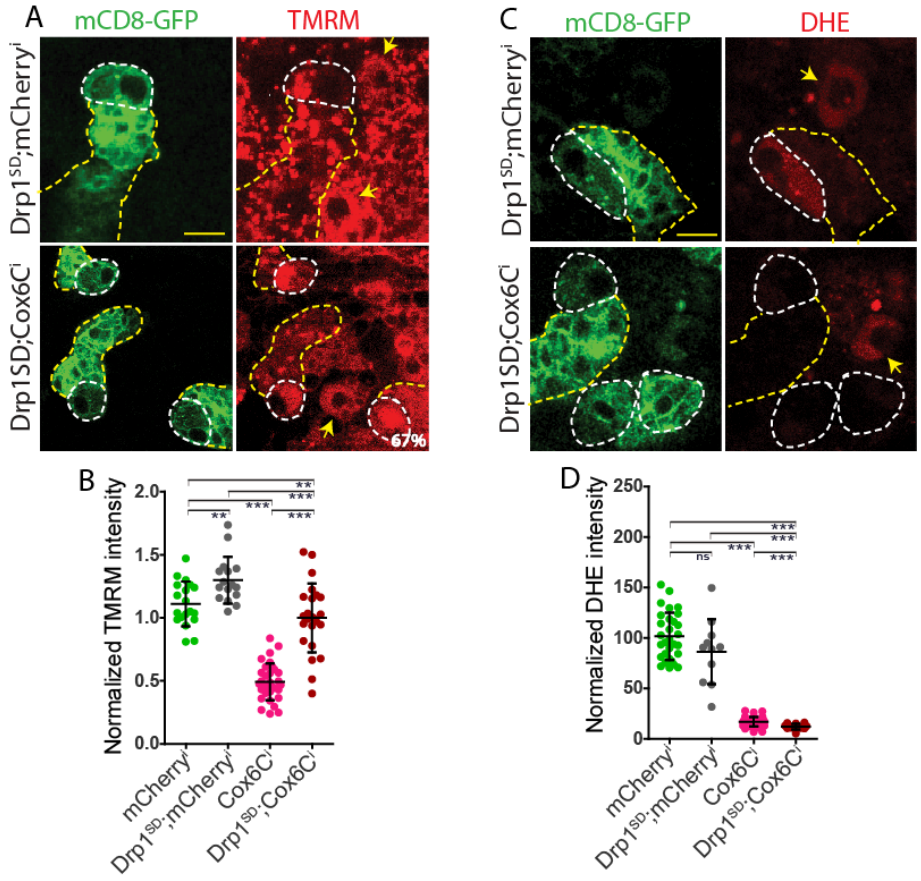


Figure 6.12: Mitochondrial fusion restores MMP loss in complex IV-depleted type II neuroblasts but could not rescue ROS levels. (A) Representative images depicting MMP detection in type II neuroblasts of indicative genotypes using TMRM dye (red). *pnt*-Gal4 mediated expression of mCD8-GFP marks the boundary of neuroblasts and lineage cells. The white dashed outline denotes type II neuroblast. Surrounding control type I neuroblasts are shown by yellow arrowheads. Scale bar- 10µm. **(B)** Quantification of TMRM intensity in type II neuroblast, normalised to the intensity of neighbouring type I neuroblast. The following genotypes were assessed: $mCherry^{i}$ (n=19 type II neuroblasts, 5 brains), $Drp1^{SD}$;$mCherry^{i}$ (16, 5), $Cox6C^{i}$ (32,3), $Drp1^{SD}$;$Cox6C^{i}$ (24,3). Data for all the single RNAi is taken from section 6.3.4. **(C)** Representative images of ROS detection in type II neuroblasts of the mentioned genotypes using DHE dye. The white dashed outline denotes type II neuroblast. Yellow arrowheads markthe surrounding type I neuroblast. Scale bar- 10µm. **(D)** Quantification of DHE intensity in type II neuroblasts normalised to background: $mCherry^{i}$ (n=37 type II neuroblasts, 4 brains), $Drp1^{SD}$;$mCherry^{i}$ (11, 5), $Cox6C^{i}$ (42,5), and $Drp1^{SD}$;$Cox6C^{i}$ (13,4). Data for all the single RNAi is taken from section 6.3.4. Mann-Whitney's t-test was performed for statistical analysis. *- $p<0.05$, **- $p<0.01$, ***- $p<0.001$.

6.3.7 Mitochondrial fusion restores Cyclin E nuclear accumulation in complex IV-depleted neuroblasts

Existing literature shows that mitochondrial morphology and activity regulate cell cycle progression through the G1/S phase (Mandal et al. 2010; Owusu-Ansah et al. 2008). As we showed in section 4.3.3, complex I depletion in type II neuroblasts induces G1/S transition defects by decreasing nuclear cyclin E accumulation; we assessed the effect of complex IV depletion on cyclin E levels. We used immunostaining to quantify cyclin E expression in complex I RNAi and control type II neuroblasts. There was a significant decrease in the nuclear accumulation of cyclin E in $Cox6C^{i}$ neuroblasts compared to the $mCherry^{i}$ control (Figure 6.13 A and B). In $Cox6C^{i}$ neuroblasts, cyclin E was retained in the cytoplasm, but in control, it was completely nuclear localised. Inducing mitochondrial fusion in $Cox6C^{i}$ neuroblasts by Drp1 depletion ($Drp1^{SD}$;$Cox6C^{i}$) restored nuclear cyclin

E accumulation. Cyclin E levels in Drp1^{SD};Cox6C^{i} neuroblasts were comparable to Drp1^{SD};mCherry^{i} fusion control and greater than Cox6C^{i} alone (Figure 6.13 A and B).

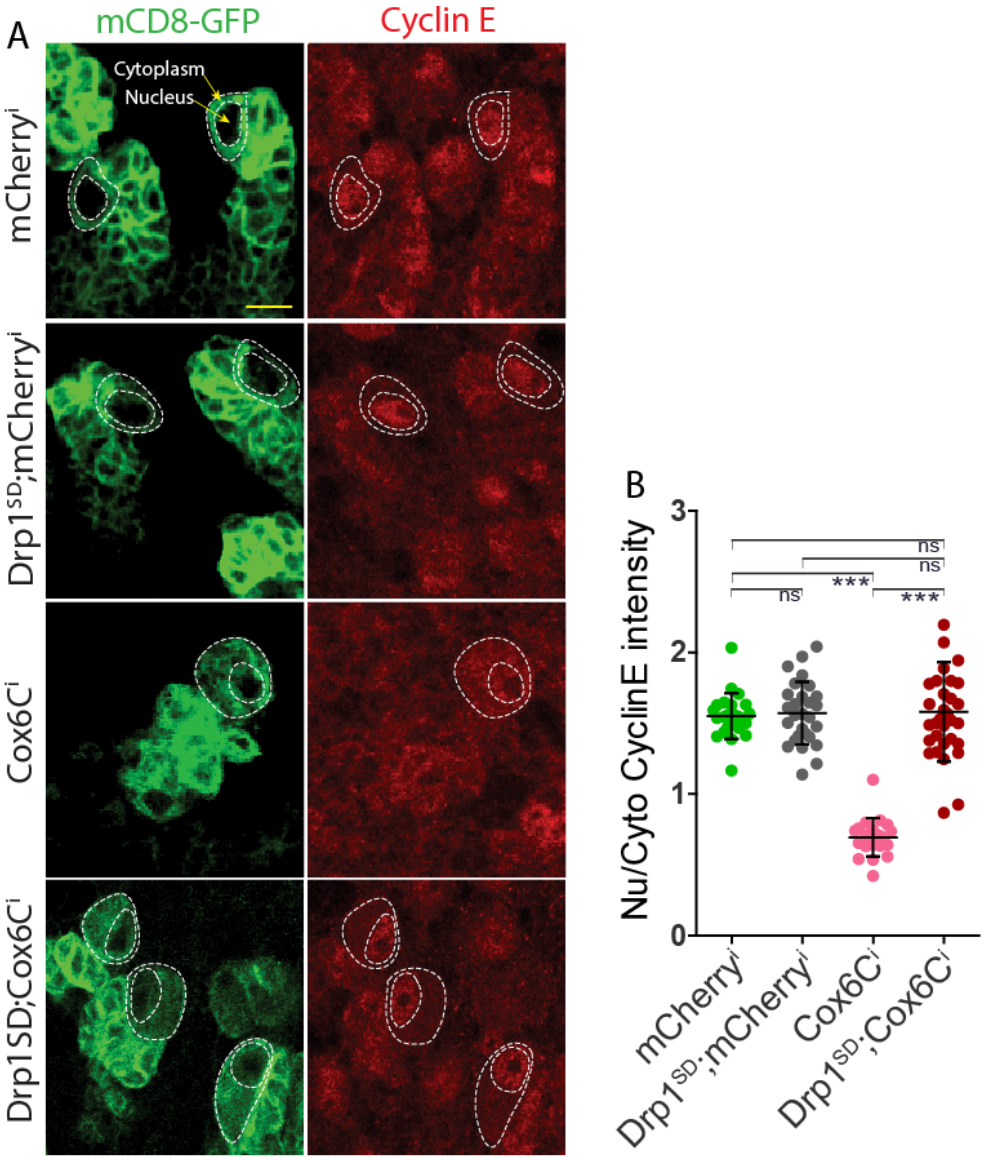


Figure 6.13: Mitochondrial fusion rescues nuclear cyclin E loss in complex IV-depleted neuroblasts. (A) Representative images showing cyclin E immunostaining (red) in type II neuroblasts of indicative genotypes. Type II neuroblasts are shown as encircled by white dashed line. Scale bar- 10µm. **(B)** Quantification of cyclin E intensity in the nucleus with respect to the cytoplasm of type II neuroblasts of the following genotypes: mCherry^{i} (n=23 type II

neuroblasts, 9 brains), $Drp1^{SD}$;$mCherry^{i}$ (28, 3), $Cox6C^{i}$ (21, 5), $Drp1^{SD}$;$Cox6C^{i}$ (32, 5). Mann-Whitney's t-test was performed for statistical analysis. ns=non-significant, ***- $p<0.001$.

6.4 Discussion

Our study established that complex IV is essential for the proliferation and differentiation of *Drosophila* type II neuroblasts. Depletion of Complex IV subunits (Cox5A, Cox6C, Cox7C, and Cox8) led to a decrease in neuroblast proliferation and a subsequent reduction in the number of mature INPs, GMCs, and neurons. Complex IV is the terminal enzyme of the ETC; it maintains MMP by transferring electrons to molecular oxygen and pumping protons across the inner mitochondrial membrane. Our TMRM analysis showed a significant loss of MMP, likely impairing ATP production and mitochondrial import processes essential for cell cycle progression (Owusu-Ansah et al. 2008). Fusion restored MMP and differentiation defects, indicating that MMP might aid in the restoration of metabolic activity.

Interestingly, ROS levels were abolished in type II neuroblasts upon depletion of Complex IV. Physiological levels of mitochondrial ROS serve as important signalling molecules in stem cell maintenance and differentiation (Khacho et al. 2016; Tothova et al. 2007). Therefore, its absence may impair ROS-dependent signalling required for proper neuroblast proliferation and differentiation. This observation is consistent with previous findings in *Drosophila* intestinal stem cells, where Complex IV depletion perturbs differentiation through overactivation of stress pathways such as FOXO (Zhang et al. 2020). Complex IV depletion-mediated proliferation and differentiation defects were rescued by fusion. However, ROS levels remained low even after inducing fusion, indicating that ROS is not the primary mediator of this rescue effect. These data contrast with our findings on Complex I RNAi neuroblasts, where hyperfusion restored ROS and rescued the phenotype (Chapter 4), suggesting complex IV-specific mechanisms of neuroblast differentiation.

We also observed that Complex IV depletion reduces nuclear accumulation of Cyclin E, an essential G1/S phase regulator. This supports previous reports that mitochondrial dysfunction impairs cell cycle entry by affecting Cyclin E localization and stability (Owusu-Ansah et al. 2008; Mandal et al. 2005, 2010). Mitochondrial fusion restored nuclear Cyclin E accumulation in $Cox6C^{i}$ neuroblasts, further linking mitochondrial dynamics to cell cycle control. These results suggest that the reduced proliferation observed upon complex IV depletion may be due to G1/S transition defects caused by improper Cyclin E localisation.

Chapter 7

Downregulation of electron transport chain complex V in neuroblast disrupts cristae morphology and results in proliferation and differentiation defects

---

7.1 Introduction

Complex V of the electron transport chain, also known as F_1F_o ATP synthase. It is the final complex in the chain that harnesses the energy stored in mitochondrial membrane potential to drive ATP synthesis. ATP synthase comprises two distinct components: the F_1, a soluble domain located in the mitochondrial matrix, and the F_0, embedded in the inner mitochondrial membrane. The F_1 domain contains three copies each of the α and β subunits, along with single copies of γ, δ, and ε subunits. The γ, δ, and ε subunits together form the central stalk of complex V. The F_0 domain possesses a c-ring which is made up of eight C subunits, as shown in bovine mitochondria (Watt et al. 2010) and single copies of subunits A, B, D, F6, and the oligomycin sensitivity-conferring protein (OSCP). The peripheral stalk, which supports the complex from the side, is formed by subunits B, D, F6, and OSCP. Additional membrane-spanning subunits—E, F, G, and A6L—are also associated with the F_0 sector (Devenish et al. 2008; Wittig and Schägger 2008). ATP synthase in the inner membrane dimerises and self-organises in rows, inducing positive membrane curvature, leading to the formation of the cristae tips. In *Drosophila*, subunits E and G have been shown to be solely responsible for ATP synthase dimerisation but not for catalytic activity (Teixeira et al. 2015; Paumard et al. 2002), while α and β subunits contribute to both dimerisation and catalytic activity. The remaining subunits are dedicated to mitochondrial respiration. Therefore, subunits E, G, α, and β play a key role in regulating cristae architecture (Teixeira et al. 2015). In yeast,

loss of subunits **E** or **G** leads to abnormal onion-like cristae structures (Paumard et al. 2002).

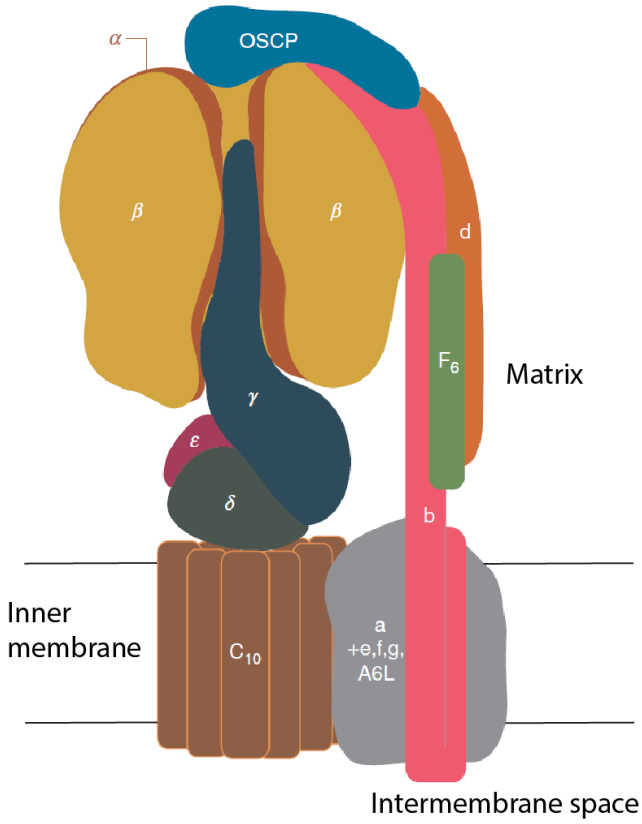


Figure 7.1. Subunit organization of mitochondrial ATP synthase (mtATPase). The F_1 domain contains subunits α, β, and the central stalk subunits γ, δ, and ε. The F_0 domain consists of the c-ring (10 copies in yeast), subunit a, and peripheral stalk subunits b, d, F6(h), and OSCP. Minor subunits (e, f, g, A6L) are present in a 1:1:1:1 ratio. The central stalk and c-ring form the rotor, while the remaining subunits form the stator. Figure adapted from (Devenish et al. 2008).

In this chapter, we have examined the effect of downregulating F_1 subunits, α and β, and F_0 subunits E, G, and B on proliferation, differentiation, and mitochondrial activity of *Drosophila* neuroblast.

7.2 Materials and methods

7.2.1 Fly stocks

7.2.1.1 Gal4 flies: *pnt*-Gal4,UAS-mCD8-GFP and *wor*-Gal4,UAS-mCD8-GFP

7.2.1.2 RNAi flies: ATP Syn E^i (BL67826), ATP Syn G^i (BL67347), ATP Syn α^i (28059), ATP Syn β^i (BL28056), ATP Syn B^i (BL28062).

The following combinations of transgenes were made by using standard fly genetics and appropriate balancers to bring the lines together:

1. $Drp1^{SD}$/CyOGFP;$mCherry^i$/TM6B
2. ATP syn E^i (BL67826)/FM7A;$Drp1^{SD}$/CyOGFP
3. ATP syn G^i (BL67347)/FM7A;$Drp1^{SD}$/CyOGFP
4. $Drp1^{SD}$/CyOGFP;ATP syn α^i (28059)/TM6B
5. $Drp1^{SD}$/CyOGFP;ATP syn β^i (BL28056)/TM6B
6. $Drp1^{SD}$/CyOGFP;ATP syn B^i (BL28062)/TM6B

7.2.2 Antibodies

Primary antibodies: Chicken anti-GFP (1:1000, Invitrogen, A10262), rabbit anti-Ase (1:10000, Yuh-Nung Jan, UCSF, USA), rat-anti-Deadpan (1:150, Abcam, ab195173), rabbit anti-Deadpan (1:800, Yuh-Nung Jan, UCSF, USA), mouse-anti-Prospero (1:20, DSHB, MR1A), rabbit anti-phosphohistone 3 (1:500, Invitrogen, PA5-17869), and rat-anti-Miranda (1:600, Abcam, 197788).

Secondary antibodies: Alexa fluor coupled secondary antibodies (Invitrogen) were used in 1:1000 dilution: anti-chicken 488, anti-mouse 568/647, anti-rabbit 488/568/647, anti-rat 488/568/647.

7.2.3 Immunostaining

Third instar larval brains of ETC RNAi and control were dissected and processed for immunostaining following the protocol mentioned in section 2.2.3.

7.2.4 Image acquisition and analysis

Fixed samples were processed for Confocal microscopy done at room temperature using LSM710 or LSM780 inverted microscope with a Plan apochromat 40x 1.4NA and 63x 1.4NA oil objective. Refer to sections, 2.2.8,2.2.9, and 2.2.10 for detailed information about image acquisition and analysis.

7.3 Results

7.3.1 Disruption of complex V in *Drosophila* neuroblast leads to decreased proliferation at the third instar larval stage

Mitochondrial activity is a critical regulator of mammalian stem cell proliferation and differentiation (Parker et al. 2015; Chen and Chan 2017). Inhibition of mitochondrial function, by halting electron transport chain complex I and V, causes stem cell proliferation defects (van den Ameele and Brand 2019; Teixeira et al. 2015). To determine the role of electron transport chain **complex V** in *Drosophila* neuroblast proliferation, we measured their mitotic index in the central nervous system of third instar larvae. Larval brains were dissected out and mitotically dividing neuroblasts were identified by co-staining them with Miranda (a neuroblast marker) and phospho-Histone 3 (pH3), which marks mitotic cells. We utilised the *wor*-Gal4 to express RNAi lines targeting Complex V subunits, ATP syn E, ATP syn G, and ATP syn β. mCD8-GFP marked the plasma membrane in the cells expressing the Gal4 and the RNA^{i}. We observed a significant reduction in the proportion of mitotically active NSCs within each brain lobe expressing ATP syn E^{i}, ATP syn G^{i}, and ATP syn β^{i} compared to mCherry^{i} control (Figure 7.2 A and B).

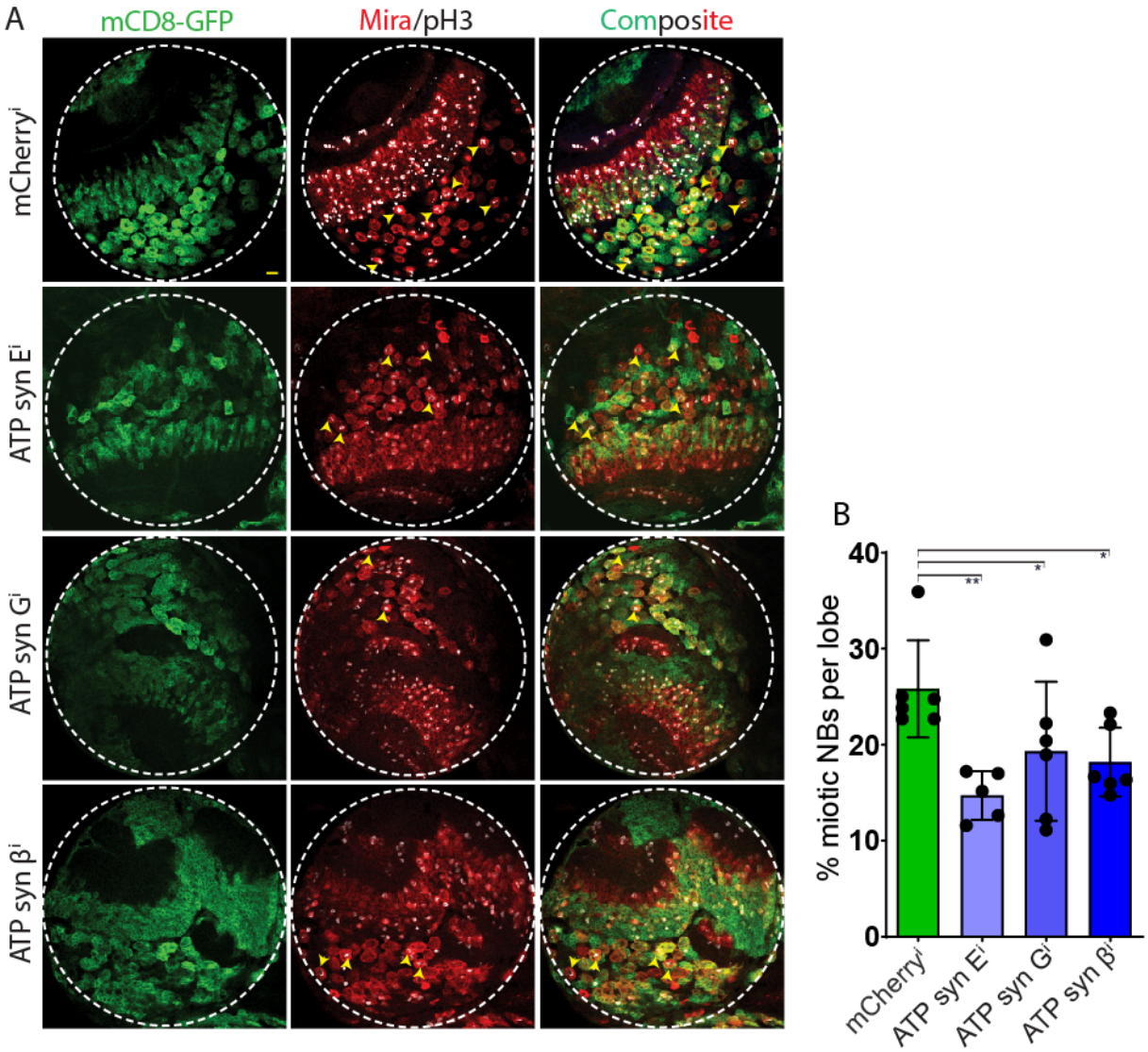


Figure 7.2: Neuroblasts in the third instar larval brain proliferate less on complex V depletion. (A) Representative images showing detection of mitotically dividing neuroblasts (yellow arrowheads) in the *Drosophila* third instar larval brain lobe (white dashed outline) of indicative genotypes. *wor*-Gal4 driven UAS-mCD8-GFP marks the boundary of stem cells and its lineage (green). Miranda label stem cell cortex (red) and mitotically dividing cells are labelled by phospho-Histone H3 (pH3) (grey). Scale bar-10μm. **(B)** Graph showing the quantification of percent mitotically dividing neuroblasts present inthe brain lobe of third instar larvae, expressing *wor*-Gal4 driven mCherry^i (n=607 NSCs, 6 brains), ATP syn E^i (490, 5), ATP syn G^i

(585,6), ATP syn β^i (590,6). Mann-Whitney's t-test was performed for statistical analysis. *- $p<0.05$, **- $p<0.01$.

7.3.2 Complex V depletion in type II neuroblasts results in a decreased number of mature INPs, GMCs, and neurons in the lineage

We evaluated the impact of complex V depletion on the differentiation of the type II neuroblast. We quantified the number of differentiated progenies, mINPs, GMCs and neurons within the type II neuroblast lineage by immunostaining for specific markers. We depleted complex V in type II neuroblast by downregulating its F_1 subunits, ATP syn α, ATP syn β, and F_0 subunits ATP syn E, ATP syn G, and ATP syn B using *pnt*-Gal4. Consistent with the decreased proliferation of neuroblast on complex V depletion (Figure 7.2), we found that the numbers of mature INPs (Ase+, Dpn+) were also reduced in ATP syn α^i, ATP syn β^i, ATP syn E^i, ATP syn G^i, and ATP syn B^i expressing type II neuroblast lineages as compared to mCherry^i expressing control (Figure 7.3 A and B). mINPs undergo asymmetric division to produce GMCs (Ase+, Dpn-). This reduction in mINP number corresponded with a decrease in the population of GMCs (Ase+ Dpn-) (Figure 7.3 A and C). GMCs divide symmetrically to form a pair of neurons or glia. Neurons show Prospero in the nucleus and are present at the base of the lineage (Bello et al. 2008; Walsh and Doe 2017). We used an anti-Prospero antibody to immunostain the brains to identify neurons. As anticipated, fewer GMCs produced a lesser number of neurons (high nuclear Prospero) in the complex IV deficient lineages than the control (Figure 7.4 A and B). During the differentiation of germline stem cells in *Drosophila melanogaster ovary*, ATP synthase subunits E, G, α, and β have been shown to mediate dimerisation and regulate cristae maturation (Teixeira et al., 2015). In this study, depletion of these subunits—presumably disrupting ATP synthase dimerisation—resulted in a reduction in the number of mINPs, GMCs, and neurons. Interestingly, the knockdown of ATP synthase subunit B, which is not involved in dimer formation, also caused similar differentiation defects. These findings suggest that both

OXPHOS and cristae morphology contribute to neuroblast differentiation, likely through distinct but complementary mechanisms.

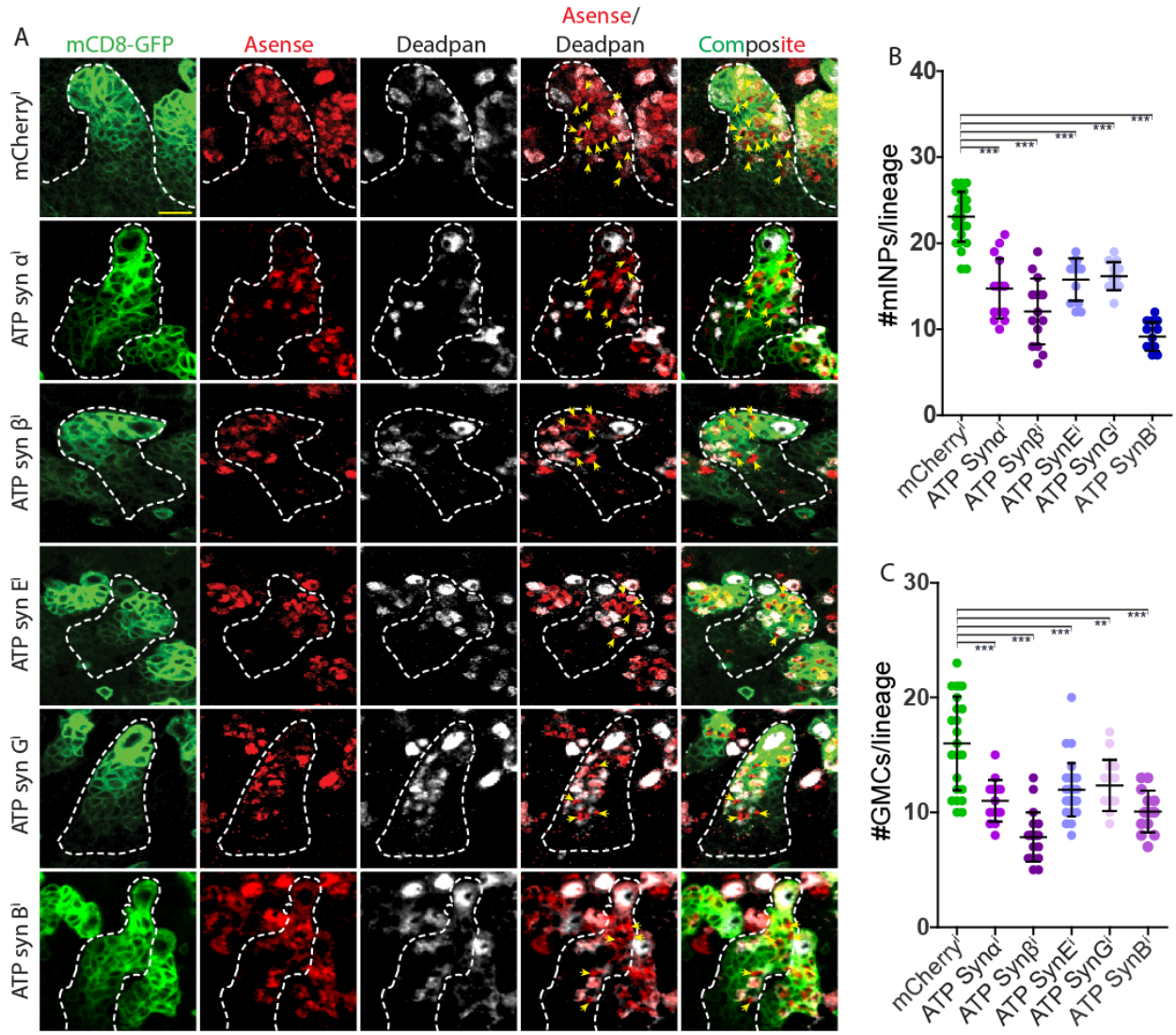


Figure 7.3: Depletion of complex V in type II neuroblasts leads to a decreased number of mature INPs and GMCs in the lineage. (A) Representative figures of mINPs and GMCs detection by immunostaining in type II neuroblast lineage of indicative genotypes. Deadpan positive cells are mature INPs (gray). Asense positive (red)-Deadpan negative cells are GMCs (Yellow arrowheads). Scale bar- 10μm. **(B)** Quantification of mature INPs in type II neuroblast

lineages of genotypes, mCherry^{i} (n=28 type II neuroblast lineages, 11 brains), ATP syn α^{i} (15,4), ATP syn β^{i} (15,4), ATP syn E^{i} (13,4), ATP syn G^{i} (13,4), and ATP syn B^{i} (14,4). **(C)** Quantification of GMCs in type II neuroblast lineages of genotypes, mCherry^{i} (n=24 type II neuroblast lineages, 5 brains), ATP syn α^{i} (15,4), ATP syn β^{i} (19,4), ATP syn E^{i} (31,4), ATP syn G^{i} (15,4), and ATP syn B^{i} (14,4). Mann-Whitney's t-test was performed for statistical analysis. **- p<0.01, ***- p<0.001.

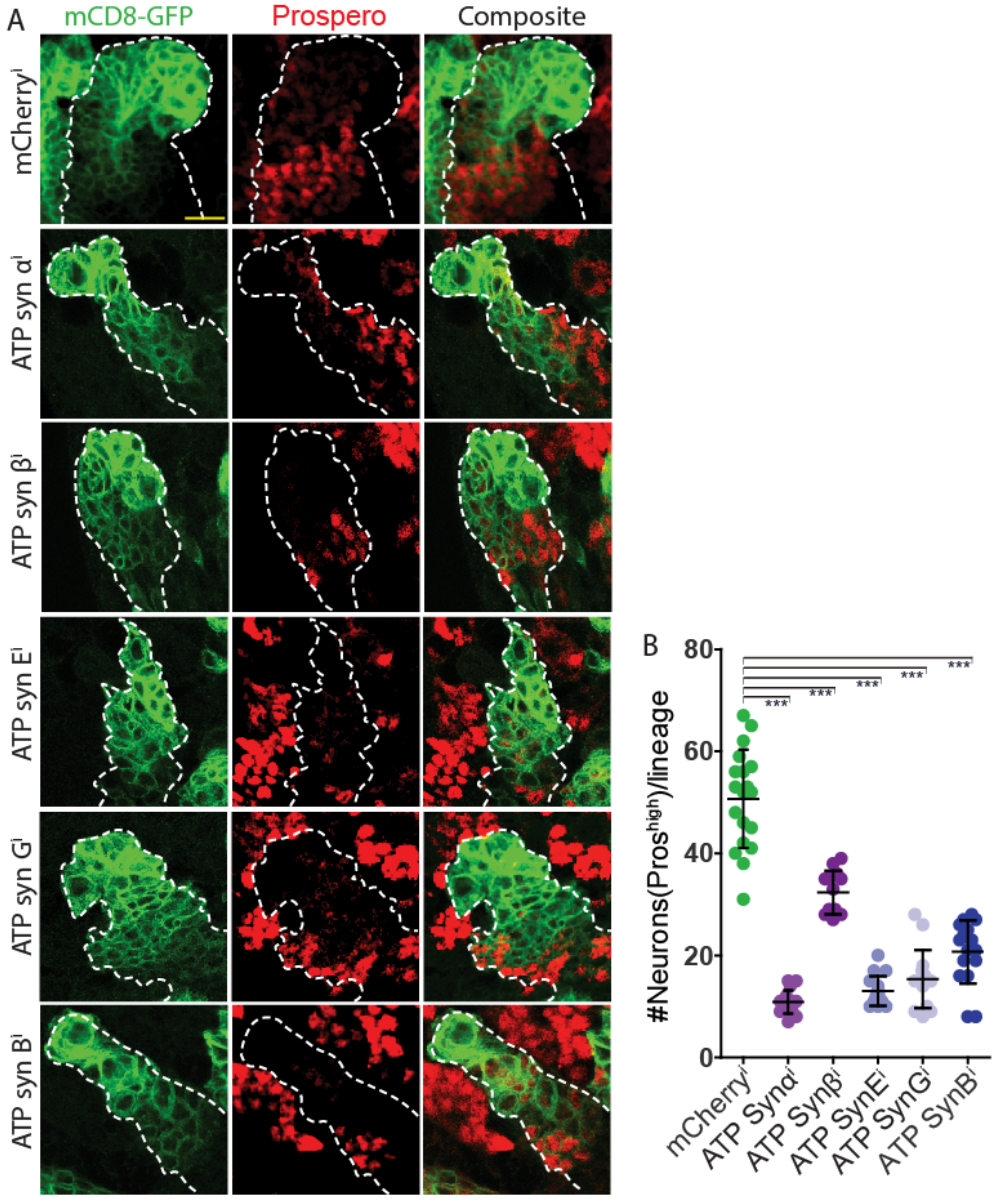


Figure 7.4: Complex V inhibition in type II neuroblast reduces the number of neurons in the lineage. (A) Representative images of neurons staining in type II neuroblast lineages of indicative genotypes. High nuclear Prospero positive cells are neurons (red). Scale bar- 10µm. **(B)** Neurons quantification in type II neuroblast lineages of genotypes, mCherry^{i} (n=19 type II neuroblast lineages, 5 brains), ATP syn α^{i} (16,4), ATP syn β^{i} (13,4), ATP syn E^{i} (15,4), ATP syn G^{i} (16,4), and ATP syn B^{i} (16,4). Mann-Whitney's t-test was performed for statistical analysis. ***- p<0.001.

7.3.3 Mitochondrial fusion fails to rescue differentiation in complex V dimer-forming subunit (α, β, E, G) knockdowns but rescues in B subunit depletion

In *Drosophila* neural stem cells, depletion of complex V is shown to cause mitochondrial fragmentation (van den Ameele and Brand 2019). In our lab previously, mitochondrial hyperfusion induced by Drp1^{SD,} a dominant-negative form of Drp1, was found to rescue the type II neuroblast differentiation defect caused by mitochondrial fragmentation on opa1 downregulation. We wanted to study whether inducing mitochondrial hyperfusion in complex V-depleted type II neuroblasts could rescue the differentiation defects. Therefor,e we generated the flies combinations, ATP Syn E^{i};Drp1^{SD}, ATP Syn G^{i};Drp1^{SD}, Drp1^{SD};ATP Syn α^{i}, Drp1^{SD};ATP Syn β^{i}, and Drp1^{SD};ATP Syn B^{i} and crossed them with type II neuroblast-specific *pnt*-Gal4. We dissected out the F1 third instar larval brain and stained them with their specific cellular markers for analysing the number of distinct differentiated cells in the lineage. We observed that hyperfusion of mitochondria could not rescue the differentiation defects caused by the depletion of ATP synthase subunits α, β, E, and G (Figure 7.5 A-C) (Figure 7.6 A and B). The number of mature INPs, GMCs and neurons were still similar to α, β, E, and G depleted type II neuroblasts. In contrast, a partial rescue was observed in the case of ATP synthase B depletion. As discussed earlier, ATP synthase α, β, E, and G subunits are involved in ATP synthase dimerisation and cristae maturation. Our analysis indicates that ATP

synthase dimerisation and proper cristae morphology are prerequisite for the rescue of differentiation defects by mitochondrial hyperfusion.

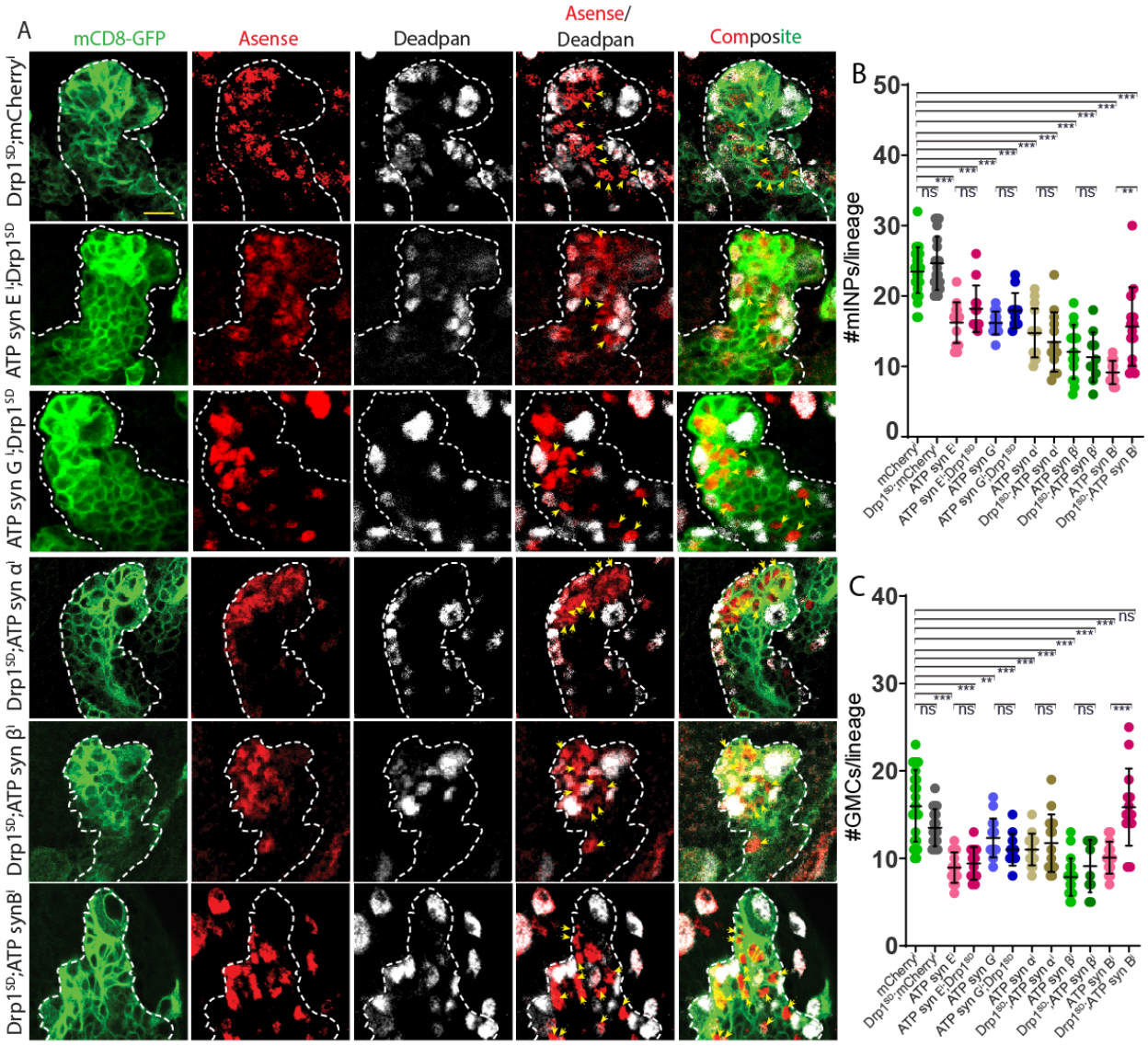


Figure 7.5: Mitochondrial fusion does not rescue the decreased number of mature INPs and GMCs in ATP syn α, β, E, and G subunits depleted type II neuroblast lineage, but rescues the ATP syn B knockdown. (A) Representative figures showing mINPs and GMCs detection by immunostaining in type II neuroblast lineage of indicative genotypes. Deadpan positive cells are mature INPs (gray). Asense positive (red)-Deadpan negative cells are GMCs

(yellow arrowheads). Scale bar- 10µm. **(B)** Quantification of mature INPs in type II neuroblast lineages of genotypes, mCherry^{i} (n=28 type II neuroblast lineages, 11 brains), Drp1^{SD};mCherry^{i} (20,5), ATP syn E^{i} (13,4), ATP syn E^{i};Drp1^{SD} (12,4), ATP syn G^{i} (13,4), ATP syn G^{i};Drp1^{SD} (11,4), ATP syn α^{i} (15,4), Drp1^{SD};ATP syn α^{i} (13,4), ATP syn β^{i} (15,4), Drp1^{SD};ATP syn β^{i} (10,4), ATP syn B^{i} (14,4), Drp1^{SD};ATP syn B^{i} (14,4). Data for all the single RNAi is taken from section 7.3.2. **(C)** Quantification of GMCs in type II neuroblast lineages of genotypes, mCherry^{i} (n=24 type II neuroblast lineages, 5 brains), Drp1^{SD};mCherry^{i} (18,5), ATP syn E^{i} (31,4), ATP syn E^{i};Drp1^{SD} (12,4), ATP syn G^{i} (15,4), ATP syn G^{i};Drp1^{SD} (11,4), ATP syn α^{i} (15,4), Drp1^{SD};ATP syn α^{i} (15,4), ATP syn β^{i} (19,4), Drp1^{SD};ATP syn β^{i} (10,4), ATP syn B^{i} (10,4), and Drp1^{SD};ATP syn B^{i} (14,4). Data for all the single RNAi are taken from section 7.3.2. Mann-Whitney's t-test was performed for statistical analysis. ns=non-significant, **- $p<0.01$, ***- $p<0.001$.

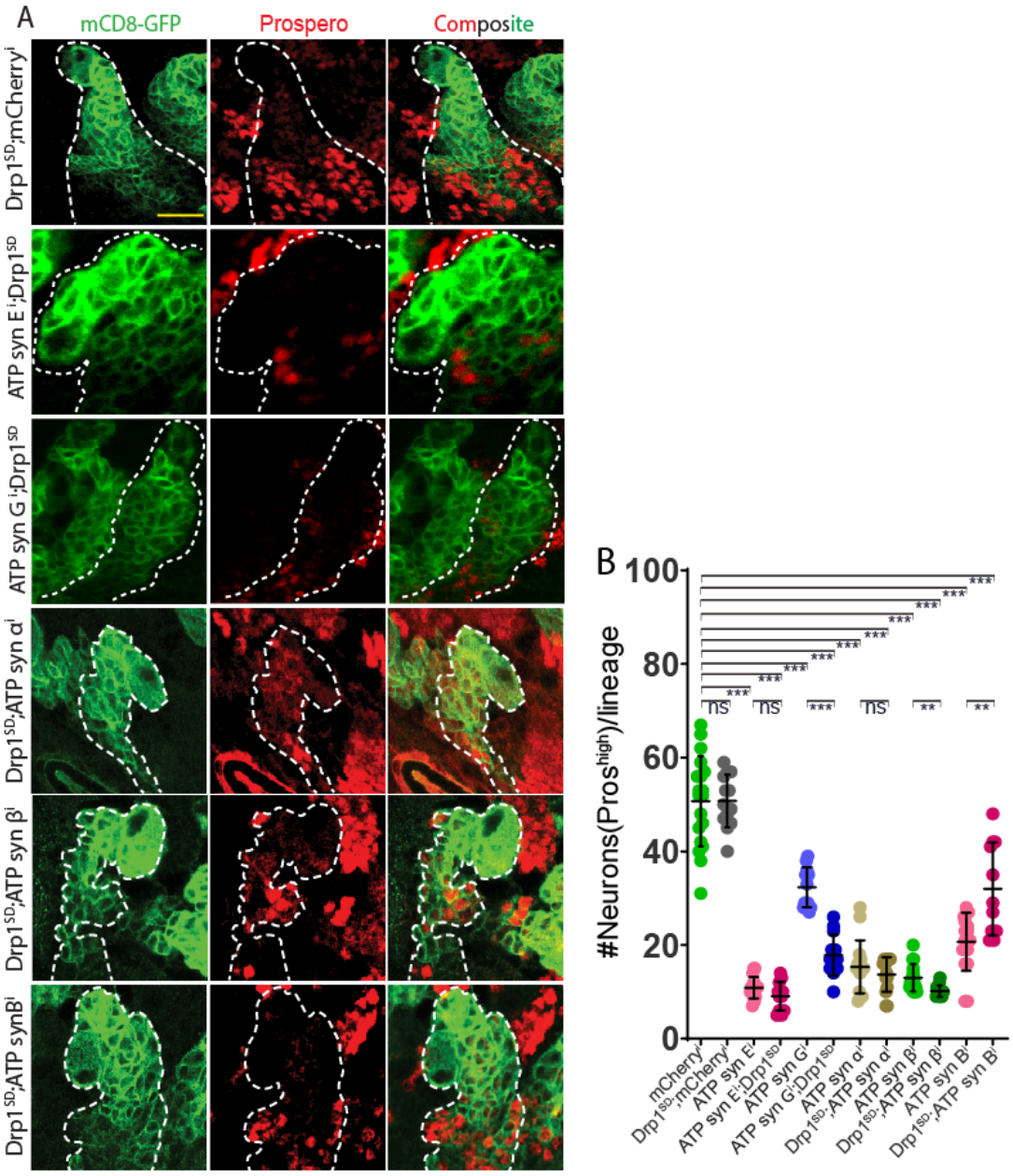


Figure 7.6: Mitochondrial fusion fails to restore the reduced numbers of neurons in lineage of type II neuroblasts lacking ATP synthase α, β, E, and G subunits but rescues in B subunit knockdown. (A) Representative images of neuron detection by immunostaining in type II neuroblast lineages of indicative genotypes. High nuclear Prospero positive cells are neurons (red). Scale bar- 10μm. **(B)** Neurons quantification in type II neuroblast lineages of genotypes, mCherry^{i} (n=19 type II neuroblast lineages, 5 brains), Drp1^{SD};mCherry^{i} (13,5), ATP

syn E^{i} (15,4), ATP syn E^{i};$Drp1^{SD}$ (12,4), ATP syn G^{i} (16,4), ATP syn G^{i};$Drp1^{SD}$ (13,4), ATP syn α^{i} (16,4), $Drp1^{SD}$;ATP syn α^{i} (14,4), ATP syn β^{i} (13,4), $Drp1^{SD}$;ATP syn β^{i} (13,4), ATP syn B^{i} (16,4), and $Drp1^{SD}$;ATP syn B^{i} (11,4). Data for all the single RNAi is taken from section 7.3.2. Mann-Whitney's t-test was performed for statistical analysis. ns=non-significant, **- $p<0.01$, ***- $p<0.001$.

7.3.4 Complex V downregulation in type II neuroblast increases ROS production and decreases MMP, which could not be reversed by mitochondrial fusion

Cristae morphology defects in type II neuroblasts are expected to impair ETC function. Therefore, we assessed mitochondrial activity in complex V-depleted type II neuroblasts by measuring cellular ROS and MMPl. Membrane potential is a functional readout of OXPHOS activity (Vander Heiden et al., 1997), while mitochondrial ROS reflects electron leakage from the ETC.

Dihydroethidium (DHE), a fluorescent probe that becomes activated upon oxidation by ROS, was used to measure cellular ROS levels. Tetramethylrhodamine Methyl Ester (TMRM), a voltage-sensitive dye that accumulates in regions of high membrane potential, was employed to assess mitochondrial membrane potential. In addition, cytochrome c was used as an indirect marker for cristae structure. As a peripheral inner membrane protein residing within cristae pockets, its proper containment depends on normal cristae architecture. Therefore, cristae morphology disruption is expected to cause cytoplasmic release of cytochrome c (Cogliati et al. 2016).

Membrane potential measurements displayed depolarisation upon depletion of ATP synthase subunits α, β, and B with $Drp1^{SD}$-mediated hyperfusion could not rescue these defects (Figure 7.7 A and B).

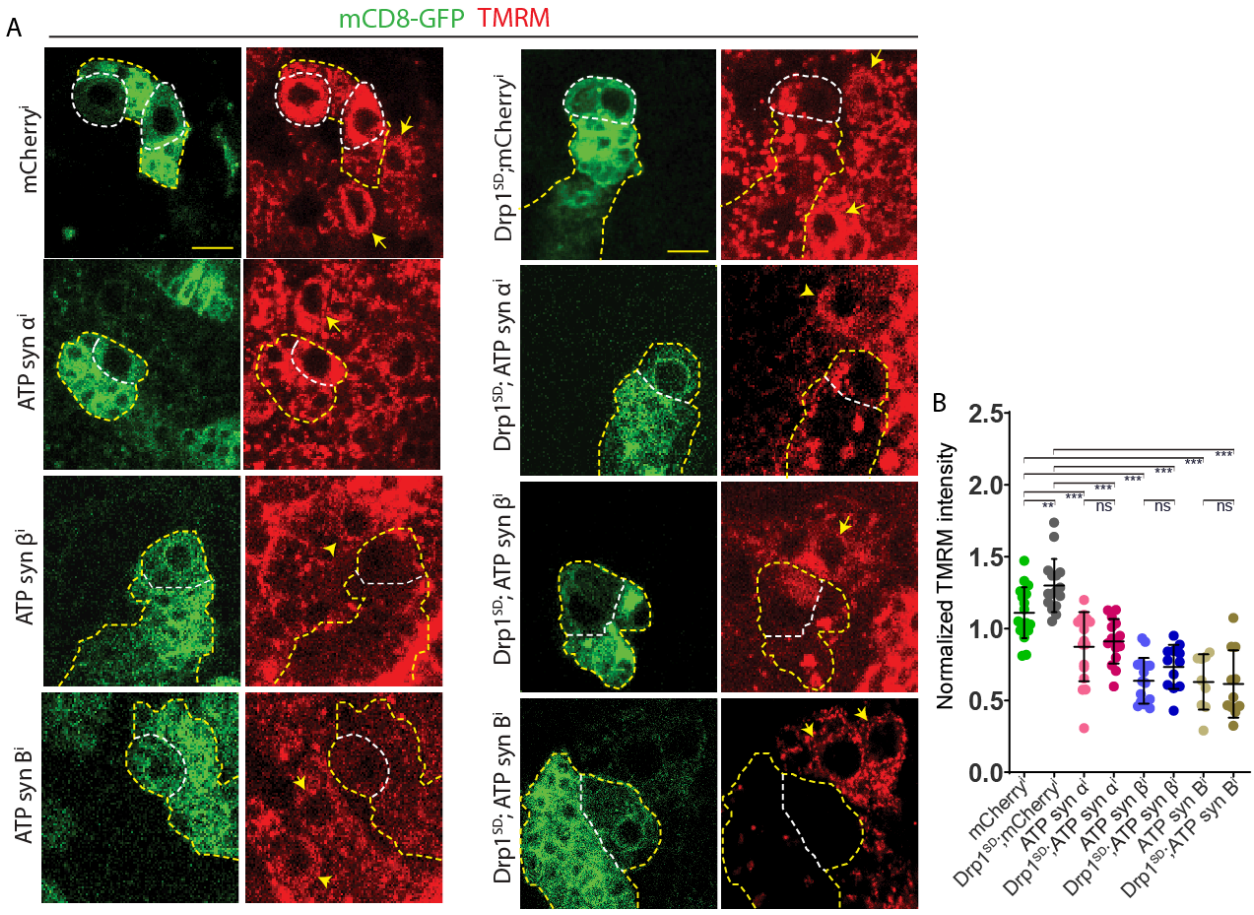


Figure 7.7: Mitochondrial fusion could not restore MMP loss in complex V-depleted type II neuroblasts (A) Representative images depicting MMP detection in type II neuroblasts of indicative genotypes using TMRM dye (red). *pnt*-Gal4 mediated expression of mCD8-GFP marks the boundary of neuroblasts and lineage cells. The white dashed outline denotes type II neuroblast. Surrounding control type I neuroblasts are shown by yellow arrowheads. Scale bar- 10µm. **(B)** TMRM intensity in type II neuroblasts was quantified and normalised to the intensity of neighbouring type I neuroblasts. The following genotypes were assessed: mCherry^i (n=19 type II neuroblasts, 5 brains), Drp1^{SD};mCherry^i (16, 5), ATP syn α^i (17,3), Drp1^{SD};ATP syn α^i (15,3), ATP syn β^i (16,3), Drp1^{SD};ATP syn β^i (13,3), ATP syn B^i (9,3), and Drp1^{SD};ATP syn B^i (11,3). Mann-Whitney's t-test was performed for statistical analysis. ns=non-significant, **- p<0.01, ***- p<0.001.

ATP synthase subunits α, β, and B depletions led to a significant rise in ROS. Co-expression of Drp1^{SD} rescued this elevation only in ATP synthase B depletion, but not with α or β subunit knockdowns (Figure 7.8 A and B). Given the established role of α and β subunits in dimerisation, this supports the idea that ATP synthase dimerisation is essential for hyperfusion-mediated rescue, and ROS regulation acting downstream, linking cristae structure to type II neuroblast differentiation.

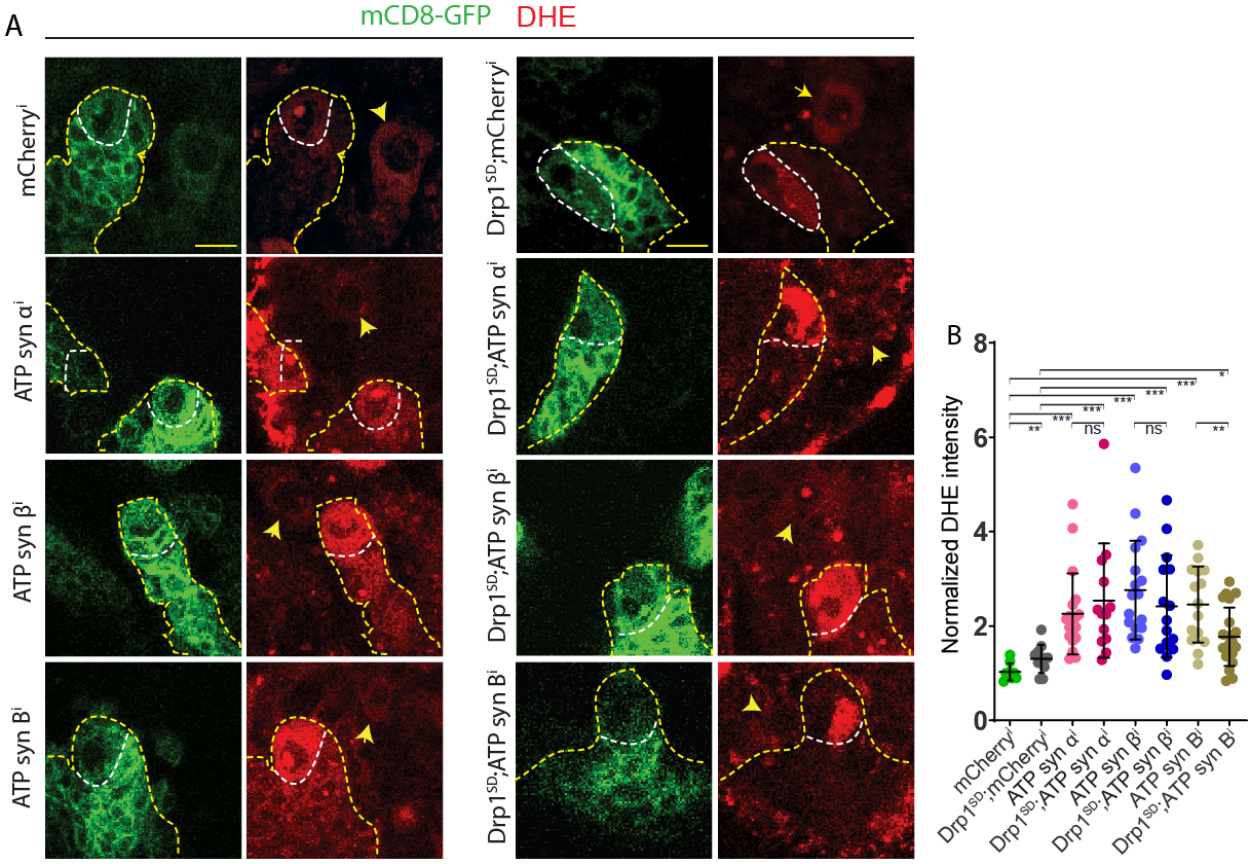


Figure 7.8: Mitochondrial hyperfusion failed to reduce elevated ROS levels in ATP synthase α and β-depleted type II neuroblasts, but suppressed ROS generation in ATP synthase B (A) Representative images of ROS detection in type II neuroblasts of the mentioned genotypes using DHE dye (red). The white dashed outline denotes type II neuroblast. Yellow arrowheads mark surrounding type I neuroblast. Scale bar- 10μm. **(B)** Quantification of DHE intensity in type II neuroblast normalised to surrounding type I

neuroblasts. Following genotypes were assessed: mCherry^{i} (n=37 type II neuroblasts, 4 brains), Drp1^{SD};mCherry^{i} (11, 5), ATP syn α^{i} (19,3), Drp1^{SD};ATP syn α^{i} (13,3), ATP syn β^{i} (15,3), Drp1^{SD};ATP syn β^{i} (15,3), ATP syn B^{i} (15,3), and Drp1^{SD};ATP syn B^{i} (21,3). Mann-Whitney's t-test was performed for statistical analysis. ns=non-significant, *- $p<0.05$,**- $p<0.01$, ***- $p<0.001$.

To further understand the role of ATP syn β subunit in maintaining the cristae architecture in neuroblast using transmission electron microscopy. Loss of the β subunit resulted in mitochondrial fragmentation (Figure 7.9 A and B) accompanied by a complete loss of cristae structure (Figure 7.9 A and C), highlighting its crucial role in preserving the inner membrane organisation. Expression of Drp1SD IN ATP syn β-depleted neuroblasts failed to restore either mitochondrial morphology or cristae integrity. This inability of induced mitochondrial fusion to compensate for the differentiation defects arising from the loss of ATP synthase dimer-forming subunits.

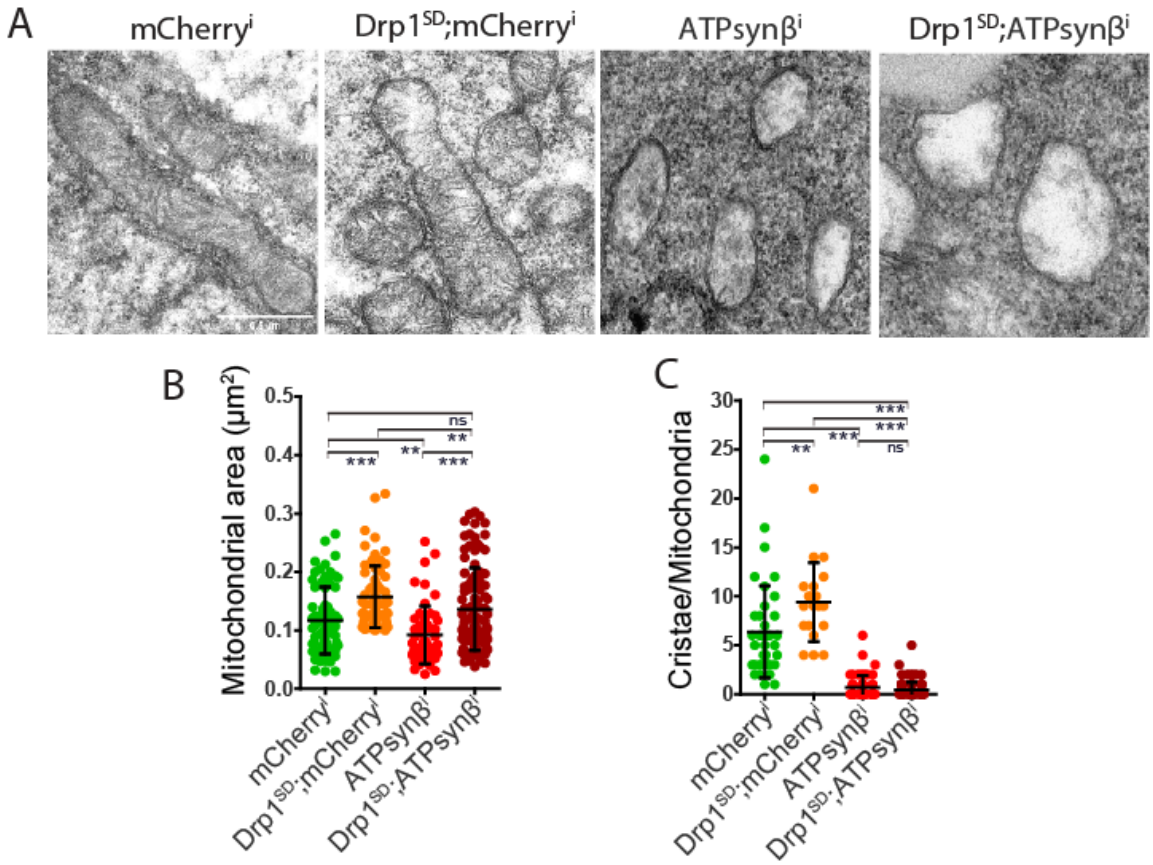


Figure 7.9. Depletion of ATP syn β subunit results in fragmented mitochondrial morphology and loss of cristae, and forced mitochondrial fusion could not rescue it. (A) Representative electron micrographs of mCherry^{i} neuroblasts (elongated and well-developed cristae mitochondria), Drp1^{SD};mCherry^{i} (fused, cristae-rich mitochondria clustered on one side of the neuroblasts), ATP syn β and and Drp1^{SD};ATP syn β^{i} (fragmented mitochondria which devoid of cristae). **(B)** Quantification of mitochondrial area in the following genotypes: mCherry^{i} (n=76 mitochondria, 10 neuroblasts, 3 brains), Drp1^{SD};mCherry^{i} (66, 8, 3), ATP syn β^{i} (54, 12, 3), Drp1^{SD};ATP syn β^{i} (104, 16, 3). **(C)** Quantification of cristae number in following genotypes: mCherry^{i} (n=39 mitochondria, 10 neuroblasts, 3 brains), Drp1^{SD};mCherry^{i} (20, 8, 3), ATP syn β^{i} (54, 12, 3), Drp1^{SD};ATP syn β^{i} (104, 16, 3)..

Cytochrome c distribution patterns further support this conclusion. Increased cytoplasmic cytochrome c levels were observed upon ATP synthase subunit α, β, and B

depletion in type II neuroblast (Figure 7.10 A and B), indicating disrupted cristae morphology. This defect was reversed in B subunit depletion upon Drp1^{SD} expression, but not rescued in α or β depletion (Figure 7.10 A and B), suggesting that hyperfusion cannot restore cristae integrity in the absence of ATP synthase dimerisation, resulting in a failure to rescue differentiation.

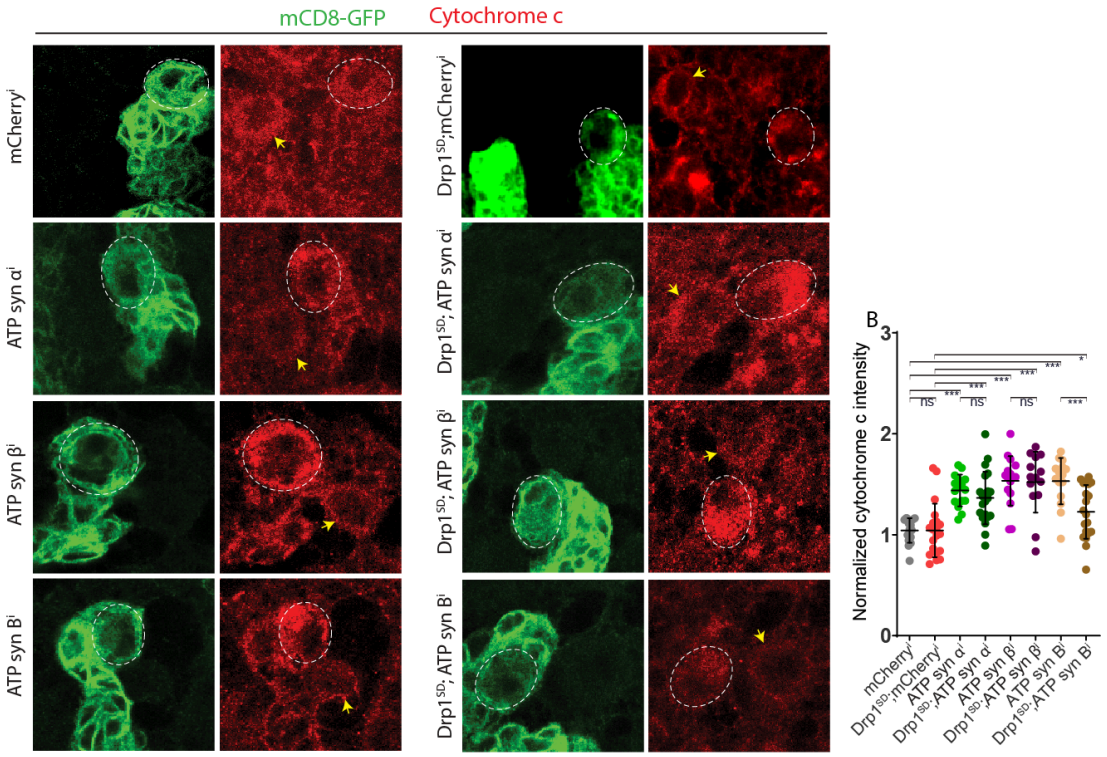


Figure 7.10: Mitochondrial hyperfusion alleviated cytoplasmic accumulation of cytochrome c in ATP synthase B-depleted type II neuroblasts but had no effect in α or β subunit knockdowns (A) Representative images of cytochrome c detection (red) in type II neuroblasts of the mentioned genotypes by immunostaining. The white dashed outline denotes type II neuroblast. Yellow arrowheads mark the surrounding type I neuroblast. **(B)** Quantification of cytochrome c intensity in type II neuroblast, normalised to control type I neuroblast. The following genotypes were assessed: mCherry^i (n=16 type II neuroblasts, 4 brains), Drp1^{SD};mCherry^i (20, 5), ATP syn α^i (16,3), Drp1^{SD};ATP syn α^i (21,3), ATP syn β^i (18,5), Drp1^{SD};ATP syn β^i (15,3), ATP syn B^i (15,5), and Drp1^{SD};ATP syn B^i (20,3). Mann-Whitney's t-test was performed for statistical analysis. ns=non-significant, *- p<0.05, ***- p<0.001.

7.4 Discussion

Our study highlights the role of ATP synthase dimer-forming subunits α, β, E, and G in type II neuroblast proliferation and differentiation. Depletion of ATP synthase subunits α, β, E, and G reduces neuroblast proliferation and their differentiation. Downregulation of ATP synthase subunit B, which is not involved in dimer formation, also led to similar differentiation defects, indicating that both OXPHOS and ATP synthase dimerisation play crucial roles in neuroblast development. In mammalian and *Drosophila* stem cells, mitochondrial dynamics and cristae morphology have been directly linked to stem cell fate decisions (Khacho et al. 2016; Teixeira et al. 2015; van den Ameele and Brand 2019). $Drp1^{SD}$-induced mitochondrial hyperfusion failed to rescue the differentiation defects in neuroblasts lacking dimer-forming subunits α, β, E, and G. However, a partial rescue was observed in ATP synthase B-depleted lineages, indicating a vital role for ATP synthase dimerisation and cristae architecture in enabling hyperfusion-mediated rescue.

Cristae disorganisation is known to impair ETC function (Cogliati et al. 2016). We observed loss of MMP and elevated ROS levels in α, β, and B subunit knockdowns. While fusion could not rescue membrane depolarisation, it rescued ROS levels only in the ATP synthase B knockdown upon $Drp1^{SD}$ expression. These results suggest that ROS regulation by hyperfusion depends on intact ATP synthase dimerisation.

Furthermore, immunostaining for cytochrome c revealed its cytoplasmic leakage in α, β, and B knockdowns, indicating disrupted cristae integrity. This Cytochrome c leakage reversed only in the B subunit knockdown on induction of mitochondrial fusion but not in α or β-depleted type II neuroblasts. Since cytochrome c typically resides in cristae pockets and its release suggests cristae disruption, these results reinforce the idea that hyperfusion cannot restore cristae integrity without functional dimer formation (Cogliati et al. 2016).

Chapter 8

Summary of thesis

Stem cells have an inherent capacity to balance self-renewal and differentiation. Traditionally viewed as energy powerhouses, mitochondria have emerged as dynamic organelles that regulate stem cell fate by modulating morphology, activity, and signaling (Seo et al. 2018). The cristae morphology, mitochondrial membrane potential (MMP), and ROS generation are related components of mitochondrial function, which shape cellular behaviour. We used the *Drosophila* third instar larval brain as a model system to study these mechanisms, specifically in type II neuroblasts that undergo asymmetric divisions to produce transit-amplifying intermediate neural progenitors (INPs), which divide asymmetrically to form ganglion mother cells (GMCs). GMCs then divide symmetrically to form neurons or glia (Boone and Doe 2008).

This thesis investigates how the interaction between mitochondrial fusion and electron transport chain (ETC) function influences the proliferation and differentiation of *Drosophila* neuroblasts (Table 2)

ETC Complex		NBs mitotic index		mINPs		GMCs		Neurons		ROS		MMP	
	Subunit KD	ETC KD	Drp1SD + ETC KD	ETC KD	Drp1SD + ETC KD	ETC KD	Drp1SD + ETC KD	ETC KD	Drp1SD + ETC KD	ETC KD	DDrp1SD + ETC KD	ETC KD	Drp1SD + ETC KD
I	ND-51, ND-39, ND-19	↓	✓	↓	✓	↓	✓	↓	✓	↑	✓	↓	✓
II	SdhD	↑	X	↑	X	↑	X	↓	-	↑	-	↓	-
IV	Cox8, Cox7C, Cox6C, Cox5A	↓	✓	↓	✓	↓	✓	↓	✓	↓	X	↓	✓
V	ATP syn α, β, E, G, B	↓	X	↓	X	↓	X	↓	X	↑	X	↓	X

Table 2: Summary of phenotypic outcomes upon depletion of ETC complexes in the type II neuroblast. This table provides an overview of the mitochondrial activity and differentiation-related phenotypes observed following the depletion of individual subunits from ETC Complexes I–V, as well as ETC knockdown in the background of mitochondrial force fusion in Drosophila type II neuroblasts. Phenotypes include alterations in neuroblast proliferation, cells in the lineage (mINPs, GMCs and neurons), membrane potential and ROS levels.

Complex I-mediated regulation of ROS levels and cell cycle progression through G1/S phase

We found that depletion of complex I in type II neuroblasts leads to mitochondrial fragmentation, reduced cristae, lower MMP, and elevated ROS levels. Increased ROS generation in neuroblasts impairs G1/S transition by reducing nuclear Cyclin E accumulation, leading to reduced proliferation of neuroblasts and mature INPs. It ultimately leads to fewer mature INPs, GMCs, and neurons in the lineage.

Fusion of mitochondria by additional depletion of Drp1 rescued these defects. It restored mitochondrial morphology, reduced ROS levels, and increased nuclear Cyclin E localisation. Overexpression of ROS scavenger enzymes like SOD2 and catalase in complex I deficient type II neuroblasts also restored differentiation by reducing ROS levels. These results suggest that optimal ROS levels are crucial for proper neuroblast proliferation and differentiation.

Divergent roles of complex II in proliferation and differentiation of type II neuroblasts

In contrast to complex I, perturbation of Complex II increased neuroblast and mINP proliferation, leading to more mature INPs and GMCs, respectively, but produced a lesser number of neurons in the lineage than control. Despite similar reductions in MMP and elevations in ROS, on complex I and II depletion, Complex II led to differentiation defects opposite to complex I, suggesting a unique mechanism distinct from MMP and ROS. Given the complex II plays a dual role in the ETC and the TCA cycle, perturbations in metabolic intermediates (e.g., FAD/$FADH_2$ ratios) may drive these abnormalities. Future analyses on metabolomic profiling in neuroblasts may help to dissect this pathway further.

Complex IV: Mitochondrial fusion leads to ROS-independent rescue in complex IV depleted type II neurblasts

Complex IV is the terminal ETC complex, which reduces oxygen into water, pumps protons into the intermembrane space, and maintains MMP. Its depletion led to the loss of MMP and complete abolishment of ROS levels, reduced Cyclin E nuclear accumulation and disrupted neuroblast proliferation and differentiation.

Forced mitochondrial fusion rescued both MMP and differentiation, but not ROS levels. This indicates that ROS may not be the primary signal leading to defects in complex IV depleted type II neuroblasts, and instead, membrane potential or metabolic flux restoration through fusion may drive rescue.

Complex V: ATP Synthase dimerisation regulates cristae architecture and differentiation

Complex V in the inner membrane dimerises and self-organises in rows, inducing positive membrane curvature and forming the cristae tips (Teixeira et al. 2015). Perturbation of complex V by downregulating its subunits involved in dimerisation—α, β, E, and G—disrupted cristae morphology, caused mitochondrial fragmentation, elevated ROS levels and led to proliferation and differentiation defects, characterised by reduced mature INPs, GMCs and neurons in the lineage. These defects could not be rescued by mitochondrial forced fusion. In contrast, the knockdown of ATP synthase subunit B, which is not involved in dimer formation, showed rescue of ROS levels and differentiation upon $Drp1^{SD}$-induced fusion. This suggests that dimerisation-dependent cristae integrity is essential for fusion-mediated rescue.

In conclusion, these studies support the role of varied mitochondrial activities and metabolites derived from the activity of each of the complexes of the ETC in differentiation of *Drosophila* type II neuroblast lineage. Whereas, the studies show a conclusive role for appropriate ROS levels in driving neuroblast type II differentiation by complex I, future analysis of the mechanism by which complex II, IV and V regulate differentiation will be revealed by evaluating the change in metabolites on their depletion.

9. References

Acton, B. M., A. Jurisicova, I. Jurisica, and R. F. Casper. 2004. “Alterations in Mitochondrial Membrane Potential during Preimplantation Stages of Mouse and Human Embryo Development.” *Molecular Human Reproduction* 10 (1): 23–32. https://doi.org/10.1093/molehr/gah004.

Agip, Ahmed-Noor A., Injae Chung, Alvaro Sanchez-Martinez, Alexander J. Whitworth, and Judy Hirst. 2023. “Cryo-EM Structures of Mitochondrial Respiratory Complex I from Drosophila Melanogaster.” *eLife* 12 (January): e84424. https://doi.org/10.7554/eLife.84424.

Ameele, Jelle van den, and Andrea H. Brand. 2019. “Neural Stem Cell Temporal Patterning and Brain Tumour Growth Rely on Oxidative Phosphorylation.” *eLife* 8 (September). https://doi.org/10.7554/eLife.47887.

Amiri, Haleh, Olof Karlberg, and Siv G. E. Andersson. 2003. “Deep Origin of Plastid/parasite ATP/ADP Translocases.” *Journal of Molecular Evolution* 56 (2): 137–150. https://doi.org/10.1007/s00239-002-2387-0.

Apitz, Holger, and Iris Salecker. 2016. “Retinal Determination Genes Coordinate Neuroepithelial Specification and Neurogenesis Modes in the Drosophila Optic Lobe.” *Development (Cambridge, England)* 143 (13): 2431–2442. https://doi.org/10.1242/dev.135004.

Archibald, J. 2014. *One Plus One Equals One: Symbiosis and the Evolution of Complex Life*. Oxford University Press.

Arnold, S., F. Goglia, and B. Kadenbach. 1998. “3,5-Diiodothyronine Binds to Subunit Va of Cytochrome-c Oxidase and Abolishes the Allosteric Inhibition of Respiration by ATP.” *European Journal of Biochemistry* 252 (2): 325–330. https://doi.org/10.1046/j.1432-1327.1998.2520325.x.

Arnold, S., and B. Kadenbach. 1997. “Cell Respiration Is Controlled by ATP, an Allosteric Inhibitor of Cytochrome-c Oxidase.” *European Journal of Biochemistry* 249 (1): 350–354. https://doi.org/10.1111/j.1432-1033.1997.t01-1-00350.x.

Ashrafi, Ghazaleh, Julia S. Schlehe, Matthew J. LaVoie, and Thomas L. Schwarz. 2014. “Mitophagy of Damaged Mitochondria Occurs Locally in Distal Neuronal Axons and Requires PINK1 and Parkin.” *The Journal of Cell Biology* 206 (5): 655–670. https://doi.org/10.1083/jcb.201401070.

Astuti, D., F. Latif, A. Dallol, et al. 2001. “Gene Mutations in the Succinate Dehydrogenase Subunit SDHB Cause Susceptibility to Familial Pheochromocytoma and to Familial Paraganglioma.” *The American Journal of Human Genetics* 69 (1): 49–54. https://doi.org/10.1086/321282.

Atwood, Scott X., and Kenneth E. Prehoda. 2009. “aPKC Phosphorylates Miranda to Polarize Fate Determinants during Neuroblast Asymmetric Cell Division.” *Current Biology: CB* 19 (9): 723–729. https://doi.org/10.1016/j.cub.2009.03.056.

Bandara, Aloka B., Joshua C. Drake, and David A. Brown. 2021. “Complex II Subunit SDHD Is Critical for Cell Growth and Metabolism, Which Can Be Partially Restored with a Synthetic Ubiquinone Analog.” *BMC Molecular and Cell Biology* 22 (1): 35. https://doi.org/10.1186/s12860-021-00370-w.

Barsoum, Mark J., Hua Yuan, Akos A. Gerencser, et al. 2006. “Nitric Oxide-Induced Mitochondrial Fission Is Regulated by Dynamin-Related GTPases in Neurons.” *The EMBO Journal* 25 (16): 3900–3911. https://doi.org/10.1038/sj.emboj.7601253.

Bayraktar, Omer Ali, Jason Q. Boone, Michael L. Drummond, and Chris Q. Doe. 2010. “Drosophila Type II Neuroblast Lineages Keep Prospero Levels Low to Generate Large Clones That Contribute to the Adult Brain Central Complex.” *Neural Development* 5 (1): 26. https://doi.org/10.1186/1749-8104-5-26.

Baysal, B. E., R. E. Ferrell, J. E. Willett-Brozick, et al. 2000. “Mutations in SDHD, a Mitochondrial Complex II Gene, in Hereditary Paraganglioma.” *Science (New York, N.Y.)* 287 (5454): 848–851. https://doi.org/10.1126/science.287.5454.848.

Bello, Bruno C., Natalya Izergina, Emmanuel Caussinus, and Heinrich Reichert. 2008. “Amplification of Neural Stem Cell Proliferation by Intermediate Progenitor Cells in Drosophila Brain Development.” *Neural Development* 3 (1): 5. https://doi.org/10.1186/1749-8104-3-5.

Berger, Itai, Eli Hershkovitz, Avraham Shaag, Simon Edvardson, Ann Saada, and Orly Elpeleg. 2008. “Mitochondrial Complex I Deficiency Caused by a Deleterious NDUFA11 Mutation.” *Annals of Neurology* 63 (3): 405–408. https://doi.org/10.1002/ana.21332.

Berndtsson, Jens, Andreas Kohler, Sorbhi Rathore, et al. 2020. “Respiratory Supercomplexes Enhance Electron Transport by Decreasing Cytochrome c Diffusion Distance.” *EMBO Reports* 21 (12): e51015. https://doi.org/10.15252/embr.202051015.

Bombelka, E., F. W. Richter, A. Stroh, and B. Kadenbach. 1986. “Analysis of the Cu, Fe,

and Zn Contents in Cytochrome C Oxidases from Different Species and Tissues by Proton-Induced X-Ray Emission (PIXE).” *Biochemical and Biophysical Research Communications* 140 (3): 1007–1014. https://doi.org/10.1016/0006-291x(86)90735-7.

Bonnay, François, Ana Veloso, Victoria Steinmann, et al. 2020. “Oxidative Metabolism Drives Immortalization of Neural Stem Cells during Tumorigenesis.” *Cell* 182 (6): 1490–1507.e19. https://doi.org/10.1016/j.cell.2020.07.039.

Boone, Jason Q., and Chris Q. Doe. 2008. “Identification of Drosophila Type II Neuroblast Lineages Containing Transit Amplifying Ganglion Mother Cells.” *Developmental Neurobiology* 68 (9): 1185–1195. https://doi.org/10.1002/dneu.20648.

Bourgeron, T., P. Rustin, D. Chretien, et al. 1995. “Mutation of a Nuclear Succinate Dehydrogenase Gene Results in Mitochondrial Respiratory Chain Deficiency.” *Nature Genetics* 11 (2): 144–149. https://doi.org/10.1038/ng1095-144.

Brand, Martin D. 2010. “The Sites and Topology of Mitochondrial Superoxide Production.” *Experimental Gerontology* 45 (7-8): 466–472. https://doi.org/10.1016/j.exger.2010.01.003.

Buescher, M., S. L. Yeo, G. Udolph, et al. 1998. “Binary Sibling Neuronal Cell Fate Decisions in the Drosophila Embryonic Central Nervous System Are Nonstochastic and Require Inscuteable-Mediated Asymmetry of Ganglion Mother Cells.” *Genes & Development* 12 (12): 1858–1870. https://doi.org/10.1101/gad.12.12.1858.

Burman, Jonathon L., Sarah Pickles, Chunxin Wang, et al. 2017. “Mitochondrial Fission Facilitates the Selective Mitophagy of Protein Aggregates.” *The Journal of Cell Biology* 216 (10): 3231–3247. https://doi.org/10.1083/jcb.201612106.

Cabrera, Carlos V. 1990. “Lateral Inhibition and Cell Fate during Neurogenesis in *Drosophila:* the Interactions between *scute, Notch* and *Delta*.” *Development (Cambridge, England)* 109 (3): 733–742. https://doi.org/10.1242/dev.109.3.733.

Cadenas, E., and K. J. Davies. 2000. “Mitochondrial Free Radical Generation, Oxidative Stress, and Aging.” *Free Radical Biology & Medicine* 29 (3-4): 222–230. https://doi.org/10.1016/s0891-5849(00)00317-8.

Chang, Xiaoru, Shuyan Niu, Mengting Shang, et al. 2023. “ROS-Drp1-Mediated Mitochondria Fission Contributes to Hippocampal HT22 Cell Apoptosis Induced by Silver Nanoparticles.” *Redox Biology* 63 (102739): 102739. https://doi.org/10.1016/j.redox.2023.102739.

Chen, Hsiuchen, and David C. Chan. 2017. “Mitochondrial Dynamics in Regulating the Unique Phenotypes of Cancer and Stem Cells.” *Cell Metabolism* 26 (1): 39–48. https://doi.org/10.1016/j.cmet.2017.05.016.

Chowdhary, Sayali, Somya Madan, Darshika Tomer, Manos Mavrakis, and Richa Rikhy. 2020. “Mitochondrial Morphology and Activity Regulate Furrow Ingression and Contractile Ring Dynamics in Drosophila Cellularization.” *Molecular Biology of the Cell* 31 (21): 2331–2347. https://doi.org/10.1091/mbc.E20-03-0177.

Chowdhary, Sayali, Darshika Tomer, Dnyanesh Dubal, Devashree Sambre, and Richa Rikhy. 2017. “Analysis of Mitochondrial Organization and Function in the Drosophila Blastoderm Embryo.” *Scientific Reports* 7 (1): 5502. https://doi.org/10.1038/s41598-017-05679-1.

Chung, Susan, Petras P. Dzeja, Randolph S. Faustino, Carmen Perez-Terzic, Atta Behfar, and Andre Terzic. 2007. “Mitochondrial Oxidative Metabolism Is Required for the Cardiac Differentiation of Stem Cells.” *Nature Clinical Practice. Cardiovascular Medicine* 4 Suppl 1 (S1): S60–7. https://doi.org/10.1038/ncpcardio0766.

Cipolat, Sara, Olga Martins de Brito, Barbara Dal Zilio, and Luca Scorrano. 2004. “OPA1 Requires Mitofusin 1 to Promote Mitochondrial Fusion.” *Proceedings of the National Academy of Sciences of the United States of America* 101 (45): 15927–15932. https://doi.org/10.1073/pnas.0407043101.

Cogliati, Sara, Jose A. Enriquez, and Luca Scorrano. 2016. “Mitochondrial Cristae: Where Beauty Meets Functionality.” *Trends in Biochemical Sciences* 41 (3): 261–273. https://doi.org/10.1016/j.tibs.2016.01.001.

Colpman, Pierce, Asish Dasgupta, and Stephen L. Archer. 2023. “The Role of Mitochondrial Dynamics and Mitotic Fission in Regulating the Cell Cycle in Cancer and Pulmonary Arterial Hypertension: Implications for Dynamin-Related Protein 1 and Mitofusin2 in Hyperproliferative Diseases.” *Cells (Basel, Switzerland)* 12 (14): 1897. https://doi.org/10.3390/cells12141897.

Deng, Hansong, Shigeo Takashima, Manash Paul, Ming Guo, and Volker Hartenstein. 2018. “Mitochondrial Dynamics Regulates Drosophila Intestinal Stem Cell Differentiation.” *Cell Death Discovery* 4 (1): 17. https://doi.org/10.1038/s41420-018-0083-0.

Devenish, Rodney J., Mark Prescott, and Andrew J. W. Rodgers. 2008. “The Structure and Function of Mitochondrial F1F0-ATP Synthases.” *International Review of Cell and Molecular Biology* 267: 1–58. https://doi.org/10.1016/S1937-6448(08)00601-1.

Doerflinger, Hélène, Nina Vogt, Isabel L. Torres, et al. 2010. “Bazooka Is Required for Polarisation of the Drosophila Anterior-Posterior Axis.” *Development (Cambridge, England)* 137 (10): 1765–1773. https://doi.org/10.1242/dev.045807.

Dubal, Dnyanesh, Prachiti Moghe, Rahul Kumar Verma, Bhavin Uttekar, and Richa Rikhy. 2022. “Mitochondrial Fusion Regulates Proliferation and Differentiation in the Type II Neuroblast Lineage in Drosophila.” *PLoS Genetics* 18 (2): e1010055. https://doi.org/10.1371/journal.pgen.1010055.

Egger, Boris, James M. Chell, and Andrea H. Brand. 2008. “Insights into Neural Stem Cell Biology from Flies.” *Philosophical Transactions of the Royal Society of London. Series B, Biological Sciences* 363 (1489): 39–56. https://doi.org/10.1098/rstb.2006.2011.

Facucho-Oliveira, Joao M., Jon Alderson, Emma C. Spikings, Stuart Egginton, and Justin C. St John. 2007. “Mitochondrial DNA Replication during Differentiation of Murine Embryonic Stem Cells.” *Journal of Cell Science* 120 (Pt 22): 4025–4034. https://doi.org/10.1242/jcs.016972.

Falkenberg, Maria, and Nils-Göran Larsson. 2009. “Structure Casts Light on mtDNA Replication.” *Cell* 139 (2): 231–233. https://doi.org/10.1016/j.cell.2009.09.030.

Fernández-Moreno, Miguel Angel, Carol L. Farr, Laurie S. Kaguni, and Rafael Garesse. 2007. “Drosophila Melanogaster as a Model System to Study Mitochondrial Biology.” *Methods in Molecular Biology (Clifton, N.J.)* 372: 33–49. https://doi.org/10.1007/978-1-59745-365-3_3.

Garcia, Christian Joel, Jahan Khajeh, Emmanuel Coulanges, Emily I-Ju Chen, and Edward Owusu-Ansah. 2017. “Regulation of Mitochondrial Complex I Biogenesis in Drosophila Flight Muscles.” *Cell Reports* 20 (1): 264–278. https://doi.org/10.1016/j.celrep.2017.06.015.

Gilkerson, Robert W., Jeanne M. L. Selker, and Roderick A. Capaldi. 2003. “The Cristal Membrane of Mitochondria Is the Principal Site of Oxidative Phosphorylation.” *FEBS Letters* 546 (2-3): 355–358. https://doi.org/10.1016/s0014-5793(03)00633-1.

Gomes, Ligia C., Giulietta Di Benedetto, and Luca Scorrano. 2011. “During Autophagy Mitochondria Elongate, Are Spared from Degradation and Sustain Cell Viability.” *Nature Cell Biology* 13 (5): 589–598. https://doi.org/10.1038/ncb2220.

Green, Douglas R., and Guido Kroemer. 2004. “The Pathophysiology of Mitochondrial Cell Death.” *Science (New York, N.Y.)* 305 (5684): 626–629. https://doi.org/10.1126/science.1099320.

Guarani, Virginia, Joao Paulo, Bo Zhai, Edward L. Huttlin, Steven P. Gygi, and J. Wade Harper. 2014. “TIMMDC1/C3orf1 Functions as a Membrane-Embedded Mitochondrial Complex I Assembly Factor through Association with the MCIA Complex.” *Molecular and Cellular Biology* 34 (5): 847–861. https://doi.org/10.1128/MCB.01551-13.

Gu, Wen, Xavier Gaeta, Anna Sahakyan, et al. 2016. “Glycolytic Metabolism Plays a Functional Role in Regulating Human Pluripotent Stem Cell State.” *Cell Stem Cell* 19 (4): 476–490. https://doi.org/10.1016/j.stem.2016.08.008.

Hannaford, Matthew Robert, Anne Ramat, Nicolas Loyer, and Jens Januschke. 2018. “aPKC-Mediated Displacement and Actomyosin-Mediated Retention Polarize Miranda in Drosophila Neuroblasts.” *eLife* 7 (January). https://doi.org/10.7554/elife.29939.

Hirst, Judy. 2009. “Towards the Molecular Mechanism of Respiratory Complex I.” *The Biochemical Journal* 425 (2): 327–339. https://doi.org/10.1042/BJ20091382.

Homem, Catarina C. F., and Juergen A. Knoblich. 2012. “Drosophila Neuroblasts: A Model for Stem Cell Biology.” *Development (Cambridge, England)* 139 (23): 4297–4310. https://doi.org/10.1242/dev.080515.

Homem, Catarina C. F., Marko Repic, and Jürgen A. Knoblich. 2015. “Proliferation Control in Neural Stem and Progenitor Cells.” *Nature Reviews. Neuroscience* 16 (11): 647–659. https://doi.org/10.1038/nrn4021.

Homem, Catarina C. F., Victoria Steinmann, Thomas R. Burkard, Alexander Jais, Harald Esterbauer, and Juergen A. Knoblich. 2014. “Ecdysone and Mediator Change Energy Metabolism to Terminate Proliferation in Drosophila Neural Stem Cells.” *Cell* 158 (4): 874–888. https://doi.org/10.1016/j.cell.2014.06.024.

Hong, Y., B. Stronach, N. Perrimon, L. Y. Jan, and Y. N. Jan. 2001. “Drosophila Stardust Interacts with Crumbs to Control Polarity of Epithelia but Not Neuroblasts.” *Nature* 414 (6864): 634–638. https://doi.org/10.1038/414634a.

Horsefield, Rob, So Iwata, and Bernadette Byrne. 2004. “Complex II from a Structural Perspective.” *Current Protein & Peptide Science* 5 (2): 107–118. https://doi.org/10.2174/1389203043486847.

Ikon, Nikita, and Robert O. Ryan. 2017. “Cardiolipin and Mitochondrial Cristae Organization.” *Biochimica et Biophysica Acta. Biomembranes* 1859 (6): 1156–1163. https://doi.org/10.1016/j.bbamem.2017.03.013.

Isshiki, T., B. Pearson, S. Holbrook, and C. Q. Doe. 2001. “Drosophila Neuroblasts Sequentially Express Transcription Factors Which Specify the Temporal Identity of Their Neuronal Progeny.” *Cell* 106 (4): 511–521. https://doi.org/10.1016/s0092-8674(01)00465-2.

Iwata, S. 1998. “Structure and Function of Bacterial Cytochrome c Oxidase.” *The Journal of Biochemistry* 123 (3): 369–375. https://doi.org/10.1093/oxfordjournals.jbchem.a021946.

Jasra, Ila Tewari, Nerea Cuesta-Gomez, Kevin Verhoeff, Braulio A. Marfil-Garza, Nidheesh Dadheech, and A. M. James Shapiro. 2023. “Mitochondrial Regulation in Human Pluripotent Stem Cells during Reprogramming and β Cell Differentiation.” *Frontiers in Endocrinology* 14 (October): 1236472. https://doi.org/10.3389/fendo.2023.1236472.

Ježek, Jan, Katrina Cooper, and Randy Strich. 2018. “Reactive Oxygen Species and Mitochondrial Dynamics: The Yin and Yang of Mitochondrial Dysfunction and Cancer Progression.” *Antioxidants (Basel, Switzerland)* 7 (1): 13. https://doi.org/10.3390/antiox7010013.

John, P., and F. R. Whatley. 1975. “Paracoccus Denitrificans and the Evolutionary Origin of the Mitochondrion.” *Nature* 254 (5500): 495–498. https://doi.org/10.1038/254495a0.

Junge, Wolfgang, and Nathan Nelson. 2015. “ATP Synthase.” *Annual Review of Biochemistry* 84 (1): 631–657. https://doi.org/10.1146/annurev-biochem-060614-034124.

Kasahara, Atsuko, Sara Cipolat, Yun Chen, Gerald W. Dorn 2nd, and Luca Scorrano. 2013. “Mitochondrial Fusion Directs Cardiomyocyte Differentiation via Calcineurin and Notch Signaling.” *Science (New York, N.Y.)* 342 (6159): 734–737. https://doi.org/10.1126/science.1241359.

Kashatus, David F., Kian-Huat Lim, Donita C. Brady, Nicole L. K. Pershing, Adrienne D. Cox, and Christopher M. Counter. 2011. “RALA and RALBP1 Regulate Mitochondrial Fission at Mitosis.” *Nature Cell Biology* 13 (9): 1108–1115. https://doi.org/10.1038/ncb2310.

Kelsom, Corey, and Wange Lu. 2012. “Uncovering the Link between Malfunctions in Drosophila Neuroblast Asymmetric Cell Division and Tumorigenesis.” *Cell & Bioscience* 2 (1): 38. https://doi.org/10.1186/2045-3701-2-38.

Khacho, Mireille, Alysen Clark, Devon S. Svoboda, et al. 2016. “Mitochondrial Dynamics

Impacts Stem Cell Identity and Fate Decisions by Regulating a Nuclear Transcriptional Program." *Cell Stem Cell* 19 (2): 232–247. https://doi.org/10.1016/j.stem.2016.04.015.

Kianian, Penny M. A., and Shahryar F. Kianian. 2014. "Mitochondrial Dynamics and the Cell Cycle." *Frontiers in Plant Science* 5 (May): 222. https://doi.org/10.3389/fpls.2014.00222.

Knoblich, Juergen A. 2010. "Asymmetric Cell Division: Recent Developments and Their Implications for Tumour Biology." *Nature Reviews. Molecular Cell Biology* 11 (12): 849–860. https://doi.org/10.1038/nrm3010.

Kohler, Andreas, Antoni Barrientos, Flavia Fontanesi, and Martin Ott. 2023. "The Functional Significance of Mitochondrial Respiratory Chain Supercomplexes." *EMBO Reports* 24 (11): e57092. https://doi.org/10.15252/embr.202357092.

Koju, Nirmala, Abdoh Taleb, Jifang Zhou, et al. 2019. "Pharmacological Strategies to Lower Crosstalk between Nicotinamide Adenine Dinucleotide Phosphate (NADPH) Oxidase and Mitochondria." *Biomedecine & Pharmacotherapie [Biomedicine & Pharmacotherapy]* 111 (March): 1478–1498. https://doi.org/10.1016/j.biopha.2018.11.128.

Kraft, Lauren M., and Laura L. Lackner. 2018. "Mitochondrial Anchors: Positioning Mitochondria and More." *Biochemical and Biophysical Research Communications* 500 (1): 2–8. https://doi.org/10.1016/j.bbrc.2017.06.193.

Kunz, Thomas, Karoline F. Kraft, Gerhard M. Technau, and Rolf Urbach. 2012. "Origin of Drosophila Mushroom Body Neuroblasts and Generation of Divergent Embryonic Lineages." *Development (Cambridge, England)* 139 (14): 2510–2522. https://doi.org/10.1242/dev.077883.

Lai, Sen-Lin, Takeshi Awasaki, Kei Ito, and Tzumin Lee. 2008. "Clonal Analysis of Drosophila Antennal Lobe Neurons: Diverse Neuronal Architectures in the Lateral Neuroblast Lineage." *Development (Cambridge, England)* 135 (17): 2883–2893. https://doi.org/10.1242/dev.024380.

Lambert, Adrian J., and Martin D. Brand. 2004. "Superoxide Production by NADH:ubiquinone Oxidoreductase (complex I) Depends on the pH Gradient across the Mitochondrial Inner Membrane." *The Biochemical Journal* 382 (Pt 2): 511–517. https://doi.org/10.1042/BJ20040485.

Lane, Nick, and William Martin. 2010. "The Energetics of Genome Complexity." *Nature* 467 (7318): 929–934. https://doi.org/10.1038/nature09486.

Lee, T., A. Lee, and L. Luo. 1999. “Development of the Drosophila Mushroom Bodies: Sequential Generation of Three Distinct Types of Neurons from a Neuroblast.” *Development (Cambridge, England)* 126 (18): 4065–4076. https://doi.org/10.1242/dev.126.18.4065.

Lee, Yang-Ja, Seon-Yong Jeong, Mariusz Karbowski, Carolyn L. Smith, and Richard J. Youle. 2004. “Roles of the Mammalian Mitochondrial Fission and Fusion Mediators Fis1, Drp1, and Opa1 in Apoptosis.” *Molecular Biology of the Cell* 15 (11): 5001–5011. https://doi.org/10.1091/mbc.E04-04-0294.

Liesa, Marc, Manuel Palacín, and Antonio Zorzano. 2009. “Mitochondrial Dynamics in Mammalian Health and Disease.” *Physiological Reviews* 89 (3): 799–845. https://doi.org/10.1152/physrev.00030.2008.

Li, Fan, Hongli Liu, Xiaojing Wu, et al. 2022. “Copper Modulates Mitochondrial Oxidative Phosphorylation to Enhance Dermal Papilla Cells Proliferation in Rex Rabbits.” *International Journal of Molecular Sciences* 23 (11): 6209. https://doi.org/10.3390/ijms23116209.

Liot, G., B. Bossy, S. Lubitz, Y. Kushnareva, N. Sejbuk, and E. Bossy-Wetzel. 2009. “Complex II Inhibition by 3-NP Causes Mitochondrial Fragmentation and Neuronal Cell Death via an NMDA- and ROS-Dependent Pathway.” *Cell Death and Differentiation* 16 (6): 899–909. https://doi.org/10.1038/cdd.2009.22.

Liu, Weiwei, and Guokai Chen. 2021. “Regulation of Energy Metabolism in Human Pluripotent Stem Cells.” *Cellular and Molecular Life Sciences: CMLS* 78 (24): 8097–8108. https://doi.org/10.1007/s00018-021-04016-0.

Liu, Wenbo, Qi Long, Keshi Chen, et al. 2013. “Mitochondrial Metabolism Transition Cooperates with Nuclear Reprogramming during Induced Pluripotent Stem Cell Generation.” *Biochemical and Biophysical Research Communications* 431 (4): 767–771. https://doi.org/10.1016/j.bbrc.2012.12.148.

Li, Youfen, Jeong-Soon Park, Jian-Hong Deng, and Yidong Bai. 2006. “Cytochrome c Oxidase Subunit IV Is Essential for Assembly and Respiratory Function of the Enzyme Complex.” *Journal of Bioenergetics and Biomembranes* 38 (5-6): 283–291. https://doi.org/10.1007/s10863-006-9052-z.

Lopez-Mejia, Isabel C., and Lluis Fajas. 2015. “Cell Cycle Regulation of Mitochondrial Function.” *Current Opinion in Cell Biology* 33 (April): 19–25. https://doi.org/10.1016/j.ceb.2014.10.006.

Lu, B., F. Roegiers, L. Y. Jan, and Y. N. Jan. 2001. “Adherens Junctions Inhibit

Asymmetric Division in the Drosophila Epithelium." *Nature* 409 (6819): 522–525. https://doi.org/10.1038/35054077.

Ludwig, B., E. Bender, S. Arnold, M. Hüttemann, I. Lee, and B. Kadenbach. 2001. "Cytochrome C Oxidase and the Regulation of Oxidative Phosphorylation." *Chembiochem: A European Journal of Chemical Biology* 2 (6): 392–403. https://doi.org/10.1002/1439-7633(20010601)2:6<392::AID-CBIC392>3.0.CO;2-N.

Malka, Florence, Olwenn Guillery, Carmen Cifuentes-Diaz, et al. 2005. "Separate Fusion of Outer and Inner Mitochondrial Membranes." *EMBO Reports* 6 (9): 853–859. https://doi.org/10.1038/sj.embor.7400488.

Mallik, Bhagaban, and C. Andrew Frank. 2022. "Roles for Mitochondrial Complex I Subunits in Regulating Synaptic Transmission and Growth." *Frontiers in Neuroscience* 16 (April): 846425. https://doi.org/10.3389/fnins.2022.846425.

Mandal, Sudip, William A. Freije, Preeta Guptan, and Utpal Banerjee. 2010. "Metabolic Control of G1-S Transition: Cyclin E Degradation by p53-Induced Activation of the Ubiquitin-Proteasome System." *The Journal of Cell Biology* 188 (4): 473–479. https://doi.org/10.1083/jcb.200912024.

Mandal, Sudip, Preeta Guptan, Edward Owusu-Ansah, and Utpal Banerjee. 2005. "Mitochondrial Regulation of Cell Cycle Progression during Development as Revealed by the Tenured Mutation in Drosophila." *Developmental Cell* 9 (6): 843–854. https://doi.org/10.1016/j.devcel.2005.11.006.

Mazumder, S., E. L. DuPree, and A. Almasan. 2004. "A Dual Role of Cyclin E in Cell Proliferation and Apoptosis May Provide a Target for Cancer Therapy." *Current Cancer Drug Targets* 4 (1): 65–75. https://doi.org/10.2174/1568009043481669.

Mirzoyan, Zhasmine, Manuela Sollazzo, Mariateresa Allocca, Alice Maria Valenza, Daniela Grifoni, and Paola Bellosta. 2019. "Drosophila Melanogaster: A Model Organism to Study Cancer." *Frontiers in Genetics* 10 (March): 51. https://doi.org/10.3389/fgene.2019.00051.

Mishra, Prashant, Valerio Carelli, Giovanni Manfredi, and David C. Chan. 2014. "Proteolytic Cleavage of Opa1 Stimulates Mitochondrial Inner Membrane Fusion and Couples Fusion to Oxidative Phosphorylation." *Cell Metabolism* 19 (5): 891. https://doi.org/10.1016/j.cmet.2014.04.014.

Mishra, Prashant, and David C. Chan. 2016. "Metabolic Regulation of Mitochondrial Dynamics." *The Journal of Cell Biology* 212 (4): 379–387. https://doi.org/10.1083/jcb.201511036.

Mitra, Kasturi, Richa Rikhy, Mary Lilly, and Jennifer Lippincott-Schwartz. 2012. "DRP1-Dependent Mitochondrial Fission Initiates Follicle Cell Differentiation during Drosophila Oogenesis." *The Journal of Cell Biology* 197 (4): 487–497. https://doi.org/10.1083/jcb.201110058.

Mitra, Kasturi, Christian Wunder, Badrinath Roysam, Gang Lin, and Jennifer Lippincott-Schwartz. 2009. "A Hyperfused Mitochondrial State Achieved at G1-S Regulates Cyclin E Buildup and Entry into S Phase." *Proceedings of the National Academy of Sciences of the United States of America* 106 (29): 11960–11965. https://doi.org/10.1073/pnas.0904875106.

Moosavi, Behrooz, Edward A. Berry, Xiao-Lei Zhu, Wen-Chao Yang, and Guang-Fu Yang. 2019. "The Assembly of Succinate Dehydrogenase: A Key Enzyme in Bioenergetics." *Cellular and Molecular Life Sciences: CMLS* 76 (20): 4023–4042. https://doi.org/10.1007/s00018-019-03200-7.

Muller, F. 2000. "The Nature and Mechanism of Superoxide Production by the Electron Transport Chain: Its Relevance to Aging." *Journal of the American Aging Association* 23 (4): 227–253. https://doi.org/10.1007/s11357-000-0022-9.

Murphy, Michael P. 2016. "Understanding and Preventing Mitochondrial Oxidative Damage." *Biochemical Society Transactions* 44 (5): 1219–1226. https://doi.org/10.1042/BST20160108.

Napiwotzki, J., and B. Kadenbach. 1998. "Extramitochondrial ATP/ADP-Ratios Regulate Cytochrome c Oxidase Activity via Binding to the Cytosolic Domain of Subunit IV." *Biological Chemistry* 379 (3): 335–339. https://doi.org/10.1515/bchm.1998.379.3.335.

Nicholls, David. 2002. "Mitochondrial Bioenergetics, Aging, and Aging-Related Disease." *Science of Aging Knowledge Environment: SAGE KE* 2002 (31): e12. https://doi.org/10.1126/sageke.2002.31.pe12.

Niemann, S., and U. Müller. 2000. "Mutations in SDHC Cause Autosomal Dominant Paraganglioma, Type 3." *Nature Genetics* 26 (3): 268–270. https://doi.org/10.1038/81551.

Ning, Kaiting, Shiqiang Liu, Baoqiang Yang, et al. 2022. "Update on the Effects of Energy Metabolism in Bone Marrow Mesenchymal Stem Cells Differentiation." *Molecular Metabolism* 58 (101450): 101450. https://doi.org/10.1016/j.molmet.2022.101450.

Nolfi-Donegan, Deirdre, Andrea Braganza, and Sruti Shiva. 2020. "Mitochondrial

Electron Transport Chain: Oxidative Phosphorylation, Oxidant Production, and Methods of Measurement." *Redox Biology* 37 (101674): 101674. https://doi.org/10.1016/j.redox.2020.101674.

Nunnari, J., W. F. Marshall, A. Straight, A. Murray, J. W. Sedat, and P. Walter. 1997. "Mitochondrial Transmission during Mating in Saccharomyces Cerevisiae Is Determined by Mitochondrial Fusion and Fission and the Intramitochondrial Segregation of Mitochondrial DNA." *Molecular Biology of the Cell* 8 (7): 1233–1242. https://doi.org/10.1091/mbc.8.7.1233.

Okamoto, K., P. S. Perlman, and R. A. Butow. 1998. "The Sorting of Mitochondrial DNA and Mitochondrial Proteins in Zygotes: Preferential Transmission of Mitochondrial DNA to the Medial Bud." *The Journal of Cell Biology* 142 (3): 613–623. https://doi.org/10.1083/jcb.142.3.613.

Okuno, Daichi, Ryota Iino, and Hiroyuki Noji. 2011. "Rotation and Structure of FoF1-ATP Synthase." *The Journal of Biochemistry* 149 (6): 655–664. https://doi.org/10.1093/jb/mvr049.

O'Rourke, Brian. 2010. "From Bioblasts to Mitochondria: Ever Expanding Roles of Mitochondria in Cell Physiology." *Frontiers in Physiology* 1 (June): 7. https://doi.org/10.3389/fphys.2010.00007.

Owusu-Ansah, Edward, and Utpal Banerjee. 2009. "Reactive Oxygen Species Prime Drosophila Haematopoietic Progenitors for Differentiation." *Nature* 461 (7263): 537–541. https://doi.org/10.1038/nature08313.

Owusu-Ansah, Edward, Amir Yavari, Sudip Mandal, and Utpal Banerjee. 2008. "Distinct Mitochondrial Retrograde Signals Control the G1-S Cell Cycle Checkpoint." *Nature Genetics* 40 (3): 356–361. https://doi.org/10.1038/ng.2007.50.

Parker, Danitra J., Archana Iyer, Shikha Shah, et al. 2015. "A New Mitochondrial Pool of Cyclin E, Regulated by Drp1, Is Linked to Cell-Density-Dependent Cell Proliferation." *Journal of Cell Science* 128 (22): 4171–4182. https://doi.org/10.1242/jcs.172429.

Paumard, Patrick, Jacques Vaillier, Bénédicte Coulary, et al. 2002. "The ATP Synthase Is Involved in Generating Mitochondrial Cristae Morphology." *The EMBO Journal* 21 (3): 221–230. https://doi.org/10.1093/emboj/21.3.221.

Perkins, Lizabeth A., Laura Holderbaum, Rong Tao, et al. 2015. "The Transgenic RNAi Project at Harvard Medical School: Resources and Validation." *Genetics* 201 (3): 843–852. https://doi.org/10.1534/genetics.115.180208.

Pernas, Lena, and Luca Scorrano. 2016. “Mito-Morphosis: Mitochondrial Fusion, Fission, and Cristae Remodeling as Key Mediators of Cellular Function.” *Annual Review of Physiology* 78 (1): 505–531. https://doi.org/10.1146/annurev-physiol-021115-105011.

Rak, Malgorzata, Paule Bénit, Dominique Chrétien, et al. 2016. “Mitochondrial Cytochrome c Oxidase Deficiency.” *Clinical Science (London, England: 1979)* 130 (6): 393–407. https://doi.org/10.1042/CS20150707.

Rambold, Angelika S., Brenda Kostelecky, Natalie Elia, and Jennifer Lippincott-Schwartz. 2011. “Tubular Network Formation Protects Mitochondria from Autophagosomal Degradation during Nutrient Starvation.” *Proceedings of the National Academy of Sciences of the United States of America* 108 (25): 10190–10195. https://doi.org/10.1073/pnas.1107402108.

Roger, Andrew J., Sergio A. Muñoz-Gómez, and Ryoma Kamikawa. 2017. “The Origin and Diversification of Mitochondria.” *Current Biology: CB* 27 (21): R1177–R1192. https://doi.org/10.1016/j.cub.2017.09.015.

Rolland, Stéphane G., Elisa Motori, Nadin Memar, et al. 2013. “Impaired Complex IV Activity in Response to Loss of LRPPRC Function Can Be Compensated by Mitochondrial Hyperfusion.” *Proceedings of the National Academy of Sciences of the United States of America* 110 (32): E2967–76. https://doi.org/10.1073/pnas.1303872110.

Samuels, Tamsin J., Yoav Arava, Aino I. Järvelin, et al. 2020. “Neuronal Upregulation of Prospero Protein Is Driven by Alternative mRNA Polyadenylation and Syncrip-Mediated mRNA Stabilisation.” *Biology Open* 9 (5): bio049684. https://doi.org/10.1242/bio.049684.

Sapkota, Anupama. 2024. “Electron Transport Chain Unveiled: Steps, Products, Diagram.” Microbe Notes, Sagar Aryal, October 15. https://microbenotes.com/electron-transport-chain/.

Schieke, Stefan M., Mingchao Ma, Liu Cao, et al. 2008. “Mitochondrial Metabolism Modulates Differentiation and Teratoma Formation Capacity in Mouse Embryonic Stem Cells.” *The Journal of Biological Chemistry* 283 (42): 28506–28512. https://doi.org/10.1074/jbc.M802763200.

Scott, R. A. 1995. “Functional Significance of Cytochrome c Oxidase Structure.” *Structure (London, England: 1993)* 3 (10): 981–986. https://doi.org/10.1016/s0969-2126(01)00233-7.

Senoo-Matsuda, Nanami, Philip S. Hartman, Akira Akatsuka, Shinichi Yoshimura, and Naoaki Ishii. 2003. “A Complex II Defect Affects Mitochondrial Structure, Leading to Ced-3- and Ced-4-Dependent Apoptosis and Aging.” *The Journal of Biological Chemistry* 278 (24): 22031–22036. https://doi.org/10.1074/jbc.M211377200.

Seo, Bong Jong, Sang Hoon Yoon, and Jeong Tae Do. 2018. “Mitochondrial Dynamics in Stem Cells and Differentiation.” *International Journal of Molecular Sciences* 19 (12): 3893. https://doi.org/10.3390/ijms19123893.

Shaka, Maria, Aranzazu Arias-Rojas, Alexandra Hrdina, Dagmar Frahm, and Igor Iatsenko. 2022. “Lipopolysaccharide -Mediated Resistance to Host Antimicrobial Peptides and Hemocyte-Derived Reactive-Oxygen Species Are the Major Providencia Alcalifaciens Virulence Factors in Drosophila Melanogaster.” *PLoS Pathogens* 18 (9): e1010825. https://doi.org/10.1371/journal.ppat.1010825.

Sharma, Lokendra K., Jianxin Lu, and Yidong Bai. 2009. “Mitochondrial Respiratory Complex I: Structure, Function and Implication in Human Diseases.” *Current Medicinal Chemistry* 16 (10): 1266–1277. https://doi.org/10.2174/092986709787846578.

Sharma, Lokendra Kumar, Hezhi Fang, Jiangtao Liu, Rasika Vartak, Janice Deng, and Yidong Bai. 2011. “Mitochondrial Respiratory Complex I Dysfunction Promotes Tumorigenesis through ROS Alteration and AKT Activation.” *Human Molecular Genetics* 20 (23): 4605–4616. https://doi.org/10.1093/hmg/ddr395.

Shen, Koning, Corinne L. Pender, Raz Bar-Ziv, et al. 2022. “Mitochondria as Cellular and Organismal Signaling Hubs.” *Annual Review of Cell and Developmental Biology* 38 (1): 179–218. https://doi.org/10.1146/annurev-cellbio-120420-015303.

Shoffner, J. M., R. L. Watts, J. L. Juncos, A. Torroni, and D. C. Wallace. 1991. “Mitochondrial Oxidative Phosphorylation Defects in Parkinson’s Disease.” *Annals of Neurology* 30 (3): 332–339. https://doi.org/10.1002/ana.410300304.

Song, Dong Hoon, Jonghyun Park, Laura L. Maurer, Wei Lu, Martin A. Philbert, and Ann Marie Sastry. 2013. “Biophysical Significance of the Inner Mitochondrial Membrane Structure on the Electrochemical Potential of Mitochondria.” *Physical Review. E, Statistical, Nonlinear, and Soft Matter Physics* 88 (6): 062723. https://doi.org/10.1103/PhysRevE.88.062723.

Song, Won-Hee, John William Oman Ballard, Young-Joo Yi, and Peter Sutovsky. 2014. “Regulation of Mitochondrial Genome Inheritance by Autophagy and Ubiquitin-Proteasome System: Implications for Health, Fitness, and Fertility.” *BioMed Research International* 2014 (June): 981867.

https://doi.org/10.1155/2014/981867.

Song, Zhiyin, Mariam Ghochani, J. Michael McCaffery, Terrence G. Frey, and David C. Chan. 2009. “Mitofusins and OPA1 Mediate Sequential Steps in Mitochondrial Membrane Fusion.” *Molecular Biology of the Cell* 20 (15): 3525–3532. https://doi.org/10.1091/mbc.e09-03-0252.

Son, Myung Jin, Bo Ram Jeong, Youjeong Kwon, and Yee Sook Cho. 2013. “Interference with the Mitochondrial Bioenergetics Fuels Reprogramming to Pluripotency via Facilitation of the Glycolytic Transition.” *The International Journal of Biochemistry & Cell Biology* 45 (11): 2512–2518. https://doi.org/10.1016/j.biocel.2013.07.023.

Sorianello, Eleonora, Maximiliano J. Katz, Julieta M. Acevedo, Mariana Melani, Joel I. Perez-Perri, and Pablo Wappner. 2025. “The Translational Inhibitor 4EBP/Thor Is Required for Drosophila Adaptation to Hypoxia.” *Scientific Reports* 15 (1): 23370. https://doi.org/10.1038/s41598-025-94457-5.

Spana, E. P., C. Kopczynski, C. S. Goodman, and C. Q. Doe. 1995. “Asymmetric Localization of Numb Autonomously Determines Sibling Neuron Identity in the Drosophila CNS.” *Development (Cambridge, England)* 121 (11): 3489–3494. https://doi.org/10.1242/dev.121.11.3489.

Stroud, David A., Elliot E. Surgenor, Luke E. Formosa, et al. 2016. “Accessory Subunits Are Integral for Assembly and Function of Human Mitochondrial Complex I.” *Nature* 538 (7623): 123–126. https://doi.org/10.1038/nature19754.

Sun, Chang, Samir Benlekbir, Padmaja Venkatakrishnan, et al. 2018. “Structure of the Alternative Complex III in a Supercomplex with Cytochrome Oxidase.” *Nature* 557 (7703): 123–126. https://doi.org/10.1038/s41586-018-0061-y.

Svensson-Ek, Margareta, Jeff Abramson, Gisela Larsson, Susanna Törnroth, Peter Brzezinski, and So Iwata. 2002. “The X-Ray Crystal Structures of Wild-Type and EQ(I-286) Mutant Cytochrome c Oxidases from Rhodobacter Sphaeroides.” *Journal of Molecular Biology* 321 (2): 329–339. https://doi.org/10.1016/s0022-2836(02)00619-8.

Taguchi, Naoko, Naotada Ishihara, Akihiro Jofuku, Toshihiko Oka, and Katsuyoshi Mihara. 2007. “Mitotic Phosphorylation of Dynamin-Related GTPase Drp1 Participates in Mitochondrial Fission.” *The Journal of Biological Chemistry* 282 (15): 11521–11529. https://doi.org/10.1074/jbc.M607279200.

Tassone, Annalisa, Maria Meringolo, Giulia Ponterio, Paola Bonsi, Tommaso Schirinzi,

and Giuseppina Martella. 2023. “Mitochondrial Bioenergy in Neurodegenerative Disease: Huntington and Parkinson.” *International Journal of Molecular Sciences* 24 (8): 7221. https://doi.org/10.3390/ijms24087221.

Teixeira, Felipe K., Carlos G. Sanchez, Thomas R. Hurd, et al. 2015. “ATP Synthase Promotes Germ Cell Differentiation Independent of Oxidative Phosphorylation.” *Nature Cell Biology* 17 (5): 689–696. https://doi.org/10.1038/ncb3165.

Ten, Vadim, and Alexander Galkin. 2019. “Mechanism of Mitochondrial Complex I Damage in Brain Ischemia/reperfusion Injury. A Hypothesis.” *Molecular and Cellular Neurosciences* 100 (103408): 103408. https://doi.org/10.1016/j.mcn.2019.103408.

Tilokani, Lisa, Shun Nagashima, Vincent Paupe, and Julien Prudent. 2018. “Mitochondrial Dynamics: Overview of Molecular Mechanisms.” *Essays in Biochemistry* 62 (3): 341–360. https://doi.org/10.1042/EBC20170104.

Tomizaki, T., E. Yamashita, H. Yamaguchi, et al. 1999. “Structure Analysis of Bovine Heart Cytochrome c Oxidase at 2.8 A Resolution.” *Acta Crystallographica. Section D, Biological Crystallography* 55 (Pt 1): 31–45. https://doi.org/10.1107/S0907444998006362.

Tothova, Zuzana, Ramya Kollipara, Brian J. Huntly, et al. 2007. “FoxOs Are Critical Mediators of Hematopoietic Stem Cell Resistance to Physiologic Oxidative Stress.” *Cell* 128 (2): 325–339. https://doi.org/10.1016/j.cell.2007.01.003.

Trevisan, Tatiana, Diana Pendin, Aldo Montagna, Sergio Bova, Anna Maria Ghelli, and Andrea Daga. 2018. “Manipulation of Mitochondria Dynamics Reveals Separate Roles for Form and Function in Mitochondria Distribution.” *Cell Reports* 23 (6): 1742–1753. https://doi.org/10.1016/j.celrep.2018.04.017.

Twig, Gilad, Alvaro Elorza, Anthony J. A. Molina, et al. 2008. “Fission and Selective Fusion Govern Mitochondrial Segregation and Elimination by Autophagy.” *The EMBO Journal* 27 (2): 433–446. https://doi.org/10.1038/sj.emboj.7601963.

Urbach, Rolf, Ralf Schnabel, and Gerhard M. Technau. 2003. “The Pattern of Neuroblast Formation, Mitotic Domains and Proneural Gene Expression during Early Brain Development in Drosophila.” *Development (Cambridge, England)* 130 (16): 3589–3606. https://doi.org/10.1242/dev.00528.

Varum, S., O. Momcilović, C. Castro, A. Ben-Yehudah, J. Ramalho-Santos, and C. S. Navara. 2009. “Enhancement of Human Embryonic Stem Cell Pluripotency through Inhibition of the Mitochondrial Respiratory Chain.” *Stem Cell Research* 3

(2-3): 142–156. https://doi.org/10.1016/j.scr.2009.07.002.

Vogel, Frank, Carsten Bornhövd, Walter Neupert, and Andreas S. Reichert. 2006. “Dynamic Subcompartmentalization of the Mitochondrial Inner Membrane.” *The Journal of Cell Biology* 175 (2): 237–247. https://doi.org/10.1083/jcb.200605138.

Walsh, Kathleen T., and Chris Q. Doe. 2017. “Drosophila Embryonic Type II Neuroblasts: Origin, Temporal Patterning, and Contribution to the Adult Central Complex.” In *bioRxiv*. BioRxiv, July 30. https://doi.org/10.1101/170043.

Wang, Zhu A., and Daniel Kalderon. 2009. “Cyclin E-Dependent Protein Kinase Activity Regulates Niche Retention of Drosophila Ovarian Follicle Stem Cells.” *Proceedings of the National Academy of Sciences of the United States of America* 106 (51): 21701–21706. https://doi.org/10.1073/pnas.0909272106.

Watt, Ian N., Martin G. Montgomery, Michael J. Runswick, Andrew G. W. Leslie, and John E. Walker. 2010. “Bioenergetic Cost of Making an Adenosine Triphosphate Molecule in Animal Mitochondria.” *Proceedings of the National Academy of Sciences of the United States of America* 107 (39): 16823–16827. https://doi.org/10.1073/pnas.1011099107.

Willows, Robin, Matthew J. Sanders, Bing Xiao, et al. 2017. “Phosphorylation of AMPK by Upstream Kinases Is Required for Activity in Mammalian Cells.” *The Biochemical Journal* 474 (17): 3059–3073. https://doi.org/10.1042/BCJ20170458.

Wittig, Ilka, and Hermann Schägger. 2008. “Structural Organization of Mitochondrial ATP Synthase.” *Biochimica et Biophysica Acta* 1777 (7-8): 592–598. https://doi.org/10.1016/j.bbabio.2008.04.027.

Wodarz, Andreas, and Wieland B. Huttner. 2003. “Asymmetric Cell Division during Neurogenesis in Drosophila and Vertebrates.” *Mechanisms of Development* 120 (11): 1297–1309. https://doi.org/10.1016/j.mod.2003.06.003.

Wollweber, Florian, Karina von der Malsburg, and Martin van der Laan. 2017. “Mitochondrial Contact Site and Cristae Organizing System: A Central Player in Membrane Shaping and Crosstalk.” *Biochimica et Biophysica Acta* 1864 (9): 1481–1489. https://doi.org/10.1016/j.bbamcr.2017.05.004.

Yang, Ziyun, Liang Wang, Cheng Yang, et al. 2021. “Mitochondrial Membrane Remodeling.” *Frontiers in Bioengineering and Biotechnology* 9: 786806. https://doi.org/10.3389/fbioe.2021.786806.

Yankovskaya, Victoria, Rob Horsefield, Susanna Törnroth, et al. 2003. “Architecture of

Succinate Dehydrogenase and Reactive Oxygen Species Generation." *Science (New York, N.Y.)* 299 (5607): 700–704. https://doi.org/10.1126/science.1079605.

Yao, Cong-Hui, Rencheng Wang, Yahui Wang, Che-Pei Kung, Jason D. Weber, and Gary J. Patti. 2019. "Mitochondrial Fusion Supports Increased Oxidative Phosphorylation during Cell Proliferation." *eLife* 8 (January). https://doi.org/10.7554/eLife.41351.

Youle, Richard J., and Alexander M. van der Bliek. 2012. "Mitochondrial Fission, Fusion, and Stress." *Science (New York, N.Y.)* 337 (6098): 1062–1065. https://doi.org/10.1126/science.1219855.

Yu, Fengwei, Chay T. Kuo, and Yuh Nung Jan. 2006. "Drosophila Neuroblast Asymmetric Cell Division: Recent Advances and Implications for Stem Cell Biology." *Neuron* 51 (1): 13–20. https://doi.org/10.1016/j.neuron.2006.06.016.

Zhang, Fan, Mehdi Pirooznia, and Hong Xu. 2020. "Mitochondria Regulate Intestinal Stem Cell Proliferation and Epithelial Homeostasis through FOXO." *Molecular Biology of the Cell* 31 (14): 1538–1549. https://doi.org/10.1091/mbc.E19-10-0560.

Zhang, Xing-Ding, Ye Wang, Jun-Chao Wu, et al. 2009. "Down-Regulation of Bcl-2 Enhances Autophagy Activation and Cell Death Induced by Mitochondrial Dysfunction in Rat Striatum." *Journal of Neuroscience Research* 87 (16): 3600–3610. https://doi.org/10.1002/jnr.22152.

Zhao, Jian, Tong Liu, Shaobo Jin, et al. 2011. "Human MIEF1 Recruits Drp1 to Mitochondrial Outer Membranes and Promotes Mitochondrial Fusion rather than Fission: MIEF1, a Key Regulator of Mitochondrial Dynamics." *The EMBO Journal* 30 (14): 2762–2778. https://doi.org/10.1038/emboj.2011.198.

Zhu, Sijun, Suzanne Barshow, Jill Wildonger, Lily Yeh Jan, and Yuh-Nung Jan. 2011. "Ets Transcription Factor Pointed Promotes the Generation of Intermediate Neural Progenitors in Drosophila Larval Brains." *Proceedings of the National Academy of Sciences of the United States of America* 108 (51): 20615–20620. https://doi.org/10.1073/pnas.1118595109.

Acton, B. M., A. Jurisicova, I. Jurisica, and R. F. Casper. 2004. "Alterations in Mitochondrial Membrane Potential during Preimplantation Stages of Mouse and Human Embryo Development." Molecular Human Reproduction 10 (1): 23–32. https://doi.org/10.1093/molehr/gah004.

Agip, Ahmed-Noor A., Injae Chung, Alvaro Sanchez-Martinez, Alexander J. Whitworth, and Judy Hirst. 2023. "Cryo-EM Structures of Mitochondrial Respiratory Complex I

from Drosophila Melanogaster.” eLife 12 (January): e84424. https://doi.org/10.7554/eLife.84424.

Ameele, Jelle van den, and Andrea H. Brand. 2019. “Neural Stem Cell Temporal Patterning and Brain Tumour Growth Rely on Oxidative Phosphorylation.” eLife 8 (September). https://doi.org/10.7554/eLife.47887.

Amiri, Haleh, Olof Karlberg, and Siv G. E. Andersson. 2003. “Deep Origin of Plastid/parasite ATP/ADP Translocases.” Journal of Molecular Evolution 56 (2): 137–150. https://doi.org/10.1007/s00239-002-2387-0.

Apitz, Holger, and Iris Salecker. 2016. “Retinal Determination Genes Coordinate Neuroepithelial Specification and Neurogenesis Modes in the Drosophila Optic Lobe.” Development (Cambridge, England) 143 (13): 2431–2442. https://doi.org/10.1242/dev.135004.

Archibald, J. 2014. One Plus One Equals One: Symbiosis and the Evolution of Complex Life. Oxford University Press.

Arnold, S., F. Goglia, and B. Kadenbach. 1998. “3,5-Diiodothyronine Binds to Subunit Va of Cytochrome-c Oxidase and Abolishes the Allosteric Inhibition of Respiration by ATP.” European Journal of Biochemistry 252 (2): 325–330. https://doi.org/10.1046/j.1432-1327.1998.2520325.x.

Arnold, S., and B. Kadenbach. 1997. “Cell Respiration Is Controlled by ATP, an Allosteric Inhibitor of Cytochrome-c Oxidase.” European Journal of Biochemistry 249 (1): 350–354. https://doi.org/10.1111/j.1432-1033.1997.t01-1-00350.x.

Ashrafi, Ghazaleh, Julia S. Schlehe, Matthew J. LaVoie, and Thomas L. Schwarz. 2014. “Mitophagy of Damaged Mitochondria Occurs Locally in Distal Neuronal Axons and Requires PINK1 and Parkin.” The Journal of Cell Biology 206 (5): 655–670. https://doi.org/10.1083/jcb.201401070.

Astuti, D., F. Latif, A. Dallol, et al. 2001. “Gene Mutations in the Succinate Dehydrogenase Subunit SDHB Cause Susceptibility to Familial Pheochromocytoma and to Familial Paraganglioma.” The American Journal of Human Genetics 69 (1): 49–54. https://doi.org/10.1086/321282.

Atwood, Scott X., and Kenneth E. Prehoda. 2009. “aPKC Phosphorylates Miranda to Polarize Fate Determinants during Neuroblast Asymmetric Cell Division.” Current Biology: CB 19 (9): 723–729. https://doi.org/10.1016/j.cub.2009.03.056.

Bandara, Aloka B., Joshua C. Drake, and David A. Brown. 2021. “Complex II Subunit

SDHD Is Critical for Cell Growth and Metabolism, Which Can Be Partially Restored with a Synthetic Ubiquinone Analog." BMC Molecular and Cell Biology 22 (1): 35. https://doi.org/10.1186/s12860-021-00370-w.

Barsoum, Mark J., Hua Yuan, Akos A. Gerencser, et al. 2006. "Nitric Oxide-Induced Mitochondrial Fission Is Regulated by Dynamin-Related GTPases in Neurons." The EMBO Journal 25 (16): 3900–3911. https://doi.org/10.1038/sj.emboj.7601253.

Bayraktar, Omer Ali, Jason Q. Boone, Michael L. Drummond, and Chris Q. Doe. 2010. "Drosophila Type II Neuroblast Lineages Keep Prospero Levels Low to Generate Large Clones That Contribute to the Adult Brain Central Complex." Neural Development 5 (1): 26. https://doi.org/10.1186/1749-8104-5-26.

Baysal, B. E., R. E. Ferrell, J. E. Willett-Brozick, et al. 2000. "Mutations in SDHD, a Mitochondrial Complex II Gene, in Hereditary Paraganglioma." Science (New York, N.Y.) 287 (5454): 848–851. https://doi.org/10.1126/science.287.5454.848.

Bello, Bruno C., Natalya Izergina, Emmanuel Caussinus, and Heinrich Reichert. 2008. "Amplification of Neural Stem Cell Proliferation by Intermediate Progenitor Cells in Drosophila Brain Development." Neural Development 3 (1): 5. https://doi.org/10.1186/1749-8104-3-5.

Berger, Itai, Eli Hershkovitz, Avraham Shaag, Simon Edvardson, Ann Saada, and Orly Elpeleg. 2008. "Mitochondrial Complex I Deficiency Caused by a Deleterious NDUFA11 Mutation." Annals of Neurology 63 (3): 405–408. https://doi.org/10.1002/ana.21332.

Berndtsson, Jens, Andreas Kohler, Sorbhi Rathore, et al. 2020. "Respiratory Supercomplexes Enhance Electron Transport by Decreasing Cytochrome c Diffusion Distance." EMBO Reports 21 (12): e51015. https://doi.org/10.15252/embr.202051015.

Bombelka, E., F. W. Richter, A. Stroh, and B. Kadenbach. 1986. "Analysis of the Cu, Fe, and Zn Contents in Cytochrome C Oxidases from Different Species and Tissues by Proton-Induced X-Ray Emission (PIXE)." Biochemical and Biophysical Research Communications 140 (3): 1007–1014. https://doi.org/10.1016/0006-291x(86)90735-7.

Bonnay, François, Ana Veloso, Victoria Steinmann, et al. 2020. "Oxidative Metabolism Drives Immortalization of Neural Stem Cells during Tumorigenesis." Cell 182 (6): 1490–1507.e19. https://doi.org/10.1016/j.cell.2020.07.039.

Boone, Jason Q., and Chris Q. Doe. 2008. "Identification of Drosophila Type II

Neuroblast Lineages Containing Transit Amplifying Ganglion Mother Cells." Developmental Neurobiology 68 (9): 1185–1195. https://doi.org/10.1002/dneu.20648.

Bourgeron, T., P. Rustin, D. Chretien, et al. 1995. "Mutation of a Nuclear Succinate Dehydrogenase Gene Results in Mitochondrial Respiratory Chain Deficiency." Nature Genetics 11 (2): 144–149. https://doi.org/10.1038/ng1095-144.

Brand, Martin D. 2010. "The Sites and Topology of Mitochondrial Superoxide Production." Experimental Gerontology 45 (7-8): 466–472. https://doi.org/10.1016/j.exger.2010.01.003.

Buescher, M., S. L. Yeo, G. Udolph, et al. 1998. "Binary Sibling Neuronal Cell Fate Decisions in the Drosophila Embryonic Central Nervous System Are Nonstochastic and Require Inscuteable-Mediated Asymmetry of Ganglion Mother Cells." Genes & Development 12 (12): 1858–1870. https://doi.org/10.1101/gad.12.12.1858.

Burman, Jonathon L., Sarah Pickles, Chunxin Wang, et al. 2017. "Mitochondrial Fission Facilitates the Selective Mitophagy of Protein Aggregates." The Journal of Cell Biology 216 (10): 3231–3247. https://doi.org/10.1083/jcb.201612106.

Cabrera, Carlos V. 1990. "Lateral Inhibition and Cell Fate during Neurogenesis in Drosophila: the Interactions between scute, Notch and Delta." Development (Cambridge, England) 109 (3): 733–742. https://doi.org/10.1242/dev.109.3.733.

Cadenas, E., and K. J. Davies. 2000. "Mitochondrial Free Radical Generation, Oxidative Stress, and Aging." Free Radical Biology & Medicine 29 (3-4): 222–230. https://doi.org/10.1016/s0891-5849(00)00317-8.

Chang, Xiaoru, Shuyan Niu, Mengting Shang, et al. 2023. "ROS-Drp1-Mediated Mitochondria Fission Contributes to Hippocampal HT22 Cell Apoptosis Induced by Silver Nanoparticles." Redox Biology 63 (102739): 102739. https://doi.org/10.1016/j.redox.2023.102739.

Chen, Hsiuchen, and David C. Chan. 2017. "Mitochondrial Dynamics in Regulating the Unique Phenotypes of Cancer and Stem Cells." Cell Metabolism 26 (1): 39–48. https://doi.org/10.1016/j.cmet.2017.05.016.

Chowdhary, Sayali, Somya Madan, Darshika Tomer, Manos Mavrakis, and Richa Rikhy. 2020. "Mitochondrial Morphology and Activity Regulate Furrow Ingression and Contractile Ring Dynamics in Drosophila Cellularization." Molecular Biology of the Cell 31 (21): 2331–2347. https://doi.org/10.1091/mbc.E20-03-0177.

Chowdhary, Sayali, Darshika Tomer, Dnyanesh Dubal, Devashree Sambre, and Richa Rikhy. 2017. “Analysis of Mitochondrial Organization and Function in the Drosophila Blastoderm Embryo.” Scientific Reports 7 (1): 5502. https://doi.org/10.1038/s41598-017-05679-1.

Chung, Susan, Petras P. Dzeja, Randolph S. Faustino, Carmen Perez-Terzic, Atta Behfar, and Andre Terzic. 2007. “Mitochondrial Oxidative Metabolism Is Required for the Cardiac Differentiation of Stem Cells.” Nature Clinical Practice. Cardiovascular Medicine 4 Suppl 1 (S1): S60–7. https://doi.org/10.1038/ncpcardio0766.

Cipolat, Sara, Olga Martins de Brito, Barbara Dal Zilio, and Luca Scorrano. 2004. “OPA1 Requires Mitofusin 1 to Promote Mitochondrial Fusion.” Proceedings of the National Academy of Sciences of the United States of America 101 (45): 15927–15932. https://doi.org/10.1073/pnas.0407043101.

Cogliati, Sara, Jose A. Enriquez, and Luca Scorrano. 2016. “Mitochondrial Cristae: Where Beauty Meets Functionality.” Trends in Biochemical Sciences 41 (3): 261–273. https://doi.org/10.1016/j.tibs.2016.01.001.

Colpman, Pierce, Asish Dasgupta, and Stephen L. Archer. 2023. “The Role of Mitochondrial Dynamics and Mitotic Fission in Regulating the Cell Cycle in Cancer and Pulmonary Arterial Hypertension: Implications for Dynamin-Related Protein 1 and Mitofusin2 in Hyperproliferative Diseases.” Cells (Basel, Switzerland) 12 (14): 1897. https://doi.org/10.3390/cells12141897.

Deng, Hansong, Shigeo Takashima, Manash Paul, Ming Guo, and Volker Hartenstein. 2018. “Mitochondrial Dynamics Regulates Drosophila Intestinal Stem Cell Differentiation.” Cell Death Discovery 4 (1): 17. https://doi.org/10.1038/s41420-018-0083-0.

Devenish, Rodney J., Mark Prescott, and Andrew J. W. Rodgers. 2008. “The Structure and Function of Mitochondrial F1F0-ATP Synthases.” International Review of Cell and Molecular Biology 267: 1–58. https://doi.org/10.1016/S1937-6448(08)00601-1.

Doerflinger, Hélène, Nina Vogt, Isabel L. Torres, et al. 2010. “Bazooka Is Required for Polarisation of the Drosophila Anterior-Posterior Axis.” Development (Cambridge, England) 137 (10): 1765–1773. https://doi.org/10.1242/dev.045807.

Dubal, Dnyanesh, Prachiti Moghe, Rahul Kumar Verma, Bhavin Uttekar, and Richa Rikhy. 2022. “Mitochondrial Fusion Regulates Proliferation and Differentiation in the Type II Neuroblast Lineage in Drosophila.” PLoS Genetics 18 (2): e1010055. https://doi.org/10.1371/journal.pgen.1010055.

Egger, Boris, James M. Chell, and Andrea H. Brand. 2008. “Insights into Neural Stem Cell Biology from Flies.” Philosophical Transactions of the Royal Society of London. Series B, Biological Sciences 363 (1489): 39–56. https://doi.org/10.1098/rstb.2006.2011.

Facucho-Oliveira, Joao M., Jon Alderson, Emma C. Spikings, Stuart Egginton, and Justin C. St John. 2007. “Mitochondrial DNA Replication during Differentiation of Murine Embryonic Stem Cells.” Journal of Cell Science 120 (Pt 22): 4025–4034. https://doi.org/10.1242/jcs.016972.

Falkenberg, Maria, and Nils-Göran Larsson. 2009. “Structure Casts Light on mtDNA Replication.” Cell 139 (2): 231–233. https://doi.org/10.1016/j.cell.2009.09.030.

Fernández-Moreno, Miguel Angel, Carol L. Farr, Laurie S. Kaguni, and Rafael Garesse. 2007. “Drosophila Melanogaster as a Model System to Study Mitochondrial Biology.” Methods in Molecular Biology (Clifton, N.J.) 372: 33–49. https://doi.org/10.1007/978-1-59745-365-3_3.

Garcia, Christian Joel, Jahan Khajeh, Emmanuel Coulanges, Emily I-Ju Chen, and Edward Owusu-Ansah. 2017. “Regulation of Mitochondrial Complex I Biogenesis in Drosophila Flight Muscles.” Cell Reports 20 (1): 264–278. https://doi.org/10.1016/j.celrep.2017.06.015.

Gilkerson, Robert W., Jeanne M. L. Selker, and Roderick A. Capaldi. 2003. “The Cristal Membrane of Mitochondria Is the Principal Site of Oxidative Phosphorylation.” FEBS Letters 546 (2-3): 355–358. https://doi.org/10.1016/s0014-5793(03)00633-1.

Gomes, Ligia C., Giulietta Di Benedetto, and Luca Scorrano. 2011. “During Autophagy Mitochondria Elongate, Are Spared from Degradation and Sustain Cell Viability.” Nature Cell Biology 13 (5): 589–598. https://doi.org/10.1038/ncb2220.

Green, Douglas R., and Guido Kroemer. 2004. “The Pathophysiology of Mitochondrial Cell Death.” Science (New York, N.Y.) 305 (5684): 626–629. https://doi.org/10.1126/science.1099320.

Guarani, Virginia, Joao Paulo, Bo Zhai, Edward L. Huttlin, Steven P. Gygi, and J. Wade Harper. 2014. “TIMMDC1/C3orf1 Functions as a Membrane-Embedded Mitochondrial Complex I Assembly Factor through Association with the MCIA Complex.” Molecular and Cellular Biology 34 (5): 847–861. https://doi.org/10.1128/MCB.01551-13.

Gu, Wen, Xavier Gaeta, Anna Sahakyan, et al. 2016. “Glycolytic Metabolism Plays a Functional Role in Regulating Human Pluripotent Stem Cell State.” Cell Stem Cell

19 (4): 476–490. https://doi.org/10.1016/j.stem.2016.08.008.

Hannaford, Matthew Robert, Anne Ramat, Nicolas Loyer, and Jens Januschke. 2018. “aPKC-Mediated Displacement and Actomyosin-Mediated Retention Polarize Miranda in Drosophila Neuroblasts.” eLife 7 (January). https://doi.org/10.7554/elife.29939.

Hirst, Judy. 2009. “Towards the Molecular Mechanism of Respiratory Complex I.” The Biochemical Journal 425 (2): 327–339. https://doi.org/10.1042/BJ20091382.

Homem, Catarina C. F., and Juergen A. Knoblich. 2012. “Drosophila Neuroblasts: A Model for Stem Cell Biology.” Development (Cambridge, England) 139 (23): 4297–4310. https://doi.org/10.1242/dev.080515.

Homem, Catarina C. F., Marko Repic, and Jürgen A. Knoblich. 2015. “Proliferation Control in Neural Stem and Progenitor Cells.” Nature Reviews. Neuroscience 16 (11): 647–659. https://doi.org/10.1038/nrn4021.

Homem, Catarina C. F., Victoria Steinmann, Thomas R. Burkard, Alexander Jais, Harald Esterbauer, and Juergen A. Knoblich. 2014. “Ecdysone and Mediator Change Energy Metabolism to Terminate Proliferation in Drosophila Neural Stem Cells.” Cell 158 (4): 874–888. https://doi.org/10.1016/j.cell.2014.06.024.

Hong, Y., B. Stronach, N. Perrimon, L. Y. Jan, and Y. N. Jan. 2001. “Drosophila Stardust Interacts with Crumbs to Control Polarity of Epithelia but Not Neuroblasts.” Nature 414 (6864): 634–638. https://doi.org/10.1038/414634a.

Horsefield, Rob, So Iwata, and Bernadette Byrne. 2004. “Complex II from a Structural Perspective.” Current Protein & Peptide Science 5 (2): 107–118. https://doi.org/10.2174/1389203043486847.

Ikon, Nikita, and Robert O. Ryan. 2017. “Cardiolipin and Mitochondrial Cristae Organization.” Biochimica et Biophysica Acta. Biomembranes 1859 (6): 1156–1163. https://doi.org/10.1016/j.bbamem.2017.03.013.

Isshiki, T., B. Pearson, S. Holbrook, and C. Q. Doe. 2001. “Drosophila Neuroblasts Sequentially Express Transcription Factors Which Specify the Temporal Identity of Their Neuronal Progeny.” Cell 106 (4): 511–521. https://doi.org/10.1016/s0092-8674(01)00465-2.

Iwata, S. 1998. “Structure and Function of Bacterial Cytochrome c Oxidase.” The Journal of Biochemistry 123 (3): 369–375. https://doi.org/10.1093/oxfordjournals.jbchem.a021946.

Jasra, Ila Tewari, Nerea Cuesta-Gomez, Kevin Verhoeff, Braulio A. Marfil-Garza, Nidheesh Dadheech, and A. M. James Shapiro. 2023. “Mitochondrial Regulation in Human Pluripotent Stem Cells during Reprogramming and β Cell Differentiation.” Frontiers in Endocrinology 14 (October): 1236472. https://doi.org/10.3389/fendo.2023.1236472.

Ježek, Jan, Katrina Cooper, and Randy Strich. 2018. “Reactive Oxygen Species and Mitochondrial Dynamics: The Yin and Yang of Mitochondrial Dysfunction and Cancer Progression.” Antioxidants (Basel, Switzerland) 7 (1): 13. https://doi.org/10.3390/antiox7010013.

John, P., and F. R. Whatley. 1975. “Paracoccus Denitrificans and the Evolutionary Origin of the Mitochondrion.” Nature 254 (5500): 495–498. https://doi.org/10.1038/254495a0.

Junge, Wolfgang, and Nathan Nelson. 2015. “ATP Synthase.” Annual Review of Biochemistry 84 (1): 631–657. https://doi.org/10.1146/annurev-biochem-060614-034124.

Kasahara, Atsuko, Sara Cipolat, Yun Chen, Gerald W. Dorn 2nd, and Luca Scorrano. 2013. “Mitochondrial Fusion Directs Cardiomyocyte Differentiation via Calcineurin and Notch Signaling.” Science (New York, N.Y.) 342 (6159): 734–737. https://doi.org/10.1126/science.1241359.

Kashatus, David F., Kian-Huat Lim, Donita C. Brady, Nicole L. K. Pershing, Adrienne D. Cox, and Christopher M. Counter. 2011. “RALA and RALBP1 Regulate Mitochondrial Fission at Mitosis.” Nature Cell Biology 13 (9): 1108–1115. https://doi.org/10.1038/ncb2310.

Khacho, Mireille, Alysen Clark, Devon S. Svoboda, et al. 2016. “Mitochondrial Dynamics Impacts Stem Cell Identity and Fate Decisions by Regulating a Nuclear Transcriptional Program.” Cell Stem Cell 19 (2): 232–247. https://doi.org/10.1016/j.stem.2016.04.015.

Kianian, Penny M. A., and Shahryar F. Kianian. 2014. “Mitochondrial Dynamics and the Cell Cycle.” Frontiers in Plant Science 5 (May): 222. https://doi.org/10.3389/fpls.2014.00222.

Kohler, Andreas, Antoni Barrientos, Flavia Fontanesi, and Martin Ott. 2023. “The Functional Significance of Mitochondrial Respiratory Chain Supercomplexes.” EMBO Reports 24 (11): e57092. https://doi.org/10.15252/embr.202357092.

Koju, Nirmala, Abdoh Taleb, Jifang Zhou, et al. 2019. “Pharmacological Strategies to

Lower Crosstalk between Nicotinamide Adenine Dinucleotide Phosphate (NADPH) Oxidase and Mitochondria." Biomedecine & Pharmacotherapie [Biomedicine & Pharmacotherapy] 111 (March): 1478–1498. https://doi.org/10.1016/j.biopha.2018.11.128.

Kraft, Lauren M., and Laura L. Lackner. 2018. "Mitochondrial Anchors: Positioning Mitochondria and More." Biochemical and Biophysical Research Communications 500 (1): 2–8. https://doi.org/10.1016/j.bbrc.2017.06.193.

Kunz, Thomas, Karoline F. Kraft, Gerhard M. Technau, and Rolf Urbach. 2012. "Origin of Drosophila Mushroom Body Neuroblasts and Generation of Divergent Embryonic Lineages." Development (Cambridge, England) 139 (14): 2510–2522. https://doi.org/10.1242/dev.077883.

Lai, Sen-Lin, Takeshi Awasaki, Kei Ito, and Tzumin Lee. 2008. "Clonal Analysis of Drosophila Antennal Lobe Neurons: Diverse Neuronal Architectures in the Lateral Neuroblast Lineage." Development (Cambridge, England) 135 (17): 2883–2893. https://doi.org/10.1242/dev.024380.

Lambert, Adrian J., and Martin D. Brand. 2004. "Superoxide Production by NADH:ubiquinone Oxidoreductase (complex I) Depends on the pH Gradient across the Mitochondrial Inner Membrane." The Biochemical Journal 382 (Pt 2): 511–517. https://doi.org/10.1042/BJ20040485.

Lane, Nick, and William Martin. 2010. "The Energetics of Genome Complexity." Nature 467 (7318): 929–934. https://doi.org/10.1038/nature09486.

Lee, T., A. Lee, and L. Luo. 1999. "Development of the Drosophila Mushroom Bodies: Sequential Generation of Three Distinct Types of Neurons from a Neuroblast." Development (Cambridge, England) 126 (18): 4065–4076. https://doi.org/10.1242/dev.126.18.4065.

Lee, Yang-Ja, Seon-Yong Jeong, Mariusz Karbowski, Carolyn L. Smith, and Richard J. Youle. 2004. "Roles of the Mammalian Mitochondrial Fission and Fusion Mediators Fis1, Drp1, and Opa1 in Apoptosis." Molecular Biology of the Cell 15 (11): 5001–5011. https://doi.org/10.1091/mbc.E04-04-0294.

Liesa, Marc, Manuel Palacín, and Antonio Zorzano. 2009. "Mitochondrial Dynamics in Mammalian Health and Disease." Physiological Reviews 89 (3): 799–845. https://doi.org/10.1152/physrev.00030.2008.

Li, Fan, Hongli Liu, Xiaojing Wu, et al. 2022. "Copper Modulates Mitochondrial Oxidative Phosphorylation to Enhance Dermal Papilla Cells Proliferation in Rex Rabbits."

International Journal of Molecular Sciences 23 (11): 6209. https://doi.org/10.3390/ijms23116209.

Liot, G., B. Bossy, S. Lubitz, Y. Kushnareva, N. Sejbuk, and E. Bossy-Wetzel. 2009. “Complex II Inhibition by 3-NP Causes Mitochondrial Fragmentation and Neuronal Cell Death via an NMDA- and ROS-Dependent Pathway.” Cell Death and Differentiation 16 (6): 899–909. https://doi.org/10.1038/cdd.2009.22.

Liu, Weiwei, and Guokai Chen. 2021. “Regulation of Energy Metabolism in Human Pluripotent Stem Cells.” Cellular and Molecular Life Sciences: CMLS 78 (24): 8097–8108. https://doi.org/10.1007/s00018-021-04016-0.

Liu, Wenbo, Qi Long, Keshi Chen, et al. 2013. “Mitochondrial Metabolism Transition Cooperates with Nuclear Reprogramming during Induced Pluripotent Stem Cell Generation.” Biochemical and Biophysical Research Communications 431 (4): 767–771. https://doi.org/10.1016/j.bbrc.2012.12.148.

Li, Youfen, Jeong-Soon Park, Jian-Hong Deng, and Yidong Bai. 2006. “Cytochrome c Oxidase Subunit IV Is Essential for Assembly and Respiratory Function of the Enzyme Complex.” Journal of Bioenergetics and Biomembranes 38 (5-6): 283–291. https://doi.org/10.1007/s10863-006-9052-z.

Lopez-Mejia, Isabel C., and Lluis Fajas. 2015. “Cell Cycle Regulation of Mitochondrial Function.” Current Opinion in Cell Biology 33 (April): 19–25. https://doi.org/10.1016/j.ceb.2014.10.006.

Lu, B., F. Roegiers, L. Y. Jan, and Y. N. Jan. 2001. “Adherens Junctions Inhibit Asymmetric Division in the Drosophila Epithelium.” Nature 409 (6819): 522–525. https://doi.org/10.1038/35054077.

Ludwig, B., E. Bender, S. Arnold, M. Hüttemann, I. Lee, and B. Kadenbach. 2001. “Cytochrome C Oxidase and the Regulation of Oxidative Phosphorylation.” Chembiochem: A European Journal of Chemical Biology 2 (6): 392–403. https://doi.org/10.1002/1439-7633(20010601)2:6<392::AID-CBIC392>3.0.CO;2-N.

Malka, Florence, Olwenn Guillery, Carmen Cifuentes-Diaz, et al. 2005. “Separate Fusion of Outer and Inner Mitochondrial Membranes.” EMBO Reports 6 (9): 853–859. https://doi.org/10.1038/sj.embor.7400488.

Mallik, Bhagaban, and C. Andrew Frank. 2022. “Roles for Mitochondrial Complex I Subunits in Regulating Synaptic Transmission and Growth.” Frontiers in Neuroscience 16 (April): 846425. https://doi.org/10.3389/fnins.2022.846425.

Mandal, Sudip, William A. Freije, Preeta Guptan, and Utpal Banerjee. 2010. “Metabolic Control of G1-S Transition: Cyclin E Degradation by p53-Induced Activation of the Ubiquitin-Proteasome System.” The Journal of Cell Biology 188 (4): 473–479. https://doi.org/10.1083/jcb.200912024.

Mandal, Sudip, Preeta Guptan, Edward Owusu-Ansah, and Utpal Banerjee. 2005. “Mitochondrial Regulation of Cell Cycle Progression during Development as Revealed by the Tenured Mutation in Drosophila.” Developmental Cell 9 (6): 843–854. https://doi.org/10.1016/j.devcel.2005.11.006.

Mazumder, S., E. L. DuPree, and A. Almasan. 2004. “A Dual Role of Cyclin E in Cell Proliferation and Apoptosis May Provide a Target for Cancer Therapy.” Current Cancer Drug Targets 4 (1): 65–75. https://doi.org/10.2174/1568009043481669.

Mirzoyan, Zhasmine, Manuela Sollazzo, Mariateresa Allocca, Alice Maria Valenza, Daniela Grifoni, and Paola Bellosta. 2019. “Drosophila Melanogaster: A Model Organism to Study Cancer.” Frontiers in Genetics 10 (March): 51. https://doi.org/10.3389/fgene.2019.00051.

Mishra, Prashant, Valerio Carelli, Giovanni Manfredi, and David C. Chan. 2014. “Proteolytic Cleavage of Opa1 Stimulates Mitochondrial Inner Membrane Fusion and Couples Fusion to Oxidative Phosphorylation.” Cell Metabolism 19 (5): 891. https://doi.org/10.1016/j.cmet.2014.04.014.

Mishra, Prashant, and David C. Chan. 2016. “Metabolic Regulation of Mitochondrial Dynamics.” The Journal of Cell Biology 212 (4): 379–387. https://doi.org/10.1083/jcb.201511036.

Mitra, Kasturi, Richa Rikhy, Mary Lilly, and Jennifer Lippincott-Schwartz. 2012. “DRP1-Dependent Mitochondrial Fission Initiates Follicle Cell Differentiation during Drosophila Oogenesis.” The Journal of Cell Biology 197 (4): 487–497. https://doi.org/10.1083/jcb.201110058.

Mitra, Kasturi, Christian Wunder, Badrinath Roysam, Gang Lin, and Jennifer Lippincott-Schwartz. 2009. “A Hyperfused Mitochondrial State Achieved at G1-S Regulates Cyclin E Buildup and Entry into S Phase.” Proceedings of the National Academy of Sciences of the United States of America 106 (29): 11960–11965. https://doi.org/10.1073/pnas.0904875106.

Moosavi, Behrooz, Edward A. Berry, Xiao-Lei Zhu, Wen-Chao Yang, and Guang-Fu Yang. 2019. “The Assembly of Succinate Dehydrogenase: A Key Enzyme in Bioenergetics.” Cellular and Molecular Life Sciences: CMLS 76 (20): 4023–4042. https://doi.org/10.1007/s00018-019-03200-7.

Muller, F. 2000. “The Nature and Mechanism of Superoxide Production by the Electron Transport Chain: Its Relevance to Aging.” Journal of the American Aging Association 23 (4): 227–253. https://doi.org/10.1007/s11357-000-0022-9.

Murphy, Michael P. 2016. “Understanding and Preventing Mitochondrial Oxidative Damage.” Biochemical Society Transactions 44 (5): 1219–1226. https://doi.org/10.1042/BST20160108.

Napiwotzki, J., and B. Kadenbach. 1998. “Extramitochondrial ATP/ADP-Ratios Regulate Cytochrome c Oxidase Activity via Binding to the Cytosolic Domain of Subunit IV.” Biological Chemistry 379 (3): 335–339. https://doi.org/10.1515/bchm.1998.379.3.335.

Nicholls, David. 2002. “Mitochondrial Bioenergetics, Aging, and Aging-Related Disease.” Science of Aging Knowledge Environment: SAGE KE 2002 (31): e12. https://doi.org/10.1126/sageke.2002.31.pe12.

Niemann, S., and U. Müller. 2000. “Mutations in SDHC Cause Autosomal Dominant Paraganglioma, Type 3.” Nature Genetics 26 (3): 268–270. https://doi.org/10.1038/81551.

Ning, Kaiting, Shiqiang Liu, Baoqiang Yang, et al. 2022. “Update on the Effects of Energy Metabolism in Bone Marrow Mesenchymal Stem Cells Differentiation.” Molecular Metabolism 58 (101450): 101450. https://doi.org/10.1016/j.molmet.2022.101450.

Nolfi-Donegan, Deirdre, Andrea Braganza, and Sruti Shiva. 2020. “Mitochondrial Electron Transport Chain: Oxidative Phosphorylation, Oxidant Production, and Methods of Measurement.” Redox Biology 37 (101674): 101674. https://doi.org/10.1016/j.redox.2020.101674.

Nunnari, J., W. F. Marshall, A. Straight, A. Murray, J. W. Sedat, and P. Walter. 1997. “Mitochondrial Transmission during Mating in Saccharomyces Cerevisiae Is Determined by Mitochondrial Fusion and Fission and the Intramitochondrial Segregation of Mitochondrial DNA.” Molecular Biology of the Cell 8 (7): 1233–1242. https://doi.org/10.1091/mbc.8.7.1233.

Okamoto, K., P. S. Perlman, and R. A. Butow. 1998. “The Sorting of Mitochondrial DNA and Mitochondrial Proteins in Zygotes: Preferential Transmission of Mitochondrial DNA to the Medial Bud.” The Journal of Cell Biology 142 (3): 613–623. https://doi.org/10.1083/jcb.142.3.613.

Okuno, Daichi, Ryota Iino, and Hiroyuki Noji. 2011. “Rotation and Structure of FoF1-ATP

Synthase." The Journal of Biochemistry 149 (6): 655–664. https://doi.org/10.1093/jb/mvr049.

O'Rourke, Brian. 2010. "From Bioblasts to Mitochondria: Ever Expanding Roles of Mitochondria in Cell Physiology." Frontiers in Physiology 1 (June): 7. https://doi.org/10.3389/fphys.2010.00007.

Owusu-Ansah, Edward, and Utpal Banerjee. 2009. "Reactive Oxygen Species Prime Drosophila Haematopoietic Progenitors for Differentiation." Nature 461 (7263): 537–541. https://doi.org/10.1038/nature08313.

Owusu-Ansah, Edward, Amir Yavari, Sudip Mandal, and Utpal Banerjee. 2008. "Distinct Mitochondrial Retrograde Signals Control the G1-S Cell Cycle Checkpoint." Nature Genetics 40 (3): 356–361. https://doi.org/10.1038/ng.2007.50.

Parker, Danitra J., Archana Iyer, Shikha Shah, et al. 2015. "A New Mitochondrial Pool of Cyclin E, Regulated by Drp1, Is Linked to Cell-Density-Dependent Cell Proliferation." Journal of Cell Science 128 (22): 4171–4182. https://doi.org/10.1242/jcs.172429.

Paumard, Patrick, Jacques Vaillier, Bénédicte Coulary, et al. 2002. "The ATP Synthase Is Involved in Generating Mitochondrial Cristae Morphology." The EMBO Journal 21 (3): 221–230. https://doi.org/10.1093/emboj/21.3.221.

Pernas, Lena, and Luca Scorrano. 2016. "Mito-Morphosis: Mitochondrial Fusion, Fission, and Cristae Remodeling as Key Mediators of Cellular Function." Annual Review of Physiology 78 (1): 505–531. https://doi.org/10.1146/annurev-physiol-021115-105011.

Rak, Malgorzata, Paule Bénit, Dominique Chrétien, et al. 2016. "Mitochondrial Cytochrome c Oxidase Deficiency." Clinical Science (London, England: 1979) 130 (6): 393–407. https://doi.org/10.1042/CS20150707.

Rambold, Angelika S., Brenda Kostelecky, Natalie Elia, and Jennifer Lippincott-Schwartz. 2011. "Tubular Network Formation Protects Mitochondria from Autophagosomal Degradation during Nutrient Starvation." Proceedings of the National Academy of Sciences of the United States of America 108 (25): 10190–10195. https://doi.org/10.1073/pnas.1107402108.

Roger, Andrew J., Sergio A. Muñoz-Gómez, and Ryoma Kamikawa. 2017. "The Origin and Diversification of Mitochondria." Current Biology: CB 27 (21): R1177–R1192. https://doi.org/10.1016/j.cub.2017.09.015.

Rolland, Stéphane G., Elisa Motori, Nadin Memar, et al. 2013. “Impaired Complex IV Activity in Response to Loss of LRPPRC Function Can Be Compensated by Mitochondrial Hyperfusion.” Proceedings of the National Academy of Sciences of the United States of America 110 (32): E2967–76. https://doi.org/10.1073/pnas.1303872110.

Samuels, Tamsin J., Yoav Arava, Aino I. Järvelin, et al. 2020. “Neuronal Upregulation of Prospero Protein Is Driven by Alternative mRNA Polyadenylation and Syncrip-Mediated mRNA Stabilisation.” Biology Open 9 (5): bio049684. https://doi.org/10.1242/bio.049684.

Schieke, Stefan M., Mingchao Ma, Liu Cao, et al. 2008. “Mitochondrial Metabolism Modulates Differentiation and Teratoma Formation Capacity in Mouse Embryonic Stem Cells.” The Journal of Biological Chemistry 283 (42): 28506–28512. https://doi.org/10.1074/jbc.M802763200.

Scott, R. A. 1995. “Functional Significance of Cytochrome c Oxidase Structure.” Structure (London, England: 1993) 3 (10): 981–986. https://doi.org/10.1016/s0969-2126(01)00233-7.

Senoo-Matsuda, Nanami, Philip S. Hartman, Akira Akatsuka, Shinichi Yoshimura, and Naoaki Ishii. 2003. “A Complex II Defect Affects Mitochondrial Structure, Leading to Ced-3- and Ced-4-Dependent Apoptosis and Aging.” The Journal of Biological Chemistry 278 (24): 22031–22036. https://doi.org/10.1074/jbc.M211377200.

Seo, Bong Jong, Sang Hoon Yoon, and Jeong Tae Do. 2018. “Mitochondrial Dynamics in Stem Cells and Differentiation.” International Journal of Molecular Sciences 19 (12): 3893. https://doi.org/10.3390/ijms19123893.

Sharma, Lokendra K., Jianxin Lu, and Yidong Bai. 2009. “Mitochondrial Respiratory Complex I: Structure, Function and Implication in Human Diseases.” Current Medicinal Chemistry 16 (10): 1266–1277. https://doi.org/10.2174/092986709787846578.

Sharma, Lokendra Kumar, Hezhi Fang, Jiangtao Liu, Rasika Vartak, Janice Deng, and Yidong Bai. 2011. “Mitochondrial Respiratory Complex I Dysfunction Promotes Tumorigenesis through ROS Alteration and AKT Activation.” Human Molecular Genetics 20 (23): 4605–4616. https://doi.org/10.1093/hmg/ddr395.

Shen, Koning, Corinne L. Pender, Raz Bar-Ziv, et al. 2022. “Mitochondria as Cellular and Organismal Signaling Hubs.” Annual Review of Cell and Developmental Biology 38 (1): 179–218. https://doi.org/10.1146/annurev-cellbio-120420-015303.

Shoffner, J. M., R. L. Watts, J. L. Juncos, A. Torroni, and D. C. Wallace. 1991. “Mitochondrial Oxidative Phosphorylation Defects in Parkinson’s Disease.” Annals of Neurology 30 (3): 332–339. https://doi.org/10.1002/ana.410300304.

Song, Dong Hoon, Jonghyun Park, Laura L. Maurer, Wei Lu, Martin A. Philbert, and Ann Marie Sastry. 2013. “Biophysical Significance of the Inner Mitochondrial Membrane Structure on the Electrochemical Potential of Mitochondria.” Physical Review. E, Statistical, Nonlinear, and Soft Matter Physics 88 (6): 062723. https://doi.org/10.1103/PhysRevE.88.062723.

Song, Won-Hee, John William Oman Ballard, Young-Joo Yi, and Peter Sutovsky. 2014. “Regulation of Mitochondrial Genome Inheritance by Autophagy and Ubiquitin-Proteasome System: Implications for Health, Fitness, and Fertility.” BioMed Research International 2014 (June): 981867. https://doi.org/10.1155/2014/981867.

Song, Zhiyin, Mariam Ghochani, J. Michael McCaffery, Terrence G. Frey, and David C. Chan. 2009. “Mitofusins and OPA1 Mediate Sequential Steps in Mitochondrial Membrane Fusion.” Molecular Biology of the Cell 20 (15): 3525–3532. https://doi.org/10.1091/mbc.e09-03-0252.

Son, Myung Jin, Bo Ram Jeong, Youjeong Kwon, and Yee Sook Cho. 2013. “Interference with the Mitochondrial Bioenergetics Fuels Reprogramming to Pluripotency via Facilitation of the Glycolytic Transition.” The International Journal of Biochemistry & Cell Biology 45 (11): 2512–2518. https://doi.org/10.1016/j.biocel.2013.07.023.

Spana, E. P., C. Kopczynski, C. S. Goodman, and C. Q. Doe. 1995. “Asymmetric Localization of Numb Autonomously Determines Sibling Neuron Identity in the Drosophila CNS.” Development (Cambridge, England) 121 (11): 3489–3494. https://doi.org/10.1242/dev.121.11.3489.

Stroud, David A., Elliot E. Surgenor, Luke E. Formosa, et al. 2016. “Accessory Subunits Are Integral for Assembly and Function of Human Mitochondrial Complex I.” Nature 538 (7623): 123–126. https://doi.org/10.1038/nature19754.

Sun, Chang, Samir Benlekbir, Padmaja Venkatakrishnan, et al. 2018. “Structure of the Alternative Complex III in a Supercomplex with Cytochrome Oxidase.” Nature 557 (7703): 123–126. https://doi.org/10.1038/s41586-018-0061-y.

Svensson-Ek, Margareta, Jeff Abramson, Gisela Larsson, Susanna Törnroth, Peter Brzezinski, and So Iwata. 2002. “The X-Ray Crystal Structures of Wild-Type and EQ(I-286) Mutant Cytochrome c Oxidases from Rhodobacter Sphaeroides.”

Journal of Molecular Biology 321 (2): 329–339. https://doi.org/10.1016/s0022-2836(02)00619-8.

Taguchi, Naoko, Naotada Ishihara, Akihiro Jofuku, Toshihiko Oka, and Katsuyoshi Mihara. 2007. “Mitotic Phosphorylation of Dynamin-Related GTPase Drp1 Participates in Mitochondrial Fission.” The Journal of Biological Chemistry 282 (15): 11521–11529. https://doi.org/10.1074/jbc.M607279200.

Tassone, Annalisa, Maria Meringolo, Giulia Ponterio, Paola Bonsi, Tommaso Schirinzi, and Giuseppina Martella. 2023. “Mitochondrial Bioenergy in Neurodegenerative Disease: Huntington and Parkinson.” International Journal of Molecular Sciences 24 (8): 7221. https://doi.org/10.3390/ijms24087221.

Teixeira, Felipe K., Carlos G. Sanchez, Thomas R. Hurd, et al. 2015. “ATP Synthase Promotes Germ Cell Differentiation Independent of Oxidative Phosphorylation.” Nature Cell Biology 17 (5): 689–696. https://doi.org/10.1038/ncb3165.

Ten, Vadim, and Alexander Galkin. 2019. “Mechanism of Mitochondrial Complex I Damage in Brain Ischemia/reperfusion Injury. A Hypothesis.” Molecular and Cellular Neurosciences 100 (103408): 103408. https://doi.org/10.1016/j.mcn.2019.103408.

Tilokani, Lisa, Shun Nagashima, Vincent Paupe, and Julien Prudent. 2018. “Mitochondrial Dynamics: Overview of Molecular Mechanisms.” Essays in Biochemistry 62 (3): 341–360. https://doi.org/10.1042/EBC20170104.

Tomizaki, T., E. Yamashita, H. Yamaguchi, et al. 1999. “Structure Analysis of Bovine Heart Cytochrome c Oxidase at 2.8 A Resolution.” Acta Crystallographica. Section D, Biological Crystallography 55 (Pt 1): 31–45. https://doi.org/10.1107/S0907444998006362.

Tothova, Zuzana, Ramya Kollipara, Brian J. Huntly, et al. 2007. “FoxOs Are Critical Mediators of Hematopoietic Stem Cell Resistance to Physiologic Oxidative Stress.” Cell 128 (2): 325–339. https://doi.org/10.1016/j.cell.2007.01.003.

Trevisan, Tatiana, Diana Pendin, Aldo Montagna, Sergio Bova, Anna Maria Ghelli, and Andrea Daga. 2018. “Manipulation of Mitochondria Dynamics Reveals Separate Roles for Form and Function in Mitochondria Distribution.” Cell Reports 23 (6): 1742–1753. https://doi.org/10.1016/j.celrep.2018.04.017.

Twig, Gilad, Alvaro Elorza, Anthony J. A. Molina, et al. 2008. “Fission and Selective Fusion Govern Mitochondrial Segregation and Elimination by Autophagy.” The EMBO Journal 27 (2): 433–446. https://doi.org/10.1038/sj.emboj.7601963.

Urbach, Rolf, Ralf Schnabel, and Gerhard M. Technau. 2003. “The Pattern of Neuroblast Formation, Mitotic Domains and Proneural Gene Expression during Early Brain Development in Drosophila.” Development (Cambridge, England) 130 (16): 3589–3606. https://doi.org/10.1242/dev.00528.

Varum, S., O. Momcilović, C. Castro, A. Ben-Yehudah, J. Ramalho-Santos, and C. S. Navara. 2009. “Enhancement of Human Embryonic Stem Cell Pluripotency through Inhibition of the Mitochondrial Respiratory Chain.” Stem Cell Research 3 (2-3): 142–156. https://doi.org/10.1016/j.scr.2009.07.002.

Vogel, Frank, Carsten Bornhövd, Walter Neupert, and Andreas S. Reichert. 2006. “Dynamic Subcompartmentalization of the Mitochondrial Inner Membrane.” The Journal of Cell Biology 175 (2): 237–247. https://doi.org/10.1083/jcb.200605138.

Walsh, Kathleen T., and Chris Q. Doe. 2017. “Drosophila Embryonic Type II Neuroblasts: Origin, Temporal Patterning, and Contribution to the Adult Central Complex.” In bioRxiv. BioRxiv, July 30. https://doi.org/10.1101/170043.

Wang, Zhu A., and Daniel Kalderon. 2009. “Cyclin E-Dependent Protein Kinase Activity Regulates Niche Retention of Drosophila Ovarian Follicle Stem Cells.” Proceedings of the National Academy of Sciences of the United States of America 106 (51): 21701–21706. https://doi.org/10.1073/pnas.0909272106.

Watt, Ian N., Martin G. Montgomery, Michael J. Runswick, Andrew G. W. Leslie, and John E. Walker. 2010. “Bioenergetic Cost of Making an Adenosine Triphosphate Molecule in Animal Mitochondria.” Proceedings of the National Academy of Sciences of the United States of America 107 (39): 16823–16827. https://doi.org/10.1073/pnas.1011099107.

Willows, Robin, Matthew J. Sanders, Bing Xiao, et al. 2017. “Phosphorylation of AMPK by Upstream Kinases Is Required for Activity in Mammalian Cells.” The Biochemical Journal 474 (17): 3059–3073. https://doi.org/10.1042/BCJ20170458.

Wittig, Ilka, and Hermann Schägger. 2008. “Structural Organization of Mitochondrial ATP Synthase.” Biochimica et Biophysica Acta 1777 (7-8): 592–598. https://doi.org/10.1016/j.bbabio.2008.04.027.

Wodarz, Andreas, and Wieland B. Huttner. 2003. “Asymmetric Cell Division during Neurogenesis in Drosophila and Vertebrates.” Mechanisms of Development 120 (11): 1297–1309. https://doi.org/10.1016/j.mod.2003.06.003.

Wollweber, Florian, Karina von der Malsburg, and Martin van der Laan. 2017. “Mitochondrial Contact Site and Cristae Organizing System: A Central Player in

Membrane Shaping and Crosstalk.” Biochimica et Biophysica Acta 1864 (9): 1481–1489. https://doi.org/10.1016/j.bbamcr.2017.05.004.

Yang, Ziyun, Liang Wang, Cheng Yang, et al. 2021. “Mitochondrial Membrane Remodeling.” Frontiers in Bioengineering and Biotechnology 9: 786806. https://doi.org/10.3389/fbioe.2021.786806.

Yankovskaya, Victoria, Rob Horsefield, Susanna Törnroth, et al. 2003. “Architecture of Succinate Dehydrogenase and Reactive Oxygen Species Generation.” Science (New York, N.Y.) 299 (5607): 700–704. https://doi.org/10.1126/science.1079605.

Yao, Cong-Hui, Rencheng Wang, Yahui Wang, Che-Pei Kung, Jason D. Weber, and Gary J. Patti. 2019. “Mitochondrial Fusion Supports Increased Oxidative Phosphorylation during Cell Proliferation.” eLife 8 (January). https://doi.org/10.7554/eLife.41351.

Youle, Richard J., and Alexander M. van der Bliek. 2012. “Mitochondrial Fission, Fusion, and Stress.” Science (New York, N.Y.) 337 (6098): 1062–1065. https://doi.org/10.1126/science.1219855.

Yu, Fengwei, Chay T. Kuo, and Yuh Nung Jan. 2006. “Drosophila Neuroblast Asymmetric Cell Division: Recent Advances and Implications for Stem Cell Biology.” Neuron 51 (1): 13–20. https://doi.org/10.1016/j.neuron.2006.06.016.

Zhang, Fan, Mehdi Pirooznia, and Hong Xu. 2020. “Mitochondria Regulate Intestinal Stem Cell Proliferation and Epithelial Homeostasis through FOXO.” Molecular Biology of the Cell 31 (14): 1538–1549. https://doi.org/10.1091/mbc.E19-10-0560.

Zhang, Xing-Ding, Ye Wang, Jun-Chao Wu, et al. 2009. “Down-Regulation of Bcl-2 Enhances Autophagy Activation and Cell Death Induced by Mitochondrial Dysfunction in Rat Striatum.” Journal of Neuroscience Research 87 (16): 3600–3610. https://doi.org/10.1002/jnr.22152.

Zhao, Jian, Tong Liu, Shaobo Jin, et al. 2011. “Human MIEF1 Recruits Drp1 to Mitochondrial Outer Membranes and Promotes Mitochondrial Fusion rather than Fission: MIEF1, a Key Regulator of Mitochondrial Dynamics.” The EMBO Journal 30 (14): 2762–2778. https://doi.org/10.1038/emboj.2011.198.